ISSN: 2408-2384 (Online)
ISSN: 1686-5456 (Print)

Environment and Natural Resources Journal

Volume 21, Number 2, March - April 2023

Environment and Natural Resources Journal (EnNRJ)

Volume 21, Number 2, March - April 2023 ISSN: 1686-5456 (Print)
ISSN: 2408-2384 (Online)

AIMS AND SCOPE

The Environment and Natural Resources Journal is a peer-reviewed journal, which provides insight scientific knowledge into the diverse dimensions of integrated environmental and natural resource management. The journal aims to provide a platform for exchange and distribution of the knowledge and cutting-edge research in the fields of environmental science and natural resource management to academicians, scientists and researchers. The journal accepts a varied array of manuscripts on all aspects of environmental science and natural resource management. The journal scope covers the integration of multidisciplinary sciences for prevention, control, treatment, environmental clean-up and restoration. The study of the existing or emerging problems of environment and natural resources in the region of Southeast Asia and the creation of novel knowledge and/or recommendations of mitigation measures for sustainable development policies are emphasized.

The subject areas are diverse, but specific topics of interest include:

- Biodiversity
- Climate change
- Detection and monitoring of polluted sources e.g., industry, mining
- Disaster e.g., forest fire, flooding, earthquake, tsunami, or tidal wave
- Ecological/Environmental modelling
- Emerging contaminants/hazardous wastes investigation and remediation
- Environmental dynamics e.g., coastal erosion, sea level rise
- Environmental assessment tools, policy and management e.g., GIS, remote sensing, Environmental Management System (EMS)
- Environmental pollution and other novel solutions to pollution
- Remediation technology of contaminated environments
- Transboundary pollution
- Waste and wastewater treatments and disposal technology

Schedule

Environment and Natural Resources Journal (EnNRJ) is published 6 issues per year in January-February, March-April, May-June, July-August, September-October, and November-December.

Publication Fees

There is no cost of the article-processing and publication.

Ethics in publishing

EnNRJ follows closely a set of guidelines and recommendations published by Committee on Publication Ethics (COPE).

Environment and Natural Resources Journal (EnNRJ)

Volume 21, Number 2, March - April 2023

ISSN: 1686-5456 (Print)

ISSN: 2408-2384 (Online)

Editorial Office Address
Research Management and Administration Section,
Faculty of Environment and Resource Studies, Mahidol University
999, Phutthamonthon Sai 4 Road, Salaya, Phutthamonthon, Nakhon Pathom, Thailand, 73170
Phone +662 441 5000 ext. 2108 Fax. +662 441 9509-10
Website: https://ph02.tci-thaijo.org/index.php/ennrj/index
E-mail: ennrjournal@gmail.com

Environment and Natural Resources Journal (EnNRJ)

Volume 21, Number 2, March - April 2023 ISSN: 1686-5456 (Print)
ISSN: 2408-2384 (Online)

CONTENT

Coagulation Study on Extracted Algal Alginate from Red Algae as Natural Coagulant for Remediation of Textile Dye Congo Red

Sivamani Sivalingam* and Vijayaraghavan Gopal

Department of Chemical Engineering, Rajalakshmi Engineering College, Thandalam-602105, Chennai, Tamilnadu, India

ARTICLE INFO

Received: 11 Oct 2022
Received in revised: 23 Nov 2022
Accepted: 7 Dec 2022
Published online: 13 Jan 2023
DOI: 10.32526/ennrj/21/202200221

Keywords:
Congo red/ Calcium alginate/ Jar test/ Turbidity/ Textile wastewater

*** Corresponding author:**
E-mail: sivamchem@gmail.com; sivamani.s@rajalakshmi.edu.in

ABSTRACT

In the present study, extracted algal alginate from red algae as natural coagulant was used for removal of textile dye congo red (CR) from water. In developing countries like India, only about 10% of the wastewater being generated is treated, whereas the remaining 90% is discharged into the water bodies as it stands. Color and turbidity are the most common problems in the disposal of wastewater. The removal of color is one of the key challenges in wastewater treatment. For the coagulation process, the synthetic textile wastewater samples had CR concentrations of 50, 100, 150, 200, and 250 mg/L and varying initial pH of 4, 5, and 6. Different dosages of calcium and alginate (1, 2, 3, 4, 5, and 6 g/L) were used to perform the experiments. The obtained results exhibited that the effectiveness of color removal was higher at lower pH 4, and the calcium and alginate dosages are dependent on the CR concentration of the synthetic textile wastewater. These investigations demonstrating the higher efficiency of calcium alginate as a coagulant, where maximum color removal achieved over 95.05%. Increasing alginate dosages and residence times can enhance the performance of coagulation. Dye color is often present in real wastewater and needs to be removed before being reused or discharged to the environment.

1. INTRODUCTION

A basic need for all living organisms is water, but water is unable to be used when it mixes with impurities creating wastewater caused by industrialization and increasing populations. Treatment of synthetic textile wastewater is one of the major problems faced by researchers and industries (Vijayaraghavan and Shanthakumar, 2016; Sivalingam et al., 2019; Sivalingam and Sen, 2019). Textile industries are using various dyes like anionic dyes (alizarin yellow, methyl orange and congo red) and cationic dyes (methylene blue, crystal violet and rhodamine B) for dying and printing purposes. After being applied, these dye colors are generating synthetic wastewater dye solutions that are discharged without any treatment into the environment. The traditional wastewater treatment is aerobic biodegradation which gives low removal efficiency thus the need to employ new techniques. The printing and dyeing industries use an extensive amount of azo dye congo red (CR), which is made from 1-naphthalene sulfonic acid. A high quantity of this dye molecule causes an allergic reaction or possibly causes it to change into a carcinogen similar to Benzidine. Moreover, due to its structural, chemical, and thermal stability and difficult in biodegrading property CR is a persistent substrate in wastewater (Pham et al., 2019; Ajoke et al., 2021).

Commonly, various kinds of wastewater treatments have been used to purify the water such as biological treatment, membrane separation, coagulation and flocculation, oxidation, photo-chemical, ion exchange, and adsorption (Chuah et al., 2005; Assimeddine et al., 2022). However, these processes require higher costs and energy than the coagulation/flocculation which is a quite simple, effective, and economically feasible method. Coagulation technique is as simple as adding some chemicals to the suspended particles to destabilize the solution where the surface of the colloids has been modified and converting all the particles into solid particles. Coagulants increase the size of minute particles in a solution by balancing electrical charges,

Citation: Sivalingam S, Gopal V. Coagulation study on extracted algal alginate from red algae as natural coagulant for remediation of textile dye congo red. Environ. Nat. Resour. J. 2023;21(2):90-101. (https://doi.org/10.32526/ennrj/21/202200221)

which counteract electrostatic repelling forces that cause repellent electrical charges (destabilized particles), that are typically negative, to be neutralized.

As coagulant aids, natural or synthetic polymers as well as inorganic metals like alum, ferric chloride, lime, etc. are used. For many years alum (aluminum sulfate) has been the most widely used coagulant. The aluminum ions, Al^{3+} that form when the alum is dissolved in water, neutralize the negative charges that the colloidal particles carry and which help to destabilize them. The alum destabilizes the particles through hydrolysis making it a hydrolyzing metal salt coagulant (Nozaic et al., 2001). When the water is slowly swirled the precipitates enmesh the destabilized particles to help them settle down while the Al ions hydrolyze and create $Al(OH)_3$. The main drawbacks of metal salt coagulations are the generally large amounts of chemicals required, simultaneously huge amounts of sludge generated and substantial pH changes throughout the treatment. Another disadvantage of alum is the concern about the suspected role of aluminum in Alzheimer's disease (Huang et al., 2000; Ozacar and Sengil, 2003).

Due to some negative impacts of synthetic polymers on human health, the current research focuses on natural polymeric materials. The natural polymeric materials such as polysaccharides have been suggested because they are easily available, low cost, low molecular weight, and high shear stability. Additional advantages of this natural polyelectrolyte include safety for human health, biodegradability, and a wider effective dose range of flocculation for various colloidal suspensions (Kawamura, 1991; Palapa et al., 2021). Therefore, inorganic coagulants have been suggested to be replaced by natural organic polymers in recent years (Salehizadeh and Shojaosadati, 2001).

Water treatment uses natural coagulants that are taken from specific types of plants, such as *Prosopis Juliflora*, *Cactus latifaria*, and *Moringa oleifera*. Both high and low turbidity water responds favorably to these coagulants. Moreover, chitosan, cationic starches, and extract of cactus, have been used to remove turbidity (Pal et al., 2005; Zhang et al., 2006). These investigations show that natural coagulants are more effective at removing color than inorganic metals and synthetic polymers.

Alginate was produced in this manner from sea brown algae. This polysaccharide is organic. Monomers of α-L guluronic acid (G) and β-D mannuronic acid (M) combine to produce the polymer. The monomers create MM, MG, and GG block structures to create alginate. According to Aylin Devrimci (Devrimci et al., 2012; Ekanayake and Manage, 2022), virtual quantity of these building blocks present in alginate structure shows better performance with metal ions. Alginate is the only polysaccharide, which naturally contains carboxyl groups in each constituent residue, and possesses various abilities for functional materials (Ikeda et al., 2000). Strong gels or insoluble polymers are created by the alginate's reaction with polyvalent metal cations, particularly calcium ions. They are divided into three major classes according to their coloration: brown algae (*Phaeophyceae*), red algae (*Rhodophyceae*), and green algae (*Chlorophyceae*) (Kharkwal et al., 2012). There are 4,000 red species, 1,500 brown species, and roughly 900 kinds of green seaweed that can be found in nature. Alginate is used in a variety of products, including frozen foods, pastry fillings, syrups, bakery goods, dry mixes, meringues, frozen desserts, cooked puddings, salad dressings, flavored meat sauces, chiffons, and dessert gels. The *Chennubhotla*, *Sargassum*, and *Turbinaria* species are used to extract algin.

The main aim of this work is to study an effective coagulation process with extracted alginate as a natural coagulant for removal of highly toxic textile industry dye CR from wastewater. This study further gives sufficient details an effect of different variables such as pH, calcium dose, alginate dose, and dye concentration respectively.

2. METHODOLOGY

2.1 Algae collection

Different species of red (*Kappaphycous allverzii*) and brown algae (*Turbinaria* sp. and *Sargassum* sp.) were taken from coastal water near Mandapam, Tamil Nadu (Vijayaraghavan and Shanthakumar, 2016) (Bay of Bengal), which can be seen in Figure 1. By severing the thallus with a knife close to the rizoid, all of the obtained samples were further processed. Algae were washed in seawater then dried under sunlight and stored in bags in a ventilated area. There are about 900 species of green seaweed among 4,000 red species and 1,500 brown species that can found in nature. The greatest variety of red seaweeds is found in subtropical and tropical waters while brown seaweeds are more common in cooler temperate waters. Seaweeds are marine algae, saltwater dwelling, and simple organisms that fall into the rather outdated general category of plants. Most of them are red (6,000 species), brown (2,000 species) or green (1,200 species).

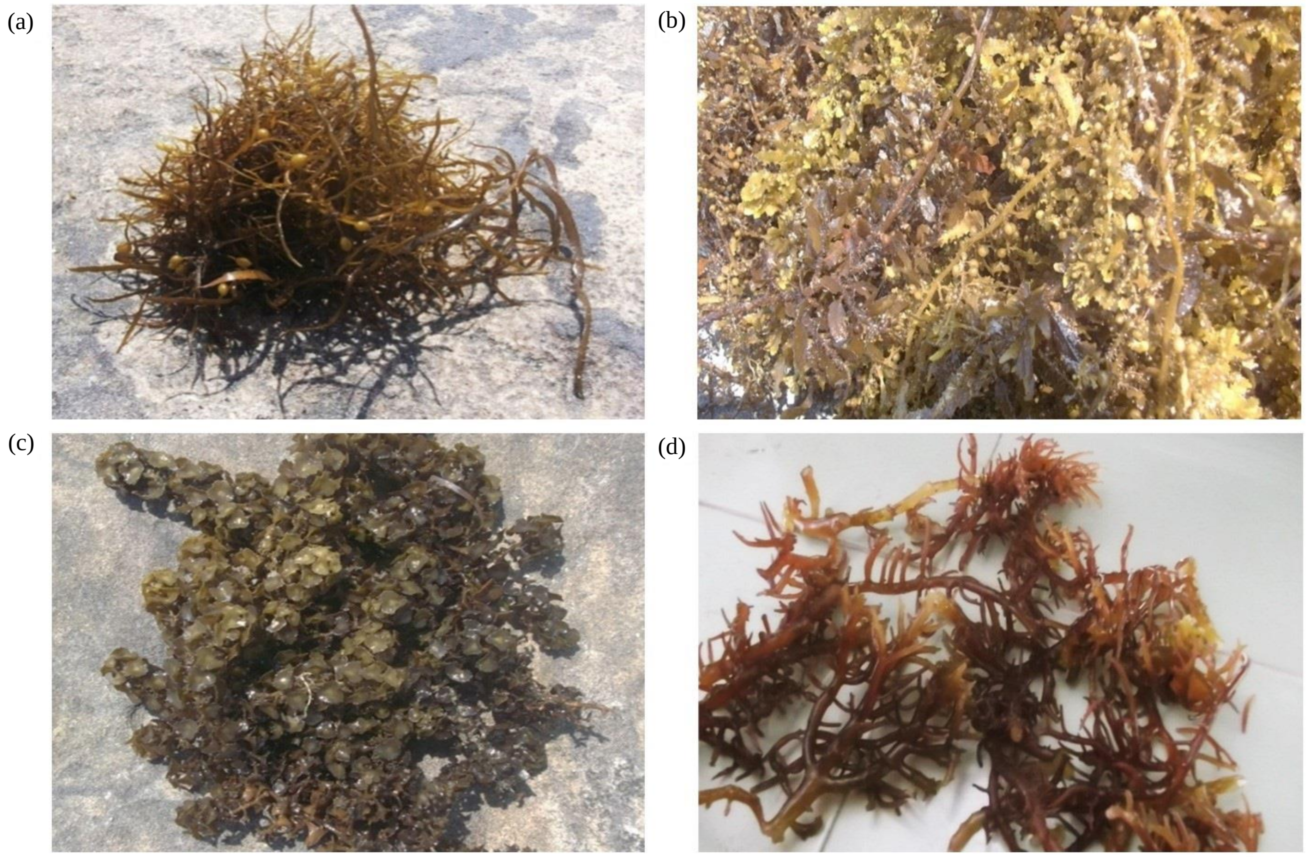

Figure 1. Various species of brown algae, (a) *Sargassum* sp. 1, (b) *Sargassum* sp. 2 and red algae (c) *Turbinaria* sp, (d) *Kaapaphycous allverzii*

2.2 Alginate preparation

Figure 2 shows the schematic diagram for the synthesis of sodium alginate. The collected algae were thoroughly washed by double-distilled water before drying for 30 h at 65 degrees. Alginates removal was done following the method from our previous work (Fenoradosoa et al., 2010; Vijayaraghavan and Shanthakumar, 2016). Twenty five gram aliquots of dried algae were soaked in 800 mL of 2% formaldehyde for 24 h at room temperature rinsed with water. Then, 800 mL of 0.2 M HCl was added and the process was continued for another 24 h. The samples were subsequently given another distilled water wash. Then, alginates were extracted for three hours at 100°C using 2% sodium carbonate. To precipitate the polysaccharides, three liters of 95% ethanol were added after the soluble fraction was filtered out. Sodium alginate was dried at 65°C after being collected and washed twice with 100 mL of acetone, and then transferred to 100 mL of water. Lastly, alginates were precipitated using ethanol (v/v) solution followed by drying at 65°C.

2.3 Dye solution preparation

Congo red dye standard solution (1,000 mg/L) was used to create the necessary concentrations of 50, 100, 150, 200, and 250 mg/L CR in synthetic textile wastewater solutions. The original concentration was made using distilled water and various pH levels of 4, 5, and 6 while mixing for an hour. With a -9.28 mV zeta potential, the CR dye surface is negatively charged. Various doses of calcium and alginates were applied to each 500 mL sample during this experiment.

2.4 UV-Vis spectrophotometer analysis

By measuring the dye sample's absorbance in distilled water at a known standard wavelength (510 nm), UV spectrophotometers can be made uniform. Using a UV spectrophotometer, the absorbance of standard dye solutions (10, 20, 30, mg/L, etc.) was measured. The congo red maximum absorbance wavelength was established at 510 nm. The absorbance of the unidentified sample concentration was then recorded. An equation is provided to determine the concentration of the unknown material and the graph between absorbance and concentration is displayed to confirm the straight line.

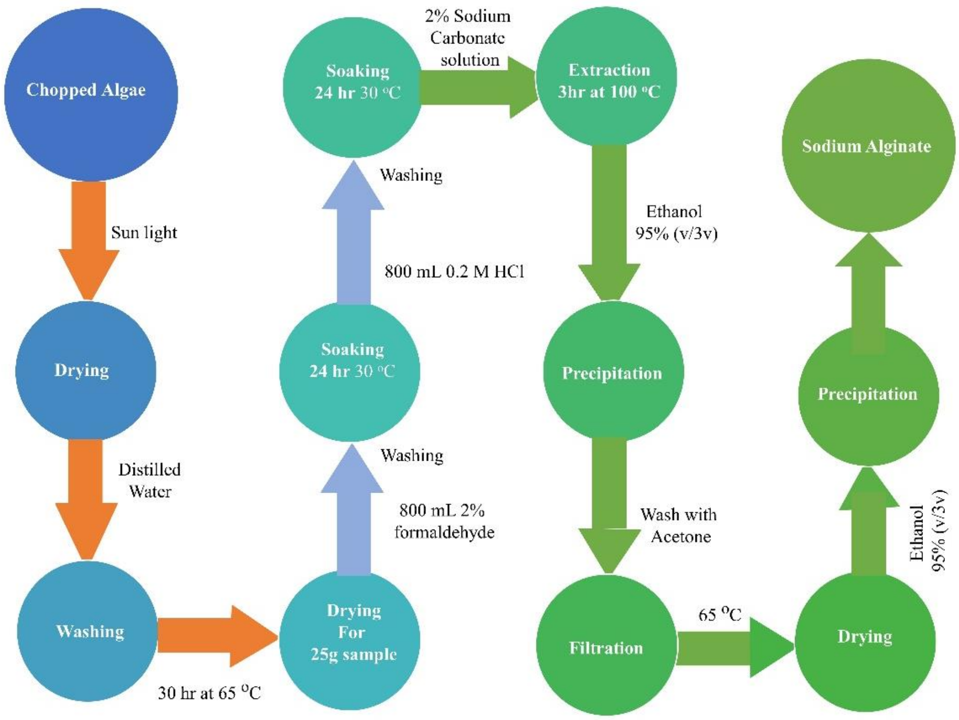

Figure 2. Preparation of sodium alginate

2.5 Experimental procedure

A typical jar test setup was used for the coagulation experiment. As alginate and congo red were both negatively charged substances calcium was introduced first followed by alginate. Colloid/colloid, polymer/colloid, and polymer/polymer pairings repulsive forces are reduced and the double layer is better compressed by the calcium during the coagulation process (Devrimci et al., 2012).

In this study, calcium was employed as CaCl and sodium alginate as alginate. Between 1 and 6 mg/L of calcium were given, and between 1 and 6 mg/L of alginate. Five minutes of gradually increased agitation at 120 rpm for calcium and 5 min of rapid agitation at 120 rpm for alginate, followed by 20 min gradual mixing at 40 rpm and 30 min of settling time were the mixing parameters of each sample used in the tests. Using Whatman filter paper number 42, the collected supernatant following sedimentation was filtered. The filtered solution was analyzed by UV spectrometry at 510 nm of maximum wavelength with the concentrations of 50, 100, 150, 200, and 250 mg/L, which offer improved treatment outcomes. The %CR dye removal was calculated by using equation (1).

$$\text{Dye removal (\%)} = \frac{C_i - C_f}{C_i} \quad (1)$$

Where C_i and C_f are the initial and final dye concentration respectively.

3. RESULTS AND DISCUSSION

3.1 Yield % of alginate

About 25 g of dry seaweeds were examined to find out how much alginate was produced. Following the extraction method shown in Figure 1, it was noted that the sodium alginate yield contents from *Sargassum* sp. 1, *Sargassum* sp. 2, *Turbinaria* sp., and *Kappaphycus allverzii*, were found to be 10.2, 9.6, 9.8, and 10.5 g, respectively. Figure 3 shows the plot between the type of seaweed used to percentage of sodium alginate yield, which was found to be 40.8, 38.4, 39.2, and 42.0% for *Sargassum* sp. 1, *Sargassum* sp. 2, *Turbinaria* sp., and *Kappaphycous allverzii*, respectively. Based on these findings, it is noticeably clear that the experimental seaweed have the potential to be rich sources of alginate, which can be used as a natural coagulant for color removal.

3.2 Scanning electron microscopy (SEM) analysis

Figure 4 (a) and (b) show the Scanning Electron Microscope images of raw alginate surface and alginate surface after coagulation process. It was observed that the surface of alginate before the coagulation process possess blistering spine flakes and fine perforations. But after coagulation treatment process it was noted that sludge formed was fully lodged with swarms of dye particles on the entire fine porous surface of alginate. Based on the SEM images, it was observed that, when comparing the surface of alginate before and after coagulation test, the surface becomes smooth and no flakes were noted. This morphological change on the surface of the alginate reveals the removal of dye from aqueous solution through coagulation process.

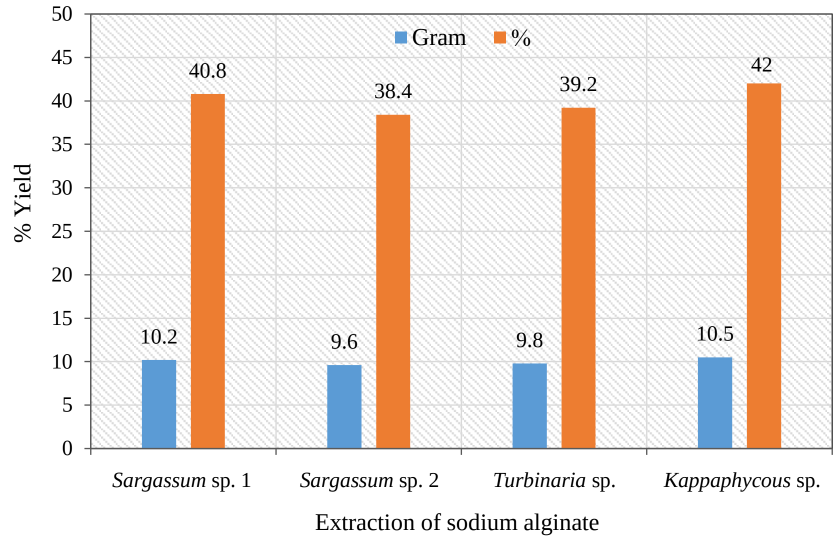

Figure 3. The yield of alginate from brown and red algae species

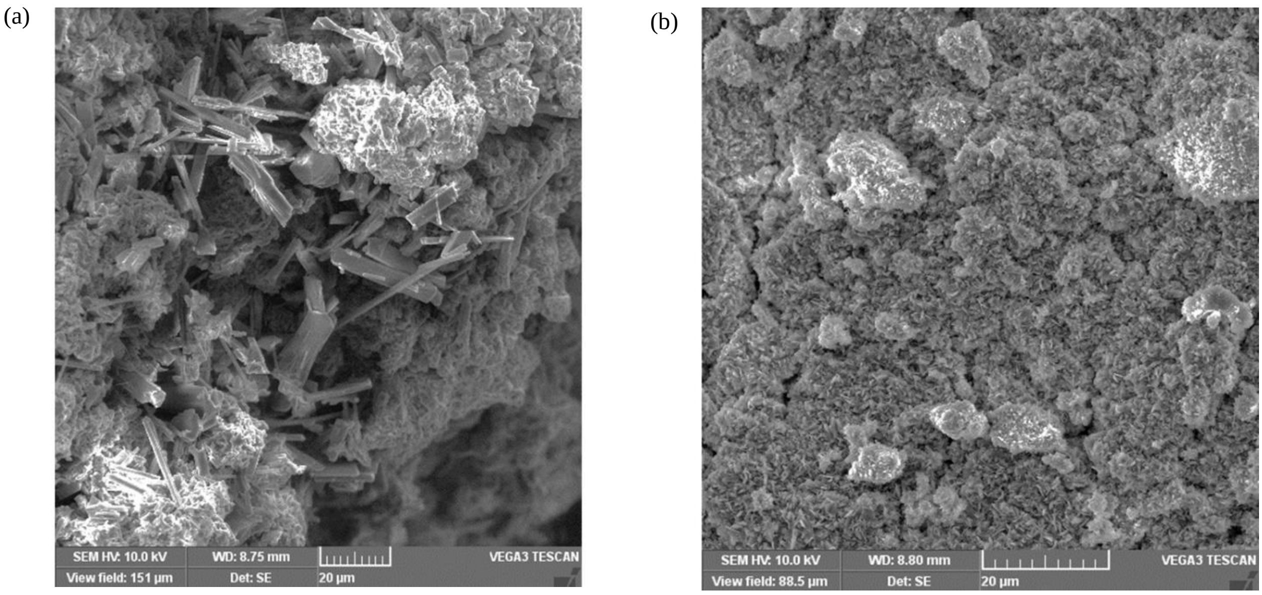

Figure 4. SEM image of (a) raw alginate (b) alginate surface loaded with congo red dye

3.3 Effects of coagulation parameters

The effects of calcium and alginate doses are shown in Figure 5(a)-(f) using synthetic textile wastewater with starting concentrations of 250 and 200 mg/L at pH values of 4, 5, and 6. Because it affects the surface characteristics of the calcium alginate and the ionization/dissociation of the CR dye molecule, the pH of the system has a significant impact on the coagulation process of CR. How dyes are removed from aqueous solutions with different technologies are crucial in wastewater treatment (Ponnusamy and Subramaniam, 2013). In this context, low pH causes an increase in the H^+ ion concentration, and the calcium alginate surface becomes positively charged by absorbing H^+ ions. Because the surface of calcium alginate is positively charged at low pH levels, an extremely strong electrostatic attraction forms between the positively charged calcium alginate surface and the anionic dye molecule that result in a decent amount of dye adsorption (Hoong and Ismail, 2018). More negatively charged sites are present in the systems when the pH increases, while fewer positively charged sites are present (Yupin et al., 2022). Electrostatic repulsion prevents the coagulation of anionic dye molecules at a negatively charged surface location on calcium alginate. In addition, the rivalry between extra OH ions and the anionic dye molecule causes the CR dye to coagulate less readily in an alkaline medium (Kristianto et al., 2019). Figure 5(a)-(c) demonstrates that CR dye removal increases with Calcium dose increases from 1-6 g/L. Moreover, while increasing pH from 4 to 6 the CR dye removal was gradually decreasing. The same phenomena occur during dye concentration decreases from 250 to 200 mg/L as can be seen in Figure 5(a)-(c). In both concentrations the dye removal was 95% at pH 4.

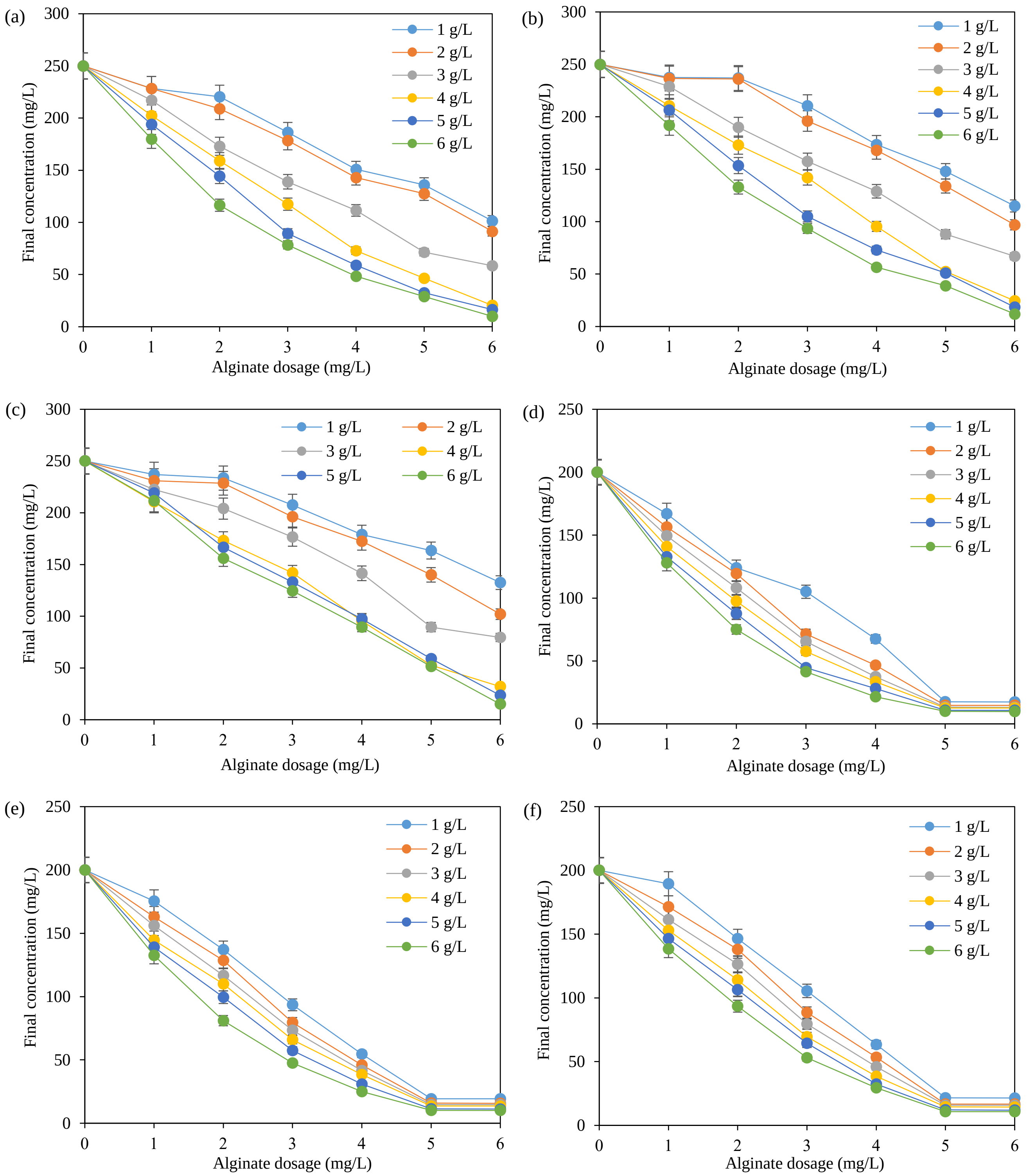

Figure 5. Effect of calcium and alginate dosage in synthetic textile wastewater at initial concentrations of 250 and 200 mg/L at different pH (a) 250 mg/L at 4 pH, (b) 250 mg/L at 5 pH, (c) 250 mg/L at 6 pH, (d) 200 mg/L at 4 pH, (e) 200 mg/L at 5 pH, (f) 200 mg/L at 6 pH

The performance at initial CR concentrations in synthetic textile wastewater of 250 and 200 mg/L is illustrated in Figure 5(a)-(f). This results clearly shows when calcium and alginate were added, the concentration value fell near 10.0 and 9.8 mg/L in 250 and 200 mg/L of synthetic textile waste water, respectively. According to the graph, dye removal efficiency changed as the alginate dose was increased while the calcium dose remained constant. On the other hand, the use of calcium in relation with the dye removal, the efficiency of calcium dose is dependent on alginate dose according to the results. The best dye removal results were obtained using calcium and alginate dosages of 6 and 6 mg/L in synthetic textile wastewater of 250 mg/L, respectively, and calcium and alginate dosages of 6 and 5 mg/L in synthetic textile wastewater of 200 mg/L. At low calcium dosages, calcium alginate generates an inappropriate gel.

When the synthetic textile waste water sample was negatively charged, the low calcium concentration was not enough to neutralize samples so the dyes remained stable. A dose of 6 mg/L of calcium dosage requires 6 and 5 mg/L of alginate dosage in 250 and 200 mg/L of synthetic textile waste water, respectively, to achieve required concentration levels. For 6 mg/L of calcium dosage with 6 and 5 mg/L of alginate dosage the percentage of dye removal values were calculated and removal rates were over 95%. These result show, in high initial concentration, the calcium alginate act as very effective coagulant in different combinations of calcium and alginate doses.

Figure 6(a)-(f) showing the results for initial concentration of synthetic textile waste water at 150 and 100 mg/L for different calcium and alginate doses. From the graphs, low final concentrations near 4.6 and 7.6 mg/L were achieved at 150 and 100 mg/L, respectively, in synthetic textile waste water for 6 mg/L of calcium dosage at different alginate doses studied. The alginate doses level at 150 and 100 mg/L were smaller than alginate dosage level at 250 and 200 mg/L. The optimum alginate dosage range at 250 and 200 mg/L was 6 and 5 mg/L for 6 mg/L of calcium dosage, respectively. On the other hand, this optimum alginate range at 150 and 100 mg/L was 4 and 3 mg/L for 5 mg/L of calcium dosage, respectively. The percentage dye removal values in 150 and 100 mg/L were over 95 % for 5 mg/L of calcium dosage. For low calcium dosage the percentage dye removal values were below 90% in both 150 and 100 mg/L. In low calcium dosage dye removal was lower but still varied depending on the different alginate dosages studied. These results show that at medium initial concentrations, the calcium alginate acts as very effective coagulant in different combination of calcium and alginate doses (Assimeddine et al., 2022).

The final concentration value for an initial concentration of 50 mg/L synthetic textile wastewater at various calcium and alginate doses is displayed in Figure 7(a)-(c). The performance at lower concentration increased when compared to the samples of higher concentration. The optimum concentration of alginate was 2 mg/L for various mg/L of calcium dosage for synthetic textile waste water samples. The final concentration values achieved as near 2.5 mg/L, with various calcium dosage. The efficiency of dye removal ranged from 94 to 96% depending on the calcium and alginate dose.

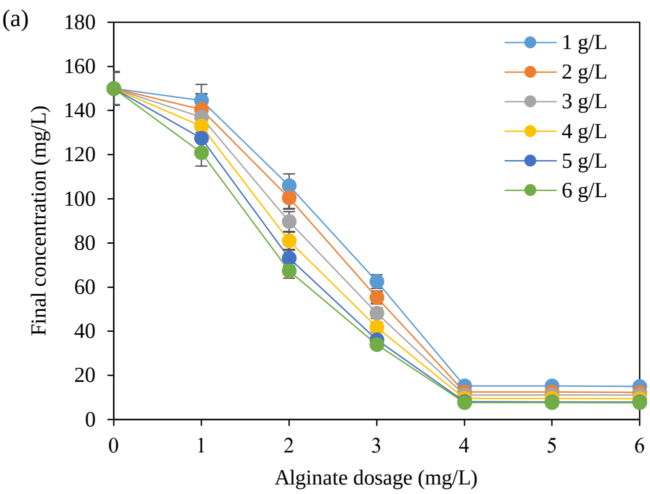

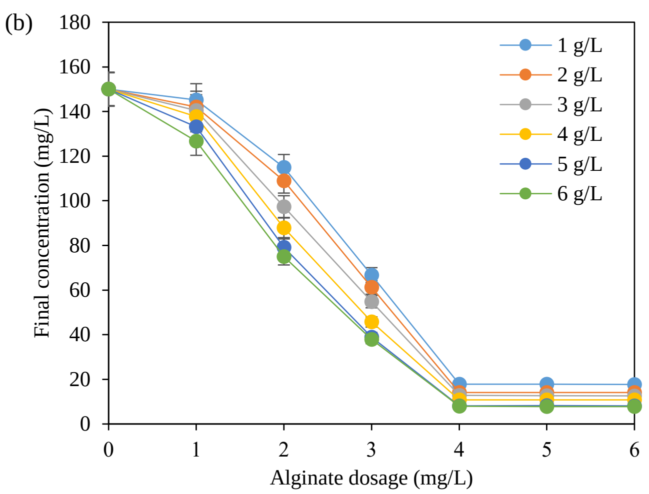

Figure 6. Effect of calcium and alginate dosage on synthetic textile wastewater at initial concentrations 150 and 100 mg/L at different pH (a) 150 mg/L at 4 pH, (b) 150 mg/L at 5 pH, (c) 150 mg/L at 6 pH, (d) 100 mg/L at 4 pH, (d) 100 mg/L at 5 pH, (d) 100 mg/L at 6 pH

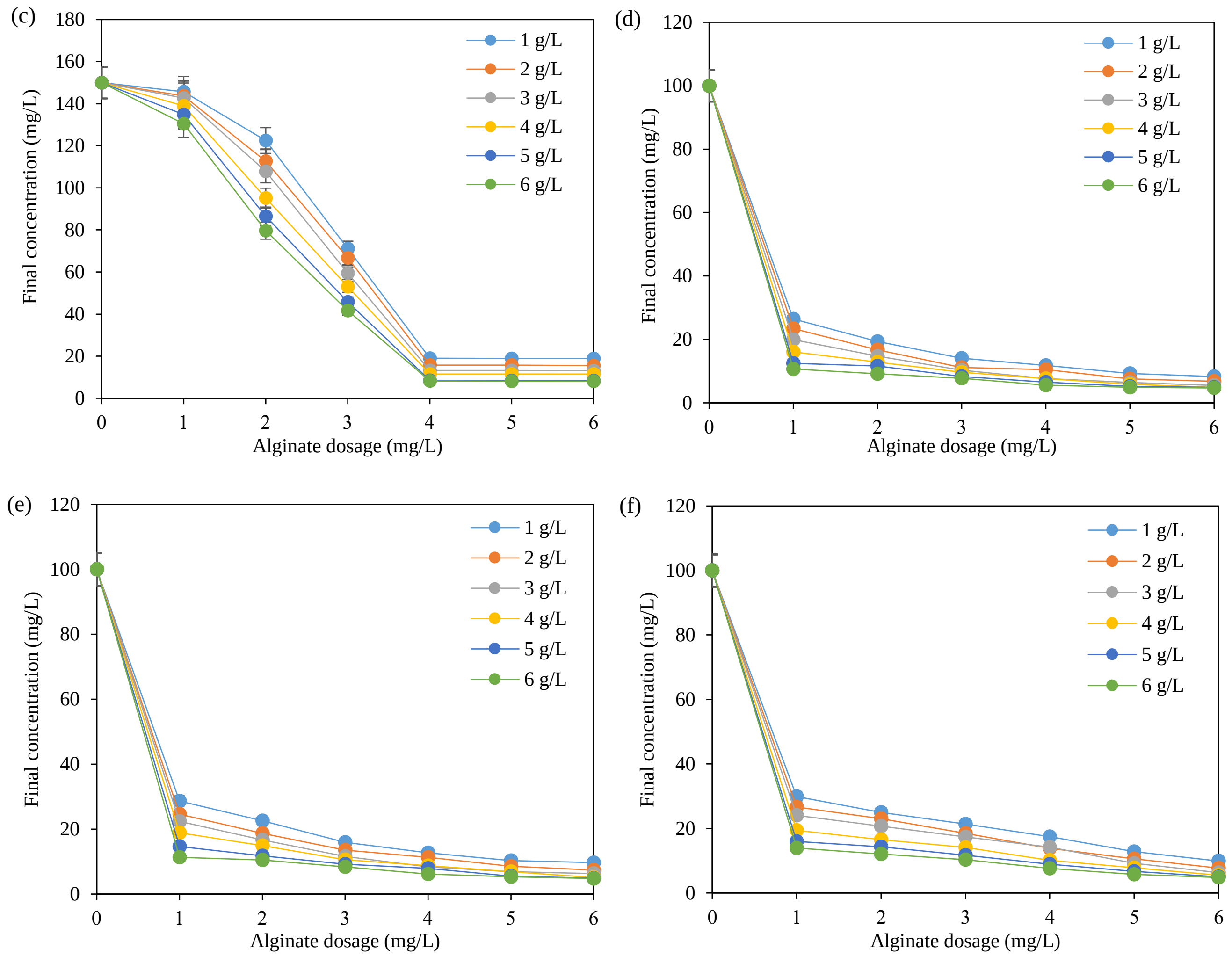

Figure 6. Effect of calcium and alginate dosage on synthetic textile wastewater at initial concentrations 150 and 100 mg/L at different pH (a) 150 mg/L at 4 pH, (b) 150 mg/L at 5 pH, (c) 150 mg/L at 6 pH, (d) 100 mg/L at 4 pH, (d) 100 mg/L at 5 pH, (d) 100 mg/L at 6 pH (cont.)

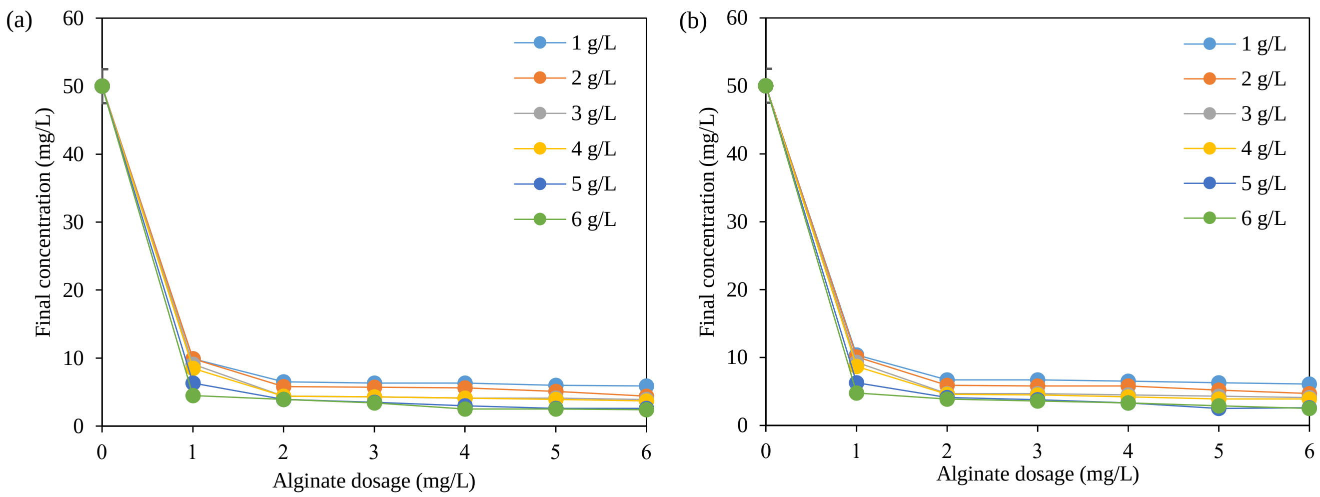

Figure 7. Effect of calcium and alginate dosage on synthetic textile wastewater at initial concentrations of 50 mg/L at different pH (a) 4 pH, (b) 5 pH, (c) 6 pH.

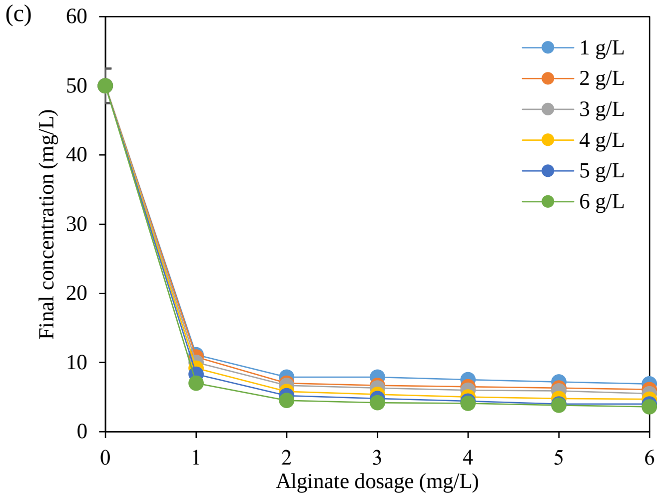

Figure 7. Effect of calcium and alginate dosage on synthetic textile wastewater at initial concentrations of 50 mg/L at different pH (a) 4 pH, (b) 5 pH, (c) 6 pH (cont.)

An increase in the dye removal efficiency was due to the absence of enough particles to constitute nuclei for the flocs to form. The calcium alginate gel formation is the main mechanism, because during or after the stage of gel formation it combines and captures particles to form particles heavy enough to settle down. However, if the flocs were not heavy particles it was not enough to settle down and separate. Calcium alginate gels might have also contributed to some extra turbidity. With these observations low concentration samples may not make floc formation, so using higher viscosity alginates gave better results than lower viscosity alginates in final concentration values. When the alginate molecular weight is higher it increases viscosity and dye removal efficiency. Molecular weight increase is directly related to the polymer chain length. So when it increases, the polymer's bridging ability increases (Palapa et al., 2021).

This kind of intraparticle bridging mechanism helps a lot to form big flocs, so that the settling of particles will be more after adding the suitable coagulant. The other factors like double layer compression, sweep flocculation and charge neutralization may influence a little. However, this bio coagulant, capable of producing a gel, will follow the intraparticle bridging mechanism commonly known as the Egg box model (Ekanayake and Manage, 2022). The presence of carboxyl groups with double bonds increases the affinity of the dye particle towards the coagulant.

Table 1. Overall best performance conditions for congo red dye removal

Initial concentration (mg/L)	pH	Alginate dosage (mg/L)	Calcium dosage (mg/L)	Final concentration (mg/L)	% of dye removal
50	4	2	4	3.9	92.20
	5	2	5	4.1	91.80
	6	2	6	4.5	91.00
100	4	3	5	8.3	91.70
	5	3	4	9.2	90.80
	6	3	6	10.3	89.70
150	4	4	5	8.1	94.60
	5	4	5	8.1	94.60
	6	4	5	8.5	94.33
200	4	5	6	9.9	95.05
	5	5	5	11.4	94.30
	6	5	6	10.8	94.60
250	4	6	6	10	95.00
	5	6	6	12	94.00
	6	6	6	15	92.50

These results have demonstrated explicitly that calcium alginate can function as a coagulant for the removal of color from synthetic textile effluent. Alginate and calcium both failed to reach the desired concentration levels when used alone. Therefore, their combined effect is thought to be necessary. A positively charged substance, such as calcium, must be added to the system due to the alginic acid polysaccharides and the utilized particles negative surface charges. According to Davis et al. (2003), the monomeric units of mannuronic acids and guluronic acids have values of 3.38 and 3.65, respectively. Alginic acid must therefore approach and bind to the surface of calcium ions. As a result, the initial stage in the calcium alginate dye removal technique is surface charge neutralization. Therefore, adding calcium before alginate improved system function. According to Simpson et al. (2004), the action of alginate is the production of calcium alginate gel, or it's held to bridge the gap between the particles by one of two methods.

The main reason to choose combinations for study is because calcium alginate dosage could often attain low concentration values. Table 1 lists the lowest concentrations that were attained together with the corresponding concentrations of calcium and alginate. At different calcium and alginate doses for samples with beginning calcium concentrations of 250, 200, 150, 100, and 50 mg/L, low target values could be achieved. These studies collectively demonstrated that the calcium coagulates more effectively.

3.4 Coagulation kinetics

Kinetic study helps to determine the rate of dye molecules removal form aqueous solution. In this view first order and second order kinetic model has been studied for CR dye removal from textile effluent by alginate as natural coagulant. The following equations are used to verify the first order (Equation 2) and second order (Equation 3) kinetic, respectively.

$$\log\left(\frac{C_i}{C_o}\right) = -kt \tag{2}$$

$$\frac{1}{C_o} - \frac{1}{C_i} = k't \tag{3}$$

Where C_i is initial dye concentration, C_0 is the Concentration of dye after time (minutes), and k is first order and k' second order rate constant (min^{-1}).

From Figure 8(a) and (b) can be seen that the first order and second order kinetics to the experimental data, respectively. These kinetic data show that the intercept for first order does not obey the kinetic equation. Therefore, the coagulation process for removal of CR dye using alginate followed a second order model (Nnaji et al., 2014; Vijayaraghavan et al., 2018).

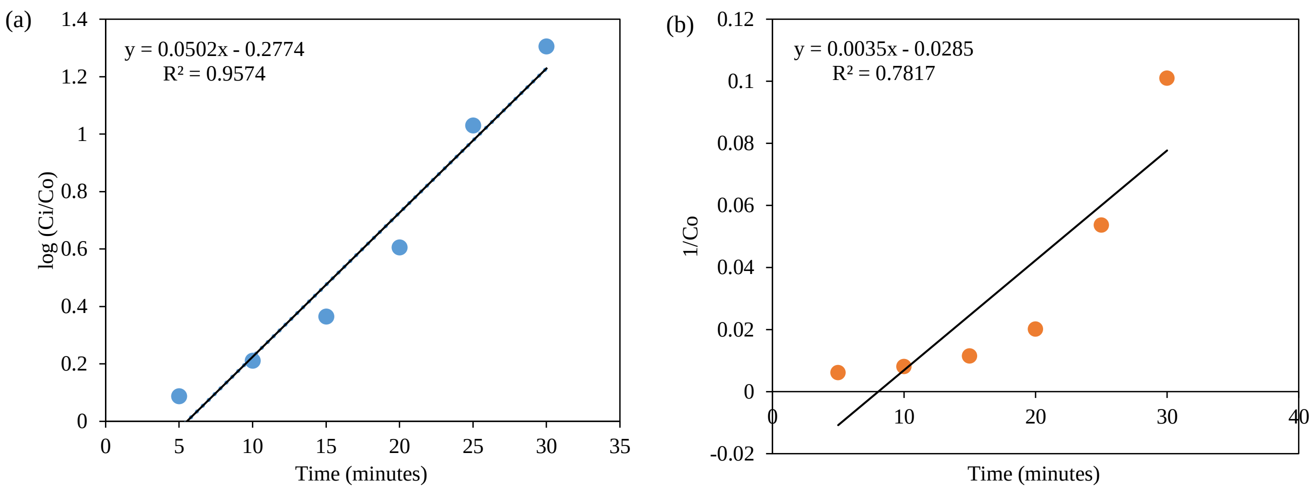

Figure 8. Kinetics study of CR dye (a) first order and (b) second order

4. CONCLUSION

The current study concluded that CR dye can be removed from aqueous solution using natural coagulant obtained from coastal water. The procured alginate worked effectively as coagulant and achieved maximum percentage removal by varying calcium and alginate doses in synthetic textile wastewater at varying concentrations (50-250 mg/L) and pH (4, 5, 6) levels. When compared to low pH at the same concentration of synthetic textile wastewater, hydroxyl group decomposition at high pH resulted in low coagulation process efficiency. In comparison with other decolorization processes, this technique attained results in a short time. The maximum removal percentage of 95.05% was achieved by the operating conditions of pH 4, calcium and alginate dosage of 6.0 g/L. The calcium alginate acted well as a coagulant and removed congo red dye from the aqueous solution effectively, which is present in textile wastewater. Our future study will recover or degrade the dye from sludge using solvent extraction. Once the dye is recovered or degraded, the treated contents can be used as a manure/fertilizer. But the limitations involved in the dye recovery process from the sludge should be large. In the present process, the quantity of sludge formed is very small amount, hence the dye recovery process can be feasible only if the process is scaled up to large quantity.

ACKNOWLEDGEMENTS

The authors would like to acknowledge their sincere thanks to Rajalakshmi Engineering College (Autonomous), Thandalam, Chennai, India for the lab support.

CONFLICT OF INTEREST

The authors hereby declare that they do not have any conflict of interest.

REFERENCES

Ajoke ARO, Mercy MA, Alhassan KE. Efficacy of chitosan as a coagulant aid to alum precipitation of congo red in wastewater. Academic Journal of Chemistry 2021;6(2):37-44.

Assimeddine M, Abdennouri M, Barka N, Elmoubarki R, Sadiq M. Natural phosphates characterization and evaluation of their removal efficiency of methylene blue and methyl orange from aqueous media. Environment and Natural Resources Journal 2022;20(1):29-41.

Chuah TG, Jumasiah A, Azni I, Katayon S, Choong SYT. Rice husk as a potentially low-cost biosorbent for heavy metal and dye removal: An overview. Desalination 2005;175(3):305-16.

Davis TA, Volesky B, Mucci A. A review of the biochemistry of heavy metal biosorption by brown algae. Water Research 2003;37(18):4311-30.

Devrimci HA, Yuksel AM, Sanin FD. Algal alginate: A potential coagulant for drinking water treatment. Desalination 2012;299:16-21.

Ekanayake MS, Manage P. Mycoremediation potential of synthetic textile dyes by *Aspergillus niger* via biosorption and enzymatic degradation. Environment and Natural Resources Journal 2022;20(3):234-45.

Fenoradosoa TA, Ali G, Delattre C, Laroche C, Petit E, Wadouachi A, et al. Extraction and characterization of an alginate from the brown seaweed *Sargassum turbinarioides* Grunow. Journal of Applied Phycology 2010;22(2):131-7.

Hoong HNJ, Ismail N. Removal of dye in wastewater by adsorption-coagulation combined system with *Hibiscus sabdariffa* as the coagulant. MATEC Web Conference 2018;152:Article No. 01008.

Huang C, Chen S, Pan JR. Optimal condition for modification of chitosan: A biopolymer for coagulation of colloidal particles. Water Research 2000;34(3):1057-62.

Ikeda A, Takemura A, Ono H. Preparation of low-molecular weight alginic acid by acid hydrolysis. Carbohydrate Polymers 2000;42(4):421-5.

Kawamura S. Effectiveness of natural polyelectrolytes in water treatment. Journal/American Water Works Association 1991;83(10):88-91.

Kharkwal H, Joshi D, Panthari P, Pant MK, Kharkwal AC. Algae as future drugs. Asian Journal of Pharmaceutical and Clinical Research 2012;5(2):99-106.

Kristianto H, Rahman H, Prasetyo S, Sugih AK. Removal of congo red aqueous solution using *Leucaena leucocephala* seed's extract as natural coagulant. Applied Water Science 2019;9(4):1-7.

Nnaji NJN, Ani JU, Aneke LE, Onukwuli OD, Okoro UC, Ume JI. Modelling the coag-flocculation kinetics of cashew nut testa tannins in an industrial effluent. Journal of Industrial and Engineering Chemistry 2014;20(4):1930-5.

Nozaic DJ, Freese SD, Thompson P. Longterm experience in the use of polymeric coagulants at Umgeni water. Water Science and Technology: Water Supply 2001;1(1):43-50.

Ozacar M, Sengil IA. Evaluation of tannin biopolymer as a coagulant aid for coagulation of colloidal particles. Colloids and Surfaces A: Physicochemical and Engineering Aspects 2003;229(1):85-96.

Pal S, Mal D, Singh RP. Cationic starch: An effective flocculating agent. Carbohydrate Polymers 2005;59(4):417-23.

Palapa NR, Normah N, Taher T, Mohadi R, Rachmat A, Lesbani A. Effectivity of indonesian rice husk as an adsorbent for removing congo red from aqueous solutions. Environment and Natural Resources Journal 2021;19(4):255-65.

Pham TV, Tran TV, Nguyen TD, Tham NTH, Quang PTT, Uyen DTT, et al. Development of response surface methodology for optimization of congo red adsorption utilizing exfoliated graphite as an efficient adsorbent. Materials Today: Proceedings 2019;22:2341-50.

Ponnusamy S, Subramaniam R. Process optimization studies of congo red dye adsorption onto cashew nut shell using response surface methodology. International Journal of Industrial Chemistry 2013;4(1):1-10.

Salehizadeh H, Shojaosadati SA. Extracellular biopolymeric flocculants: Recent trends and biotechnological importance. Biotechnology Advances 2001;19(5):371-85.

Simpson NE, Stabler CL, Simpson CP, Sambanis A, Constantinidis I. The role of the $CaCl_2$-guluronic acid interaction on alginate encapsulated βTC3 cells. Biomaterials 2004;25:2603-10.

Sivalingam S, Kella T, Maharana M, Sen S. Efficient sono-sorptive elimination of methylene blue by fly ash-derived nano-zeolite X: Process optimization, isotherm and kinetic studies. Journal of Cleaner Production 2019;208:1241-54.

Sivalingam S, Sen S. Efficient removal of textile dye using nanosized fly ash derived zeolite-x: Kinetics and process optimization study. Journal of Taiwan Institute of Chemical Engineering 2019;96:305-14.

Vijayaraghavan G, Shanthakumar S. Performance study on algal alginate as natural coagulant for the removal of congo red dye. Desalination and Water Treatment 2016;22:6384-92.

Vijayaraghavan G, Shanthakumar S. Effective removal of acid black 1 dye in textile effluent using alginate from brown algae as a coagulant. Iranian Journal of Chemistry and Chemical Engineering. 2018;37(4):145-51.

Yupin K, Neamhom T, Singhkant C, Sreesai S, Polprasert S. Color removal of pulp and paper mill wastewater using residual eucalyptus wood. Environment and Natural Resources Journal 2022;20(4):419-25.

Zhang J, Zhang F, Luo Y, Yang H. A preliminary study on cactus as coagulant in water treatment. Process Biochemisty 2006;41(3):730-3.

Optimization and Kinetic Study of Phosphorus Dissolution from Primary Settled-Nightsoil Sludge

Wanida Pimpeach[1,3], Withida Patthanaissaranukool[2,3], Chongchin Polprasert[1,3], Supawadee Polprasert[2,3], Suwisa Mahasandana[1,3], and Bunyarit Panyapinyopol[1,3*]

[1]Department of Sanitary Engineering, Faculty of Public Health, Mahidol University, Bangkok 10400, Thailand
[2]Department of Environmental Health Sciences, Faculty of Public Health, Mahidol University, Bangkok 10400, Thailand
[3]Center of Excellence on Environmental Health and Toxicology (EHT), OPS, MHESI, Bangkok 10400, Thailand

ARTICLE INFO

Received: 28 Sep 2022
Received in revised: 6 Dec 2022
Accepted: 8 Dec 2022
Published online: 31 Jan 2023
DOI: 10.32526/ennrj/21/202200213

Keywords:
Co-solution of metals/ Interactions mechanism/ Phosphorus recovery/ Septage sludge/ Sludge extraction/ Waste management

*** Corresponding author:**
E-mail: bunyarit.pan@mahidol.ac.th

ABSTRACT

In this study, chemical extraction using different acid concentrations, solids concentrations, and reaction time with subsequent interactions mechanism were carried out to evaluate the potential of phosphorus (P) recovery from primary settled-nightsoil sludge (PSNS). The response surface methodology (RSM) with Box-Behnken experimental design and one-way ANOVA analysis were also employed to establish optimal P leaching conditions. The extraction efficiency relied mainly on acid and solids concentration. The second-order polynomial model was successfully developed for extracting process designs. Approximately 93% of P could effectively be extracted from PSNS of 20,000 mg/L with 0.5 M of H_2SO_4 at reaction time of 45 min (optimum condition). Kinetic studies showed that the pseudo-second order was fit to describe leaching of P and metals. Moreover, the rate of kinetic constants (k_2) of the P, Fe, Mg, and Ca under optimum condition were found to be 0.1607, 0.1099, 0.0317, and 0.0053 g/mg·min, respectively. The 99% leaching of maximum extracted P concentration at the equilibrium (9.6673 mg/g) took place in less than one hour. The findings of a suitable simple and low-cost method P dissolution from PSNS not only provides understanding of leaching kinetics, but also helps to pave a way of recovering P from a renewable resource in the field of waste utilization.

1. INTRODUCTION

The importance of global phosphate rock (PR) reserves shortage in the next 50 to 100 years has been reported (Van Vuuren et al., 2010; Cordell et al., 2009). Global food security has been threatened with phosphorus (P) scarcity problems in countries with limited PR deposits, especially Thailand (Cordell et al., 2011; Thitanuwat et al., 2016). It becomes necessary to develop a sustainable method to recover P from the other sources. Several waste materials have been identified as potentially useful sources of P (Shiba and Ntuli, 2017; Li et al., 2022a; Ramaswamy et al., 2022), but research on P recovery from human excreta remains fairly limited. The studies of Liu et al. (2008) and Cordell et al. (2009) estimated the annual global quantity of reused P totals 0.3 to 1.5 million metric tons of P generated from human excreta and greywater. In view of the characteristics of Human Fecal Sludge (HFS) such as their high levels of key plant nutrients, mainly nitrogen (N), phosphorus (P), and potassium (K), it provides a potential source for recovery (Jonsson et al., 2005; Vinnerås et al., 2006; Wignarajah et al., 2006; Calloway and Margen, 1971).

Separate collection of septage sludge is implemented only in a few countries, especially in Thailand. The Bangkok Metropolitan Administration (BMA)'s central nightsoil treatment plants can generate 5,324.8 tons of primary settled nightsoil sludge (PSNS) annually that contains considerable amounts of phosphorus (9.6 g P/kg, total solids) (Thitanuwat et al., 2016). The generated PSNS is commonly composted with green garbage to produce organic fertilizer used in public parks and roadsides. However, such use can often cause environmental

Citation: Pimpeach W, Patthanaissaranukool W, Polprasert C, Polprasert S, Mahasandana S, Panyapinyopol B. Optimization and kinetic study of phosphorus dissolution from primary settled-nightsoil sludge. Environ. Nat. Resour. J. 2023;21(2):102-112. (https://doi.org/10.32526/ennrj/21/202200213)

problems, especially the potential presence of pathogens particularly helminth eggs in fecal sludge, which is a major public health concern (WHO, 2006; Heinss et al., 1998). For this reason, the direct application of PSNS in the agricultural field is consequently limited. Therefore, it remains essential to intercept pathogens spread from PSNS before land application.

Numerous studies of P recovery using crystallization have been extensively reported with the objectives to recover P from leachate in the form of both magnesium ammonium phosphate (struvite) (Xu et al., 2012) and calcium phosphate (Ding et al., 2022). Struvite is best known as a slow-release fertilizer proven technically feasible and economically beneficial (Li et al., 2022b). However, pre-treatment is needed to release P from PSNS into solution thereby enhancing P availability for P recovery. The common method widely used to extract phosphorus from wastes is acid or acid-based leaching (Fang et al., 2020; Khaing et al., 2022). Moreover, influencing factors including pH, extraction time, liquid to solid ratio (L:S ratio), molar concentration of acid solution, and sludge concentration have also been investigated (Ali and Kim, 2016; Shiba and Ntuli, 2017). Acid concentration is a significant factor for enhancing P leaching process. The work of Shiba and Ntuli (2007) reported that the highest leaching efficiency of P from sewage sludge could be achieved at an extraction time for 2 h with 1 M of sulfuric acid and solid loading of 5%. In addition, nearly 100% of total P was released form incinerated sewage sludge ash when using 0.19 M H_2SO_4, extraction time of 2 h, and L:S ratio of 20 (Ottosen et al., 2013). Various types of acid and alkali have been extensively studied. P extraction efficiency using inorganic acids is higher than that of other extractants. Among these different inorganic acids, sulfuric acid has found high extraction efficiency (Shiba and Ntuli, 2017; Fang et al., 2018). However, after acid leaching, the inorganic constituents are not only P but also other metals such as Ca and Mg left in the leachates. Therefore, from the viewpoint of effective P recovery, chemical precipitation can be employed in line with extraction (Ali and Kim, 2016). Nevertheless, there are little information is available concerning P extraction from PSNS. Therefore, it is interesting to investigate effects of independent variables on leaching of PSNS.

A large number of studies have investigated individual and interaction effects of variables on extraction and adsorption/desorption efficiencies using response surface methodology (RSM) (Reuna and Väisänen, 2018; Rasoulzadeh et al., 2021a; Mohammadi et al., 2017). The obtained results from RSM can be used for optimizing process capability (Asgari et al., 2020; Rasoulzadeh et al., 2021b). In addition, RSM also provides reasonable regression equations which are used for process design (Luyckx et al., 2020). Some studies employed adsorption adsorption-desorption mechanism to determine reaction pathway and equilibrium (Rathi and Kumar, 2021; Rasoulzadeh et al., 2021c). Various studies have been performed using nonlinear adsorption kinetic models, especially, pseudo-second order (Rasoulzadeh et al., 2021c; Barca et al., 2019).

This work was to establish chemical P extraction technology for P recovery process together with utilization of primary settled-nightsoil sludge as a sustainable P-rich resource rather than to dispose it as a waste, in order to solve the shortage of natural P resources in the near future. Optimum conditions and factors affecting P extraction were evaluated using response surface methodology (RSM) and ANOVA. In addition, the second-order polynomial model was successfully developed for extracting process designs which could maximize P leaching efficiency with low energy consumption. The kinetics of P leaching were presented so as to determine the rate constants and maximum equilibrium capacities of extraction. Also, because leaching generates a metal laden solution, this works aimed to study the leaching of major elements such as Fe, Ca, and Mg. Successful results obtained from this study are expected to minimize waste by 3R (reduce, reuse, and recycling). Using PSNS as a renewable resource to produce phosphate containing fertilizers offers solutions to many problems and helps ensure future supplies of phosphates, while addressing waste management issues.

2. METHODOLOGY

2.1 Descriptions of PSNS

PSNS was collected from a dewatering process of the Nong Khaem nightsoil treatment plant under the Bangkok Metropolitan Administration (BMA). Samples were dried at 105ºC for three days and then homogenized in a bucket. The composite samples were placed in sealed bags at a laboratory. Subsequently, the dried PSNS was crushed by a pestle and mortar to obtain a fine powder. The powdered samples were sieved by passing through a 2 mm screen and the resulting sludge with particle sizes smaller than 2 mm were separated and stored in a polyethylene bottle at room temperature in the laboratory.

2.2 Experimental design for acid leaching and optimization

The extraction experiments were conducted at room temperature. PSNS was measured in 10,000, 20,000, 30,000, and 50,000 mg and then mixed with 1 L of acid solution ranging from 0.01 to 0.50 M H_2SO_4). Extraction time ranged from 0.25 to 2.00 h at ambient temperature. The leachates were then filtered through a 10 µm filter (Whatman no.93) and the pH recorded afterwards. The schematic of this research is presented in Figure 1. To determine interaction effects of three variables on P leaching efficiency, the response surface methodology (RSM) of design expert® 13 Software with Box-Behnken design (BBD-RSM) was selected to design P extraction experiments which were performed randomly under 15 conditions with three central points. The coded variables and their values are shown in Table 1. The following three influential parameters were investigated: extraction time (A), acid concentration (B), and solids concentration (C). To verify the relationship of independent parameters and their interactions on response (P extraction), the statistical analysis was established with 0.05 confidence level. Thus, the optimum condition for P extraction, the quadratic equation model was employed as represented by Equation (1).

$$y = \beta_0 + \beta_A A + \beta_B B + \beta_C C + \beta_{AA} A^2 + \beta_{BB} B^2 + \beta_{CC} C^2 + \beta_{AB} AB + \beta_{AC} AC + \beta_{BC} BC \quad (1)$$

Where; y is the predicted response (P extraction efficiency (%)); β_0 is constant coefficient; β_A, β_B and β_C are coefficients of linear expressions; β_{AA}, β_{BB}, and β_{CC} are quadratic coefficients; β_{AB}, β_{AC}, and β_{BC} are interaction coefficients; A, B, and C represent three independent variables viz. extraction time (A), acid concentration (B), and solids concentration (C).

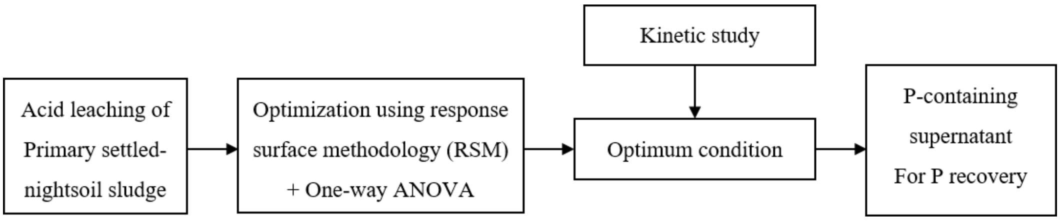

Figure 1. Schematic diagram for optimization and kinetic study of P extraction from primary settled-nightsoil sludge

Table 1. The 3-levels Box-Behnken design with coded and actual variables for optimization of P leaching from primary settled-nightsoil sludge

Variables	Units	Coded levels		
		-1	0	1
Extraction time	h	0.25	1.00	2.00
Acid concentration	M	0.01	0.10	0.50
Solids concentration	mg/L	10,000	30,000	50,000

2.3 Analytical methods

A spectrophotometer (Evolution 201 UV-Visible) using the vanadomolybdophosphoric acid colorimetric method was employed to determine P concentration in both solid and aqueous phases. The total solids (TS), total volatile solids (VS), and total kjeldahl nitrogen (TKN) were analyzed using the procedure described in the Standard Methods (APHA, 2012). Metal analyses were performed by means of atomic absorption spectrometry (AAS) according to standard methods (APHA, 2012). The pH was measured using a pH meter (YSI 1200).

2.4 Statistical analysis

All experimental conditions were described as observed mean and standard error (±SE), and statistical analysis was established as significant at $p<0.05$. Statistical analyses were performed using SPSS Statistics, Version 18.0. Standard deviation, mean averages and standard error were used in this study. One-way ANOVA (analysis of variance) was used to test the data for significant differences in the effect of variance of acid concentration, solids concentration, and extraction times on P extraction.

All batch experiments were repeated in triplicate and the mean value was accepted as the final value.

2.5 Calculations

Extraction efficiency of P was defined as the percentage of P released from PSNS (solid phrase) in relation to the initial P in solution, calculated as Equation (2):

$$\text{P extraction (\%)} = \frac{([PO_4^{3-} - P]_{released} * (L{:}S)\ ratio)}{M_{input}} \times 100 \qquad (2)$$

Where; $[PO_4^{3-} - P]_{released}$ is the concentration of P in solution obtained at each reaction time (mg/L), L:S ratio is the liquid (sulfuric acid solution (L)) to solid amount of PSNS (g) ratios, and M_{input} is mass of P in the primary settled-nightsoil sludge at the beginning.

3. RESULTS AND DISCUSSION

3.1 Characteristic of PSNS

The characteristics of PSNS are presented in Table 2, demonstrating that the main components of PSNS were P, N, Ca, Mg, and Fe. The total P was found to be 1.0 wt.% which appeared to be an alternative resource for P recovery. The Ca concentration was much higher than Mg and Fe. The Ca concentration related to the ranges of generation rates in feces 0.1-3.6 (g Ca/cap/day) (wet basis) (Wignarajah et al., 2006). Similarly, Mg concentration was very low, having a range in feces of 0.15-0.35 (g Mg/cap/day) (wet basis) (Eastwood et al., 1984; Calloway and Margen, 1971). PSNS contains relatively lower concentrations of Fe than incinerated sewage sludge ash (ISSA) (Kleemann et al., 2017).

Table 2. Characteristics of primary settled-nightsoil sludge

Parameters	Unit	Primary settled-nightsoil sludge
C/N ratio	-	10-17
pH	-	6.13
Moisture	%	74.50±2.36
Volatile solid	%	69.10±2.80
Total phosphorus	mg/kg	10,260±420
Total kjeldahl nitrogen	mg/kg	36,750±90
Calcium: Ca	mg/kg	33,357±1,727
Magnesium: Mg	mg/kg	2,018±60
Iron: Fe	mg/kg	8,408±333
Parasites eggs	eggs/g	<1 (12.5% detected probability) (Trichuris trichiura) <1 (12.5% detected probability) (Hook worm Egg) >30 (12.5% detected probability) (Nematode larva) >30 (12.5% detected probability) (Teania spp.eggs) >20 (12.5% detected probability) (Ascaris spp.eggs)

3.2 Second-order model and ANOVA analysis

Based on the results obtained from comparison of different models, the experimental data were fitted to a second-order polynomial model and regression coefficients obtained (Table 3). The goodness-of-fit of the model can be checked from the coefficient of determination (R^2) which was high, 99.94%, implying good correlation between the predicted values and the observed data. The adjusted R^2-value of 99.83% indicated that all factors included in the model were significant and affecting the response variable. The high predicted R^2-value of 99.32% proved that this model could predict proper responses for new observations. High values of both adjusted and predicted R^2 also meant that the model fit to the data.

Table 3. Comparing models on summary statistics

Source	Sequential p-value	Lack of fit p-value	R^2	Adjusted R^2	Predicted R^2
Linear	0.1558	0.0016	0.3663	0.1935	-0.1384
2FI	0.9995	0.0011	0.3674	-0.1070	-1.4282
Quadratic	<0.0001	0.5057	0.9994	0.9983	0.9932

The ANOVA analysis results for the quadratic models of primary settled- nightsoil sludge (PSNS) leaching were provided in Table 4; the F-value of 921.09 implied that the model was accurate. The corresponding p-value was less than 0.0001 which could identify the significance of terms. Thus, the model was proven significant and could be used to optimize leaching. Figure 2 displays the external student residuals and normal% probability plot. The plots illustrated that no abnormality occurred in this experimentation and model. Moreover, it could be observed that the actual values obtained from the experiment were close to the predicted values calculated by the quadratic models, indicating that the equation was reliable (Table 5).

The quadratic equations for the leaching of PSNS in terms of coded factors and actual factors were obtained as shown in Equation (3) and Equation (4).

$$y = 135.48 + 1.48A + 32.18B - 4.00C - 2.64A^2 - 78.71B^2 + 3.50C^2 + 0.5819(A \times B) + 0.7107(A \times C) + 0.7107(A \times C) + 1.46(B \times C) \quad (3)$$

$$Y = 28.75432 + 7.54273A + 788.09344B \; 0.000847C - 3.44762A^2 - 1311.30244B^2 + 8.75324 \times 10^{-9}C^2 + 2.71458(A \times B) + 0.000041(A \times C) + 0.000299(B \times C) \quad (4)$$

Where; y is the predicted response (P extraction efficiency (%)); A, B, and C represent three independent variables: extraction time (A), acid concentration (B) and solids concentration (C).

Table 4. ANOVA table for quadratic model of primary settled nightsoil sludge leaching at ambient temperature (response: % P extraction)

Source	Sum of squares	df	Mean square	F-value	p-value	
Model	11,235.46	9	1,248.38	921.09	<0.0001	Significant
A-extraction time	15.12	1	15.12	11.16	0.0206	
B-acid concentration	8,214.68	1	8,214.68	6,060.99	<0.0001	
C-solids concentration	108.36	1	108.36	79.95	0.0003	
AB	1.64	1	1.64	1.21	0.3215	
AC	2.04	1	2.04	1.50	0.2748	
BC	10.26	1	10.26	7.57	0.0402	
A^2	24.46	1	24.46	18.04	0.0081	
B^2	6,945.27	1	6,945.27	5,124.38	<0.0001	
C^2	45.19	1	45.19	33.35	0.0022	
Residual	6.78	5	1.36			
Lack of fit	4.24	3	1.41	1.11	0.5057	Not significant
Pure error	2.54	2	1.27			
Cor total	11,242.24	14				

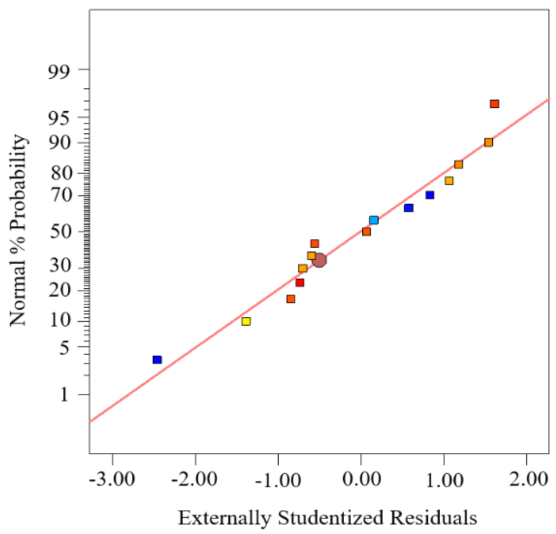

Figure 2. Studentized residuals and normal% probability plot

Table 5. Experimental design matrix of BBD-RSM in actual factors with experimental and predicted values

Run order	Standard order	Actual levels of variables			Experiment value	Predicted value
		Extraction time (h)	Acid concentration (M)	Solids concentration (mg/L)		
1	14	1.00	0.10	30,000	84.7	83.4
2	10	1.00	0.50	10,000	94.4	94.7
3	13	1.00	0.10	30,000	82.7	83.4
4	11	1.00	0.01	50,000	22.8	22.3
5	15	1.00	0.10	30,000	82.8	83.4
6	8	2.00	0.10	50,000	81.9	81.4
7	2	2.00	0.01	30,000	21.6	22.9
8	6	2.00	0.10	10,000	90.5	89.8
9	4	2.00	0.50	30,000	88.4	88.4
10	9	1.00	0.01	10,000	33.6	33.5
11	5	0.25	0.10	10,000	88.5	89.0
12	12	1.00	0.50	50,000	89.2	89.5
13	7	0.25	0.10	50,000	77.0	77.7
14	3	0.25	0.50	30,000	84.8	84.2
15	1	0.25	0.01	30,000	21.7	21.0

3.3 Effect of three variables on P extraction efficiency

Figure 3 (a-c) illustrates interactive effect of acid concentration, solids concentration, and reaction times on P extraction efficiency. The results showed that most P was still extracted when acid concentrations were above 0.15 M. An increase in solid loading caused a small decrease in the percentage of P extracted. In addition, the extended contact time did not result in more P leaching. The plot also showed at higher solids concentrations (above 30,000 mg/L) and lower acid concentrations, P leaching decreased as shown in green (50% P extraction line). Thus, solids concentration must be in the range 10,000 to 30,000 mg/L to maximize leaching efficiency. Shiba and Ntuli (2017) studied P extraction of sewage sludge and claimed that the amount of P extracted increased with rise of solids loading up to 50 g/L which totaled about 82% of P extracted. However, solids concentrations between 50 to 100 g/L exhibited low P extraction efficiency (Nosrati et al., 2013). In this work, decreasing P extraction efficiency started to reduce after solids concentrations were above 30,000 mg/L. This may be due to the presence of high total volatile suspended solids (about 69.1%) in the PSNS which easily releases P. Therefore, it could be claimed with confidence that solids concentration is one factor affecting P extraction efficiency.

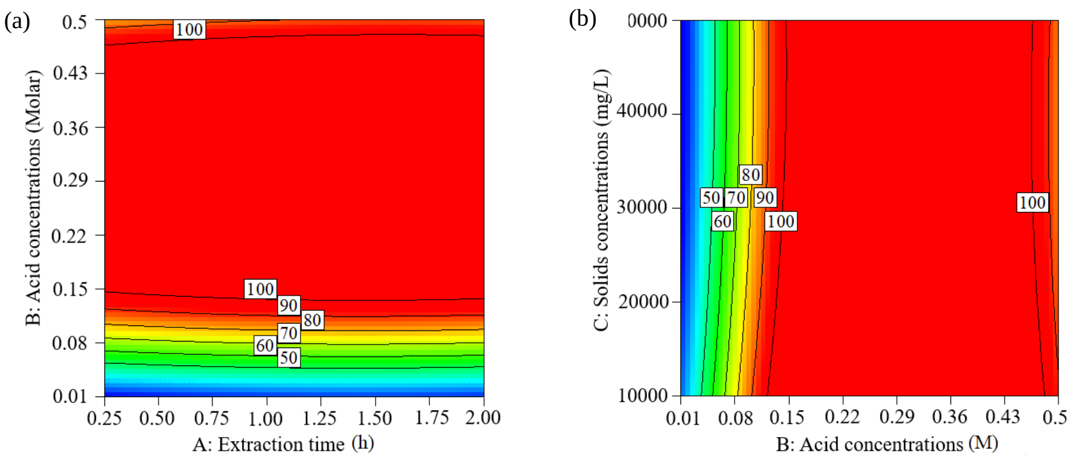

Figure 3. P extraction (%) at ambient temperature with respect to: (a) contour plots of extraction time (h) and acid concentration (M) with solids concentration at 50,000 mg/L, (b) contour plots of acid concentration (M) and solids concentration (mg/L) with extraction time at 0.25 h, and (c) contour plots of extraction time (h) and solids concentration (mg/L) with acid concentration of 0.1 M

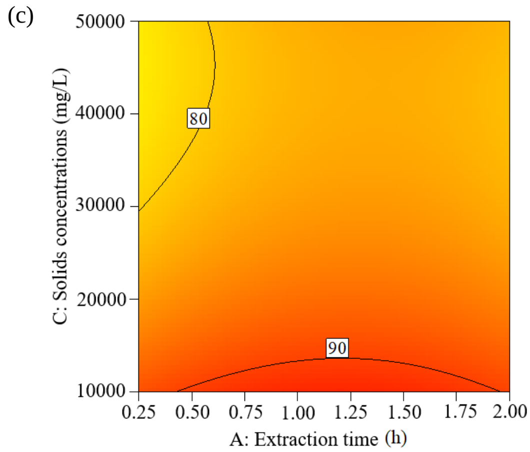

Figure 3. P extraction (%) at ambient temperature with respect to: (a) contour plots of extraction time (h) and acid concentration (M) with solids concentration at 50,000 mg/L, (b) contour plots of acid concentration (M) and solids concentration (mg/L) with extraction time at 0.25 h, and (c) contour plots of extraction time (h) and solids concentration (mg/L) with acid concentration of 0.1 M (cont.)

3.4 Optimization of P extraction

Based on the above results, high P extraction efficiency (>85%) was obtained at acid concentrations range from 0.1 and 0.5 M, and with solids concentrations of 10,000 to 30,000 M. In addition, higher extraction times did not achieve greater P extraction, this was discussed in section 3.5. However, from an economic point of view, using high solids concentration with low acid concentration is more interesting due to the lower extraction liquid costs for optimal P extraction. Figure 4 shows comparative results of P extraction under various acid:solids loading ratios (g:g), revealing only the results of leaching that have high P extraction efficiency (>80%). A single factor analysis of variance test indicated that the difference in mean of % P extraction between an acid:solids loading ratio of 5.2:1 and 2.6:1 was not statistically significant (p-value=1.000). Conversely, comparing the mean %P extraction at 2.6:1 and 1.7:1 of leaching, comparing between using solids concentrations of 20,000 mg/L and 30,000 mg/L at an acid concentration of 0.5 M, respectively, showed a significant difference in mean values (p-value <0.0001). Therefore, the acid:solids loading ratio of 2.6:1 with 0.5 M H_2SO_4 and solids concentration of 20,000 mg/L (L:S ratio=50) was chosen for optimum leaching condition.

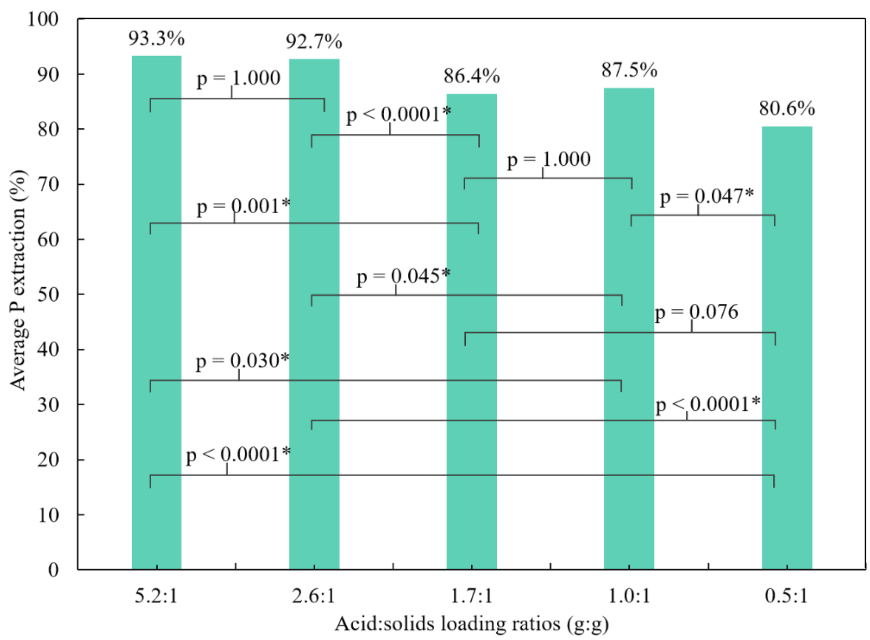

Figure 4. Comparative results of P extraction under various acid:solids loading ratios (*The mean difference was significant at the 0.05 level).

This optimum condition is also comparable to what other studies obtained from different leaching methods of P from wastes. Compared with organic acid, inorganic acid approaches, especially H_2SO_4, have been more widely investigated to extract P from wastes because of high leaching efficiency, up to 82-100% (Table 6) (Khaing et al., 2022; Shiba and Ntuli, 2017; Wang et al., 2018; Fang et al., 2018). Similarly, due to the double concentration of H^+ ions, sulfuric acid can release more P than nitric acid at the same concentration (Fang et al., 2018). Other researchers also reported that more than 95% P extraction efficiency was achieved after 120 min, while the leaching efficiency rapidly increased up to 15 min, and then slowly increased afterwards. Thus, many studies suggested that within 2 h was the optimum duration for leaching P from ISSA (Wang et al., 2018; Fang et al., 2018). Related research has also investigated the influencing factors for P extraction from sludge. As discussed above, an L:S ratio of 50 was considered the optimum condition for this study. However, an L:S ratio of 20 with 0.1 to 1 M of H_2SO_4 was sufficient for leaching P from sewage sludge and ISSA (Shiba and Ntuli, 2017; Wang et al., 2018; Fang et al., 2018).

Table 6. Comparison of P extraction efficiency from different conditions of leaching and sludge types

Type of wastes	Type of acid	Molar of acid (mol/L)	L:S ratio ($mL_{(acid)}$ /$g_{(sludge)}$)	Quantity of acid ($g_{(acid)}$/$g_{(dried\ sludge)}$)	Extraction time (h)	Temperature (°C)	% P extraction	Reference
Primary settled nightsoil sludge	H_2SO_4	0.50	50	2.50	0.75	Room temperature	93.6	This study
Waste activated sludge	H_2SO_4	0.10	35	0.30	0.50	Room temperature	97.0	Khaing et al. (2022)
Incinerated sewage sludge ash	H_2SO_4	0.05	150	0.70	2.00	Room temperature	>95.0	Liang et al. (2019)
Sewage sludge	H_2SO_4	1.00	20	2.00	2.00	100	82.0	Shiba and Ntuli (2017)
WAO residual	Citric acid	1.00	10	1.90	24.00	Room temperature	61.0	Barca et al. (2019)
WAO residual	HCl	1.00	10	0.40	24.00	Room temperature	65.0	
Incinerated sewage sludge ash	H_2SO_4	0.10	20	0.20	2.00	Room temperature	88.3	Wang et al. (2018)
Incinerated sewage sludge ash	H_2SO_4	0.20	20	0.40	2.00	Room temperature	94.0	Fang et al. (2018)

Remark :WAO residual=Solid residues obtained from wet air oxidation of sewage sludge

3.5 Extraction kinetics

The study of leaching kinetics involves understanding the mechanism of interactions between solid matrix and solvent in leaching. Various models exist to describe the kinetics of adsorption or desorption. The ones that have been used most commonly in previous studies are nonlinear adsorption kinetic models such as pseudo-first order, pseudo-second order, and intraparticle diffusion (Barca et al., 2019; Rasoulzadeh et al., 2021b; Rathi and Kumar, 2021). In this study, the rate of adsorption/desorption of the optimum condition follows the pseudo-second order kinetics equation:

$$(\frac{t}{q_t} = \frac{1}{k_2 q_e^2} + \frac{1}{q_e} \times t)$$

Where: q_t denotes extraction capacity at time t (mg/g); q_e denotes extraction capacity at equilibrium (mg/g); and k_2=the constant rate of the pseudo second order (g/(mg·min)).

Figure 5, shows the high determination coefficient for P, Fe, Mg, and Ca extraction of 0.9999, 0.9999, 0.9897, and 0.9944, respectively, indicating that the extraction of these four elements was probably controlled by chemical desorption rather than diffusion (Ho and McKay, 1998; Rasoulzadeh et al., 2021b). This also proved that at the beginning of extraction, the leaching rate is fast and much lower until equilibrium is reached (Dutta et al., 2016). The experimental results also showed that after 45 min extracted P was around 99% of maximum extracted P concentration at the equilibrium (9.6673 mg/g) obtained from the model which could be chosen as the optimum time to extract P from primary settled-nightsoil sludge (Table 7). Referring to Figure 5, the kinetic constants (k_2) of the leaching under optimum condition had the order of P (k_2=0.1607 g/mg·min) > Fe (k_2=0.1099 g/mg·min) > Mg (k_2=0.0317 g/mg·min) > Ca (k_2= 0.0053 g/mg·min), meaning that P was extracted faster than other elements in the same contact time.

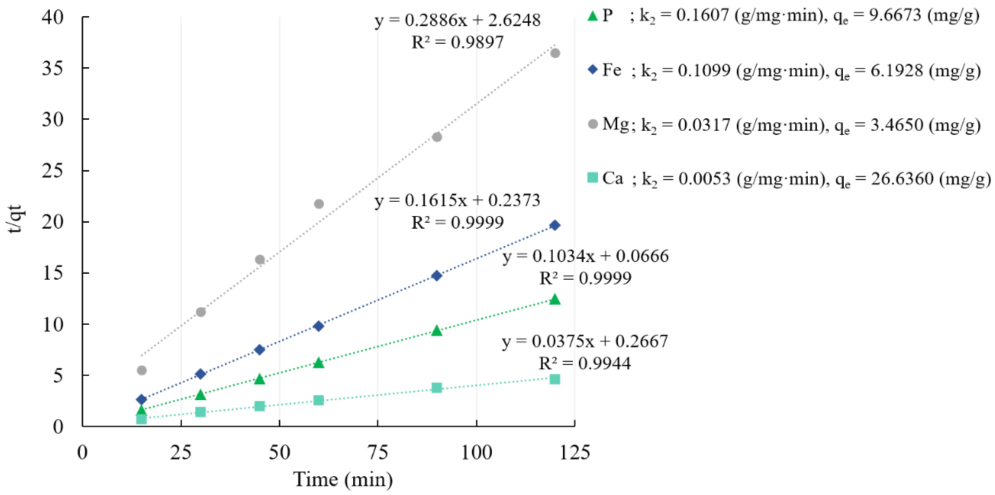

Figure 5. Pseudo-second-order kinetic modeling results of the P, Fe, Mg, and Ca extraction from primary settled-nightsoil sludge using solids concentration of 20,000 mg/L and 0.5 M H_2SO_4. (k_2=the constant rate of the pseudo second order, q_e=extracted concentration at the equilibrium)

Table 7. The acid leaching results using for pseudo-second order kinetic

Time (min)	% P extraction	% Fe extraction	% Mg extraction	% Ca extraction	P		Fe		Mg		Ca	
					q_t (mg/g)	t/q_t	q_t (mg/g)	t/q_t	q_t (mg/g)	t/q_t	q_t (mg/g)	t/q_t
15	90.67	86.90	81.60	64.00	9.3026	1.612	5.657	2.652	2.719	5.516	20.421	0.735
30	91.95	89.50	80.10	67.60	9.4340	3.180	5.825	5.150	2.670	11.236	21.567	1.391
45	93.23	92.00	82.70	70.40	9.5653	4.704	5.988	7.515	2.755	16.334	22.458	2.004
60	93.23	93.70	82.70	73.90	9.5653	6.273	6.102	9.833	2.755	21.777	23.567	2.546
90	93.23	93.70	95.50	74.00	9.5653	9.409	6.102	14.750	3.181	28.292	23.608	3.812
120	93.87	93.80	98.70	81.30	9.6310	12.460	6.105	19.656	3.289	36.489	25.929	4.628

4. CONCLUSION

In order to establish a simple, low-cost method for extracting P from PSNS, acid leaching with three independent variables (extraction time, acid concentration, and solids concentration) was investigated. A 3-levels Box-Behnken experimental design based on response surface methodology (RSM) and one-way ANOVA was applied to determine influence of experiments variables subsequent with optimal P extraction condition. The results were fitted into a second-order polynomial equation. The analysis of variance results obtained from RSM showed that three factors (extraction time, concentration of acid, and solids concentration) are statistically significant ($p<0.05$). Thus, it was observed that efficiency of P extraction increased with rise of acid concentration (over 0.15) and extraction time and dropped on increasing solids concentration. The optimal condition for the acid concentration, solids concentration, and reaction time of 0.5 M H_2SO_4, 20,000 mg/L, and 45 min, respectively, could be determined. Under this condition, the low-energy consumption with maximum P extraction efficiency of 92.7% was achieved. Kinetic study of optimum condition was performed. The mechanism of extraction is best described by pseudo-second order, which confirms the leaching of P, Ca, Fe, and Mg controlled by a chemical desorption. The results of kinetic constants (k_2) indicated that extraction of P was rapidly completed compared to extraction of other elements. Therefore, it is concluded that PSNS could be potentially used as an alternative recourse of P recovery.

ACKNOWLEDGEMENTS

The authors gratefully acknowledge Thailand research Fund (TRF), the National Research Councill of Thailand (NRCT), and the Thailand Science Research and Innovation (TSRI) for the financial support through the Royal Golden Jubilee Ph.D. Scholarship Program (Grant numbers: PHD/0190/2559). This work is also part of a 2019 research project, "Techno-economic assessment of phosphorus recycling from septage sludge in Bangkok Metropolis" supported by Biodiversity-based Economy Development Office (Public Organization) (BEDO) and Mahidol University Thailand (Grant numbers: 38/2562). This work is supported for publication by the China Medical Board (CMB), Faculty of Public Health, Mahidol University, Bangkok, Thailand. This research work is supported in part by the grant from Center of Excellence on Environmental Health and Toxicology (EHT), OPS, Ministry of Higher Education,

Science, Research and Innovation. The authors would like to acknowledge Assoc. Prof. Dr. Chongchin Polprasert for his initiative and guidance in experimental procedure and analyzing the P extraction from PSNS.

REFERENCES

Ali UT, Kim DJ. Phosphorus extraction and sludge dissolution by acid and alkali treatments of polyaluminum chloride (PAC) treated wastewater sludge. Bioresource Technology 2016; 217:233-8.

American Public Health Association (APHA). Standard Methods for the Examination of Water and Waste Water: 22nd ed. Washington DC, USA: APHA; 2012.

Asgari E, Mohammadi F, Nourmoradi H, Sheikhmohammadi A, Rostamifasih Z, Hashemzadeh B, et al. Heterogeneous catalytic degradation of nonylphenol using persulphate activated by natural pyrite: Response surface methodology modelling and optimization. International Journal of Environmental Analytical Chemistry 2020;102(17):1-20.

Barca C, Martino M, Hennebert P, Nicolas R. Kinetics and capacity of phosphorus extraction from solid residues obtained from wet air oxidation of sewage sludge. Waste Management 2019;89:275-83.

Calloway DH, Margen S. Variation in endogenous nitrogen excretion and dietary nitrogen utilization as determinants of human protein requirement. Journal of Nutrition 1971;101(2):205-16.

Cordell D, Drangert JO, White S. The Story of phosphorus: Global food security and food for thought. Global Environmental Change 2009;19:292-305.

Cordell D, Rosemarin A, Schröder J, Smit A. Towards global phosphorus security: A systems framework for phosphorus recovery and reuse options. Chemosphere 2011;84:747-58.

Ding Y, Dai X, Wu B, Liu Z, Dai L. Targeted clean extraction of phosphorus from waste activated sludge: From a new perspective of phosphorus occurrence states to an innovative approach through acidic cation exchange resin. Water Research 2022;215:Article No. 118190.

Dutta R, Sarkar U, Mukherjee A. Pseudo-kinetics of batch extraction of *Crotalaria juncea* (Sunn hemp) seed oil using 2-propanol. Industrial Crops and Products 2016;87:9-13.

Eastwood MA, Brydon WG, Baird J, Elton R, Helliwell S, Smith J, et al. Fecal weight and composition, serum lipids, and diet among subjects aged 18 to 80 years not seeking health care. The American Journal of Clinical Nutrition 1984;40(3): 628-34.

Fang L, Li JS, Guo MZ, Cheeseman CR, Tsang CWD, Donatello S, et al. Phosphorus recovery and leaching of trace elements from incinerated sewage sludge ash (ISSA). Chemosphere 2018;193:278-87.

Fang L, Wang Q, Li J-S, Poon CS, Cheeseman CR, Donatello S, et al. Feasibility of wet-extraction of phosphorus from incinerated sewage sludge ash (ISSA) for phosphate fertilizer production: A critical review. Critical Reviews in Environmental Science and Technology 2020;51(9):939-71

Heinss U, Larmie SA, Strass M. Solids Separation and Pond Systems for the Treatment of Faecal Sludge in the Tropics. Lessons Learnt and Recommendations for Preliminary Design, SANDEC Report No 5/98. Dubendorf, Switzerland: EAWAG/SANDEC Publications; 1998.

Ho YS, McKay G. A comparison of chemisorption kinetic models applied to pollutant removal on various sorbents. Process Safety and Environmental Protection 1998;76:332-40.

Jonsson H, Baky A, Jeppsson U, Hellström D, Kärrman E. Composition of Urine, Faeces, Greywater and Biowaste for Utilisation in the URWARE Model. Urban Water Report: Volume 6. Gothenburg, Sweden: Urban Water, Chalmers University of Technology; 2005.

Khaing KT, Polprasert C, Mahasandana S, Pimpeach W, Patthanaissaranukool W, Polprasert S. Phosphorus recovery and bioavailability from chemical extraction of municipal wastewater treatment's waste activated sludge: A case of Bangkok Metropolis, Thailand. Environment and Natural Resources Journal 2022;20(4):369-78.

Kleemann R, Chenoweth J, Clift R, Morse S, Pearce P, Saroj D. Comparison of phosphorus recovery from incinerated sewage sludge ash (ISSA) and pyrolysed sewage sludge char (PSSC). Waste Management 2017;60:201-10.

Li X, Shen S, Xu Y, Hongliang D, Lu X. Transformation and fate of non-reactive phosphorus (NRP) in enhanced biological phosphorus removal process with sidestream phosphorus recovery. Science of the Total Environment 2022a;839: Article No. 156275.

Li X, Zhao X, Zhang J, Hao J, Zhang Q. Struvite crystallization by using active serpentine: An innovative application for the economical and efficient recovery of phosphorus from black water. Water Research 2022b;221:Article No. 118678.

Liang S, Chen H, Zeng X, Li Z, Yu W, Xiao K, et al. A comparison between sulfuric acid and oxalic acid leaching with subsequent purification and precipitation for phosphorus recovery from sewage sludge incineration ash. Water Research 2019;159:242-51.

Liu Y, Villalba G, Ayres RU, Schroder H. Global phosphorus flows and environmental impacts from a consumption perspective. Journal of Industrial Ecology 2008;12:229-47.

Luyckx L, Geerts S, Caneghem JV. Closing the phosphorus cycle: Multi-criteria techno-economic optimization of phosphorus extraction from wastewater treatment sludge ash. Science of the Total Environment 2020;713:Article No. 135543.

Mohammadi A, Nemati S, Mosaferi M, Abdollahnejhad A, Almasian M, Sheikhmohammadi A. Predicting the capability of carboxymethyl cellulose-stabilized iron nanoparticles for the remediation of arsenite from water using the response surface methodology (RSM) model: Modeling and optimization. Journal of Contaminant Hydrology 2017; 203:85-92.

Nosrati A, MacCarthy J, Addai-Mensah J. Acid leaching and rheological behaviour of siliceous goethite Ni laterite ore: Effect of solid loading and temperature. Proceedings of Chemeca 2013 Challenging Tomorrow; 2013 Jan 1; Australia; 2013.

Ottosen ML, Kirkelund MG, Jensen EP. Extracting phosphorous from incinerated sewage sludge ash rich in iron or aluminum. Chemosphere 2013;91:963-9.

Ramaswamy J, Solaiappan V, Albasher G, Alamri O, Alsultan N, Sathiasivan K. Process optimization of struvite recovered from slaughterhouse wastewater and its fertilizing efficacy in amendment of biofertilizer. Environmental Research 2022;211:Article No. 113011.

Rasoulzadeh H, Sheikhmohammadi A, Abtahi M, Alipour M, Roshan B. Predicting the capability of diatomite magnano composite boosted with polymer extracted from brown seaweeds for the adsorption of cyanide from water solutions using the response surface methodology: Modelling and optimization. International Journal of Environmental Analytical Chemistry 2021a;101:1-14.

Rasoulzadeh H, Sheikhmohammadi A, Abtahi M, Roshan B, Jokar R. Eco-friendly rapid removal of palladium from aqueous solutions using alginate-diatomite magnano composite. Journal of Environmental Chemical Engineering 2021b;9:Article No. 105954.

Rasoulzadeh H, Sheikhmohammadi A, Asgari E, Hashemzadeh B. The adsorption behaviour of triclosan onto magnetic bio polymer beads impregnated with diatomite. International Journal of Environmental Analytical Chemistry 2021c; 101:1-13.

Rathi BS, Kumar PS. Application of adsorption process for effective removal of emerging contaminants from water and wastewater. Environmental Pollution 2021;280:Article No. 116995.

Reuna S, Väisänen A. Optimizing the H_3PO_4 leaching conditions of post-precipitated sewage sludge using response surface methodology. Journal of Environmental Management 2018; 226:70-5.

Shiba CN, Ntuli F. Extraction and precipitation of phosphorus from sewage sludge. Waste Management 2017;60:191-200.

Thitanuwat B, Polprasert C, Englande Jr AJ. Quantification of phosphorus flows throughout the consumption system of Bangkok Metropolis, Thailand. Science of the Total Environment 2016;542(Pt B):1106-16.

Van Vuuren DP, Bouwman AF, Beusen AHW. Phosphorus demand for the 1970-2100 period: A scenario analysis of resource depletion. Global Environmental Change 2010; 20(3):428-39.

Vinnerås B, Palmquist H, Balmér P, Weglin J, Jensen A, Andersson Å, et al. The characteristics of household wastewater and biodegradable waste-a proposal for new Swedish norms. Urban Water Journal 2006;3:3-11.

Wang Q, Li JS, Tang P, Fang L, Poon SC. Sustainable reclamation of phosphorus from incinerated sewage sludge ash as value-added struvite by chemical extraction, purification and crystallization. Journal of Cleaner Production 2018;181:717-25.

Wignarajah K, Litwiller E, Fisher J, Hogan J. Simulated human faeces for testing human waste processing technologies in spaces systems. SAE Technical Paper Series, 2006-012180. Proceedings of the 36th International Conference on Environmental Systems (ICES); 2006 Jul 17-20; Norfolk, Virgini: USA; 2006.

World Health Organization (WHO). Guidelines for the safe use of wastewater, excreta and greywater. In: Excreta and Greywater Use in Agriculture: Volume 4. Geneva, Switzerland; WHO Publications; 2006.

Xu H, He P, Gu W, Wang G, Shao L. Recovery of phosphorus as struvite from sewage sludge ash. Journal of Environmental Sciences 2012;24:1533-8.

Environment and Natural Resources Journal 2023; 21(2): 113-126

Farmer's Perception and Factors Influencing Adoption of Adaptation Measures to Cope with Climate Change: An Evidence from Coastal Bangladesh

Hassan Md. Naveed Anzum[1], Tapos Kumar Chakraborty[2*], and Himel Bosu[2]

[1]*Department of Climate and Disaster Management, Faculty of Applied Science and Technology, Jashore University of Science and Technology, Jashore-7408, Bangladesh*

[2]*Department of Environmental Science and Technology, Faculty of Applied Science and Technology, Jashore University of Science and Technology, Jashore-7408, Bangladesh*

ARTICLE INFO

Received: 28 Apr 2022
Received in revised: 22 Sep 2022
Accepted: 26 Sep 2022
Published online: 27 Jan 2023
DOI: 10.32526/ennrj/21/202200186

Keywords:
Agriculture/ Adaptation/ Bangladesh/ Climate change/ Coastal areas

*** Corresponding author:**
E-mail:
taposchakraborty@just.edu.bd

ABSTRACT

Farmers in the south-west coastal Bangladesh are frequently affected by climate change due to their proximity to the Bay of Bengal and heavy reliance on agriculture for their livelihoods. In this case, farmers need to know the best implementation methods (adaptation strategies) to reduce crop losses in a changing climate. The present research evaluated the perceptions of farmers to climate change and determine the socio-economic factors which influence the farmers in choosing the right adaptation decisions. Data were collected through close-ended and open-ended structured questionnaire from 52 coastal households and analyzed through descriptive statistics and logistic regression using SPSS V.16. Results revealed that almost all farmers perceived increasing temperature and changes in rainfall patterns over the last 15 years. In response to a changing climate, farmers adopted 13 adaptation strategies where irrigation ranked the first and crop insurance was the last. The logit analysis suggests that household age, education, family income, family member, farm size, farming experience, organizational participations, and training received have a significant influence on farmer's adaptation choices. Despite various support and technological interventions being available, changing weather, natural disaster pattern, lower income, and lack of credit facilities ranked as the highest problems farmers encountered during adaptation. This study helps to identify important household characteristics that can be applied in the future to formulate and implement a successful adaptation policy. Finally, this study recommends that effective training and early warning systems and provision of credit and market access facilities are necessary to enhance farmer's resilience to climate change.

1. INTRODUCTION

Geographically, Bangladesh lies between 20°34' to 26°38' N latitude and 88°01' to 92°42' E longitude, covers an area of 147,570 km^2 (BBS, 2012) of which 47,211 km^2 is coastal area, which covers 32% of the total land area of the country (Huq and Rabbani, 2011). The 711 km long coast, consisting of 19 coastal districts, which occupies 35.1 million people (BBS, 2011), are known as the most climate change vulnerable areas in Bangladesh (Sarker et al., 2020; Alam et al., 2020; Kabir et al., 2016) due to its close proximity to sea, lower elevation, funnel shaped coast, recurrence of natural disasters, high population density, and dependency on agriculture (MOEF, 2005; DOE, 2007; Shahid and Behrawan, 2008; Abedin and Shaw, 2013). However, several indicators such as sea level rise, saline water intrusion, higher temperature, erratic rainfall, frequency and intensity of cyclones, storm surge, and coastal flooding, have proved that the impacts of climate changes are already happening (Khan et al., 2011; Rana et al., 2011; Thurlow et al., 2012; Yu et al., 2010). In every year during the pre-monsoon (April and May) and post-monsoon (October and November) season, coastal areas are affected by

Citation: Anzum HMN, Chakraborty TK, Bosu H. Farmer's perception and factors influencing adoption of adaptation measures to cope with climate change: An evidence from coastal Bangladesh. Environ. Nat. Resour. J. 2023;21(2):113-126. (https://doi.org/10.32526/ennrj/21/202200186)

cyclones. A report from the GoB (2009) showed that from the year 1877 to 1995, coastal regions have experienced 154 cyclones and, on average, every two to three years a severe cyclone hits these coastal regions that have caused a great immediate and long term impact on coastal agriculture (Uddin, 2012), particularly rice production (MOEF, 2005; Yamin et al., 2005). In addition, a result from BBS (2021b) showed that flood (56.41%), river/coastal erosion (14.99%), and cyclones (14.25%) were the most responsible disasters that caused the highest damage and losses in Bangladesh and the first most affected sector was land degradation including reduced valuation (52.56%) where a crop (28.90%) was the second most affected sector.

Coastal agriculture contributes about 25% of the total rice production in the country (BBS, 2013) and generates livelihoods and food security for 70% of the coastal dwellers (Lázár et al., 2015). These areas have been continuously exposed to drought, floods, cyclones, storm surges, salinity intrusion, water-logging, and riverbank erosion. A longitudinal data analysis conducted by Islam et al. (2022) showed that cyclone and saline-prone areas of the country are more vulnerable compared to drought and flood-affected areas of cereal food consumption. Among the other hazards, salinity intrusion is a great threat to coastal agriculture (Molla, 2016; Shaibur et al., 2017), which impedes the growth of vegetation, and deteriorates the natural environment, agricultural ecosystem, and biodiversity; that highly influences the socio-economic conditions of these areas (Hoque et al., 2013; Shaibur et al., 2019). Coastal agriculture is gradually facing incredible challenges due to the inverse relationship between agriculture and climate change, which is responsible for large-scale loss of agricultural production by changing crop physiology (Chakraborty et al., 2000) and severely affecting farming activities (Uddin et al., 2014). However, in this case, several researchers have considered that adaptation is the best possible option for fighting against these negative impacts of climate change (Huang and Sim, 2021; Dorward et al., 2020; Turner-Walker et al., 2021).

Climate change adaptation is defined as the adjustments of a system (natural and human) to reduce the negative effects of climate change and to enhance the favorable opportunities of climate change (Parry et al., 2007; Adger et al., 2003). Adaptation strategies can be adopted by farmer's willingness (autonomous adaptation) or by government/organization supported policies (planned adaptation) and also achieved at different stages such as individual/farm, regional, national, sub-national, local, and international (Asrat and Simane, 2018). However, the farm level adaptation will be effective if the farmers have a clear understanding of climate change and its associated risk. In this case, knowledge, and access to information act as the principle driver. The most common agricultural adaptations are: increasing irrigation facilities, use of new crop varieties, crop rotation, crop diversification, crop intensification, changing planting times, cultivating short-duration varieties, mix crop cultural and livestock farming systems, monitoring weather forecasts on radio, homestead gardening, planting trees and migration, and water resource exploitation (Ahmed et al., 2021; Aidoo et al., 2021; Alam et al., 2017; Habiba et al., 2012). Moreover, adaptation decisions are influenced by different factors including socioeconomic status (farmer’s age, gender, education level, farm-size, family size, family income, off farm income, experience of farming, training received), access to climate information, agricultural subsidies, better access to electricity and institutional facilities, accessibility of technology, remaining infrastructure, more secure tenure rights, an awareness of climatic effects, perceptions about the impact and intensity of climate change, drought severity, extent of groundwater depletion, agro ecological system, existing policies, and capacity (Aidoo et al., 2021; Jha and Gupta, 2021; Uddin et al., 2017; Alam, 2015). These influencing factors are needed to design suitable adaptation policies for specific areas based on sensitivity and vulnerability. But, unfortunately, there is no exploratory research on which adaptation strategies are the best suited for the saline-prone vulnerable coastal areas and how the farmers adapt with their agricultural activities during these extreme climate variability and events. Also, no specific scientific study has been conducted yet in Bangladesh regarding farmer’s perception and factors influencing the adaptation decision to cope with climate change. Most of the study conducted so far in Bangladesh regarding farmer’s perception and response to climate change has focused only on drought-prone areas (Alam, 2015; Alauddin and Sarker, 2014; Sarker et al., 2013; Habiba et al., 2012), saline-prone areas (Kabir et al., 2017; Uddin et al., 2017; Hasnat et al., 2016; Rashid et al., 2014), riverbank erosion-prone areas (Alam et al., 2017; Ahmed, 2015; Karim, 2014) and riverine char islands (Ahmed et al., 2021). Therefore, there is an urgent necessity to identify the strategies that are best suited to support farmers and farming communities in this period of climate change and to identify the factors influencing farmers' adoption of adaptation strategies to cope with climate change. So, a research initiative was needed for this purpose. In this context, the current research paper ascertains farmer's perceptions on various climatic events from farmers experience, agricultural practices, adaptation strategies, constraints, etc., and also determines the underlying socio-economic factors which influence the farmers adaptation decisions.

2. METHODOLOGY

2.1 The study area

Khulna, a south-western coastal district of Bangladesh, was selected to conduct this study. The fourth largest city of Bangladesh in respect of area, Khulna, is considered as one of the worst affected coastal districts due to recurrent natural disasters like cyclones, storm surges, tidal flow, river bank erosion, salinity intrusion, and even drought during the summer season. Khulna district, covers an area of 4,394 km^2 (of which 607.80 km^2 is riverine and 2,028.22 km^2 is under forest), which represents 2.97% of the country's total area (BBS, 2021a). This area is characterized by Ganges tidal floodplain agro-ecological zones (AEZs), and is the most vulnerable climate change affected coastal zone among the 30 AEZs (Rahman et al., 2018). The climate of this district is characterized by a hot summer and a mild winter. The monthly average maximum temperature goes up to 31.1°C during the month of May and the monthly average minimum temperature falls down to 21.8°C in the month of January. The annual rainfall recorded in 2011 was 162.3 mm (BBS, 2021b). The main agricultural products are: rice, jute, sesame, betel nut, and fruits and vegetables, and the major occupation of the villagers are rice cultivation, although the area has been known as a shrimp cultivation area since the 1990s (Barai et al., 2019). Khulna district consists of nine upazilas (sub-districts) and 67 unions (officially called union parishad or union council, the smallest administrative unit in Bangladesh) with having a population of 2,318,527 with 547,347 households (in 2011 census) with the density of 537 persons/km^2. Among the nine upazilas (sub-districts) of Khulna District, Dacope upazila was the worst victim of tropical cyclone Aila, formed on 25th May, 2009 (Roy et al., 2009). Due to the high tidal surge of cyclone Aila, seven unions of Dacope upazila were inundated by high saline water and about 100,000 people have lost their livelihoods. This intrusion of high saline water into agricultural land caused damages to about 1,094 ha of crop land and thus the land also became unsuitable for crop production (Kumar et al., 2010) which eventually caused suffering to the farmers of these unions. Another research on assessing climate change vulnerability of Dacope upazila, Bangladesh was conducted by Razzaque et al. (2019), where they found out of seven unions, the Kamarkhola union of Dacope upazila was highly vulnerable to climate change stress and is in the frontline to face various disasters like cyclones, storm surges and salinity in soil and water. Thus, it is the most fragile area in the aspect of climate change point of view.

Therefore, by following the above discussion with considering the worse scenarios of the affected unions, the Kamarkhola union of dacope upazila (sub-district) of Khulna District, Bangladesh was selected purposively to understand the perceptions of farmers regarding climate change and the factors determining their adaptation decisions to cope with these climate change situations.

Kamarkhola union covers an area of 29.20 km^2, with 3,670 households and a population of 15,407 (population density 154 persons/km^2), out of which 60% are farmers. Geographically, this union is bounded by Dhaki River and Bhodra River in the North, Sutarkhali union in the South, Bhadra River on the East, and Dhaki River on the West. Average literacy rate of this union is 47%. The main occupation of this union is farming. Major crops/products grown in this region are: rice cultivation and fish culture, and the major source of income comes from agriculture. The total number of poor people and landless families are 705 and 338 respectively (BBS, 2011). Here, the study area where we conducted our research is shown in (Figure 1).

2.2 Sampling questionnaire and data collection

The present research was conducted on Kamarkhola union of Dacope upazila in Khulna district of south-western coastal Bangladesh. About 3,670 households with a population of 15,407 (out of which 60% are farmers) live in this union. Out of total households, 500 household heads were first identified through conducting a household census survey by considering the following criteria: those who are the head of the household and who are related with agriculture. Then, with the help of a background survey and the opinion of local experts, 52 farmers were randomly selected from 500 households considering the following criteria: whose primary occupation is agriculture, who are actively involved in agriculture, and who have more than 15 years of farming experience.

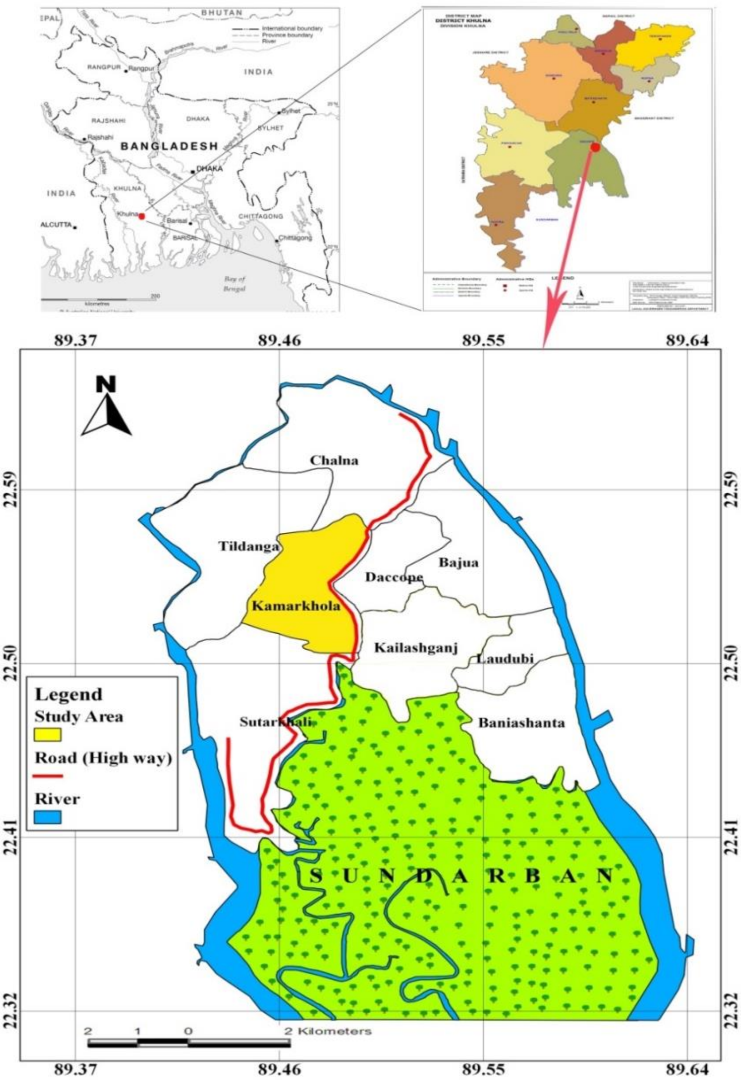

Figure 1. Map of the study area (Kamarkhola Union)

This study was conducted based on primary data sources, and a simple random sampling technique was applied to collect the data. The data collection methods were personal interviews and field observation by using closed-ended (with multiple response options) and open-ended (without multiple response options) structured questions focusing on questions regarding demographic and socioeconomic information, perceptions on the changes of climatic variables over the past 15 years, adaptation techniques to cope with climate change, and problems faced by the farmers during adaptation. This pre-tested structured questionnaire for interview schedule was set up in English but during data collection, the question was translated into Bengali. The questionnaire used was pre-tested on some selected households in the study area before the actual survey started. All the secondary data were collected from various related government and non-government offices, statistical reports, articles, published materials, and official websites. The data were collected from different ages of farmers of having short, medium, and long range of experiences, including various farm sizes, to get data representative of the whole union.

The data collection from personal interviews were gathered through farmer's self-elicitation answer by using a 4-point Likert scale (3=high, 2=medium, 1=low, and 0=not at all) (Sarker et al., 2020; Akanda and Howlader, 2015; Alam et al., 2017; Uddin et al., 2014). After an extensive literature review, 13 adaption strategies/options were selected. The farmers were asked to rate the strategy for how effective they believed the strategy would be as a suitable adaptation options. Moreover, we selected 33 statements according to the major climatic events (8) perceived by the farmers, major adaptation strategies (13) adopted by the farmers, and the major problems (12) faced by the farmers during adaptation. Then we selected eight socio-economic characteristics as an attitudinal statements which were amended from the existing literature, e.g., Uddin et al. (2017), Ahmed et al. (2021), Uddin et al. (2014), and Jha and Gupta (2021). These attitudinal statements give a proper perception about how climate change affects agriculture and what strategies they prefer.

2.3 Variables of the study for empirical model

In this study, adaptation was selected as a dependent variable, where the value of adaptation strategies was assigned as "1" for those farmers who had taken at least one adaptation strategies from the adaptation list to minimize the negative impact of climate change, on the other hand "0" value was assigned to those farmers who had never taken any types of adaptation strategies from the selected list. However, the socio-economic characteristics of the farmers were selected as independent variables (Table 1) which were collected from the extensive literature review of some research scholars, e.g., Uddin et al. (2017) Ahmed et al. (2021) Uddin et al. (2014), and Jha and Gupta (2021) as it increases the level of perceptions about climate change and its associated risk as well as influences the farmer's in taking various adaptation decisions to cope with climate change (Diggs, 1991; West et al., 2008).

Table 1. Definition of variables of binary logistic model

Dependent variable	Independent variable
The value of "1" for who take adaptation strategies and "0" otherwise	X_1=Age of the farmer, measured in years
	X_2=Farmer's education level: "1" if able to read and write; and "0" otherwise
	X_3=Number of family members of the household
	X_4=Family income, measured in Bangladeshi taka per month
	X_5=Farm size, measured in acres
	X_6= Farming experience, measured in years
	X_7=Training received, "1" if received and 0 otherwise
	X_8=Organizational participation: "1" if participated and "0" otherwise

Different types of adaptation models are traditionally used in adaptation studies, for example: probit model (Maddison, 2007; Aidoo et al., 2021), socio-cognitive model (Grothmann and Patt, 2005), multinomial choice model (Hassan et al., 2008), multinomial logit (MNL) model (Deressa et al., 2009), and binary logit regression model (Jha and Gupta, 2021; Uddin et al., 2017; Ahmed et al., 2021; Uddin et al., 2014). Multinomial logistic regression is the extension of binary logit regression. It is used when the dependent variables of the study are three and above, whereas, binary logit is used when the dependent variable of the study is two. According to their formulation and results, both the probit and logit models are the same, but the probit models are most used for experimental data and do not give accuracy in robustness as it cannot approve the modeler to adjust for covariates. On the other hand, logit models confirm the rise of estimated probability and never cross the range of 0 to 1. This model is recognized as the best fit and is widely accepted by all. So, by considering all of these conditions and factors, the binary logit regression model was applied in this study to determine how the demographic and socio-economic factors influence the farmer's in taking the adaptation decisions to cope with climate change. This logit model was expressed in Equation (1-3) (Gujarati and Porter, 2009).

$$P_i = \frac{1}{1} + e^{-(\beta_\theta + \beta_i X_i)} \tag{1}$$

For simplicity, equation (1) can be written as:

$$P_i = \frac{1}{1} + e^{-Zi} \tag{2}$$

Where; Pi: probability of adaptation of the i^{th} respondent; e^{zi}: stands for the irrational number e raised to the power of Z_i; Z_i is a function of N-explanatory variables and expressed in equation (3) as follows:

$$Z_i = \beta_\theta + \beta_1 X_1 + \beta_2 X_2 + \cdots\cdots\cdots + \beta_n X_n + \mu_i \tag{3}$$

Where; β_θ=Constant term; μ_i=the error term, which has a standard logistic distribution; $\beta_1 \ldots \beta_n$=regression co-efficient; $X_1 \ldots X_n$= explanatory variables presented in (Table 1).

2.4 Data analysis process

The data analysis was performed by descriptive statistics and binary logit regression model using SPSS (V.16). The descriptive statistical tools were used to analyze and present the demographic and socio-economic characteristics of the farmers, the perceptions of farmers to various climatic events, their major adaptation practices, and the major problems that were faced during adaptation. Factors influencing farmer's perception were analyzed in a logistic regression model framework. In this research, we implemented Environmental Hazard Index (EHI), Adaptation Strategy Index (ASI), and Problem Facing Index (PFI) to determine the perceptions of farmers regarding climate change, to find out the rank of adaptation strategies, and to identify the problems of farmers for adopting climate change adaptation strategies respectively where the calculation equation were adopted from Ndamani and Watanabe (2017).

2.4.1 EHI: EHI help to investigate the perception of farmers regarding the climate change issues. In this study, perceptions regarding climate change impact were collected from eight climate change concerns, which were perceived by the farmers. The ranking was computed by using the Equation (4) as:

$$\mathrm{EHI} = \mathrm{EH_n} \times 0 + \mathrm{EH_l} \times 1 + \mathrm{EH_m} \times 2 + \mathrm{EH_h} \times 3 \qquad (4)$$

Where; EHI=environmental hazard index; EH_n=number of farmers who were affected by no environmental hazards; EH_1=number of farmers who were affected by low environmental hazards; EH_m=number of farmers who were affected by medium environmental hazards; EH_h=number of farmers who were affected by high environmental hazards.

2.4.2 ASI: The ASI is used to find out the rank of adaptation strategies, which are necessary for farmers to continue their farming activities. Here thirteen adaptation strategies were selected from kinds of literature and the priorities of adaptation strategies to climate change were calculated by using the Equation (5) as:

$$\mathrm{ASI} = \mathrm{AS_n} \times 0 + \mathrm{AS_l} \times 1 + \mathrm{AS_m} \times 2 + \mathrm{AS_h} \times 3 \qquad (5)$$

Where; ASI=adaptation strategy index; AS_n=number of farmers who stated no agricultural adaptation to climate change; AS_l=number of farmers who stated low agricultural adaptation to climate change; AS_m=number of farmers who stated medium agricultural adaptation to climate change; AS_h=number of farmers who stated high agricultural adaptation to climate change.

2.4.3 PFI: PFI is applied to identify the problems of farmers for adopting the climate change adaptation strategies. In this case, twelve problems were listed, where farmers expressed their opinion and the ranking of the problems was calculated by applying the Equation (6) as:

$$\mathrm{PFI} = \mathrm{P_n} \times 0 + \mathrm{P_l} \times 1 + \mathrm{P_m} \times 2 + \mathrm{P_h} \times 3 \qquad (6)$$

Where; PFI=problem facing index; P_n=number of farmers who stated the problem as not encountered; P_l=number of farmers who stated the problem as low; P_m=number of farmers who stated the problem as moderate; P_h=number of farmers who stated the problem as high.

All the index (EHI, ASI, and PFI) scores were ranging from 0 to 208, where '0' indicating the minimum and '208' indicating maximum and finally ranking was made in the order of maximum to minimum score.

3. RESULTS AND DISCUSSION

3.1 Demographic and socio-economic status of the respondents

The variables that describe the demographic and socio-economic characteristics of the respondents in this study were household head's age, education level, family member, farm size, family income, farming experience, training received, and organizational participation which are presented in (Table 2).

Data shows that 36% of the household head were in the young age group (≤35) followed by 35% and 29% within the middle age (36-50) and old age (>50) group, respectively, where the average age of the respondents were around 43 years which represents the age between young to middle-aged (71%). Uddin et al. (2017) found that most of the farmers in the coastal areas of Bangladesh were young to middle-aged.

Another important characteristic considered in this socio-demographic analysis was the level of education. Data in Table 2 shows that more than half of the respondents (52%) combined have completed their primary (1-5), secondary (6-10) and above secondary (>10) level of education while (48%) of the respondents have a low level (illiterate and can sign only) of education. There was not a single household head found who had completed graduation or above. So, we can conclude that majority 79% (including can sign only) of the farmers in this study area were literate and the average years of schooling was around four years. Data from the Bangladesh National Portal showed that a total of 17 educational institution existed in Kamarkhola union, where the number of government and non-government primary schools was six and seven, respectively, while there were only four secondary schools, and no higher secondary schools were found in this study area. So, for this, the level of education from primary to above secondary is gradually decreasing. Uddin et al. (2017) also found the similar types of literacy rates in their research.

Family size is also considered an important variable in demographic analysis. From the table, we can see that about half (50%) of the respondents have a small family (up to 4) members, while 44% have a medium (5-7), and 6% a large (>8) number of family members. The average number of family members was 4.83, which is similar to the national average family-sized 4.54 (BBS, 2021b).

In addition, about 83% of the respondents have a small farm (up to 2 acres), while only 13% of the respondents had medium (2.01-5.00 acres) and 4% had large farm sizes (>5 acres). The most common monthly family income (73%) belonged to the medium income group (BDT 5,001-10,000) while the rest (19%) and (8%) were fall under the low (up to BDT 5,000) and high income (>10,000 BDT) groups, respectively. The monthly average income of the farmers was BDT (Bangladeshi Taka) 7,538 (89 USD), which is less than the national monthly average income of BDT 9,353 (111 USD) (Uddin et al., 2017). The main sources of family income came from crop production, fish culture, cattle rearing, and non-farming sources (e.g., day labor).

Table 2. Demographic and socio-economic status of the respondents (n=52)

Characteristics	Categories	Scoring method	Respondent (%)	Mean±SD
Age	Young (up to 35)	Year	36	43.55±15.06
	Middle aged (36-50)		35	
	Old (Above 50)		29	
Education level	Illiterate (0)	Year of schooling	21	3.99±1.08
	Can sign only (0.5)		27	
	Primary (1-5)		31	
	Secondary (6-10)		19	
	Above secondary (>10)		2	
Family member	Small (Up to 4)	Number	50	4.83±1.65
	Medium (5-7)		44	
	Large (Above 8)		6	
Farm size	Small (Up to 2 ac)	Acres	83	4.68±4.14
	Medium (2.01-5.00 ac)		13	
	Large (Above 5 ac)		4	
Family income	Low (Up to 5,000)	BDT/month	19	7,538±2,654
	Medium (5,001-10,000)		73	
	High (Above 10,000)		8	
Farming experience	Short (3-19)	Years	62	18.19±12.67
	Medium (20-30)		25	
	Long (Above 30)		13	
Training received	Yes	Dummy	8	
	No		92	
Organizational participation	Yes	Dummy	31	
	No		69	

Additionally, 62% of the farmers have short range (3-19) years of farming experience while 25% and 13% have the medium level (20-30) years and long range (>30) years of farming experience, respectively. The average farming experience of the surveyed farmers was about 19 years, which is a critical factor that influences farmers for making adaptation decisions and better understanding climate change events (Asrat and Simane, 2018). The study from Uddin et al. (2017) also showed the same results where the farmers of southwest coastal Bangladesh have an average 20 years of farming experience.

Nearly 92% of the farmers had no training experience regarding climate change impact on agriculture and about 69% of the farmers did not participate in any agricultural organizational program.

3.2 EHI based on farmer's perception

The results from the environmental hazard index (EHI) showed that increased temperature and reduction in rainfall were ranked the first and second environmental hazard. Kabir (2015) also found similar results. He found that about 95% and 89% participants of southwestern coastal Bangladesh perceived an increase of annual temperature and decrease of rainfall pattern, respectively.

In addition, salinity was the third environmental hazard of concern and is considered as the most common disaster in the coastal areas of Bangladesh. Islam et al. (2015) had found that after just nine years (from 2000 to 2009) in the southwestern coastal region of Bangladesh, salinity level was changed from 23.93 dS/m to 28.64 dS/m.

Other changes in various climatic events perceived by the farmers of this study were long summers (4th), erratic rainfall due to delayed monsoons (5th), floods (6th), cyclones (7th), and short winters (8th); which are presented in (Figure 2).

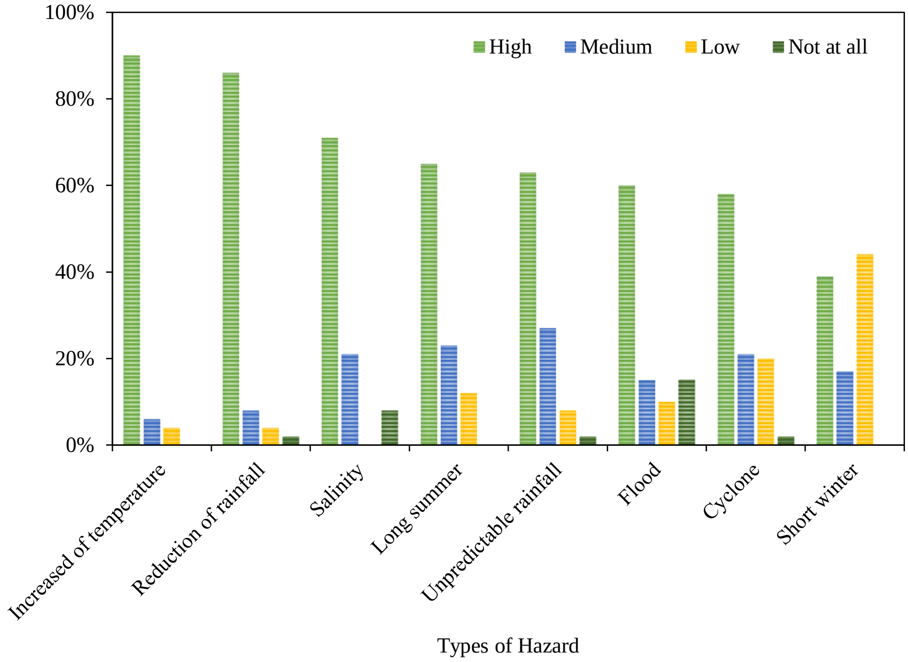

Figure 2. Farmer's perception of changes in different climatic events

However, the perception of farmers about climate change and climatic variability also matched with the scientific report that had been provided by Mondal et al. (2012).

Analysis of the findings concluded that farmers had a good perception on local climate change and climate variability, which provokes them to adopt various adaptation strategies for reducing the negative effects of climate change.

3.3 ASI based on farmer's perception

The results of Adaptation Strategy Index (ASI) are presented in (Table 3). Out of 13 adaptation strategies, increased use of irrigation was ranked the first, which is the most vital among farmers because irrigation makes the nutrients available for the plants and also influences crop production. About 80.2% of Himachal Pradesh farmers in India think that irrigation is the best adaptation strategies to climate change impacts (Loria and Bhardwaj, 2016).

The second adaptive strategy was crop diversification, which is most favorite to farmers because through practicing diversified cropping strategy, they can minimize their risk due to crop failure, and can earn more by increasing crop yield; which ultimately causes increasing opportunities for the farmers to expand their farm. About 57.9% of Indian farmers (Loria and Bhardwaj, 2016), and 61% of Kenya farmers (Judith et al., 2017) think that crop diversification at the farm level is a good adaptation option to cope with climate change.

Table 3. Rank order of the major adaptation strategies adopted by the farmers (n=52)

Adaptation strategies	High	Medium	Low	Not at all	ASI	Rank
Increased use of irrigation	116 (56%)	63 (40%)	2 (2%)	1 (2%)	182	1st
Practicing crop diversification	112 (54%)	51 (33%)	10 (9%)	2 (4%)	175	2nd
Find off-farm job	100 (48%)	51 (33%)	14 (13%)	3 (6%)	168	3rd
Integrated farming system	72 (35%)	60 (38%)	18 (17%)	5 (10%)	155	4th
Use of salinity tolerant varieties	72 (35%)	57 (37%)	12 (11%)	9 (17%)	150	5th
Cultivating short duration crops	60 (29%)	63 (40%)	14 (14%)	9 (17%)	146	6th
Practicing crop rotation	52 (14%)	54 (40%)	22 (19%)	10 (27%)	138	7th
Use of drought tolerant varieties	40 (19%)	57 (37%)	20 (19%)	13 (25%)	130	8th
Practicing intercropping	28 (14%)	63 (40%)	20 (19%)	14 (27%)	125	9th
Agroforestry	28 (14%)	60 (38%)	16 (15%)	17 (33%)	121	10th
Soil conservation techniques	36 (17%)	9 (6%)	40 (39%)	20 (38%)	105	11th
Zero tillage	16 (8%)	24 (15%)	26 (25%)	27 (52%)	93	12th
Crop insurance	8 (2%)	0 (0%)	12 (11%)	44 (85%)	64	13th

Finding an off-farm job was the third most important adaptation strategy; it was applied by those farmers whose farm income was gradually decreasing by adverse climatic conditions. Both Morton (2007) and Loria and Bhardwaj (2016) have found similar results.

The fourth strategy was the integrated farming practices. It is more popular throughout the country due to its large economic benefits (Uddin and Takeya, 2005).

Due to the salinity in soil and water of this study area, the use of saline tolerant varieties (5th) was also an important adaptation strategy among farmers (Abedin et al., 2012). Next in order of adaptation techniques are the followings: short-duration crops > practicing crop rotation > drought-tolerant varieties > practicing intercropping > agroforestry > soil conservation techniques > zero tillage > crop insurance (Table 3). Similar types of work were done by Varadan and Kumar (2014) and Uddin et al. (2014).

3.4 PFI based on farmer's perception

The problems faced by the farmers during adaptation were identified by the perception of farmers and were listed in rank order by using Problem Facing Index (PFI) presented in Table 4. The results indicate that changing weather and natural disaster pattern was ranked first where farmers faced a lot of problems, for example: crop loss, crop failure, low yield production, increasing pest infestation, etc. due to high temperatures, shortage of rainfall, and recurrent natural calamities. Although we know that the agriculture of Kamarkhola union is highly influenced by weather and climatic condition. According to Howlader and Akanda (2016), the farmers of Patuakhali district of Bangladesh also faced a similar problem.

The second most important problem faced by the farmers was insufficient family income, and due to low income they could not adopt new technologies to continue their agricultural practices. Lack of credit facilities is another problem faced by farmers during adaptation and with their low household income and lack of adequate financial or micro-credit institutions to provide them with credit facilities, this acts as an additional barrier for farmers when adopting climate change adaptation strategies. According to Judith et al. (2017), in Kenya, about 61% farmers did not have enough money, which was the main barrier for adopting agricultural adaptation.

Table 4. Rank order of the problems faced by the farmers (n=52)

Problems	High	Medium	Low	Not at all	PFI	Rank
Changing of weather and natural disaster pattern	176 (85%)	24 (15%)	0 (0%)	0 (0%)	200	1st
Insufficient family income	148 (71%)	45 (29%)	0 (0%)	0 (0%)	193	2nd
Unavailability of credit facilities	152 (73%)	30 (19%)	4 (4%)	2 (4%)	188	3rd
Lack of available water (Irrigation)	140 (67%)	9 (6%)	16 (15%)	6 (12%)	171	4th
Lack of access of information	140 (67%)	9 (6%)	14 (14%)	7 (13%)	170	5th
Lack of market access	112 (54%)	21 (14%)	20 (19%)	7 (13%)	160	6th
Unavailability of salinity tolerant species	104 (51%)	33 (21%)	16 (16%)	7 (12%)	160	7th
Shortage of farm inputs	84 (40%)	54 (35%)	12 (12%)	77 (13%)	157	8th
Traditional practices/beliefs	80 (38%)	39 (25%)	30 (29%)	4 (8%)	153	9th
Non-availability of storage and processing of agro-product	60 (29%)	27 (17%)	18 (17%)	19 (37%)	124	10th
Government's inadvertence to monitor climate risk management programs	64 (31%)	15 (10%)	16 (15%)	24 (44%)	119	11th
Poor soil fertility	32 (15%)	21 (14%)	20 (19%)	27 (52%)	100	12th

Lack of available water for irrigation was ranked as the fourth problem and was considered the biggest problem for farmers in coastal areas because the agricultural system is completely dependent on water for irrigation, but the sources of irrigation facilities are affected by various kinds of natural disasters like floods, droughts, cyclones, and salinity intrusion.

Uddin et al. (2014) found that the lack of irrigation water was the top most problem for crop cultivation in the southwest coast of Bangladesh.

Next in order of the problems faced by the farmers during adaptations are the following: inadequate access of information > lack of market access > unavailability of salinity tolerant species > shortage of farm inputs > traditional practices/beliefs > non-availability of storage and processing of agro-product > government's inadvertence to monitor climate risk management programs > poor soil fertility (Table 4). Similar types of work were done by Satishkumar et al. (2013) and Uddin et al. (2014).

3.5 Empirical model results

The result of the regression model (Table 5) showed that age positively influenced the farmer's adaptation strategies to climate change impacts. It highlighted that the adoption of adaptation strategies was significantly increased among young and middle-aged farmers, rather than old farmers, and they were more interested in taking adaptation decisions and preferred modern techniques for combatting climatic impacts. Akanda and Howlader (2015) and Adeogun et al. (2008) have found the same result that age acts as a positive influencing factor for farmer's adaptation strategies.

The findings of the regression model showed that education was positive and significantly related to farmer's adoption of climate change adaptation strategies because an educated farmer is more knowledgeable and skilled rather than an uneducated farmer. Educated farmers have a clear perception about climate change-related impacts and future scenarios, and also have better access to different types of information and facilities, etc., which influence a farmer to take better adaptation decisions than others. Quayum and Ali (2012) and Adeogun et al. (2008) have found the same result that education positively influences a farmer for adopting new adaptation technology.

On the other hand, there was a negative relationship between family size and farmer's adaptation strategies. The levels of adaptation strategies are gradually reduced with the increasing number of family members. Uddin et al. (2014) have found a similar result.

Family income has a significant positive relation between adoptions of adaptation strategies. The farmers with high household incomes are more adaptive than the farmers with less family income because the high-income families earn money from diverse sources such as off-farm activities. So they can tackle climate change effects and can continue their agricultural activities. In contrast, the reverse relationship is found in the lower-income families. Uddin et al. (2014) and Nhemachena and Hassan (2007), also explained a similar relationship.

Table 5. The results of binary logistic regression model

Dependent variable	Independent variable	β-value	Std. error	p value
Adoption of adaptation strategies to climate change	(Constant)	0.407	0.575	0.483
	Age	0.017	0.006	0.010*
	Education	0.003	0.059	0.959
	Family size	-0.001	0.035	0.977
	Family income	0.00004	0.000	0.042*
	Farm size	-0.016	0.013	0.209
	Farming experience	-0.017	0.008	0.038*
	Training received	0.088	0.229	0.704
	Organizational participation	-0.281	0.116	0.020*

*95% significant level

The regression model also represented a negative relationship between farm size and adaptation strategies to climate change impacts. Large farm size requires large farm inputs such as large investment, labor force, seeds, agro-chemicals, fertilizers, irrigation, etc. which creates a problem for proper management. So, the large farm is not able to take adaptation decisions effectively. Uddin et al. (2014) and Adeogun et al. (2008) found that farm size negatively influences the adoption of adaptation strategies.

A negative and meaningful relationship was found between farming experience and adoption of adaptation strategy. Experienced farmers are not interested to take adaptation strategies regarding climate change impact. They expressed their interest in traditional methods rather than modern agricultural practices. A similar outcome was also found by Howlader and Akanda (2016) and Adeogun et al. (2008).

Another positive relationship was found between training received and adaptation to climate change. Through receiving training, farmers can easily determine climate change issues and can take more adaptation strategies for minimizing the negative effects of climate change than those who do not receiving any training. Uddin et al. (2014) also found a positive relationship between training and the adoption of adaptation strategies.

Organizational participation was negative and significantly related to farmer's adaptation strategies to climate change impact. The farmers who are not interested in participating in different types of organizational agricultural program, and don't have diversified knowledge about agricultural-related information, modern farming practices, etc., don't take part in any role in climate change adaptation measures. Moreover, they follow traditional methods rather than modern farming techniques. This result is also supported by Loria and Bhardwaj (2016).

4. CONCLUSION

Kamarkhola union (study area) is one of the most vulnerable areas to climate change due to: impact of repeated natural calamities every year, low adaptive capacity due to resource constraints, poverty and high dependence on agriculture for livelihood which greatly impacts on agricultural sector. The urgent need in this situation is to give utmost priority to farmer's understanding of climate change and the factors affecting them to adopt the best adaptation decisions to cope with these situations. However, farmer's perception of climate change is a prerequisite for introducing adaptation strategies, so policymakers would benefit from such understanding to introduce new adaptation strategies at the policy level. In terms of understanding farmer's perceptions of climate change based on their past experiences and long-term observation of climate variables like temperature and precipitation levels, the survey results show that farmer's perceptions of climate variability are very similar to what is happening in reality; for example, increase in temperature and reduction of rainfall, long summer and shorter winter, and erratic rainfall due to delayed monsoon is very common today. This eventually causes the formation of cyclones, storm surges, coastal flooding, and saline water intrusion in the coastal area. To cope with these adverse conditions, most farmers adopt strategies related to sustaining agricultural practices, changing farm systems and income-generating activities using their own local strategies, indigenous knowledge and skills to overcome difficulties during adaptation as well as increase their level of financial status. Among all the strategies, irrigation, off-farm jobs, and integrated farming are the most adopted practices. Furthermore, adaptation decisions are significantly influenced by age, education, family income, family members, farm size, and farming experiences. To ensure the effectiveness and sustainability of adaptation practices, the study recommends increasing the provision of effective training and early warning systems and credit and market access facilities.

ACKNOWLEDGEMENTS

Author would like to thanks to the coastal dwellers of Khulna Districts, Nongovernment and Government Officers of Khulna District for providing us the valuable information regarding the research. This study was conducted by students self-fund and this research did not receive any specific grant from funding agencies in the public, commercial, or non-profit sectors.

REFERENCES

Abedin MA, Habiba U, Shaw R. Health: Impacts of salinity, arsenic, and drought in south-western Bangladesh. In: Shaw R, Tran P, editors. Environment Disaster Linkages (Community, Environment and Disaster Risk Management, Vol. 9). Bingley: Emerald Group Publishing Limited; 2012. p. 165-93.

Abedin MA, Shaw R. Agriculture adaptation in coastal zone of Bangladesh. In: Shaw R, Mallick F, Islam A, editors. Climate Change Adaptation Actions in Bangladesh. Tokyo, Japan: Springer; 2013.p. 207-25.

Adeogun OA, Ajana AM, Ayinla OA, Yarhere MT, Adeogun MO. Application of logit model in adoption decision: A study of hybrid clarias in Lagos State, Nigeria. American-Eurasian Journal of Agriculture and Environmental Science 2008; 4(4):468-72.

Adger WN, Huq S, Brown K, Declan C, Mike H. Adaptation to climate change in the developing world. Progress in Development Studies 2003;3(3):179-95.

Ahmed I. People of Many Rivers: Tales from the Riverbanks. Bangladesh: University Press Limited; 2015.

Ahmed Z, Guha GS, Shew AM, Alam GMM. Climate change risk perceptions and agricultural adaptation strategies in vulnerable riverine char islands of Bangladesh. Land Use Policy 2021;103:Article No. 105295.

Aidoo DC, Boateng SD, Freeman CK, Anaglo JN. The effect of smallholder maize farmers' perceptions of climate change on their adaptation strategies: The case of two agro-ecological zones in Ghana. Heliyon 2021;7(11):e08307.

Akanda MGR, Howlader MS. Coastal farmers' perception of climate change effects on agriculture at Galachipa Upazila under Patuakhali District of Bangladesh. Global Journals of Science Frontier Research: Agriculture and Veterinary 2015;15(4):31-9.

Alam GMM, Alam K, Mushtaq S, Sarker MN, Hossain M. Hazards, food insecurity and human displacement in rural riverine Bangladesh: implications for policy. International Journal of Disaster Risk Reduction 2020;43:Article No. 101364.

Alam GMM, Alam K, Mushtaq S, Clarke ML. Vulnerability to climatic change in riparian char and river-bank households in Bangladesh: Implication for policy, livelihoods and social development. Ecological Indicator 2017;72:23-32.

Alam K. Farmers' adaptation to water scarcity in drought-prone environments: A case study of Rajshahi District, Bangladesh. Agricultural Water Management 2015;148:196-206.

Alauddin M, Sarker MAR. Climate change and farm-level adaptation decisions and strategies in drought-prone and groundwater-depleted areas of Bangladesh: An empirical investigation. Ecological Economics 2014;106:204-13.

Asrat P, Simane B. Farmers' perception of climate change and adaptation strategies in the Dabus watershed, North-West Ethiopia. Ecological Process 2018;7(7):1-13.

Bangladesh Bureau of Statistics (BBS). Disaster Prone Area Atlas of Bangladesh: Khulna Zilla. Bangladesh Bureau of Statistics, Statistics and Informatics Division, Ministry of Planning, Government of the People's Republic of Bangladesh; 2021a.

Bangladesh Bureau of Statistics (BBS). Final Draft Report on Bangladesh Disaster-related Statistics 2021: Climate Change and Natural Disaster Perspectives. Bangladesh Bureau of Statistics, Statistics and Informatics Division, Ministry of Planning, Government of the People's Republic of Bangladesh; 2021b.

Bangladesh Bureau of Statistics (BBS). Statistical Year Book of Bangladesh-2011. Bangladesh Bureau of Statistics, Planning Division, Ministry of Planning, Government of the People's Republic of Bangladesh; 2011.

Bangladesh Bureau of Statistics (BBS). Statistical Year Book of Bangladesh-2012. Bangladesh Bureau of Statistics, Planning Division, Ministry of Planning, Government of the People's Republic of Bangladesh; 2012.

Bangladesh Bureau of Statistics (BBS). Statistical Yearbook of Bangladesh-2013. Bangladesh Bureau of Statistics, Statistic Division, Ministry of Planning, Government of the People's Republic of Bangladesh; 2013.

Barai KR, Harashina K, Satta N, Annaka T. Comparative analysis of land-use pattern and socioeconomic status between shrimp- and rice-production areas in southwestern coastal Bangladesh: a land-use/cover change analysis over 30 years. Journal of Coastal Conservation 2019;23(3):531-42.

Chakraborty S, Tiedemann AV, Teng PS. Climate change: potential impact on plant diseases. Environmental Pollution 2000;108(3):317-26.

Department of Environment (DOE). Climate Change and Bangladesh: Bangladesh Government and United Nations Development Programme. Dhaka: Department of Environment; 2007.

Deressa TT, Hassan RM, Ringler C, Alemu T, Yesuf M. Determinants of farmers' choice of adaptation methods to climate change in the Nile Basin of Ethiopia. Global Environmental Change 2009;19(2):248-55.

Diggs DM. Drought experience and perception of climatic change among Great Plains farmers. Great Plains Research: A Journal of Natural and Social Sciences 1991;1:114-32.

Dorward P, Osbahr H, Sutcliffe C, Mbeche R. Supporting climate change adaptation using historical climate analysis. Climate and Development 2020;12(5):469-80.

Grothmann T, Patt A. Adaptive capacity and human cognition: The process of individual adaptation to climate change. Global Environmental Change 2005;15(3):199-13.

Government of Bangladesh (GoB). Bangladesh Climate Change Strategy and Action Plan. Government of the People's Republic of Bangladesh; 2009.

Gujarati DN, Porter DC. Basic Econometrics. 5th ed. New York: McGraw-Hill/Irwin; 2009. p. 946.

Habiba U, Shaw R, Takeuchi Y. Farmer's perception and adaptation practices to cope with drought: Perspectives from Northwestern Bangladesh. International Journal of Disaster Risk Reduction 2012;1(1):72-84.

Hasnat MA, Hossain N, Muhibbullah M, Sarwar MD, Shormin T. Impacts of climate change on agriculture and changing adaptive strategies in the coastal area of Lakshmipur District, Bangladesh. Current World Environment 2016;11(3):700-14.

Hassan C, Rashid M, Nhemachena. Determinants of African farmers' strategies for adapting to climate change: Multinomial choice analysis. African Journal of Agricultural and Resource Economics 2008;2(1):Article No. 22.

Hoque MA-A, Saika U, Sarder BC, Biswas KK. Environmental and socio-economic impacts of salinity intrusion in the coastal area: A case study on Munshigong Union, Shymnagor, Satkhira. Jahangirnagar University Environmental Bulletin 2013;2:41-9.

Howlader MS, Akanda MG. Problems in adaptation to climate change effects on coastal agriculture by the farmers of Patuakhali District of Bangladesh. American Journal of Rural Development 2016;4(1):10-4.

Huang K, Sim N. Adaptation may reduce climate damage in agriculture by two thirds. Journal of Agricultural Economics 2021;72(1):47-71.

Huq S, Rabbani G. Adaptation Technologies in Agriculture: The Economics of rice farming technology in climate-vulnerable areas of Bangladesh. In: Christiansen L, Olhoff A, Traerup S, editors. Technologies for Adaptation: Perspectives and Practical Experiences. Denmark: UNEP Riso Centre on Energy, Climate and Sustainable Development; 2011.

Islam MA, Shitangsu PK, Hassan MZ. Agricultural vulnerability in Bangladesh to climate change induced sea level rise and options for adaptation: A study of a coastal Upazila. Journal of Agriculture and Environment for International Development 2015;109(1):19-39.

Islam MS, Samreth S, Islam AHMS, Sato M. Climate change, climatic extremes, and households' food consumption in Bangladesh: A longitudinal data analysis. Environmental Challenges 2022;7:Article No. 100495.

Jha CK, Gupta V. Farmer's perception and factors determining the adaptation decisions to cope with climate change: An evidence from rural India. Environmental and Sustainability Indicators 2021;10:Article No. 100112.

Judith C, Mbogoh SG, Chris AO, Patrick I. Smallholder farmers' perceptions and responses to climate change in multi-stressor environments: The case of Maasai agro-pastoralists in Kenya's rangelands. American Journal of Rural Development 2017;5(4):110-16.

Kabir H. Impacts of climate change on rice yield and variability; an analysis of disaggregate level in the southwestern part of Bangladesh especially Jessore and Sathkhira Districts. Journal of Geography and Natural Disasters 2015;5:Article No. 148.

Kabir MJ, Cramb R, Alauddin M, Roth C, Crimp S. Farmers' perceptions of and responses to environmental change in southwest coastal Bangladesh. Asia Pacific Viewpoint 2017;58(3):362-78.

Kabir R, Khan HTA, Ball E, Caldwell K. Climate change impact: the experience of the coastal areas of Bangladesh affected by cyclones Sidr and Aila. Journal of Environmental and Public Health 2016;2016:Article No. 9654753.

Karim AHMZ. Flood and riverbank erosion displacees: Their indigenous survival strategies in two coastal villages in Bangladesh. Asian Social Science 2014;10(4):16-26.

Khan AE, Xun WW, Ahsan H, Vineis P. Climate change, sea-level rise, and health impacts in Bangladesh. Environment: Science and Policy for Sustainable Development 2011;53(5):18-33.

Kumar U, Baten MA, Masud AA, Osman KS, Rahman MM. Cyclone Aila: One Year on Natural Disaster to Human Sufferings. Dhaka, Bangladesh: Unnayan Onneshan-The Innovators; 2010.

Lázár AN, Clarke D, Adams H, Akanda AR, Szabo S, Nicholls RJ, et al. Agricultural livelihoods in coastal Bangladesh under climate and environmental change: A model framework. Environmental Science: Processes and Impacts 2015; 17(6):1018-31.

Loria N, Bhardwaj SK. Farmers' response and adaptation strategies to climate change in low-hills of Himachal Pradesh in India. Nature Environment and Pollution Technology 2016;15(3):895-1001.

Maddison D. The Perception of and Adaptation to Climate Change in Africa. Policy Research Working Paper 4308. Washington DC, USA: World Bank Publications; 2007.

Ministry of Environment and Forest (MOEF). National Adaptation Program of Action (NAPA). Dhaka, Bangladesh: Ministry of Environment and Forest, Government of Bangladesh; 2005.

Molla IH. Environment and climate change in Bangladesh: Challenges and the role of public administration. Resources and Environment 2016;6(1):1-8.

Mondal MS, Islam AK, Madhu MK. Spatial and temporal distribution of temperature, rainfall, sunshine and humidity in context of crop agriculture. Comprehensive Disaster Management Program, Ministry of Food and Disaster Management, Government of the People's Republic of Bangladesh; 2012.

Morton JF. The impact of climate change on smallholder and subsistence agriculture. Proceedings of the National Academy of Sciences 2007;104(50):19680-5.

Ndamani F, Watanabe T. Determinants of farmers' climate risk perceptions in agriculture-a rural Ghana perspective. Water (Switzerland) 2017;9(3):Article No. 201.

Nhemachena C, Hassan R. Micro-Level Analysis of Farmers' Adaption to Climate Change in Southern Africa. IFPRI Discussion Paper 00714. Washington DC, USA: International Food Policy Research Institute; 2007. p 1-40.

Parry ML, Canziani O, Palutikof J, Van der Linden P, Hanson C. Climate Change 2007: Impacts, Adaptation and Vulnerability: Working group II contribution to the fourth assessment report of the IPCC. Cambridge, UK: Cambridge University Press; 2007.

Quayum M, Ali AM. Adoption and diffusion of power tillers in Bangladesh. Bangladesh Journal of Agricultural Research 2012;37(2):307-25.

Rahman HMT, Hickey GM, Ford JD, Egan MA. Climate change research in Bangladesh: Research gaps and implications for adaptation-related decision-making. Regional Environmental Change 2018;18(5):1535-53.

Rana SMM, Kamruzzaman M, Rajib MA, Rahman MM. Changes in cyclone pattern with climate change perspective in the coastal regions of Bangladesh. Environmental Research, Engineering and Management 2011;56(2):20-7.

Rashid MH, Afroz S, Gaydon D, Muttaleb A, Poulton P, Roth C, et al. Climate change perception and adaptation options for agriculture in Southern Khulna of Bangladesh. Applied Ecology and Environmental Sciences 2014;2(1):25-31.

Razzaque MA, Alamgir M, Rahman MM. Climate change vulnerability in Dacope Upazila, Bangladesh. Journal of Scientific Research and Reports 2019;21(4):1-12.

Roy K, Kumar U, Mehedi H, Sultana T, Ershad DM. Cyclone Aila 2009: Initial Assessment Report with Focus on Khulna District. Khulna, Bangladesh: Unnayan Onneshan-Humanity Watch- NijeraKori; 2009. p. 6-31.

Sarker MAR, Alam K, Gow J. Assessing the determinants of rice farmers' adaptation strategies to climate change in Bangladesh. International Journal of Climate Change Strategies and Management 2013;5(4):382-403.

Sarker MNI, Wu M, Alam GMM, Shouse RC. Life in riverine islands in Bangladesh: Local adaptation strategies of climate vulnerable riverine island dwellers for livelihood resilience. Land Use Policy 2020;94:Article No. 104574.

Satishkumar N, Tevari P, Singh A. A study on constraints faced by farmers in adapting to climate change in rainfed agriculture. Journal of Human Ecology 2013;44(1):23-8.

Shahid S, Behrawan H. Drought risk assessment in the western part of Bangladesh. Natural Hazards 2008;46(3):391-13.

Shaibur MR, Khan MH, Rashid MS. Climate change may cause natural disasters in Shyamnagar, Satkhira: The Southwestern parts of Bangladesh. Bangladesh Journal of Environmental Science 2017;32:101-10.

Shaibur MR, Rizvi MM, Islam MK, Shamsunnahar. Salinity causes ecosystem disruption and biodiversity losses in beel Khuksia: Keshabpur, Jashore, Bangladesh. Environmental and Biological Research 2019;1(1):1-11.

Thurlow J, Dorosh P, Yu W. A stochastic simulation approach to estimating the economic impacts of climate change in Bangladesh. Review of Development Economics 2012; 16(3):412-28.

Turner-Walker S, Anantasari E, Retnowati A. Integration into development: Translating international frameworks into village-level adaptation. In: Climate Change Research, Policy and Actions in Indonesia. Cham: Springer International Publishing; 2021. p. 53-77.

Uddin ME. Household food security status of marginal farmers in selected storm surge prone coastal area of Bangladesh. The Agriculturist 2012;10(1):98-103.

Uddin MN, Bokelmann W, Dunn ES. Determinants of farmers' perception of climate change: a case study from the coastal region of Bangladesh. American Journal of Climate Change 2017;6(1):151-65.

Uddin MN, Bokelmann W, Entsminger JS. Factors affecting farmers' adaptation strategies to environmental degradation and climate change effects: A farm level study in Bangladesh. Climate 2014;2(4):223-41.

Uddin MT, Takeya H. Resource interdependence and enterprise combination of integrated farming in some selected areas of Bangladesh. Pakistan Journal of Biological Sciences 2005; 8(3):405-12.

Varadan R, Kumar P. Indigenous knowledge about climate change: Validating the perceptions of dryland farmers in Tamil Nadu. Indian Journal of Traditional Knowledge 2014; 13(2):390-7.

West CT, Roncoli C, Ouattara F. Local perceptions and regional climate trends on the Central Plateau of Burkina Faso. Land Degradation and Development 2008;19(3):289-304.

Yamin F, Rahman A, Huq S. Vulnerability, adaptation and climate disasters: A conceptual overview. IDS Bulletin 2005;36(4): 1-14.

Yu W, Alam M, Hassan A, Khan AS, Ruane AC, Rosenzweig C, et al. Climate Change Risks and Food Security in Bangladesh. Routledge; 2010.

Agricultural Land Dryness Distribution Using the Normalized Difference Drought Index (NDDI) Algorithm on Landsat 8 Imagery in Eromoko, Indonesia

Mujiyo Mujiyo*, Ramadhina Nurdianti, Komariah, and Sutarno

Department of Soil Science, Faculty of Agriculture, Universitas Sebelas Maret, Surakarta 57126, Indonesia

ARTICLE INFO

Received: 28 Apr 2022
Received in revised: 22 Sep 2022
Accepted: 26 Sep 2022
Published online: 30 Jan 2023
DOI: 10.32526/ennrj/21/202200157

Keywords:
Estimation model/ Land drought category/ Soil evaporation/ Soil moisture

*** Corresponding author:**
E-mail: mujiyo@staff.uns.ac.id

ABSTRACT

The study area, Eromoko, has agricultural land covering 79.76% of the area, which experiences drought every year, causing a decrease in crop yields. Information on agricultural land dryness is needed to reduce the impact of dryness conditions on the agricultural sector. The effect of drought can be minimized using the transformation of the Normalized Difference Drought Index (NDDI) algorithm on Landsat 8 Imagery because it is considered capable of being used for land drought analysis that is accurate and efficient in time and cost. This study created a model for estimating soil moisture with actual soil moisture as the dependent variable and NDDI as the independent variable in several agricultural land uses in Eromoko. The results showed that the estimation model could estimate soil moisture with accuracy in plantations at 85.31%, irrigated paddy fields at 75.99%, rainfed paddy fields at 76.62%, and moors at 88.48%. The dryness category in the study area is 3,314.82 ha (35% of the total area). The variability of land use greatly affects the drying conditions. Dryness conditions can be reduced by controlling the dryness factors. Mitigation efforts to maintain soil moisture include irrigation planning based on the estimation model, applying bio-mulch and organic mulch, organic fertilization, and meeting water requirements in the harvesting period.

1. INTRODUCTION

Drought causes insufficient soil moisture for plant needs due to a lack of long-term rainfall (Liu et al., 2021). Drought in Indonesia is related to the El-Nino Southern Oscillation (ENSO) phenomenon, where rainfall has decreased sharply compared to normal conditions during the dry season. Central Java Province is one of the regions in Indonesia that is affected by the ENSO phenomenon. The impact is a decrease in rainfall in September-October-November (Hidayat et al., 2018), and drought may become a major disaster in areas with low rainfall intensity (Wild, 1993).

Drought is characterized by a water shortage for domestic and agricultural use, affecting soil moisture content and watersheds (Orimoloye et al., 2020). Dry agricultural land is limited by high soil particle cohesion due to low groundwater potential, which inhibits plant root growth. This condition causes plant growth to be disrupted and results in low crop productivity. Drought causes a decrease in paddy yields by up to 68% (Polthanee and Promkhambut, 2014). The dry season in Wonogiri Regency causes paddy production to decrease and the area of fallow land to increase (Central Bureau of Statistics of Wonogiri Regency, 2020). Corn yields in rainfed land have reduced due to drought (Popova et al., 2014), and teak crops are affected because of the decreasing trunk diameter and height, and wood quality with irregular stem shape (Eliyani et al., 2005).

Agricultural land in Eromoko District dominates the area, as much as 79.76% of the total area, so most of the population's livelihood is in farming. In the dry season, drought is the main problem because of the low rainfall creating drought and decreasing food production yields to crop failure (Ignatius, 2013). Eromoko is located in the Wonosari geological formation. It has a limestone parent rock

Citation: Mujiyo, Nurdianti R, Komariah, Sutarno. Agricultural land dryness distribution using the normalized difference drought index (NDDI) algorithm on Landsat 8 imagery in Eromoko, Indonesia. Environ. Nat. Resour. J. 2023;21(2):127-139. (https://doi.org/10.32526/ennrj/21/202200157)

(Bronto et al., 2009) with limestone parent material that has soil problems in water availability (Finch et al., 2014) because of a shortage of water in the root layer soil due to the water movement into the soil (Maulana, 2019).

Drought disasters due to low rainfall directly correlate with unavoidable global CO_2 emissions (Benti and Abara, 2019), but the impact on agriculture can be minimized by monitoring to obtain information on the latest land drought conditions. The method by the National Agency for Disaster Countermeasure, and Indonesian Agency for Meteorological, Climatological, and Geophysics, is based on regional rainfall data (National Disaster Management Coordinating Board, 2007). The observation data of climate stations do not have a sustainable spatial range to obtain spatial characters and patterns of dry conditions (Gu et al., 2007). The use of variables from remote sensing can provide more comprehensive information on drought conditions. Remote sensing data is needed to monitor and evaluate agricultural land's drought conditions. Using remote sensing data in the form of Landsat 8 images can be one solution for the drought monitoring method because of its high spatial and temporal resolution and also efficient use of time and cost (Hazaymeh and Hassan, 2017). Landsat 8 imagery has a spatial resolution of 30 meters and a temporal resolution of 16 days (USGS, 2008), so it can be used to assess agricultural land dryness. The results of the Normalized Difference Drought Index (NDDI) transformation into a drought index are used to provide information on the dryness of agricultural land. This index is used because it is the result of calculations from the Normalized Difference Vegetation Index (NDVI) and Normalized Difference Water Index (NDWI) transformations so that it has a higher sensitivity level to drought (Dobri et al., 2021).

This study aimed to identify dry conditions with a soil moisture estimation model, and find the factors of land characteristics and soil conditions that determine dry conditions, so that they can provide recommendations regarding appropriate mitigation efforts in the agricultural area of Eromoko District, Wonogiri Regency, Indonesia. Variables of soil moisture content (pF 2.5 and 4.2) and NDDI were used in simple regression analysis to obtain a model for soil moisture estimation. This estimation model is then used to obtain a dry category on agricultural land and also used to determine the area that requires additional irrigation water and the required volume of water.

2. METHODOLOGY

2.1 Study area

The study was conducted on agricultural land consisting of a plantation, irrigated paddy fields, rainfed paddy fields, and a moor in Eromoko District, Wonogiri Regency, Indonesia. The study area was located at coordinates 110°45'38,814" - 110°53'39,955" E and 7°53'41,425" - 8°1'52,644" S (Figure 1). Eromoko has an agricultural land area of 9,600 ha (79.76% of the Eromoko area) (Central Java Geoportal, 2019). The plantation has dominant plants of teak, acacia, and mahogany. The irrigated paddy fields are used for paddy and maize cultivation in the dry season. Some rainfed paddy fields and the moor have springs and pump wells are used for seasonal crop cultivation. Rainfed paddy fields are used for tobacco and bulrush, while the moor is used for cassava and bulrush.

Geologically, the study area is located in the Wonosari Formation and has limestone parent rocks (Bronto et al., 2009). Soil types at the research site are Alfisol and Inceptisol. The topography is in the form of various slopes with a range of 2% up to 40%. Eromoko District is a dry land with an annual rainfall of 1,600 up to 1,800 mm/year, classified as low-intensity rainfall. The lowest daily temperature in a year is 18.5ºC, and the highest is 37ºC (Research Agency for Solo Watershed Area, 2020).

2.2 Land observation and sampling method

The study approaches remote sensing data used, field surveys, laboratory analysis, and statistical data analysis. The variables observed in this study were the NDDI, soil moisture content, soil water retention (pF 2.5 and 4.2), and agricultural land characteristics in Eromoko District. The variability of land characteristics provided an image of Landsat 8 by radiometric and geometric corrections (Burapapol and Nagasawa, 2016). The working map is based on an overlay of land use, soil types, slopes, and rainfall map (Figure 2), and the result is named a land unit. The selection of sample points based on the similarity of land units assumes that it has similar land characteristics.

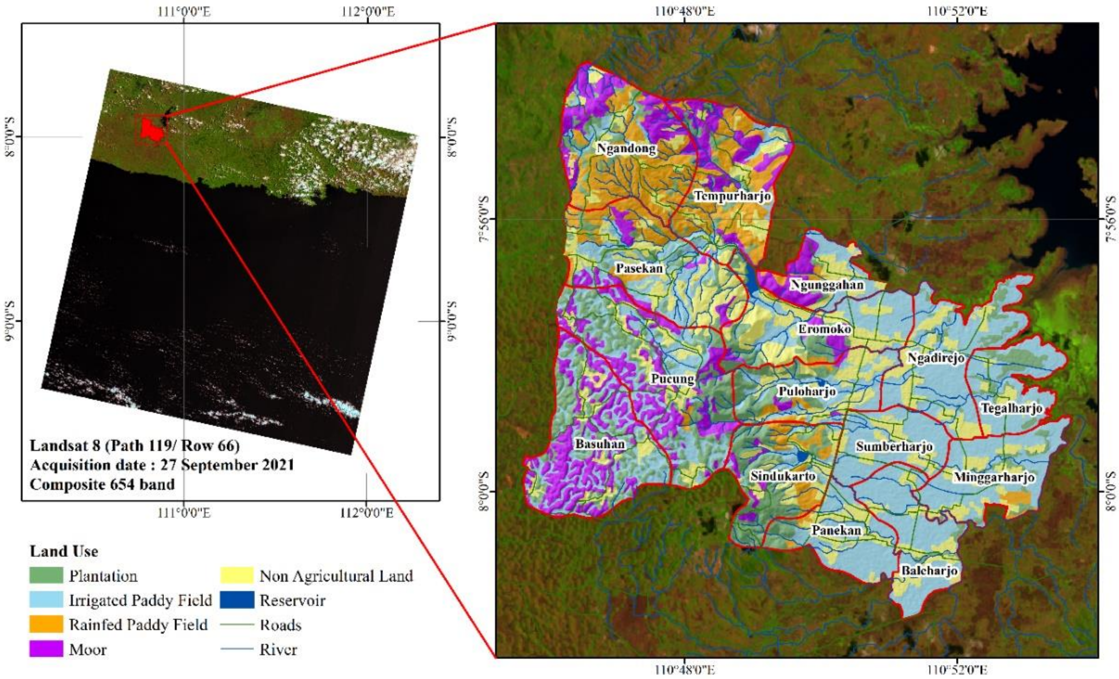

Figure 1. Study area location

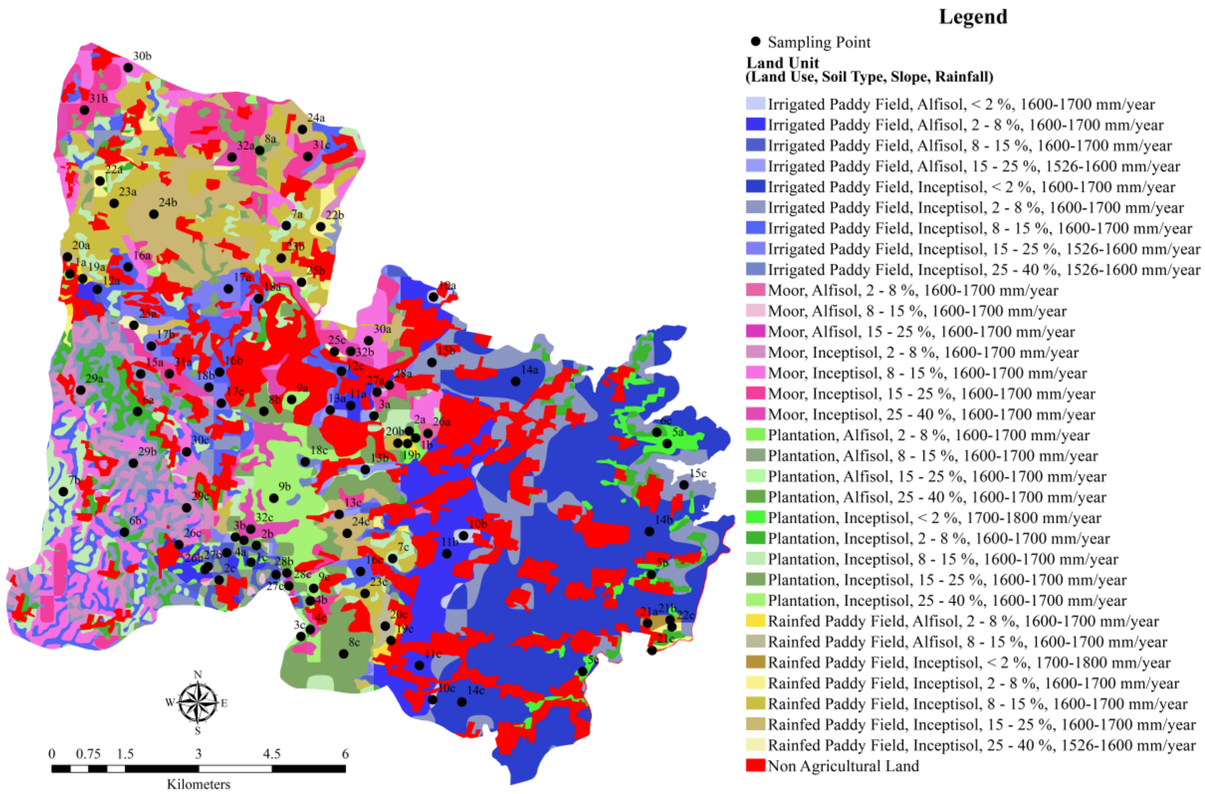

Figure 2. Land unit of study area

Sample points are determined by using the purposive random sampling technique. Based on the land characteristics map results, the agricultural land in Eromoko District is divided into 32 land units, each repeated three times. Hence, the total is 96 sample points. Soil samples were collected by a ring sampler with a diameter of 7.63 to 7.93 cm at each observation point. The type of sample is an undisturbed sample. Soil samples were then used to analyze actual soil moisture content, soil moisture content at pF 2.5 (field capacity), and soil moisture content at pF 4.2 (permanent wilting point).

2.3 Laboratory analysis

Soil parameters that needed laboratory analysis were actual soil moisture (using the gravimetric method) and soil water retention (using the pressure plate apparatus method). The principle of the gravimetric method is the measurement of water loss based on the weight of the soil sample before and after being dried at a temperature of 110ºC in an oven (Adimihardja et al., 2006). The principle of the pressure plate apparatus method is applying pressure which is equal to the ability of the soil to pass water naturally, providing water for plants, and the moisture content of the soil where plants are unable to absorb water. Applying pressure to the saturated soil sample at an interval of 48 h until it reaches the given equilibrium point determines the moisture content (Sudirman et al., 2006).

2.4 Satellite image processing

Remote sensing data used in this study are Landsat 8 imagery red channel (band 4), near-infrared (band 5), and short-wave infrared (band 6). The satellite image recording time was on September 27th in, 2021. Processing of satellite image data was done in several steps:

2.4.1 Pre-processing

(1) Radiometric correction

Satellite image used for index processing went through radiometric correction. This stage aims to improve image quality which is influenced by the position of the sun and the atmosphere when recording. The study area has varied topography so radiometric correction is necessary (Fawzi and Husna, 2021) to change the digital number value to the reflectance value (Muchsin et al., 2022).

(2) Study area cropping

Image cropping aims to narrow the work area so the processing process can focus on the research area. The radiometrically corrected image is then cropped based on the research area's map of agricultural land use.

2.4.2 Processing

The algorithm used is a combination of the NDVI (greenness of vegetation) and NDWI (vegetation wetness). The NDDI algorithm is considered more accurate in detecting drought on agricultural land than using the NDVI or NDWI algorithms separately (Dobri et al., 2021). The NDDI transformation formula (Gu et al., 2007) is:

$$\mathrm{NDDI} = \frac{(\mathrm{NDVI} - \mathrm{NDWI})}{(\mathrm{NDVI} + \mathrm{NDWI})}$$

Where: NDVI=(Band 5 - Band 4)/(Band 5 + Band 4); NDVI=(Band 5 - Band 6)/(Band 5 + Band 6); Low NDVI and NDWI values will result in high NDDI values, meaning that the area is experiencing drought. The higher the NDDI value produced, the drier an area is.

2.5 Drought distribution

The dryness distribution on agricultural land in the study area was obtained from data on actual soil moisture content, soil moisture retention (pF 2.5 and 4.2), and soil moisture content estimation model resulting from NDDI transformation on Landsat 8 imagery. Each parameter is described as follows:

2.5.1 Soil moisture estimation model and its accuracy

Linear regression analysis is used to obtain an estimation model of soil moisture. The soil moisture data was used as the dependent variable, and the NDDI value as the independent variable. The soil moisture estimation model produces estimated soil moisture data. The estimation model accuracy test is carried out to see how accurate the model is. The accuracy test was performed using standard deviation calculation, standard error estimate (SE), minimum % error, maximum % error, minimum accuracy, and maximum accuracy (Akbari and Jatmiko, 2016).

2.5.2 Agricultural land drought spatial distribution

The dryness category of agricultural land was obtained by overlaying estimated moisture content and soil water retention data (pF 2.5 and 4.2). The dryness category is classified according to Table 1 (Adimihardja et al., 2006).

Table 1. Dryness category

Category	Description
Dry	Soil moisture < pF 4.2
Moist	Soil moisture pF 4.2 < actual soil moisture < soil moisture pF 2.5
Wet	Soil moisture actual > soil moisture pF 2.5

2.6 Dryness determinant factor

The dryness determinant factor describes the effect of land use variability (as land characteristics) on the dryness category. The dryness determinant factor was carried out by Analysis of Variance (ANOVA) and continued by DMRT to find the difference of dryness condition between several land uses, and considered as dryness factor.

3. RESULTS AND DISCUSSION

3.1 NDDI transformation on Landsat 8 imagery

Atmospheric factors strongly influence the recorded image data, so radiometric corrections are made to change the pixel value into the unit value of radiation energy received by the sensor. The radiometric correction process converts the digital number to reflectance value. The difference between the image before and after radiometric correction is seen based on the range of raster values before and after correction (Figure 3).

Original image data has a digital number value with a value range of thousands. The image data result of the radiometric correction has a reflectance value with a unit value. The digital number range value in band 6 is 5247 up to 41942. In band 5 it is 5635 up to 57789, and in band 4 it is 6237 up to 54771. The results of radiometric correction produced a range of reflectance in band 6 of 0.0057 up to 1, in band 5 of 0.0147 up to 1, and in band 4 of 0.028 up to 1 (Figure 3). Landsat 8 imagery that is used in index transformation needs to go through radiometric correction (Fawzi and Husna, 2021). Agricultural land dryness assessment through remote sensing is based on the greenness and wetness of vegetation through the use of a vegetation index which can then be developed into a drought index or determining dryness of area (Renza et al., 2010). Meteorological monitoring and prediction of drought are monitored through weather data from meteorological stations. The NDDI transformation combines the data obtained from NDVI and NDWI in a broader and more accurate range of transformation values with a difference of up to 5%. Through radiation absorption, NDVI measures the chlorophyll and mesophyll content of the vegetation canopy. In contrast, NDWI measures the humidity of the vegetation canopy based on the results of the moisture content and mesophyll content of the vegetation canopy spots. In the NDVI and NDWI transformations, the higher the resulting value, the higher the density and wetness of the vegetation in the area. Whereas in the NDDI transformation, the higher value indicates the drier an area.

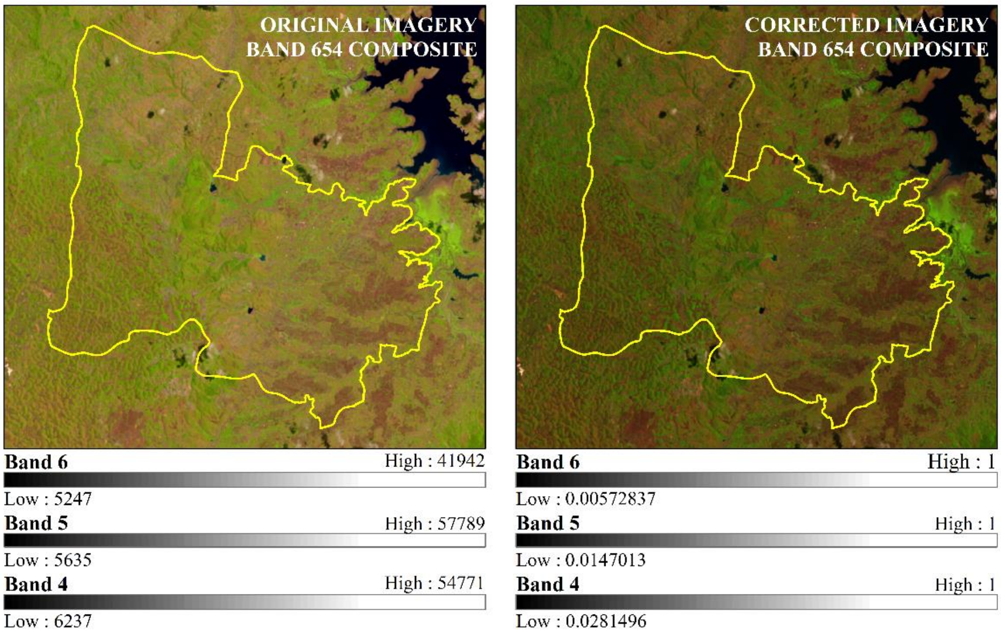

Figure 3. Radiometric correction

Based on the results of the index transformation in Figure 4, NDVI has a range of -0.179 up to 0.789 with a mean value of 0.49 and a standard deviation of 0.12. A higher NDVI value (dark green) indicates a greater density and photosynthetic capacity of the vegetation canopy (Gu et al., 2007). The results of the NDWI transformation have a range of -0.212 up to 0.610, with a mean value of 0.10 and a standard deviation of 0.11. A higher NDWI value (dark blue) indicates an area with high vegetation canopy wetness (Gao, 1996). The NDDI transformation combines the values of NDVI and NDWI to produce information on dry areas (dark red). The results of the NDDI transformation have a range of -1 up to 2 with a mean value of 0.76 and a standard deviation of 0.35. Areas that do not experience drought and are not dry areas are indicated by a Z-score <0, while areas experiencing drought are dry areas indicated by a Z-score >0 (Gulácsi and Kovács, 2018). Eromoko's agricultural land that has no dry conditions or did not experience drought was 6,078 ha, while dry conditions occurred in an area of 3,505 ha.

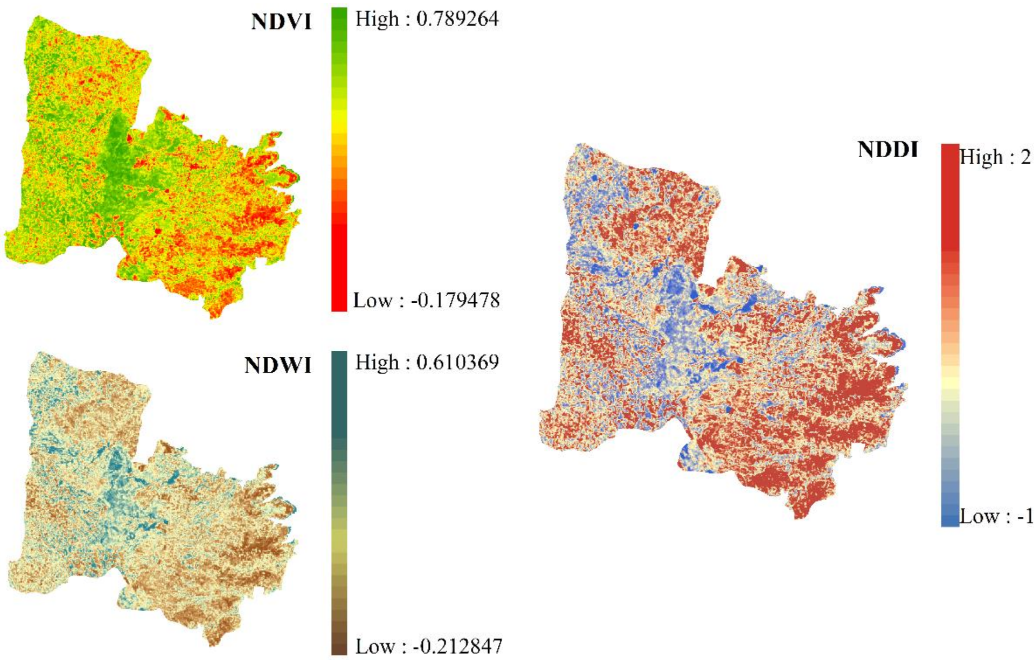

Figure 4. The transformation results

3.2 The distribution of agricultural land drought

This study uses estimated soil moisture data and actual soil moisture at pF 2.54 and 4.20 to determine the dryness category. Estimated soil moisture was obtained from linear regression analysis where actual soil moisture data was used as the dependent variable and NDDI value as an independent variable. Using one parameter without a combination of other parameters or indicator cannot determine condition in multi-scale and multi-impact drought (Hayes et al., 2012). Additional field hydrologic parameter, such as soil moisture, is needed to determine drought properties (Gulácsi and Kovács, 2018).

The condition of the soil moisture content in the study area shows different values for each land use. Moor and plantation land use have no additional moisture content, while irrigation paddy field and rainfed paddy field soil moisture levels are higher than other agricultural land uses. The condition of the actual average moisture content in several agricultural land uses in Eromoko are moor (25.38 %vol), plantation (26.40 %vol), rainfed paddy field (28.88 %vol), and irrigation paddy field (38.25 %vol), so it can be concluded that the condition of agricultural land in the study area has conditions of moderate moisture content and dryness category at dry to moist levels that is affected differently by land use.

In the estimation model of soil moisture content obtained in the study area, it can be predicted that in each increase in NDDI value, the soil moisture in the plantation decreases by 20.275%, in irrigated paddy fields by 28.525%, in rainfed paddy fields by 49.585%, and in moor 17.073% (shown in Table 2). Estimated soil moisture cannot be estimated accurately or is not always the same as the actual soil moisture content. Estimated soil moisture content can approach the actual soil moisture content but is less able to predict soil moisture content with a high value. Estimated soil moisture in the study area has a maximum accuracy to be used on a plantation, irrigated paddy fields, rainfed paddy fields, and moor of 85.31%, 75.99%, 76.62%, and 88.48%, respectively (Table 2). Based on the study results by Burapapol and Nagasawa (2016), the accuracy of the estimated soil moisture model was found to be 76.65% and consistent with actual and estimated soil moisture. The moisture content accuracy model produced in this study ranges from 74.76% up to 88.48% in the dryness category, so it has sufficient value to predict dry conditions for each agricultural land use in the study area. The spatial resolution of Landsat 8 imagery and cloud pixels estimates low groundwater content in an area (Fawzi and Husna, 2021). In addition, there are paddy cultivation activities that are in the ripening phase, where there are paddy panicles and yellowing leaves, so NDDI cannot show detailed results of the paddy condition that is experiencing dry conditions or not (Sukmono, 2018).

Table 2. Accuracy of soil moisture estimation model

Agricultural land	Soil moisture estimation	Standard error	Minimum accuracy (%)	Maximum accuracy (%)
Plantation	-20.275(NDDI) + 39.804	4.02	84.21	85.31
Irrigation paddy field	-28.525(NDDI) + 54.528	9.41	74.76	75.99
Rainfed paddy fields	-49.585(NDDI) + 60.945	6.98	75.03	76.62
Moor	-17.073(NDDI) + 36.640	3.03	87.59	88.48

The distribution map of estimated soil moisture on agricultural land in the Eromoko was made based on the soil moisture estimation model calculation on the results of the NDDI transformation. The darker blue indicates the higher soil moisture in the area, while the darker red on the map shows the lower soil moisture. Figure 5 shows that the dry conditions of the study area are seen from the estimation model results, which show areas with a dominance of low soil moisture content and high NDDI values. The estimated soil moisture using NDDI can indicate dry vegetation Burapapol and Nagasawa (2016).

Estimated soil moisture has a very significant positive correlation with leaf moisture content, so an increase will follow any increase in predicted water content in leaf water content which can be an indication of dry vegetation. Dry conditions and crop water requirements can be identified by determining tissue water status at the organ and canopy to improve the sustainability of food security and water use in agricultural land (Browne et al., 2020). Identification of dry vegetation and remote sensing monitoring with leaf water content could accurately reflect the level of dry plants and predict plant growth and development capabilities (Song et al., 2021). The estimated soil moisture content in this study provides the information that the leaf water content of vegetation in the Eromoko agricultural land mostly has low water content and impacts low crop production.

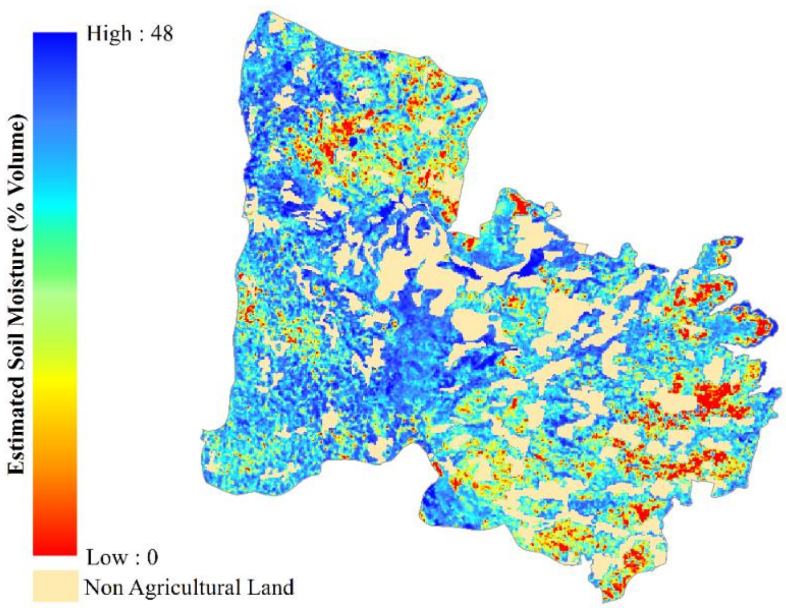

Figure 5. Distribution of estimated soil moisture

The dryness category is determined based on the estimated soil moisture amount toward soil moisture at field capacity (pF 2.54) and permanent wilting point (pF 4.20) amount (Figure 6). Field capacity represents the maximum amount of soil moisture in the soil, and field capacity is a condition of soil moisture that plants cannot uptake because the soil holds the water too tight. The difference between the amount of soil moisture at field capacity and permanent wilting point represents soil moisture availability (Voroney, 2018). Based on Table 1, it can assume that areas with the dry category are experiencing drought in the dry period of the year, and areas with the moist and wet category are not experiencing drought. The overlay of the estimated soil moisture map with soil moisture at pF 2.54 and 4.20 map result is shown in Figure 7. The agricultural land dryness condition is dominated by the moist category of 5,205.20 ha (55.17% of the study area), the dry category of 3,314.82 ha (35.13% of the study area), and the wet category of 915.30 ha (9.70% of the study area) (Figure 7). Each land use has the highest percentage of dryness conditions in the moist category, followed by the dry and wet categories (Table 3).

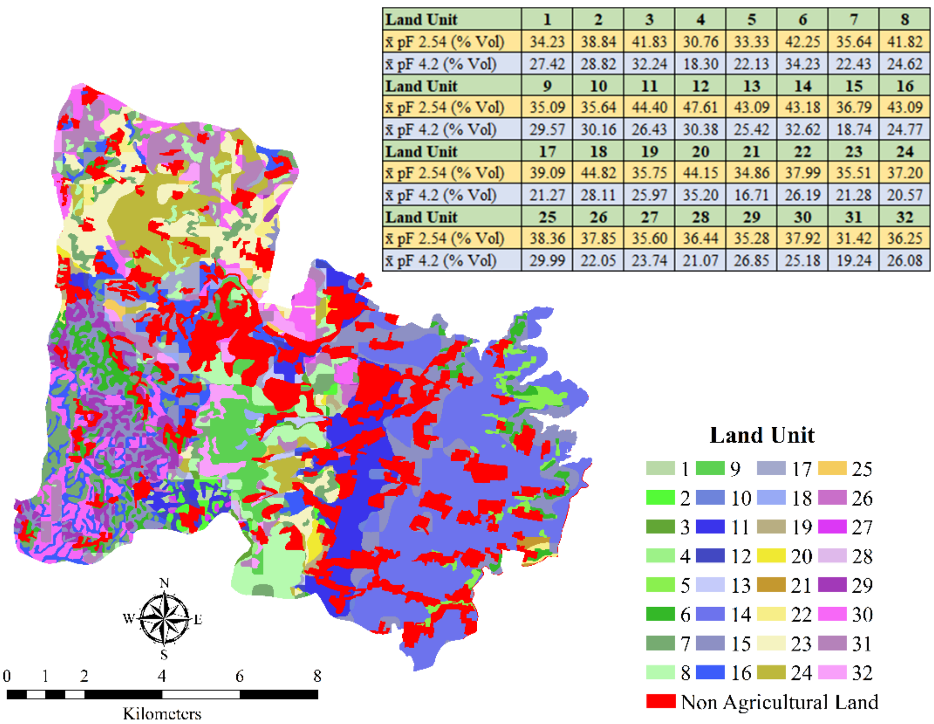

Land Unit	1	2	3	4	5	6	7	8
x̄ pF 2.54 (% Vol)	34.23	38.84	41.83	30.76	33.33	42.25	35.64	41.82
x̄ pF 4.2 (% Vol)	27.42	28.82	32.24	18.30	22.13	34.23	22.43	24.62
Land Unit	**9**	**10**	**11**	**12**	**13**	**14**	**15**	**16**
x̄ pF 2.54 (% Vol)	35.09	35.64	44.40	47.61	43.09	43.18	36.79	43.09
x̄ pF 4.2 (% Vol)	29.57	30.16	26.43	30.38	25.42	32.62	18.74	24.77
Land Unit	**17**	**18**	**19**	**20**	**21**	**22**	**23**	**24**
x̄ pF 2.54 (% Vol)	39.09	44.82	35.75	44.15	34.86	37.99	35.51	37.20
x̄ pF 4.2 (% Vol)	21.27	28.11	25.97	35.20	16.71	26.19	21.28	20.57
Land Unit	**25**	**26**	**27**	**28**	**29**	**30**	**31**	**32**
x̄ pF 2.54 (% Vol)	38.36	37.85	35.60	36.44	35.28	37.92	31.42	36.25
x̄ pF 4.2 (% Vol)	29.99	22.05	23.74	21.07	26.85	25.18	19.24	26.08

Figure 6. Soil moisture at field capacity (pF 2.54) and permanent wilting point (pF 4.20)

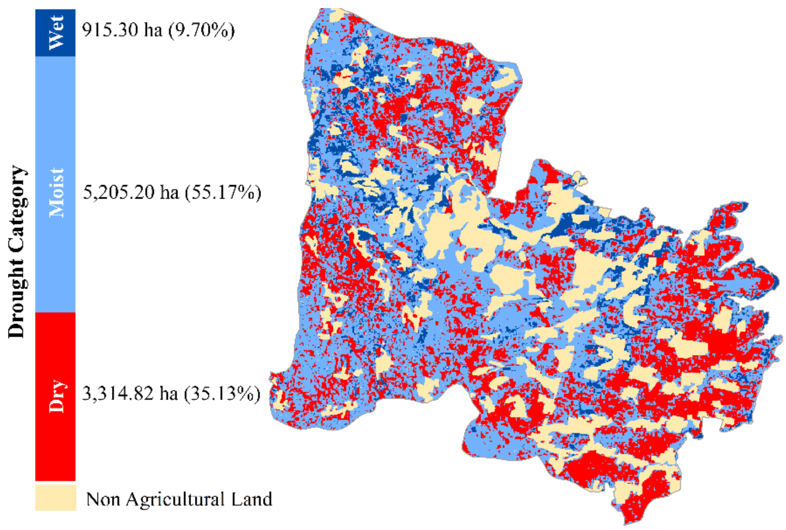

Figure 7. Distribution of agricultural land drought

Table 3. Dryness category in study area

Agricultural land	Dryness category	Area (ha)
Plantation	Dry	724.47
	Moist	1,273.79
	Wet	26.03
Irrigated paddy field	Dry	1,499.33
	Moist	2,153.85
	Wet	630.04
Rainfed paddy field	Dry	540.22
	Moist	641.48
	Wet	230.36
Moor	Dry	550.80
	Moist	1,136.07
	Wet	28.86

The plantation has the highest percentage area in a moist category based on the condition of the planted land having dense canopy, which causes little sunlight to reach the soil resulting in low evaporation (Shahidan et al., 2007). The existence of teak gives lower light intensity, as much as 45.13% (5 years teak) and 38.76% (7 years teak), which will reduce evaporation and micro temperature so the soil moisture will be maintained (Maharani et al., 2022). A cover crop of the plantation is often found to cause a decrease in solar radiation received by the soil and maintain soil moisture by evaporation (Kaye and Quemada, 2017; O'Connell and Snyder, 1999). The majority of teak plantations found in Eromoko are cultivated on dry land with rocky soil, high slope, and no irrigation, making this land use drier in the dry season. The teak tree has a wide leaf shape that can intercept rainwater, so the raindrops that fall on the leaves' surface will accumulate and form more giant raindrops. The accumulated raindrops fall to the ground surface with a greater kinetic energy that can result in large runoff (Kusumandari et al., 2020). The infiltration runs faster on land with high vegetation cover (Archer et al., 2016). Similar results were also reported by (Yang et al., 2014), who found that the introduced vegetation has lower soil moisture and is drier than mature trees because of the low soil infiltration.

The irrigated paddy fields are mostly cultivated with paddy that is in the generative phase towards the harvest phase in the third cropping period, and the soil conditions are moist to dry (Ghazali et al., 2020), while the soil conditions in the vegetative to generative phase is wet to moist (Domiri, 2017). The need for water during the productive phase of lowland paddy is lower than during the vegetative phase because the water requirement for the growth of plant parts is higher in the vegetative stage. Irrigated paddy fields that were mostly in the dry category were caused by the harvested condition and were not being cultivated, so the moisture content in the soil evaporated but did not receive water input (Ghazali et al., 2020). Growing paddy crops during this stage increases the water on the soil surface and decreases the evaporation beneath the canopy. Irrigated paddy fields are land with intensive tillage, which causes a decrease in the ability of the soil to hold water and reaches a permanent wilting point on day 5 after irrigating at a depth of 0-20 cm (Wahyunie et al., 2012).

Rainfed paddy fields and the moor is dry land that theoretically experience the greatest percentage of the dry category during the dry season. According to the study results, the moist category dominates in dry land. Some of the lands that have springs or pump wells are still used for irrigating cultivation during the dry season. Most of the dry land is planted with teak at the land edge and boundary so that the canopy can reduce the solar radiation received by the soil (Shahidan et al., 2007). The condition of land that has a dry category in rainfed paddy fields and the moor is caused by the absence of cover trees around the land so that the water in the soil continues to evaporate. Still, there is no water input, or it is not used for cultivation.

Hydrological indicators such as evapo-transpiration, infiltration, and water stage strongly connect with land cover and land use (Srivastava et al., 2020). In the study area, the variability of land use has a very significant effect on the dryness distribution (F-count=4.706; p-value=0.001; n=96). Dry condition in moor is not significantly different compared to plantation and rainfed paddy fields, while the dry condition in rainfed paddy fields was not significantly different compared to moor and irrigated fields. The highest dry condition occurred on a plantation, while the lowest occurred in irrigated paddy fields (Table 4). Land use affects dry conditions because it is related to water input and different types of vegetation resulting in the quantity of evaporation and sunlight absorption into the soil.

The plantation has the lowest available water potential compared to dry land (forest and moor), with low organic matter content resulting in a decreased ability of the soil water holding capacity (Faiz and Prijono, 2021), and also low soil moisture content that continues to decrease along the increasing age of the tree due to the increased crop water requirements

(Abdallah et al., 2020). Rainfed and irrigated paddy fields are still used for cultivation, so the water irrigation is still conducted by farmers, resulting in moist to wet conditions.

Table 4. The difference dryness category means on several land use

Land use	n	Dryness category mean
Plantation	27	1.4444[a]
Moor	21	1.5714[ab]
Rainfed paddy field	21	1.8571[bc]
Irrigated paddy field	27	2.1852[c]

The values followed by the same letter are not significantly different at = alpha 0.05.

The moor has no significantly different dry conditions compared to the plantation because in the dry season and post-harvest period, most of the land is not used for cultivation, and there is no water input from irrigation or rainfall. The effect of soil tillage on rainfed paddy fields and moor makes the soil more easily eroded, which can decrease the availability of soil organic matter that does not support the process of water absorption into the soil and soil water holding capacity (Busari et al., 2015).

3.3 Drought mitigation recommendations

To minimize the effects of drought conditions in the study area, mitigation activities are taken to fix the factors that determine dry conditions, such as adopting appropriate agricultural technologies (Adunya and Benti, 2020). The condition of available soil moisture content of less than 50% would disrupt plant growth (Adimihardja et al., 2006). In this study, the recommended mitigation effort is to add irrigation water. Furrow-irrigated paddy with organic matter can avoid drought stress and dry condition of soil because it can increase infiltration and soil moisture and reduce surface runoff (Tarigan et al., 2019).

The calculation of the additional irrigation water to reach 60% at pF 4.2 (field capacity) is carried out to maintain sufficient water conditions for plants and the efficiency of the distribution of irrigation water reserves. Based on data on the spatial distribution of estimated soil moisture content and soil moisture retention, information on the additional irrigation water volume is presented in Figure 8.

Estimated soil moisture can be used to predict and manage irrigation water. Agricultural land with the highest percentage requiring additional irrigation water is 85.82% of the moor, with a total area of 1,472.40 ha of additional irrigation water needs. Irrigated paddy fields are land with a lower percentage of the area that needs additional irrigation water, which is 62.22%. The location of irrigated paddy fields is traversed by rivers that have water flow during the dry season so that they still get a supply of water all year.

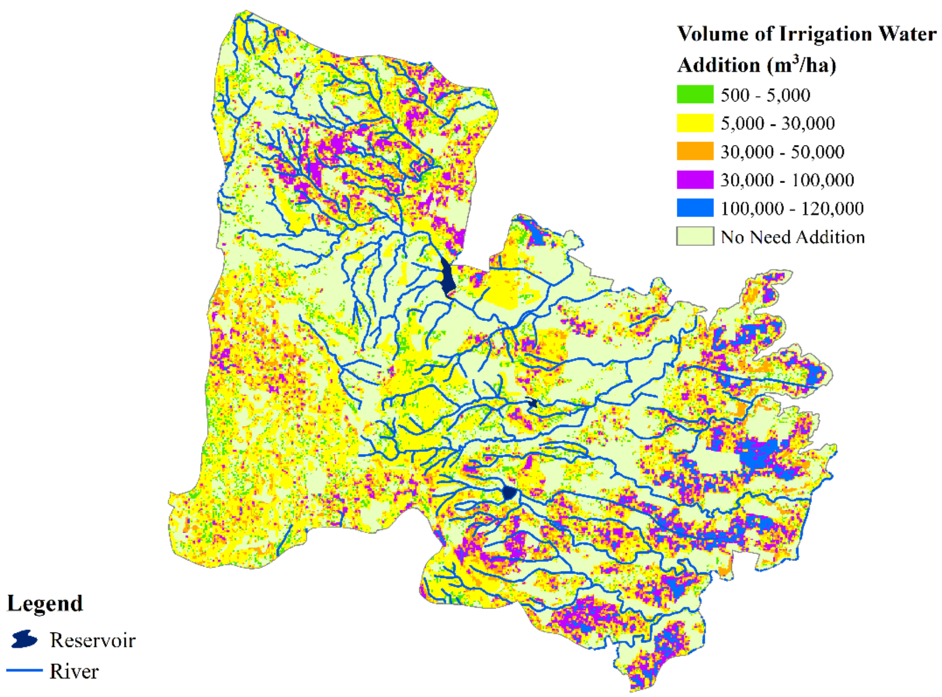

Figure 8. Irrigation water volume requirements on agricultural land

Minggarharjo Village has the largest need for additional water irrigation (21,961,825.89 m^3) and the second largest area of irrigated paddy fields (449.33 ha) in Eromoko District (Table 5), so it becomes a priority village for additional water irrigation. Irrigation water for Minggarharjo Village can be obtained from the irrigation canals of Song Putri Reservoir (Central Java Geoportal, 2019). In addition to using additional irrigation water, there are several recommendations for mitigation efforts to reduce the impact of drought on agricultural land by increasing soil water holding capacity. Using organic mulch as a cover crop *Crotalaria juncea* can increase soil water holding capacity by 56.9% and soil moisture content by up to 68.5% at a depth of 30 cm on plantation land (Reddy and Ramkumar, 2011).

The application of organic mulch gave better results than the control to create an optimal growing environment for the growth of areca nut seedlings because it provides water content to support the growth after germination (Syaranamual et al., 2022). Using cow dung and compost as organic fertilizer can hold water in the soil and be used by plants, thereby increasing plant growth and water use efficiency (Vengadaramana and Jashothan, 2012). Paddy cultivation without flooding with straw mulch application can optimize water use in drought areas in southeastern China (Qin et al., 2006). In dry lands that depend on rainfall as input for irrigation water, water harvesting is one of the efforts to fulfill crop water needs (Velasco-Muñoz et al., 2019). Harvesting of rainwater is carried out in the rainy season by making a rorak/dam so that water reserves can be utilized during the dry season and extend the planting period (Noelle et al., 2018).

Table 5. The volume of additional water irrigation and area of irrigation paddy field

Location	Additional irrigation water (m^3)	Area of irrigation paddy field (ha)
Minggarharjo	21,961,826	449.33
Tempurharjo	20,998,964	71.12
Baleharjo	18,265,298	443.56
Pucung	18,167,012	387.73
Basuhan	17,777,906	346.45
Ngadirejo	16,773,782	594.83
Tegalharjo	15,912,524	338.03
Ngandong	15,302,497	58.85
Sindukarto	14,615,865	76.46
Panekan	12,680,052	326.92
Sumberharjo	7,971,619	367.31
Eromoko	7,883,831	267.48
Ngunggahan	5,632,634	120.91
Pasek	5,535,389	308.75
Puloharjo	4,740,333	212.25

4. CONCLUSION

The estimation model of soil moisture can be used to estimate soil moisture in a range of about 74.76% up to 88.48%, with maximum accuracy in each plantation at 85.31%, irrigated paddy fields at 75.99%, rainfed paddy fields at 76.62%, and the moor at 88.48%. The moist category in 5,205.05 ha dominates the distribution of the dryness in agricultural land at Eromoko. The dry category is 3,314.82 ha and the wet category is 915.30 ha. The variability of land use greatly affects dryness conditions. Dryness conditions can be minimized by fixing the dryness factors. Dryness mitigation efforts can be made by calculating irrigation needs obtained through the results of the estimation model of soil moisture and soil water retention data, the use of organic mulch, the addition of organic matter, and water requirements in the harvesting period. By mapping dryness conditions on agricultural land, future land use can be adjusted between the actual physical condition of the soil and its utilization in more detail. A future perspective is an estimation of land dryness based on each land use using GIS technology can be carried out regularly by policyholders and the government as an alternative way to minimize drought disasters, decreased crop productivity, and soil degradation.

ACKNOWLEDGEMENTS

This research was supported by Universitas Sebelas Maret under the research grant 2022. The authors would thank to GIFU Laboratory Station, Government of Eromoko District, Wonogiri survey team (M. Arsya, M. Agan, Reza EP) and Tiara Hardian for their participation in the paper elaboration.

REFERENCES

Abdallah MAB, Durfee N, Mata-Gonzalez R, Ochoa CG, Noller JS. Water use and soil moisture relationships on western juniper trees at different growth stages. Water 2020;12(6): 26-31.

Adimihardja A, Haryati U, Juarsah I. Determination of soil moisture content using the gravimetric method. In: Technical Manual for Soil Physics Analysis. Bogor: Indonesian Center for Agricultural Land Resources Research and Development; 2006. p. 132-42.

Adunya T, Benti FC. The impacts of climate-induced agricultural drought on four cereal crops: A case study in Bako Tibe District, Oromia National Regional State, Ethiopia. Caraka Tani: Journal of Sustainable Agriculture 2020;35(1):135-46.

Akbari AN, Jatmiko RH. Utilization of landsat 8 oil images and geographic information systems for soil organic matter content mapping in Karanganyar Regency. Jurnal Bumi Indonesia 2016;5(1):10-1.

Archer NAL, Otten W, Schmidt S, Bengough AG, Shah N, Bonell M. Rainfall infiltration and soil hydrological characteristics below ancient forest, planted forest and grassland in a temperate northern climate. Ecohydrology 2016;9(4):585-600.

Benti F, Abara M. Trend analyses of temperature and rainfall and their response to global CO_2 emission in Masha, Southern Ethiopia. Caraka Tani: Journal of Sustainable Agriculture 2019;34(1):67-75.

Bronto S, Mulyaningsih S, Hartono G, Astuti. Parangjoho and songputri reservoirs: Alternative eruption sources for the semilir formation in the Eromoko area, Wonogiri Regency, Central Java. Indonesian Journal on Geoscience 2009; 4(2):79-92.

Browne M, Yardimci NT, Scoffoni C, Jarrahi M, Sack L. Prediction of leaf water potential and relative water content using terahertz radiation spectroscopy. Plant Direct 2020; 4(4):e00197.

Burapapol K, Nagasawa R. Mapping soil moisture as an indicator of wildfire risk using landsat 8 images in Sri Lanna National Park, Northern Thailand. Journal of Agricultural Science 2016;8(10):107-19.

Busari MA, Kukal SS, Kaur A, Bhatt R, Dulazi AA. Conservation tillage impacts on soil, crop and the environment. International Soil and Water Conservation Research 2015;3(2):119-29.

Central Bureau of Statistics of Wonogiri Regency. Harvest Area and Rice Production in Wonogiri Regency 2020. Wonogiri: Central Bureau of Statistics of Wonogiri Regency; 2020.

Central Java Geoportal. Geospatial data and information [Internet]. 2019 [cited 2021 Jul 15]. Available from: http://geoportal.jatengprov.go.id/.

Dobri RV, Sfîcă L, Amihăesei VA, Apostol L, Țîmpu S. Drought extent and severity on arable lands in romania derived from normalized difference drought index (2001-2020). Remote Sensing 2021;13(8):Article No. 1478.

Domiri DD. The new method for detecting early planting and bare land condition in paddy field by using vegetation bare water index. Proceedings of the 2nd International Conference of Indonesian Society for Remote Sensing (ICOIRS 2016); 2017 Dec 17-20; The Sahid Rich Jogja, Yogyakarta: Indonesia; 2016.

Eliyani, Handoko, Koesmaryono Y. Water deficit effect on growth of young fast growing teak (*Tectona grandis* L.F.). Agromet 2005;19(1):11-20.

Faiz AM, Prijono S. Differences in the ability of soil to hold water on various slopes of coffee land in the Sumbermanjing Wetan area, Malang Regency. Jurnal Tanah Dan Sumberdaya Lahan 2021;8(2):481-91.

Fawzi NI, Husna VN. Landsat 8: A Basic Processing Theory and Technique. Bengkulu: Elmarkazi Publisher; 2021.

Finch HJS, Samuel AM, Lane GPF. Soils and soil management. In: Lockhart and Wiseman's Crop Husbandry Including Grassland. 9th ed. England: Woodhead Publishing; 2014. p. 37-62.

Gao B-C. NDWI: A normalized difference water index for remote sensing of vegetation liquid water from space. Remote Sensing of Environment 1996;58:257-66.

Ghazali MF, Wikantika K, Harto AB, Kondoh A. Generating soil salinity, soil moisture, soil pH from satellite imagery and its analysis. Information Processing in Agriculture 2020; 7(2):294-306.

Gu Y, Brown JF, Verdin JP, Wardlow B. A five-year analysis of MODIS NDVI and NDWI for grassland drought assessment over the central Great Plains of the United States. Geophysical Research Letters 2007;34(6):1-6.

Gulácsi A, Kovács F. Drought monitoring of forest vegetation using modis-based normalized difference drought index in Hungary. Hungarian Geographical Bulletin 2018;67(1):29-42.

Hayes MJ, Svoboda MD, Wardlow BD, Anderson MC, Kogan F. Drought monitoring: Historical and current perspectives. In: Remote Sensing of Drought: Innovative Monitoring Approaches. CRC Press; 2012. p. 1-19.

Hazaymeh K, Hassan QK. A remote sensing-based agricultural drought indicator and its implementation over a semi-arid region, Jordan. Journal of Arid Land 2017;9(3):319-30.

Hidayat AM, Efendi U, Agustina L, Winarso PA. The correlation of the nino 3.4 index and the southern oscillation index (SOI) with variations in rainfall in Semarang. Journal of Science and Weather Modification Technology 2018;19(2):75-81.

Ignatius SR. Potential water resources and calculation of rainwater storage volume to overcome water shortage in South Wonogiri. Journal of Rural and Development 2013; 4(2):157-66.

Kaye JP, Quemada M. Using cover crops to mitigate and adapt to climate change: A review. Agronomy for Sustainable Development 2017;37(4):1-17.

Kusumandari A, Pratiwi I, Widiasmoro S. Run off prediction by using small plots at teak forest, dry land and settlement areas in Pitu village, Ngawi, East Java. IOP Conference Series: Earth and Environmental Science 2020;449:Article No. 012040.

Liu C, Yang C, Yang Q, Wang J. Spatiotemporal drought analysis by the standardized precipitation index (SPI) and standardized precipitation evapotranspiration index (SPEI) in Sichuan Province, China. Scientific Reports 2021;11(1):1-14.

Maharani D, Sudomo A, Swestiani D, Murniati, Sabastian GE, Roshetko JM, et al. Intercropping tuber crops with teak in

Gunungkidul Regency, Yogyakarta, Indonesia. Agronomy 2022;12(2):1-20.

Maulana FW. Aquifer potential of Eromoko Village, Eromoko District, Wonogiri Regency, Central Java Province based on geoelectrical data. Teknomineral 2019;1(2):79-87.

Muchsin F, Harmoko A, Prasasti I, Rahayu MI, Pradhono KA, Technology RS. Comparison of the radiometric correction of landsat-8 images based on object spectral response. International Journal of Remote Sensing and Earth Sciences 2022;18(2):177-88.

National Disaster Management Coordinating Board. Introduction to Disaster Characteristics and Mitigation Efforts in Indonesia. National Disaster Management Coordinating Board; 2007.

Noelle NM, Weru WP, Rodrigue SJ, Karlin G. The effects of drought on rice cultivation in sub-Saharan Africa and its mitigation: A review. African Journal of Agricultural Research 2018;13(25):1257-71.

O'Connell NV, Snyder RL. Cover crops, mulch lower night temperatures in citrus. California Agriculture 1999;53(5):37-40.

Orimoloye IR, Kalumba AM, Mazinyo SP, Nel W. Geospatial analysis of wetland dynamics: Wetland depletion and biodiversity conservation of Isimangaliso Wetland, South Africa. Journal of King Saud University - Sciences 2020; 32(1):90-6.

Polthanee A, Promkhambut A. Impact of climate change on rice-based cropping systems and farmers' adaptation strategies in Northeast Thailand. Asian Journal of Crop Science 2014;6(3):262-72.

Popova Z, Ivanova M, Martins D, Pereira LS, Doneva K, Alexandrov V, et al. Vulnerability of Bulgarian agriculture to drought and climate variability with focus on rainfed maize systems. Natural Hazards 2014;74(2):865-86.

Qin J, Hu F, Zhang B, Wei Z, Li H. Role of straw mulching in non-continuously flooded rice cultivation. Agricultural Water Management 2006;83(3):252-60.

Reddy RM, Ramkumar. Prospect and importance of green mulching on the soil status of tropical tasar plantation fields in India. Nature Precedings 2011;1-13.

Renza D, Martinez E, Arquero A, Sanchez J. Drought estimation maps by means of multidate landsat fused images. Proceedings of the 30th EARSeL Symposium Remote Sensing for Science, Education, and Natural and Cultural Heritage; 2010 31 May-3 Jun; París, Francia; 2010.

Research Agency for Solo Watershed Area. Daily rainfall data [Internet]. 2020. [cited 2021 Jul 15]. Available from: https://bbwsbengawansolo.id/.

Shahidan MF, Salleh E, Mustafa KMS. Effects of tree canopies on solar radiation filtration in a tropical microclimatic environment. Proceedings of the 24th Conference on Passive and Low Energy Architecture (PLEA2007); 2007 Nov 22-24; National University of Singapore, Singapore; 2007.

Song X, Zhou G, He Q. Critical leaf water content for maize photosynthesis under drought stress and its response to rewatering. Sustainability 2021;13(13):1-14.

Srivastava A, Kumari N, Maza M. Hydrological response to agricultural land use heterogeneity using variable infiltration capacity model. Water Resources Management 2020; 34(12):3779-94.

Sudirman, Sutono S, Juarsah I. Determination of groundwater retention in the laboratory. In: Technical Manual for Soil Physics Analysis. Bogor: Indonesian Center for Agricultural Land Resources Research and Development; 2006. p. 167-76.

Sukmono A. Rice fields drought identification using a combination of leaf water content index and vegetation index with landsat 8 imagery. Elipsoida: Jurnal Geodesi Dan Geomatika 2018;1(2):44-50.

Syaranamual S, Sipyan D, Tuhumena VL. The seedlings growth performance of areca nut palm (*Areca catechu* L.) Under different types of organic mulching. Caraka Tani: Journal of Sustainable Agriculture 2022;37(2):233-42.

Tarigan PL, Tohari T, Suryanto P. Physiological response of upland rice varieties to furrow with organic matter on agroforestry system with kayu putih (*Melaleuca leucadendra* L.). Caraka Tani: Journal of Sustainable Agriculture 2019; 34(2):223-31.

USGS. Landsat missions [Internet]. 2008 [cited 2021 Mar 31]. Available from: https://www.usgs.gov/core-science-systems/nli/landsat/landsat-8?qt-science_support_page_related_con=0#qt-science_support_page_related_con.

Velasco-Muñoz JF, Aznar-Sánchez JA, Batlles-delaFuente A, Fidelibus MD. Rainwater harvesting for agricultural irrigation: An analysis of global research. Water 2019;11(7):1-18.

Vengadaramana A, Jashothan PT. Effect of organic fertilizers on the water holding capacity of soil in different terrains of Jaffna peninsula in Sri Lanka. Journal of Natural Product Plant Resources 2012;2(4):500-3.

Voroney P. Soils for Horse Pasture Management. Horse Pasture Management: Elsevier Inc.; 2018. p. 65-79.

Wahyunie RE, Baskoro DPT, Sofyan M. Water retention capacity and resistence of soil penetration in intensive tillage system and conservation soil tillage. Journal of Soil Science and Environment 2012;14(2):73-8.

Wild A. Soils and the Environment: An Introduction. Melbourne: Cambridge University Press; 1993.

Yang L, Wei W, Chen L, Chen W, Wang J. Response of temporal variation of soil moisture to vegetation restoration in semi-arid Loess Plateau, China. Catena 2014;115:123-33.

Characteristics of Dissolved Organic Matter and Trihalomethane Forming Potential Occurrence in Watersheds with Different Upstream Land Use

Mila Dirgawati and Mohamad Rangga Sururi*

Institut Teknologi Nasional Bandung, Environmental Engineering Study Program, Bandung, Indonesia

ARTICLE INFO

Received: 19 Aug 2022
Received in revised: 12 Dec 2022
Accepted: 20 Dec 2022
Published online: 13 Feb 2023
DOI: 10.32526/ennrj/21/202200179

Keywords:
Upstream land use/ Chromophoric dissolved organic matter/ Total organic matter/ Dissolved organic matter/ Trihalomethanes forming potential

*** Corresponding author:**
E-mail: rangga@itenas.ac.id

ABSTRACT

Dissolved organic matter (DOM) is the most important natural organic matter (NOM) fraction which reacts with chlorine to form harmful trihalomethanes (THMs) in water bodies. The characteristics of DOM could be affected by land use in the catchment, hence comprehensive study to understand DOM in the water body is important. This study was conducted in two watersheds with different upper stream land use to determine: (1) water characteristics, total organic matter (TOM), and DOM quality and quantity based on optical and absorption properties; (2) fluorescence dissolved organic matter (FDOM) compounds; (3) TOM and DOM relationships; and (4) THMs forming potential (THMFP) in both watersheds. Samples were collected from the upper Cimahi and Cijanggel Rivers which are dominated by settlements and plantations, respectively. Water characteristics were determined by pH, electroconductivity (EC), nitrite, and nitrate in unfiltered and filtered samples. TOM and DOM were characterized by chemical oxygen demand (COD) and chromophoric DOM (CDOM) parameters (A_{254}, A_{355}, A3/4), and organic compounds were determined as FDOM compounds. The measured pH, nitrate, and nitrite in the settlements-impacted watershed were greater than those in the plantations-impacted watershed. The main FDOM compounds in the settlement-impacted river were tryptophan microbial byproduct (T1) and tryptophan aromatic protein (T2), fulvic acid (A), and humic acid (C). Meanwhile, in the plantations-impacted river were T1, A, and C. THMFP was detected in both rivers which were greater in the plantations-impacted watershed than the settlements-impacted watershed.

1. INTRODUCTION

The occurrence of organic matter in a water body is originated from the natural degradation process of organic substances in water as well as human activities. Dissolved Organic Matter (DOM) is the most important organic matter in the water body and it is the largest fraction of organic carbon in aquatic ecosystems (Leehneer and Croué, 2003). The presence of DOM in watersheds can originate from allochthonous input and autochthonous production. The main source of allochthonous is the terrestrial humic-rich compound which has aromatic characteristics (McKnight et al., 2001; Wolfe et al., 2002). Meanwhile autochthonous originates from the production by endogenous algae and macrophytes of protein-like compounds, as well as from organic matter degradation by microbes (McKnight et al., 2001; Wolfe et al., 2002). The quality of raw water sources for drinking water in most urban areas is deteriorated by urbanization, industrialization, climatic and environmental conditions, and changing land use, particularly in the upper catchment area where the water intake is typically located. The spatial and temporal variations of DOM characters in urban rivers can be mediated by local anthropogenic land uses, as reported by Baker et al. (2003). In a typical natural water body, the bioavailability of protein-like compounds is lower than those of humic-like compounds (Aschermann et al., 2016; Notodarmojo et al., 2017). However, other studies have reported that the local urban land uses are related to considerable changes in the inputs of the terrestrial humic-like compounds in the Zhujiang River (Meng et al., 2013) and Lake Tianmu (Shi et al., 2020). Sururi et al. (2021) have reported pollution in the Cikapundung River, the

Citation: Dirgawati M, Sururi MR. Characteristics of dissolved organic matter and trihalomethane forming potential occurrence in watersheds with different upstream land use. Environ. Nat. Resour. J. 2023;21(2):140-152. (https://doi.org/10.32526/ennrj/21/202200179)

main raw water source for Bandung City, Indonesia, by direct discharges of cattle manure, domestic and agricultural wastes, leading to an increment of protein-like DOM such as tryptophan in this urban river. Raw water with an abundant tryptophan-like compound enhances microbial metabolism stimulation, hence adding difficulties for conventional water treatment (WTP) which is mostly implemented in Indonesia and other developing countries to maximumly remove DOM (Sururi et al., 2020). However, in developing countries including Indonesia, the presence of organic matter is indicated by total organic matter (TOM) measurement instead of DOM and its optical properties parameters, due to limited water monitoring facilities and capability. Hence the influences of urban land use on DOM characteristics are poorly understood, and the specific characteristics of DOM compounds that react in and affect the drinking water treatment process remain unclear (Shi et al., 2021; Sururi et al., 2020). Given the fact that the river watershed is influenced by intense local urban activity, it is urgent to understand the effects of urban land use on the changes in DOM quantity and quality of water.

The composition and origin of DOM can be recognized as an important indicator of human impacts in a water body, specifically by the light-absorbing DOM fraction or chromophoric DOM (CDOM). CDOM parameters were able to indicate the origin of DOM (Dainard and Guéguen, 2013) and related to DOM composition (Artinger et al., 2000). CDOM parameters have been reported to be associated with DOM characteristics of conducting biogeochemical processing such as photochemical or microbial degradation (Korshin et al., 2009). Moreover, CDOM is very related to fluorescent dissolved organic matter or FDOM which represents the CDOM fraction that fluoresces. Hence FDOM is often used as a surrogate for CDOM particularly for tracking DOM in natural water bodies (Coble, 2007). CDOM parameters have also been linked to the presence of harmful trihalomethanes (THMs) in a watershed (Sururi et al., 2019). Nonetheless, previous studies in Indonesia did not focus on the characteristics of DOM and the THMs forming potential (THMFP) in the upstream watershed which is potentially affected by the land use feature. This study is the first to fill in the gap by investigating the characteristics of DOM and THMFP based on the land use differences of the catchment area in Indonesia.

We hypothesized that upstream land use can significantly alter the source and composition of DOM and THMFP in the raw water. Hence to test the hypotheses, we conducted two field sampling campaigns in two headwater rivers with different land use characteristics during the rainy season. The specific objectives of this study which was conducted in two watersheds with different upper stream land use were to determine (1) water characteristics, TOM and DOM quality and quantity based on their light-absorbing properties; (2) FDOM parameters and compounds; (3) TOM and DOM relationships; and (4) THMFP occurrence in both watersheds. A comprehensive understanding of the influence of land use on the characteristic of DOM in raw water sources is important to decide the best strategies for the water treatment process to ensure the production of safe drinking water in Indonesia. In addition, the link between TOM and DOM as well as their parameters will determine which parameter is better used for monitoring organic matter in raw water.

2. METHODOLOGY

2.1 Study area and sampling locations

This study was conducted in two urban watersheds with different land use in the catchment area: Cimahi River and Cijanggel River, West Java Province. The catchment of the Cimahi River consists of Citereup and Cibabat villages, with residentials occupying around 44% of the total area, followed by protected areas (29%) and green open spaces (10%). The catchment of the Cijanggel River includes Cihanjuangrahayu and Kertawangi Villages with plantations as the predominant land use (53% of the total area), followed by residentials which occupy 16% of the total area. The water sampling locations in the upper Cimahi River were located around 150 m before the intake of the conventional Water Treatment Plant (WTP). The water sampling point at the Cijanggel River was located approximately 100 m before the location of the water Cijenggel intake. The sampling locations can be seen in Figure 1.

2.2 Sampling period and methods

Grab sampling was carried out in the rainy season only. A more frequent sampling period was conducted in the Cimahi River than in the Cijanggel River because the catchment of the Cimahi River was considered more urbanized and impacted by human activities than that the Cijanggel River. The water sampling was carried out for 7 days between 13 Aug 2021-10 Sep 2021 at the Cimahi River, and 5 days from 8 to 12 Oct 2021 at the Cijanggel River.

2.3 Sample measurements and analysis

The analysis was conducted for two types of water samples: unfiltered and filtered samples. The characteristics of TOM were investigated using unfiltered samples which were obtained directly from the water samples without conducting any filtration process. The filtered samples were used to investigate the characteristics of DOM, which were were obtained by passing the samples through Advantec cellulose filter papers with a diameter of 47 mm and a pore size of 0.45 µm to remove suspended particulate matter.

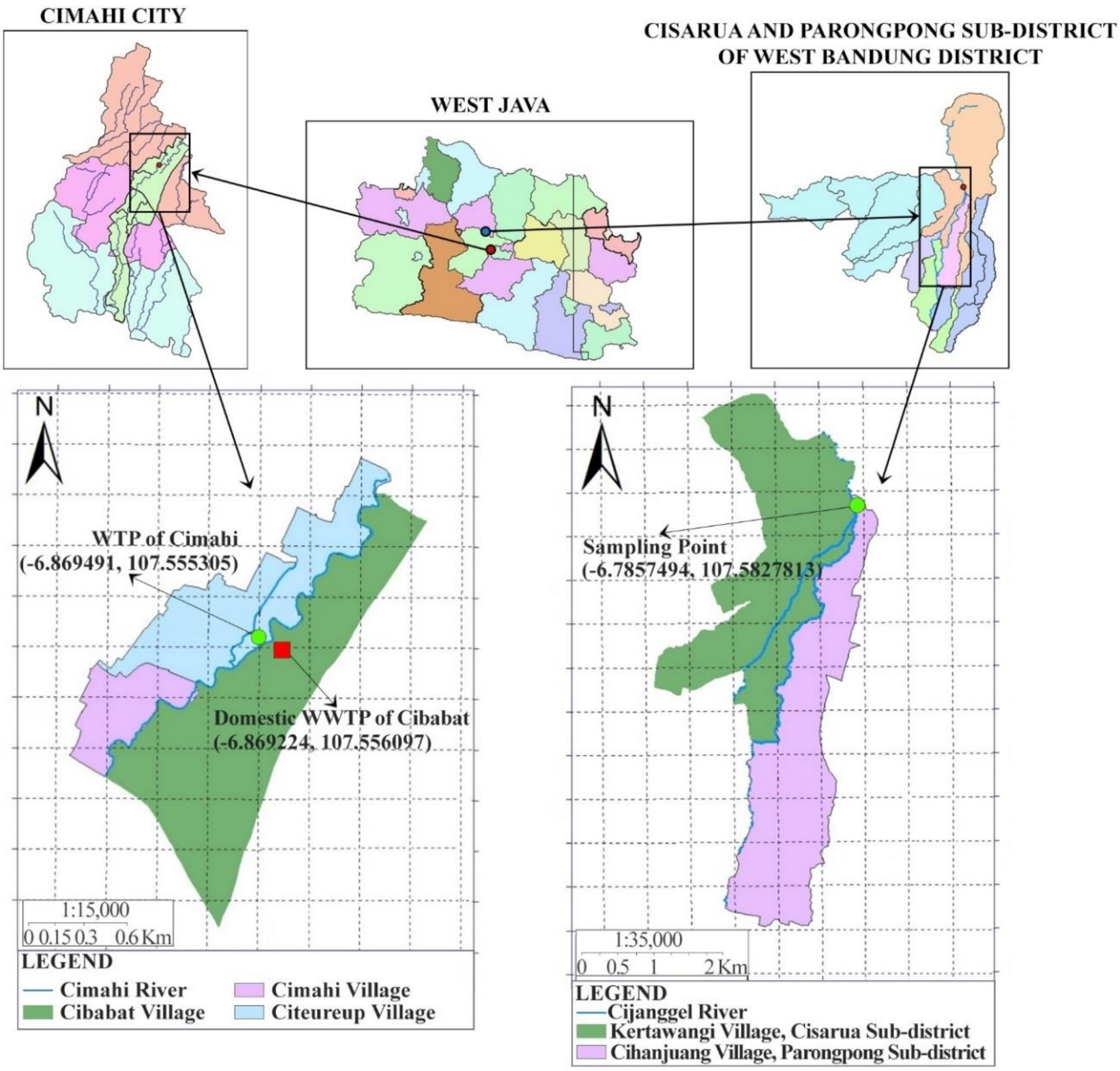

Figure 1. Study area and sampling locations

2.3.1 Water quality parameters

Common parameters of water quality such as pH, electroconductivity (EC), nitrate, and nitrite were measured to identify the influence of these parameters on the presence of organic matter in the water body. pH parameter is considered to affect the degradation process of organic compounds in water (Weishaar et al., 2003). EC indicates the ability of an aqueous solution to carry an electric current and the conductivity of the water is predominantly caused by dissolved material (Roosmini et al., 2018; Morrison et al., 2001). Nitrate and nitrite represent the presence of nutrients causing eutrophication in the water body which further shift the microbial processing of DOM (Liu et al., 2019; Williams et al., 2016). pH and EC parameters were measured using OJAUS STARTER 300 Portable Meters ST300, and LUTRON CD-4303 Conductivity Meter, respectively, with the procedure following the Standard methods 2510. The concentration of nitrate was determined based on the Standard Method 4500-NO_2-B, and nitrite was based on the Standard Method 4500-NO_3-B. Both nitrate and nitrite parameters were measured using UV-VIS

Spectrophotometer Thermo Scientific, Evolution 100-Series Evolution 201 UV-VIS.

2.3.2 Organic matter parameters

The presence of organic matter in water was indicated by the following parameters: lability organic, i.e., chemical oxygen demand (COD); CDOM parameters such as the absorbance which was measured at 254 nm wavelength (A_{254}), the absorbance at 355 nm wavelength (A_{355}), and ratio of humic to fulvic (A3/4); as well as FDOM parameters and compounds. COD is the most common parameter measured in raw water in Indonesia. A_{254} indicates organic constituents such as humic substances and groups of aromatic compounds (Korshin et al., 2009). A_{355} represents CDOM of terrestrial origin (Dainard and Guéguen, 2013) and is considered to have a significant relationship with THMFP in a polluted tropical river (Sururi et al., 2019; Sururi et al., 2020). The ratio A3/4 was determined to indicate the proportion of humic acid and fulvic acid (Artinger et al., 2000). The analysis of COD followed the Standard Method Protocol 5220C with the closed reflux method. The CDOM parameters were analyzed according to the Standard method 5910B with the spectrophotometric method using Thermo Scientific UV-VIS Spectrophotometer, Evolution 200-series. The analysis of these parameters was carried out at the Environmental Laboratory of Environmental Engineering Study Program, Institut Teknologi Nasional (ITENAS) Bandung.

2.3.3 FDOM parameters and compounds

The FDOM in both sampling locations was measured in the filtered samples only. The FDOM was determined based on a matrix excitation-emission fluorescence spectrum method which was recorded through Shimadzu RDOM5301 Spectro fluoro-photometer. The fluorescence excitation emission matrix (FEEM) was determined at excitation wavelengths ranging from 240 to 450 nm with 5 nm intervals and an emission range of 250 to 600 nm at 1 nm increments. A preliminary analysis was conducted before the visual interpretation to correct the measured FEEM from instrument-specific biases. As suggested by (Murphy et al., 2010), the Raman scatter peaks were reduced by subtracting the Raman signal from a Milli-Q water blank. The sequential steps are: (1) correct the observed spectral; (2) correct the inner filter; (3) normalize the Excitation and Emission Matrix (EEMs) to the Raman peak area; and (4) remove the Raman scatter.

FDOM parameters used in this study were Fluorescence Index (FI) and Biological Index (BIX). The value of FI indicated the contribution of algal and microbial from terrestrial DOM (McKnight et al., 2001). The FI was determined as the ratio of fluorescence intensities of 450 nm emission wave-length to 500 nm at the same excitation wavelength measured at 370 nm excitation wavelength (McKnight et al., 2001). Meanwhile, the contribution of the autochthonous process in the raw water was identified based on the value of the Biological Index (BIX) since BIX values were an indication of the relative importance of biological or microbial DOM (Huguet et al., 2009). The BIX value was obtained by dividing the fluorescence at excitation 310 nm and emission at 380 nm (ex=310, em=380) by that at excitation 310 nm and emission at 430 nm (ex=310, em=430).

FDOM compound lies in a specific region, thus a specific FDOM compound was identified based on single excitation and emission wavelength pair or its unique position in the fluorescence map. Tryptophan-derived-microbial byproduct ("T1") exists at an excitation region of >250 nm and emission of 280-350 nm, aromatic tryptophan ("T2") is located at an excitation region of >250 and emission of 330-350 nm. Furthermore, fulvic acid-like ("A") is at excitation peaks of 320-340 nm and emission of 410-420 nm, and humic-like ("C") at excitation peaks of 370-390 nm and emission of 460-480 nm (Chen et al., 2003).

2.3.4 Trihalomethane forming potential (THMFP)

The measurement of THMFP was measured according to the Standard Method 5710B (APHA, 2017). The NaOCl solution and phosphate buffer were added for adjusting and buffering the pH to 7, and the samples were incubated for 7 days at 25°C. The residual-free chlorine was then measured at the end of the 7 days. THMs were measured by Gas Chromatography (GC) Agilent 7890 A and Agilent 5975C Mass Selective Detector (MSD), and the extraction process was performed based on the EPA 551.1 method (USEPA, 1995). The sample was injected using Agilent 7693 Series for Automatic Liquid Sampling. The obtained data was then processed by Agilent MSD ChemStation software. The measurement of THMFP was conducted at the Integrated Laboratory of Politeknik Kesehatan

Bandung. The concentrations of the identified THMs were obtained by measuring the mixed standard of THMs: chloroform ($CHCl_3$), dichlorobromomethane ($CHBrCl_2$), chlorodibromomethane ($CHBr_2Cl$), and bromoform ($CHBr_3$) from Supelco Sigma Aldrich. Straight-line calibration curves were developed by plotting the absorbances of the standard solutions against the THMs concentrations with regression coefficients within the range of 0.93-0.99. The concentration of individual THM compound (mg/L) was obtained after the response (sample's measurement result) was entered into the regression equation of the calibration curve. The total THMFP is expressed in terms of identified THM equivalents using this standard equation (APHA, 2017):

$$\text{Total THMFP} = A + 0.728B + 0.574C + 0.472D \quad (1)$$

Where; A=chloroform concentration (µg $CHCl_3$/L); B=dichlorobromomethane concentration (µg $CHBrCl_2$/L); C=chlorodibromomethane concentration (µg $CHBr_2Cl$/L); and D=bromoform concentration (µg $CHBr_3$/L).

2.4 Statistical analysis

The average differences between each TOM parameter and the corresponding DOM parameter were determined based on t-test analysis. A statistically significant difference between the pair was indicated by a t-test value <0.5, whereas no significant difference between the pair was indicated by a t-test value >0.5 (Awad et al., 2016). The correlation analysis between TOM and DOM parameters and compounds was conducted and the significance of the correlations in the statistics was evaluated using p-values. SPSS 19.0 software package: IBM SPSS Statistics was used to conduct all statistical analyses.

3. RESULTS AND DISCUSSION

3.1 Water characteristics

The measurement results of water quality parameters in unfiltered and filtered samples at the Cimahi and Cijanggel Rivers during the rainy season can be seen in Table 1. The value of pH was in the neutral range (6.49-7.24) in the unfiltered and filtered samples of the two sampling locations. The average concentration of nitrite and nitrate in the unfiltered and filtered samples of the Cimahi River was higher than those at the Cijanggel River. The remaining nitrate and nitrite concentrations in the filtered samples of Cimahi River were 48% (3.16 mg/L) and 34% (7.64 mg/L), respectively. Meanwhile, in Cijanggel River, the nitrate and nitrite concentration in the unfiltered samples were 6.9% (0.16 mg/L) and 37% (0.45 mg/L), respectively. The higher concentrations of nitrate than nitrite in the Cimahi and Cijenggel Rivers add to evidence that pollution from domestic waste has been occurring for a long time (Sawyer and McCarty, 2003). The results were consistent since the land use in the catchment of the upper Cimahi River is dominated by settlements, and there was domestic wastewater pollution, especially from open defecation and effluent of the domestic wastewater treatment plant (WWTP).

Table 1. The water quality analysis result at each sampling point

Parameter	Cimahi River (N=7) ($\bar{X}$±SD)		Cijanggel River (N=5) ($\bar{X}$±SD)	
	Unfiltered samples	Filtered samples	Unfiltered samples	Filtered samples
pH	7.01±0.23	7.21±0.31	6.54±0.05	6.29±0.13
Electroconductivity (mhos/cm)	232.89±14.10	211.48±26.55	234.00±15.70	228.20±13.10
Nitrite (mg/L)	6.58±3.56	3.16±2.21	2.30±1.99	0.16±0.06
Nitrate (mg/L)	21.87±4.75	7.64 ±1.68	1.21±0.36	0.45±0.28

The average conductivity of the sample in the unfiltered sample in the Cimahi samples (232.89 mhos/cm) did not differ from that in the Cijanggel samples (234 mhos/cm). The values of the unfiltered samples slightly decreased to 211.48 mhos/cm in the Cimahi River and 228.2 mhos/cm in the Cijenggel River. The results suggest that the EC content is slightly higher in dissolved conditions than in particulates (Laghari et al., 2018; Shrestha and Basnet, 2018). Another important thing is that the EC value in the unfiltered sample taken from the plantation-impacted watershed (Cijanggel River) was higher than that of the settlements-impacted watershed (Cimahi River). The results were consistent with greater nutrient concentrations such as nitrate in the Cimahi River. Nitrate is known to have a negative relationship with

EC (r=-0.227/p=0.0025) (Wang and Yin, 1997). Moreover, the measured EC in the two sampling points did not differ from the measured EC in the Cikapundung River, an urban river that is polluted by domestic and animal wastes (132-306 mhos/cm in the unfiltered samples; and 82-201 mhos/cm in the filtered samples) (Roosmini et al., 2018). The EC was predominantly contributed by dissolved material (Tommassen, 2014), and the EC value is increasing in a polluted watershed (Il'ina et al., 2018).

3.2 Organic matter characteristics

TOM characteristics in the unfiltered samples and DOM characteristics in filtered samples are presented in Table 2 and Figure 2. The lability organic matter which was indicated by the COD parameter has indicated that the measured concentrations in the unfiltered and filtered samples in the plantation-impacted watershed (Cijenggel River) were below the maximum limit for COD concentration in raw water quality standard for drinking water (10 mg/L). However, the residential-impacted watershed (Cimahi River) exceeded the raw water standard. The ratio of the COD in the filtered sample to the COD in the unfiltered sample has suggested that most of the organic lability is in the dissolved fraction with a ratio of 0.8 for Cimahi River and 0.6 for Cijanggel River. These results confirm that the load of organic pollution in the watershed with dominant residential land use in the catchment was greater than that of the catchment dominated by plantation activities. Moreover, the sampling point at the settlement-impacted watershed (Cimahi River) was located after the outlet of the Cibabat Communal WWTP. Compare to another urban river in Bandung (Cikapundung River) with COD in the unfiltered samples of 19.94 mg/L (Sururi et al., 2018), the measured COD in the Cimahi River did not greatly differ. This was because the main sources of organic pollution in these two watersheds were similar to domestic wastewater and cattle manures.

A_{254} and A_{355} represent the content of humic compounds and other aromatic groups in water samples (Sururi et al., 2020). A_{355} in DOM fraction ($A_{355\text{-DOM}}$) was the potential to be used as a THMFP surrogate parameter in an urban river polluted by organic matter (Sururi et al., 2019; Sururi et al., 2020). Table 2 and Figure 3 shows the value of A_{254} and A_{355} in the Cimahi River samples were greater than those of the Cijanggel River. The ratio of A_{254} in the filtered to unfiltered samples was 0.42 in Cimahi River and 0.89 in Cijenggel River which suggests that A_{254} in the plantation-impacted watershed (Cijenggel River) was dominantly in dissolved fraction.

Table 2. Measured organic characteristics in Cimahi and Cijenggel River

Parameter (unit)	Cimahi River (N=7) ($\bar{X}$±SD)		Cijanggel River (N=5) ($\bar{X}$±SD)	
	Unfiltered	Filtered	Unfiltered	Filtered
COD (mg/L)	31.04±4.25	25.65±5.03	3.65±2.89	2.18±3.09
A_{254} (cm^{-1})	0.36±0.25	0.15±0.06	0.09±0.02	0.08±0.01
A_{355} (cm^{-1})	0.22±0.22	0.06 ±0.03	0.02±0.00	0.02±0.00
A3/4	1.72±0.42	3.34±2.96	6.95±3.30	19.45±17.23

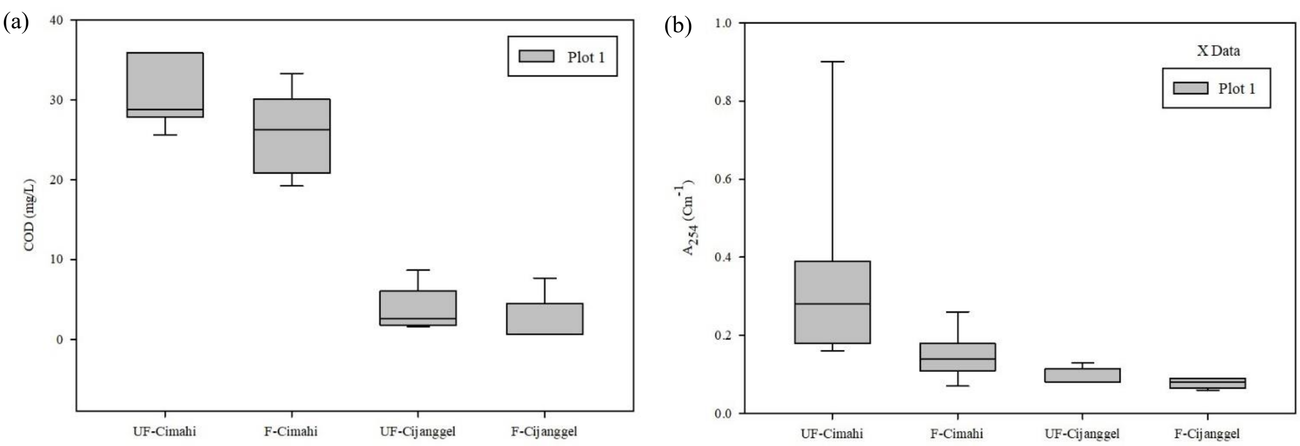

Figure 2. Measured organic characteristics: (a) COD, (b) A_{254}, (c) A_{355}, and (d) A3/4 in Cimahi and Cijenggel River

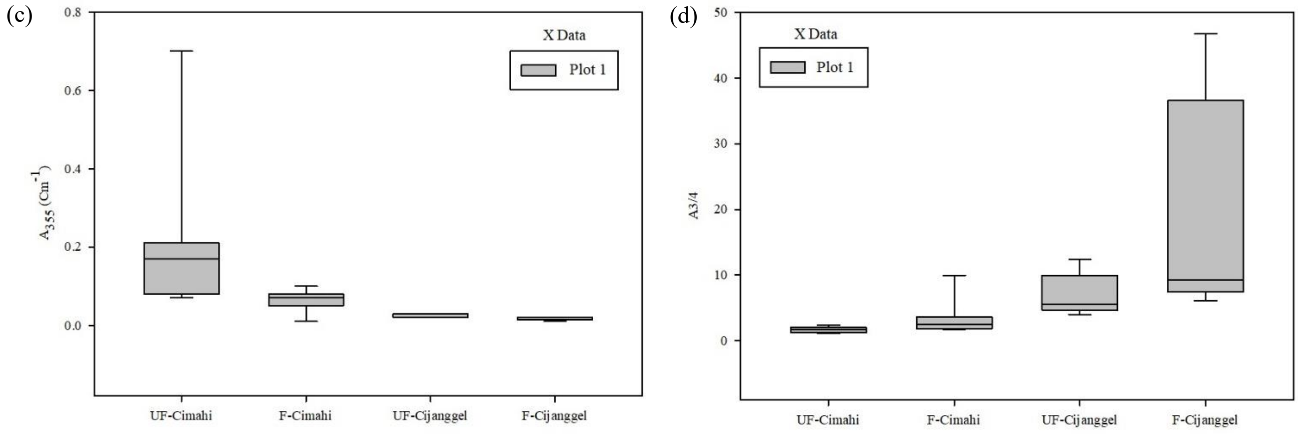

Figure 2. Measured organic characteristics: (a) COD, (b) A_{254}, (c) A_{355}, and (d) A3/4 in Cimahi and Cijenggel River (cont.)

The ratio of the filtered to unfiltered A_{355} in the Cimahi River was 0.27, yet the ratio for the Cijanggel River was substantially greater (1), indicating that the Cijanggel River has greater dissolved terrestrial aromatic compounds than the settlement-impacted river (Table 2). However, the value for A_{254} and A_{355} in the Cimahi River greater than the Cijenggel River. Previous findings have shown polluted water bodies contained considerable aromatic compounds, although non-humic protein content was dominant (Sururi et al., 2021; Sururi et al., 2020). This was because protein (tyrosine-like compound) and tryptophan which are classified as aromatic (Sururi et al., 2021; Sururi et al., 2020) were present in the raw water source. The absorption ratio (A3/4 index) has shown that the humic acid was more dominant than the fulvic acid, particularly in the plantation-impacted watershed (Table 2 and Figure 3), indicating the organic compound in Cijanggel River was more aromatic than in Cimahi River. The greater absorption ratio (>3.5) in the Cijanggel River is an indication of greater humification, aromaticity, and molecular weight of humic substances (Artinger et al., 2000). However, White et al. (1997) have found that hydrophobic compounds consist of acidic compounds such as fulvic acid and humic acid which are derived from the natural decomposition of lignin and originated from anthropogenic activity. These have contributed to the higher concentration of DOM in the Cimahi River than in the Cijanggel River.

3.3 FDOM parameters and compounds

As seen in Table 3 and Figure 3, the FI value in Cimahi samples was 2.12 (FI>1.4), adding evidence that the presence of DOM in the water body mostly originated from microbial biomass (Cory and McKnight, 2005). There was also a contribution of fresh DOM entering the water body as indicated by the BIX of 1.15 (BIX>1). Another previous study has found that BIX>1 could also be an indication that the tryptophan-like compound was more predominant than the humic-like compound (Gabor et al., 2014).

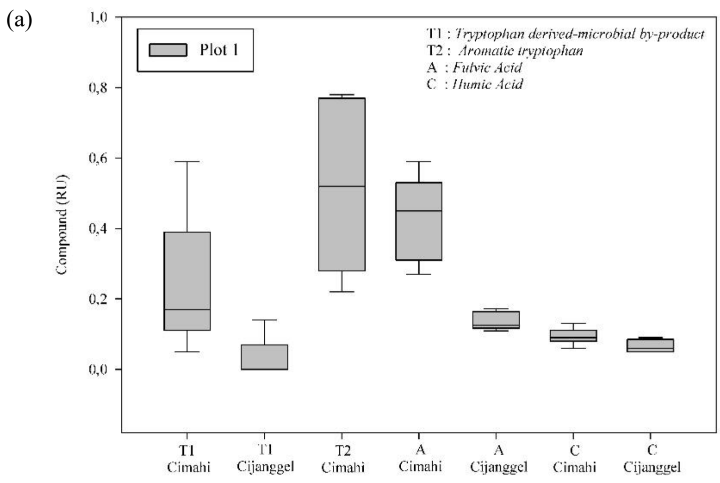

Figure 3. The measurement results for (a) FDOM compounds, (b) FI, and (c) BIX

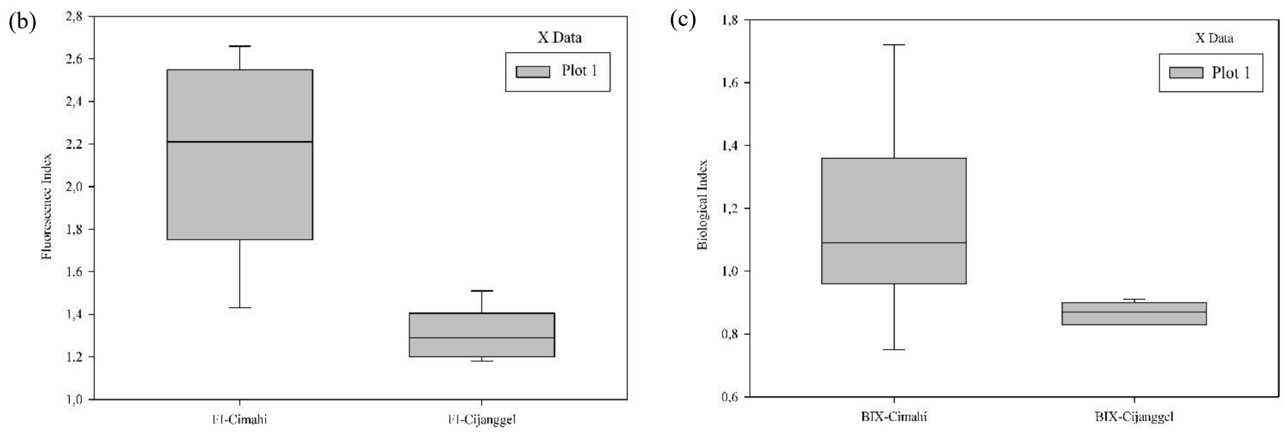

Figure 3. The measurement results for (a) FDOM compounds, (b) FI, and (c) BIX (cont.)

Moreover, the results of the FI and BIX values have confirmed the organic pollution in the settlement-impacted watershed (Cimahi River), similar to those found in a main urban river in Bandung City (Cikapundung River) during the dry season when the water quality worsened (FI=1.55-3.23; BIX=0.62-1.33) (Sururi et al., 2021). FDOM in watersheds impacted by anthropogenic activities typically has lower molecular weight with hydrophobic and aromatic characteristics (Zhao et al., 2009; Zhao et al., 2006).

The FI value measured in the plantation-impacted watershed (Cijanggel River) was lower than that of the settlement-impacted watershed (Cimahi River). In the plantation-impacted watershed, DOM predominantly originated from plant litter or terrestrial soil as indicated by the FI of 1.30. In addition, Cory and McKnight (2005) and McKnight et al. (2001) have suggested that an FI value <1.4 show the presence of terrestrial-derived humic (Table 3). Meanwhile, the average value of the BIX was 0.87 (BIX<1) which an indicative of intermediate contributions of auto-chthonous processes to the presence of DOM in this water body (Huguet et al., 2009).

Table 3. Measured FDOM parameters and compounds

Compound and parameters	Cimahi River ($\bar{X}$±SD)	Cijenggel River ($\bar{X}$±SD)
Biological index (FI)	2.12±0.43	1.30±0.13
Fluorescence index (BIX)	1.15±0.31	0.87±0.04
Tryptophan derived- microbial byproduct (T1), in Raman unit (RU)	0.25±0.19	0.03±0.06
Aromatic tryptophan (T2), in Raman unit (RU)	0.50±0.22	-
Fulvic acid (A), in Raman unit (RU)	0.43±0.12	0.14±0.03
Humic acid (C), in Raman unit (RU)	0.09±0.02	0.07±0.02

The FEEM contour map as seen in Figure 4 shows an overlap of peak locations which could occur when the high-intensity peaks mask changes to low-intensity peaks (Carstea et al., 2016). However, the unique position of the FDOM compound can be determined based on the fluorescence map reference of a specific FDOM compound (Chen et al., 2003; Li et al., 2020). Although there are unavoidable uncertainties in the peak locations, the peak-picking method has the potential to provide real-time monitoring results, and sufficiently diagnose a specific compound at single excitation and emission wavelength pair (Baker et al., 2015). Compared to the plantation-impacted watershed (Cimahi River), the settlement-impacted watershed (Cimahi River) contains greater protein compounds such as tryptophan-like compound which originated from microbial activities (T1), and aromatic tryptophan-like compound (T2).

Figure 4 shows the differences in the FEEM contours of FDOM from the two watersheds, which were typical for all sampling periods. The measured quantity of protein in the settlement-impacted watershed was 0.25 RU for T1 and 0.50 RU for T2, which is consistent with the greater quantity of FI, BIX, and nitrate concentrations in this watershed (Table 3). The influence of allochthonous DOM in Cimahi River shows by the presence of fulvic acid (compound

A) which was detected at 0.43 RU and humic acid (Compound C) which was detected at 0.09 RU only. The FEEM contours for the Cimahi River show similarities to those contours obtained from polluted rivers such as the Tyne River in England which was impacted by domestic wastes (Baker et al., 2004), and in Cikapundung River in Indonesia which has been polluted by manure wastes (Sururi et al., 2020). The main compound in the plantation-impacted watershed (Cijanggel River) was compound A (0.14 RU) followed by compound C (0.07 RU). Nonetheless, Compound T1 was the only protein-type compound detected in this watershed (0.03 RU). These results have shown that the plantation-impacted watershed was dominated by allochthonous DOM which differs from the settlement-impacted watershed which was dominated by the tryptophan-like compound. A similar fact is shown by other polluted urban rivers (Marhaba et al., 2006; Sururi et al., 2020) where the identified proteins were tryptophan and tyrosine, indicating that the source of DOM is generally anthropogenic such as settlement, and cattle manure.

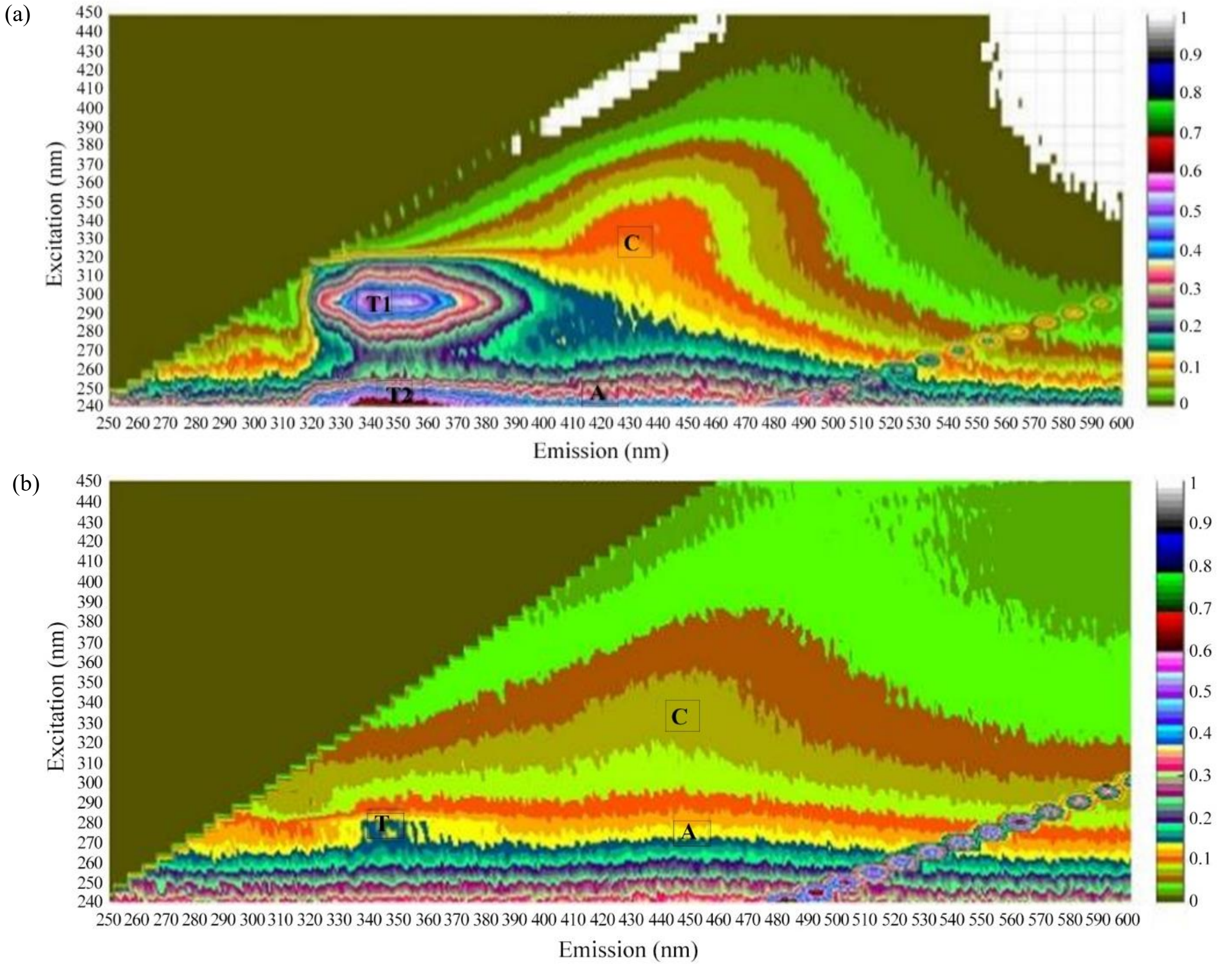

Figure 4. Example of FEEM contour at (a) Cimahi River and (b) Cijanggel River

3.4 Relationships between TOM and DOM parameter

Leven's test confirms the homogeneity of the obtained data with $p>0.05$. Based on the t-test analysis, the average values of COD, A_{254}, and A_{355} in the unfiltered (TOM) did not significantly differ from the corresponding parameter in filtered (DOM) samples in Cijanggel and Cimahi River. There was no significant correlation for A_{254} between the unfiltered and filtered samples ($r=-0.39$, $p=0.51$ in Cijanggel River) as well as A_{355} between the unfiltered-filtered pair ($r=0.41$, $p=0.49$ in Cijanggel River; $r=0.65$, $p=0.11$ in Cimahi River), implying the quantity and characteristic of DOM could not be indicated by the measurement of quantity and characteristic of TOM. These results were consistent with a study reported by Sururi et al. (2019) that found either A_{254} or A_{355} in the unfiltered samples was weakly correlated with A_{254} and A_{355} in the filtered samples during the rainy season in the urban river with abundant DOM compound.

However, there was a significant relationship for COD of the unfiltered vs filtered samples in both watersheds (r=0.96; p=0.01 for the Cijanggel River and (r=0.80; p=0.03 for the Cimahi River), as well as for A_{254} pair in Cimahi River only (r=0.76; p=0.04). The results provide evidence that either in the settlement- or plantations-impacted watershed, the measured COD concentration in the unfiltered samples could represent the COD concentration in the filtered samples during the rainy season. However, it was only in the settlement-impacted watershed during the rainy season that the optical properties of CDOM measured in 254 nm wavelength (A_{254}) in TOM could represent the quantity of A_{254} in DOM samples.

3.5 THMFP occurrences

Figure 5 shows the concentrations of $CHCl_3FP$, $CHBrCl_2FP$, $CHBr_2ClFP$, $CHBr_3FP$, and TTHMFP which were calculated based on Equation 1. The TTHMFP which was measured in the plantation-impacted watershed (Cijanggel River) was 0.09 µg/L, exceeding the standard THMs of 0.08 µg/L, the TTHMFP in the settlement-impacted watershed (0.07 µg/L) was slightly below the maximum limit. The $CHCl_3FP$ was the most dominant THMs detected in these two different watersheds (0.068 µg/L in Cijanggel River, and 0.057 µg/L in Cimahi River), suggesting these raw water sources did not contain an abundance of brominated species. The domination of $CHCl_3$ was also reported in other tropical natural water bodies in the Riau region, Indonesia (Zevi et al., 2022). Another THMs compound was $CHBr_3$ with a concentration of 0.016 µg/L at Cijanggel River and 0.024 at Cimahi River. The average concentration of $CHBrCl_2FP$ was 0.019 and 0.006 µg/L at Cijanggel River and Cimahi River respectively. Meanwhile, the lowest potential of THMs formation was observed for $CHBr_2Cl$ with an average concentration of 0.003 µg/L. This was predictable since dichlorobromomethane has been the most typical THMs compound in peat water in Indonesia (Qadafi et al., 2021).

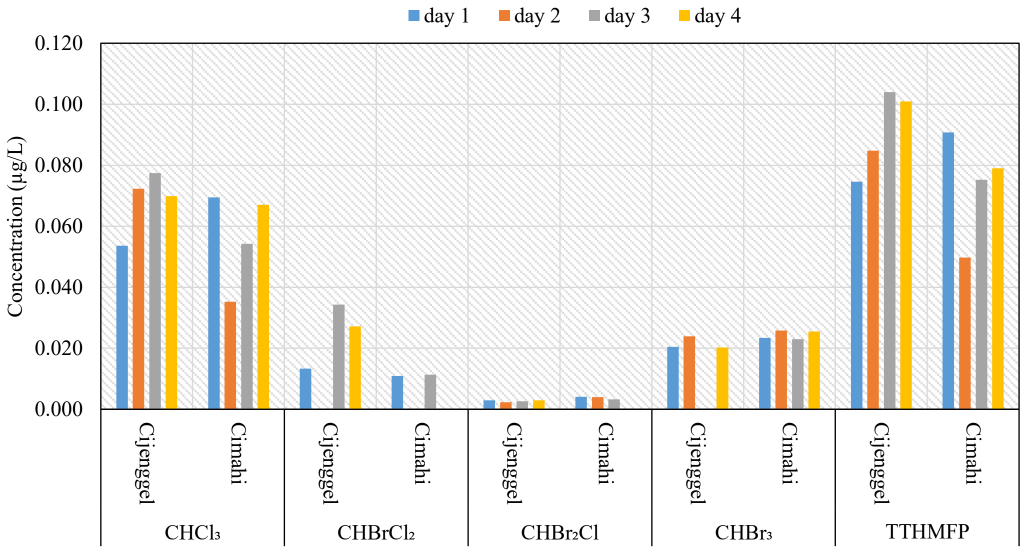

Figure 5. THMFP occurrences (µg/L) in Cimahi River and Cijanggel River (4 days measurement)

The greater concentrations of measured TTHMFP in the settlement-impacted watershed (Cijanggel River) than that in the settlement-impacted watershed (Cimahi River) were attributable to the lower concentrations of the protein-like compound in Cijengel River as indicated by the FI and BIX values in this watershed. The protein-like compound is not the main precursor of THMs. Thus, DOM would be degraded by microorganisms instead of reacting with chlorine to form THMs (Hur et al., 2013). Another reason was the Cijanggel River contained greater fulvic acid than that the Cimahi River (Table 2), consistent the greater absorption ratio (A3/4>3.5) which confirmed the Cijanggel River have greater humification, aromaticity, and molecular weight of humic compounds (Artinger et al., 2000). DOM with lower molecular weight than humic compounds such as fulvic acid has been considered the main precursor of THMs (Hua et al., 2015; Marhaba and Van, 2000; Xia et al., 2016). In addition, low molecular weight

DOM is reactive to electrophiles such as chlorine which is an electron-rich organic compound (Scully et al., 1988), leads to the greater formation of THMs.

4. CONCLUSION

Overall, upstream land use affected the quantity and quality of DOM in the Cimahi and Cijanggel Rivers. Cimahi River, an urban river with a settlement-dominated catchment had much higher concentrations of nitrate, nitrite, as well as TOM and DOM than those at Cijanggel River, an urban river with a plantation-dominated catchment. The FI and BIX values confirm the DOM compounds in both watersheds originated from different sources. The protein-like compounds which included tryptophan microbial by-product (i.e., T1) and tryptophan aromatic protein (i.e., T2) were the most dominant compounds in the upstream of the settlement-dominated catchment with a quantity of 0.75 RU for total protein-like (0.25 RU for T1, and 0.50 RU for T2). Other identified compounds were fulvic acid (i.e., C) at a quantity of 0.43 RU and humic acid (i.e., A) at a quantity of 0.09 RU. Nonetheless, the plantation-dominated catchment enhanced the propensity of the predominant DOM compounds in the watershed comprised compound A (0.14 RU) and C (0.07 RU), followed by T1 protein-like compound (0.03 RU). Moreover, a watershed with greater humic-like compounds has greater TTHMFP concentrations. Different land use also affects the relationship between TOM and DOM parameters. A significant relationship was seen between unfiltered COD and filtered COD in the plantation-dominant catchment. Hence, the measurement of the COD parameter in TOM fraction could represent the quantity of DOM in such watersheds. Among the optical parameters of the TOM and DOM fraction relationship, only A_{254} exhibited a positive correlation in the settlement-dominant catchment during the rainy season, thus the measured A_{254} in the TOM fraction could be a surrogate for A_{254} in the DOM fraction.

ACKNOWLEDGEMENTS

The authors would like to acknowledge the Lembaga Penelitian dan Pengabdian Masyarakat (Centre of Research and Community Development) of Institut Teknologi Nasional, Bandung for funding this research (Grant ID:365/B.05/LP2M-Itenas/V/2021), Adam Dzaky Rahman and Khaerul Candra for assisting water sampling and analysis.

REFERENCES

Artinger R, Buckau G, Geyer S, Fritz P, Wolf M, Kim J. Characterization of groundwater humic substances: Influence of sedimentary organic carbon. Applied Geochemistry 2000;15(1):97-116.

Aschermann G, Jeihanipour A, Shen J, Mkongo G, Dramas L, Croué JP, et al. Seasonal variation of organic matter concentration and characteristics in the Maji ya Chai River (Tanzania): Impact on treatability by ultrafiltration. Water Research 2016;101:370-81.

Awad J, Van Leeuwen J, Chow C, Drikas M, Smernik RJ, Chittleborough DJ, et al. Characterization of dissolved organic matter for prediction of trihalomethane formation potential in surface and sub-surface waters. Journal of Hazardous Materials 2016;308:430-9.

American Public Health Association (APHA). Standard Methods for the Examination of Water and Wastewater. Washington, DC, USA: APHA; 2017.

Baker A, Inverarity R, Charlton M, Richmond S. Detecting river pollution using fluorescence spectrophotometry: Case studies from the Ouseburn, NE England. Environmental Pollution 2003;124(1):57-70.

Baker A, Ward D, Lieten SH, Periera R, Simpson EC, Slater M. Measurement of protein-like fluorescence in river and waste water using a handheld spectrophotometer. Water Research 2004;38(12):2934-8.

Baker A, Cumberland SA, Bradley C, Buckley C, Bridgeman J. To what extent can portable fluorescence spectroscopy be used in the real-time assessment of microbial water quality? Science of the Total Environment 2015;532:14-9.

Carstea EM, Bridgeman J, Baker A, Reynolds DM. Fluorescence spectroscopy for wastewater monitoring: A review. Water Research 2016;95:205-19.

Chen W, Westerhoff P, Leenheer JA, Booksh K. Fluorescence excitation-emission matrix regional integration to quantify spectra for dissolved organic matter. Environmental Science and Technology 2003;37(24):5701-10.

Coble PG. Marine optical biogeochemistry: The chemistry of ocean color. Chemical Reviews 2007;107(2):402-18.

Cory RM, McKnight DM. Fluorescence spectroscopy reveals ubiquitous presence of oxidized and reduced quinones in dissolved organic matter. Environmental Science and Technology 2005;39(21):8142-9.

Dainard PG, Guéguen C. Distribution of PARAFAC modeled CDOM components in the North Pacific Ocean, Bering, Chukchi and Beaufort Seas. Marine Chemistry 2013;157: 216-23.

Gabor RS, Baker A, McKnight DM, Miller MP. Fluorescence indices and their interpretation. In: Cobble GP, Lead J, Baker A, Reynold DM, Spencer RGM, editors. Aquatic Organic Matter Fluorescence. Cambridge University Press; 2014. p. 303.

Hua G, Reckhow D, Abusallout I. Correlation between SUVA and DBP formation during chlorination and chloramination of NOM fractions from different sources. Chemosphere 2015; 130:82-9.

Huguet A, Vacher L, Relexans S, Saubusse S, Froidefond JM, Parlanti E. Properties of fluorescent dissolved organic matter in the Gironde Estuary. Organic Geochemistry 2009; 40(6):706-19.

Hur J, Lee MH, Song H, Schlatman MA. Microbial transformation of dissolved organic matter from different sources and its influence on disinfection byproduct formation potentials. Environmental Science and Pollution Research 2013; 20(6):4176-87.

Il'ina KV, Gavrilova N, Bondarenko E, Andrianova MJ, Chusov A. Express-techniques in study of polluted suburban streams. Magazine of Civil Engineering 2018;77(1):241-54.

Korshin G, Chow CW, Fabris R, Drikas M. Absorbance spectroscopy-based examination of effects of coagulation on the reactivity of fractions of natural organic matter with varying apparent molecular weights. Water Research 2009;43(6):1541-8.

Laghari AN, Walasai GD, Jatoi AR, Shaikh FA, Siyal ZA. Performance analysis of water filtration units for reduction of pH, turbidity, solids and electricity conductivity. Engineering, Technology and Applied Science Research 2018; 8(4):3209-12.

Leehneer J, Croué J. Characterizing dissolved aquatic organic matter. Environmental Science and Technology 2003;1:19-26.

Li L, Wang Y, Zhang W, Yu S, Wang X, Gao N. New advances in fluorescence excitation-emission matrix spectroscopy for the characterization of dissolved organic matter in drinking water treatment: A review. Chemical Engineering Journal 2020; 381:Article No. 122676.

Liu T, Hu S, Guo J. Enhancing mainstream nitrogen removal by employing nitrate/nitrite-dependent anaerobic methane oxidation processes. Critical Reviews in Biotechnology 2019;39(5):732-45.

Marhaba TF, Mangmeechai A, Chaiwatpongsakorn C, Pavasant P. Trihalomethanes formation potential of shrimp farm effluents. Journal of Hazardous Materials 2006;136(2):151-63.

Marhaba TF, Van D. The variation of mass and disinfection by-product formation potential of dissolved organic matter fractions along a conventional surface water treatment plant. Journal of Hazardous Materials 2000;74(3):133-47.

McKnight DM, Boyer EW, Westerhoff PK, Doran PT, Kulbe T, Andersen DT. Spectrofluorometric characterization of dissolved organic matter for indication of precursor organic material and aromaticity. Limnology and Oceanography 2001;46(1):38-48.

Meng F, Huang G, Yang X, Li Z, Li J, Cao J, et al. Identifying the sources and fate of anthropogenically impacted dissolved organic matter (DOM) in urbanized rivers. Water Research 2013;47(14):5027-39.

Morrison G, Fatoki O, Persson L, Ekberg A. Assessment of the impact of point source pollution from the Keiskammahoek Sewage Treatment Plant on the Keiskamma River-pH, electrical conductivity, oxygen-demanding substance (COD) and nutrients. Water SA 2001;27(4):475-80.

Murphy KR, Butler KD, Spencer RG, Stedmon CA, Boehme JR, Aiken GR. Measurement of dissolved organic matter fluorescence in aquatic environments: An interlaboratory comparison. Environmental Science and Technology 2010; 44(24):9405-12.

Notodarmojo S, Mahmud, Larasati A. Adsorption of natural organic matter (NOM) in peat water by local indonesia tropical clay soils. International Journal of Geomate 2017; 13(38):111-9.

Qadafi M, Notodarmojo S, Zevi Y. Performance of microbubble ozonation on treated tropical peat water: Effects on THM4 and HAA5 precursor formation based on DOM hydrophobicity fractions. Chemosphere 2021;279:Article No. 130642.

Roosmini D, Notodarmojo S, Sururi M. The characteristic of natural organic matter (NOM) of water from Cikapundung River Pond. Proceedings of the Earth and Environmental Science International Conference Series; 2018 Nov 5; Yogyakarta: Indonesia; 2018.

Sawyer CN, McCarty PL. Chemistry for Environmental Engineers. 5th ed. New York, USA: Mc Graw-Hill Book Company; 2003.

Scully FE, Howell GD, Kravitz R, Jewell JT, Hahn V, Speed M. Proteins in natural waters and their relation to the formation of chlorinated organics during water disinfection. Environmental Science and Technology 1988;22(5):537-42.

Shi W, Zhuang WE, Hur J, Yang L. Monitoring dissolved organic matter in wastewater and drinking water treatments using spectroscopic analysis and ultra-high resolution mass spectrometry. Water Research 2021;188;Article No. 116406.

Shi Y, Zhang L, Li Y, Zhou L, Zhou Y, Zhang Y, et al. Influence of land use and rainfall on the optical properties of dissolved organic matter in a key drinking water reservoir in China. Science of the Total Environment 2020;699:Article No. 134301.

Shrestha AK, Basnet N. The correlation and regression analysis of physicochemical parameters of river water for the evaluation of percentage contribution to electrical conductivity. Journal of Chemistry 2018;2018:Article No. 8369613.

Sururi MR, Dirgawati M, Roosmini D, Notodarmodjo S. Characterization of fluorescent dissolved organic matter in an affected pollution raw water source using an excitation-emission matrix and PARAFAC. Environment and Natural Resources Journal 2021;19(6):459-67.

Sururi MR, Notodarmojo S, Roosmini D. Aquatic organic matter characteristics and THMFP occurrence in a tropical river. International Journal of Geomate 2019;17(62):203-11.

Sururi MR, Notodarmojo S, Roosmini D, Putra PS, Maulana YE, Dirgawati, M. An investigation of a conventional water treatment plant in reducing dissolved organic matter and trihalomethane formation potential from a tropical river water source. Journal of Engineering and Technological Sciences 2020;52(2):271-88.

Sururi MR, Roosmini D, Notodarmojo S. Chromophoric and liability quantification of organic matters in the polluted rivers of Bandung Watershed, Indonesia. Proceedings of the 2nd International Conference on Engineering and Technology for Sustainable Development (ICET4SD 2018); 2018 Sept 13-14; Yogjakarta: Indonesia; 2018.

Tommassen G. On the Correlation between Turbidity, Conductivity and COD [dissertation]. Delf: Technische Universiteit Delft; 2014.

United States Environmental Protection Agency (USEPA). USEPA Method 551.1: Determination of Chlorination Disinfection Byproducts, Chlorinated Solvents and Halogenated Pesticides/Herbicides in Drinking Water by Liquid-Liquid Extraction and Gas Chromatography with Electron Capture Detection. Office of Research and Development: USEPA; 1995.

Wang X, Yin ZY. Using GIS to assess the relationship between land use and water quality at a watershed level. Environment International 1997;23(1):103-14.

Weishaar JL, Aiken GR, Bergamaschi BA, Fram MS, Fujii R, Mopper K. Evaluation of specific ultraviolet absorbance as an indicator of the chemical composition and reactivity of dissolved organic carbon. Environmental Science and Technology 2003;37(20):4702-8.

White MC, Thompson JD, Harrington GW, Singer PC. Evaluating criteria for enhanced coagulation compliance. Journal American Water Works Association 1997;89(5):64-77.

Williams C, Frost PC, Morales-Williams AM, Larson JH, Richardson WB, Chiandet AS, et al. Human activities cause distinct dissolved organic matter composition across freshwater ecosystems. Global Change Biology 2016; 22(2):613-26.

Wolfe AP, Kaushal SS, Fulton JR, McKnight DM. Spectrofluorescence of sediment humic substances and historical changes of lacustrine organic matter provenance in response to atmospheric nutrient enrichment. Environmental Science and Technology 2002;36(15):3217-23.

Xia CF, Ma DF, Gao BY, Hu XX, Yue QY, Meng YJ, et al. Characteristics and trihalomethane formation reactivity of dissolved organic matter in effluents from membrane bioreactors with and without filamentous bulking. Bioresource Technology 2016;211:183-9.

Zevi Y, Qadafi M, Notodarmojo S. The Presence of trihalomethanes and haloacetic acids in tropical peat water. Journal of Engineering and Technological Sciences 2022; 54(3):1-13.

Zhao ZY, Gu JD, Li HB, Li XY, Leung KMY. Disinfection characteristics of the dissolved organic fractions at several stages of a conventional drinking water treatment plant in Southern China. Journal of Hazardous Materials 2009;172(2-3):1093-9.

Zhao ZY, Gu JD, Fan XJ, Li HB. Molecular size distribution of dissolved organic matter in water of the Pearl River and trihalomethane formation characteristics with chlorine and chlorine dioxide treatments. Journal of Hazardous Materials 2006;134(1-3):60-6.

Accumulation of Microplastics and Histological Analysis on Marine Fish from Coastal Waters of Baru and Trisik Beaches, Special Region of Yogyakarta

Raden Roro Risang Ayu Dewayani Putri, Bambang Retnoaji, and Andhika Puspito Nugroho*

Faculty of Biology, Universitas Gadjah Mada, Special Region of Yogyakarta 55281, Indonesia

ARTICLE INFO

Received: 23 Sep 2022
Received in revised: 14 Dec 2022
Accepted: 21 Dec 2022
Published online: 14 Feb 2023
DOI: 10.32526/ennrj/21/202200207

Keywords:
Microplastics/ Surface seawater/ Marine fish/ Histology

*** Corresponding author:**
E-mail: andhika_pn@ugm.ac.id

ABSTRACT

River flow to the sea is regarded as a pathway for the dispersion and pollution of microplastics. The hydrodynamics of the coastal water of Baru and Trisik Beaches may increase microplastic concentrations in this estuarine-marine area. This research evaluated the microplastic concentration in surface seawater and microplastic accumulation in consumed marine fish and performed histological analysis on the demersal marine fish intestine under natural exposure. Sample collection was carried out at 12 stations with three replications. The microplastics analysis was performed on marine fish (dorsal muscle, gills, and gastrointestinal tract) and seawater, and microplastic characterization was based on physical and chemical characteristics. Environmental parameters for statistical analysis included air and water temperature, pH, dissolved oxygen, and salinity of seawater. Histological analysis of the intestine was performed on fish from three stations with two demersal fish species. The latter analysis included the length of the villi, the depth of the crypt cells, epithelial denudation with hematoxylin-eosin staining, and the number of goblet cells with periodic acid Schiff alcian blue staining. The results showed that the microplastic concentration was distributed throughout the fish sample for each of the stations. Microplastic concentrations for surface seawater showed the same pattern as marine fish. Microplastic accumulation in marine fish indicated the transfer of microplastic particles to various organs in the fish's body. The histological analysis indicated, microplastic internalization in the intestine tissue, damaging intestinal structures. Further research is needed as consuming marine fish contaminated by microplastics may present increasing health risks.

1. INTRODUCTION

Anthropogenic activities around rivers, estuaries, beaches, and coastal waters are the main sources of marine debris. Henceforward, plastic use will continue to increase and constitute 80 to 85% of marine debris (Auta et al., 2017). Global use of plastics is threatening marine life and human health (Lundebye et al., 2022). In the aquatic ecosystem, plastic waste is degraded by physical, chemical, and biological processes into smaller sizes (i.e., microplastics and nanoplastics) (Jovanović, 2017). Microplastics (MPs) size is less than 5 mm with different shapes, colors, and polymers (Barboza et al., 2020; Lundebye et al., 2022). Microplastics are transported from estuaries and beaches via ocean currents, gyres, and garbage patches (Lebreton et al., 2012; Wieczorek et al., 2018; van Sebille et al., 2020). Moreover, MPs can migrate and concentrate in surface seawaters, potentially accumulating in the estuaries and marine biota (Amelia et al., 2021; Auta et al., 2017; Zhang et al., 2020).

Marine fish, such as demersal and pelagic fish, act as a potential food source for humans, but can also accumulate and transfer MPs to other trophic levels (Carbery et al., 2018; Cedervall et al., 2012; Koongolla et al., 2020). Additive chemicals adsorbed onto the surface of MPs can also accumulate in marine fish organs (Woodall et al., 2014; Yu et al., 2019). Microplastics have been documented in marine fish organs such as the gastrointestinal tract (GIT), gills, muscle, skin, and liver (Abbasi et al., 2018; Barboza et al., 2020; Koongolla et al., 2020; Maaghloud et al.,

Citation: Putri RRRAD, Retnoaji B, Nugroho AP. Accumulation of microplastics and histological analysis on marine fish from coastal waters of Baru and Trisik Beaches, Special Region of Yogyakarta. Environ. Nat. Resour. J. 2023;21(3):153-170. (https://doi.org/10.32526/ennrj/21/202200207)

2020). Demersal fish are bottom feeders and have the potential to swim and enter river-estuaries, which also accumulate MPs from water and benthic biota (Brodeur et al., 2021). Pelagic fish swimming near surface seawater, accumulate MPs from these waters and consume neritic organisms (Brodeur et al., 2021).

Several investigations have looked into the effects of MPs on marine fish from polluted areas, but histological analysis of marine fish organs is still limited (Haave et al., 2021). The controversial issue is the potential of MPs to affect the organs in the laboratory and natural conditions. In histopathology studies, MPs have been identified as having adverse effects, especially on fish intestines (Jovanović et al., 2018). Microplastic polymers cause inflammation due to leucocyte infiltration, and a loss of crypt and villi cells in the intestine of *Girella laevifrons* (Ahrendt et al., 2020). A study by Mbugani et al. (2022) reported that MPs caused histomorphological damage, such as induced intestinal wall degeneration, reactions on epithelial, goblet, and cryptic glandular cells, leucocytic infiltration, and blood congestion.

On the other hand, the histological section of the intestinal tract of zebrafish fed with different type and sizes of feed found MP particles in intestine tissues, but MPs did not induce any histopathological effects (Batel et al., 2020). The histological analysis of marine fish from natural habitats in the study of Haave et al. (2021) also did not reveal any tissue reaction that could be related to the accumulation of MPs. However, histological studies in fish tissue exposed under natural conditions clearly demonstrated the internalization or translocation of MPs. Histological information about marine fish from the natural state is important to determine the possible effects of MPs accumulation, which can be used as a reference to the effects of MPs on humans.

Baru and Trisik Beaches (BTB) are tourist destinations, famous fishing grounds, and sea turtle conservation areas important for local communities (Prakoso, 2018; Sahubawa et al., 2015). These two areas are also separated by the Progo River Estuary (PRE), which has become one of the hotspots of plastic pollution as described by Tasseron et al. (2020) and van Sebille et al. (2020). These coastal waters are also vulnerable to MPs contamination due to plastic waste disposal, mainly from tourist areas. Therefore, MPs can enter the ocean from rivers and coastline run-offs (Pequeno et al., 2021; Zhang et al., 2020), leading to the increase MPs in seawater and possibly accumulating in marine biota. However, to the authors' knowledge, no studies are available on MP pollution in the coastal waters of BTB.

This study evaluated MP concentrations in the coastal waters near the PRE, used as a local fishing ground for demersal-pelagic fish. The abundance and characteristics (sizes, colors, shapes, and polymers) of MPs were analyzed in the fish organs, including the dorsal muscle, gills, and gastrointestinal tract (GIT). In addition, we performed histological analysis of the fish intestines comprised of the paraffin method, hematoxylin eosin (HE), and periodic acid- Schiff-Alcian Blue (PAS-AB) staining. The correlation of MPs accumulation in the intestines by histological structure analysis was further studied to determine the structural damage on epithelium denudation, and villi, crypt, and goblet cells. Microplastic polymers were analyzed with Fourier transform infrared (FTIR) technique. The relationship between MP concentrations in surface seawaters, marine fish organs, and environmental parameters at each station was analyzed using principal component analysis (PCA). Our results provided vital information for the accumulation of MPs in demersal-pelagic fish that may be useful for long-term risk management of human health.

2. METHODOLOGY

2.1 Study area

This study was conducted at the coastal waters of BTB, Special Region of Yogyakarta, Indonesia. The BTB is located near a lowland consisting of a settlement area, field, sand mine, shrimp farm, tourist areas, and seafood restaurants. The PRE separates the BTB by black sand (Prakoso, 2018; Sahubawa et al., 2015). Surface seawater and marine fish were collected from October to November 2021 (west wind season). Twelve sampling stations with three replications each were selected in the BTB based on the visual level of plastic pollution and fishing activities related to the catchment of demersal and pelagic fish, according to a study by Koongolla et al. (2020).

The 12 sampling stations were divided into two lines: line 1 (stations 1 to 6), which was one mile away from the beach, and line 2 (stations 7 to 12), which was one mile away from line 1 (Figure 1). Sampling performed in line 1 evaluated the concentration of MPs in the tidal zone and estuary, while sampling in line 2 analyzed the concentration of MPs in the territorial sea. Stations 1 (7°59′55,917″ S 110°12′ 18,446″ E) to 6 (7°58′38,246″ S 110°9′57,561″ E) are classified as fishing grounds near the tourist location, which are densely populated. In addition, stations 3 and 4 are situated close to the PRE. Stations 7 (8°0′38,443″ S 110°11′47,511″ E) to 12 (7°59′19,893″ S 110°9′25,442″ E) are infamous fishing grounds.

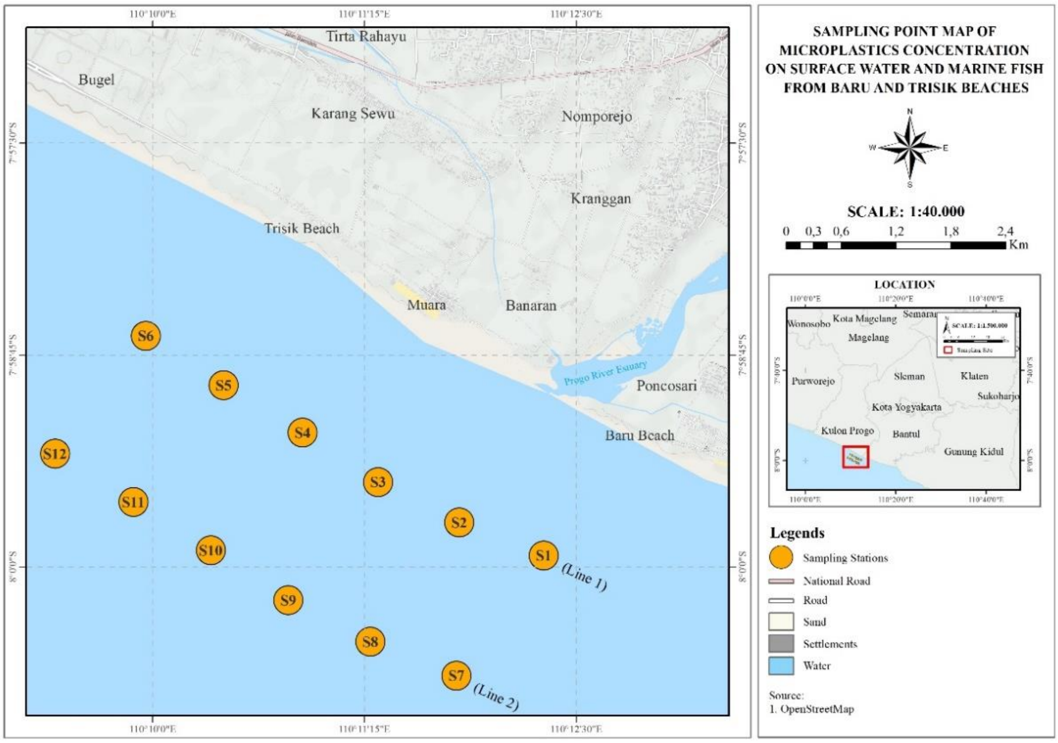

Figure 1. The sampling stations of surface seawater and marine fish collected in BTB

2.2 Sample collection

Surface seawater and marine fish samples from the 12 stations were collected from a fisherman's boat using a 15 PK capacity machine. Seawater was sampled in triplicate (at each station) at a depth of 0-60 cm from the surface referring to McNeish et al. (2018) and Sun et al. (2018), into a 5 L container and closed to avoid contamination (Yan et al., 2019; Zhang et al., 2020). Marine fish samples were collected using a gill net (length 50 m). Marine fish from all stations were identified and stored in an icebox. Marine fish species at each station were measured as the relative frequency (%) to the total number and recommended MPs biomonitoring species referring to Ali et al. (2020). Environmental factors measured in triplicate at each station included air and water temperature, pH, dissolved oxygen (DO), and salinity of seawater.

2.3 MPs extraction

Microplastics were extracted from surface seawater according to the methods described by Sun et al. (2018), Yan et al. (2019), and Zhang et al. (2020). For marine fish, MPs were extracted according to Karami et al. (2017), Koongolla et al. (2020), and Maaghloud et al. (2020). The surface seawater was filtered using a 0.45 µm filter paper (Whatman TM, UK) to filter MPs <5 mm (Zhang et al., 2020). The filter papers were stored in Petri dishes and labeled for identification and characterization.

Fish were captured and measured for length and weight. This research also identified the fish species using an identification book and database. Fish were dissected and separated into the gills, GIT, and dorsal muscles based on the recommendations of Barboza et al. (2020). Each organ was prepared, weighed, and analyzed in the laboratory to prevent contamination. Microplastics were extracted using 10% KOH (Barboza et al., 2020; Karami et al., 2017; Koongolla et al., 2020). The fish organ samples were dried in an oven at 60ºC for 24 h to dissolve the organic compounds. After digestion, the solution was filtered on a 0.45 µm filter paper (WhatmanTM, UK). The filter paper was air-dried at room temperature and then stored in a Petri dish to identify the MPs. A control filter paper (i.e., filtered distilled water) was also included in MP identification. Extraction was performed as described above. The control sample was used against the laboratory samples to check for contamination (McNeish et al., 2018).

2.4 Microplastics characterization

Microplastics were observed using a Leica ICC50E and Optilab microscope. The characterization was based on size, shape, color, and polymer type according to GESAMP (2015), Hidalgo-Ruz et al. (2012), and McNeish et al. (2018). Microplastic sizes were classified into small (<1.5 mm), medium (1.5-3.3 mm), and large (>3.3 mm) and measured with Image Raster. The shape was classified into fragments, fibers, films, foams, and pellets. The color was classified into white, blue, green, red, yellow, brown, black, and transparent.

Polymers were characterized using Fourier transform infrared spectroscopy (FTIR) with a wavelength range of 4,000-400 cm^{-1}. The spectra were analyzed with OMNIC Software (Thermo Fisher Scientific Inc.) as described by Barboza et al. (2020) and Koongolla et al. (2020). The FTIR tests were based on the MPs shape and color. Analyzed spectrum data were compared with the reference database matching >85% to determine the type of polymers.

2.5 Histological analysis

The histological structure was analyzed in the intestine of two demersal species from stations S1, S3, and S6. Two demersal fish species were selected based on the highest number of demersal fish, commercial species, and amphidromous species. In addition, the two demersal species were used to evaluate MPs accumulation in coastal water of BTB and PRE. Three stations were selected based on the visual plastic pollution in line 1, station S1 was near Baru Beach, S3 was close to the PRE, and S6 was nearby Trisik Beach. Samples from these three stations were used to determine MPs accumulation on the beaches and estuary.

The MPs structure was analyzed in triplicate from fish intestine samples by the paraffin method as described elsewhere Ahrendt et al. (2020), Limonta et al. (2019), and Ratucoreh and Retnoaji (2018). The GIT samples were excised mid-intestinal for histological analysis, and the other sections were used for MPs extraction. Intestine samples were washed using 0.9% NaCl, fixed with a 10% neutral buffer formalin (NBF) solution, and then washed with 70% alcohol until clear. This intestine sample was dehydrated with an alcohol series starting from 70%, 80%, 90%, 96%, to 100%. It was cleared and infiltrated with toluene solution and paraffin at 60°C. This organ was sectioned with a rotary microtome at 5 µm. The coupe was pasted on object glass and stained with HE and PAS-AB. Before staining the coupes, all coupes of the intestine section were observed under the microscope to detect MPs particles. The MP particles were carefully collected from the coupes and separated with paraffin for FTIR tests. After MPs were retrieved from the intestinal tissue, paraffin blocks were cut again to obtain coupes for staining.

The coupes on object glass were deparaffinized with xylol for 30 min and washed in the alcohol series starting from 96%. The samples were dipped into hematoxylin for 10 s and washed with running water for 10 min. The samples were dipped into distilled water and the alcohol series starting from 30% to 70%. Afterward, the samples were stained with eosin Y for 1 min and washed in the alcohol series, starting from 70% to 96%. The samples were sealed with Canada balsam and a cover glass. The PAS-AB staining method commenced with deparaffinization and hydration using the alcohol series. The sample was dipped into alcian-blue for 5 min and washed with distilled water, slides were dipped into periodic acid 1% for 5 min, followed by Schiff reagent for 5 min. The slides were washed with warm distilled water, dehydrated with distilled water series, and mounted with xylol. The samples were sealed with Canada balsam and a cover glass. The histological analysis assessed the occurrence and localization of possible MPs particles in the tissues with a LEICA microscope (Haave et al., 2021).

2.6 Statistical analysis

Statistical analysis was conducted using Microsoft Excel 2013, SPSS v.25, and Xlstat. One-way ANOVA and Tukey test were performed to compare the MP concentrations in the surface seawater and marine fish at each station and the relationship between MPs in fish species. The relationship of MPs in surface seawater with environmental factors was analyzed with one-way ANOVA, Duncan, and Pearson correlation tests. The correlation of MPs in surface seawater and marine fish with environmental parameters was determined by PCA. One-way ANOVA and Kruskal-Wallis’s test analyzed the internalization of MPs in the intestine. Analysis of histology data (villi length, depth of crypt cells, and the number of goblet cells) of MPs in the GIT was tested by one-way ANOVA, Duncan, and Pearson correlation.

3. RESULTS AND DISCUSSION

3.1 Microplastics in surface seawater

Monitoring MPs in the BTB showed that the pollutant contaminated surface seawater at all stations. Microplastics in the surface seawater were significantly different at each station ($p<0.05$) (Figure 2(a)). Small particles (<1.5 mm) dominated the size of MPs (Figure 2(b)). Similar results have been reported by Zhang et al. (2020), which demonstrated MP pollution in the east coastal areas of Guangdong, South China, and the Pearl River estuary. The authors verified the degradation of plastics into MPs in the mentioned coastal waters and estuary. In this study, MPs potentially re-entered the coastal waters by ocean currents, waves, and wind, and may increase in the water column, and seafloor (Haave et al., 2021). Bastesen et al. (2021) reported similar results, where the Norwegian coastline over 100,000 km had a high concentration of MPs from the Norwegian Coastal Current and winds from the southwest.

The highest MP concentration (25 particles/L) was observed at station 3 (Figure 2(a)). This station is an estuary area receiving strong anthropogenic pressures from rivers, Rodrigues et al. (2020) on surface seawater at a Portuguese Estuary and Marine Park. In addition, fishing activities may increase the concentration of MPs from fishing lines or fishing tools.

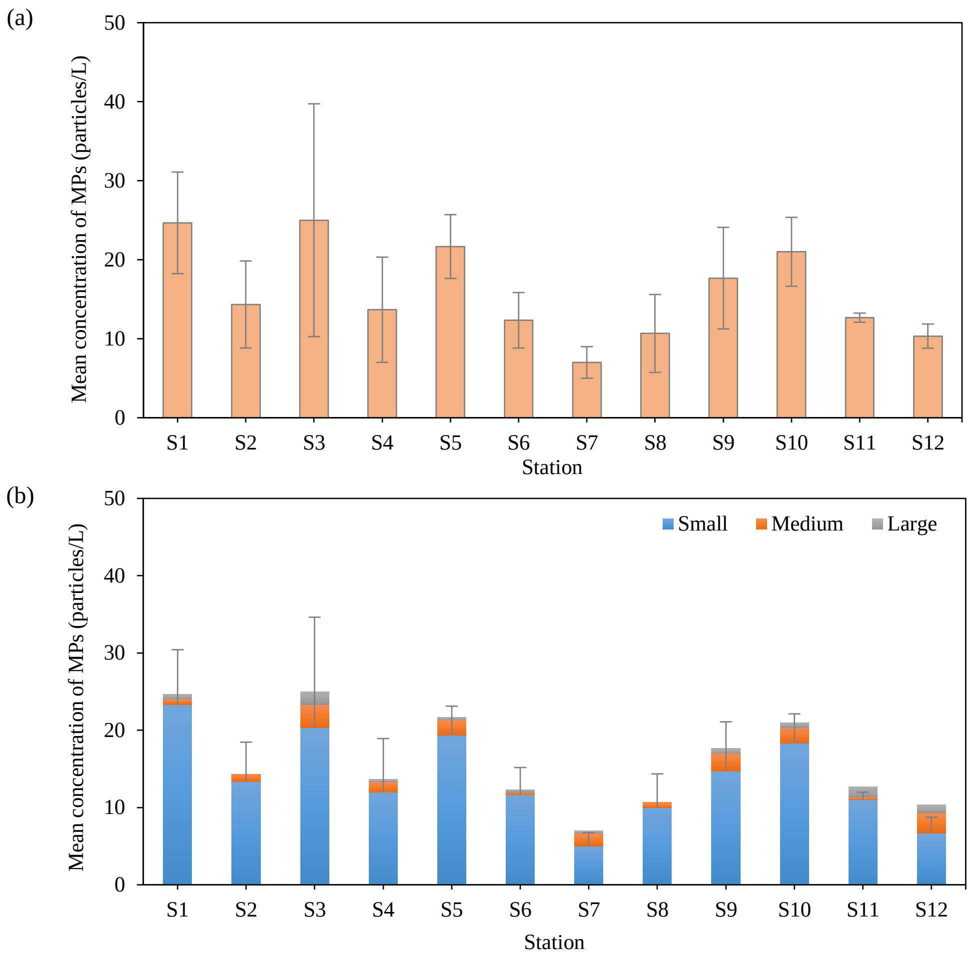

Figure 2. Concentration of MPs (a) and concentration of MPs in three size fractions (b) in surface seawater.

When comparing MPs concentration in surface seawaters at BTB, our results showed that lines 1 and 2 had 12.3-25.0 particles/L and 7-21 particles/L, respectively. The stations at line 1 had a higher concentration of MPs, suggesting MP pollution at these stations might be ascribed to their proximity to the shoreline (about 1 mile) and the mouth of the PRE. It also indicates that the high concentration of MPs in the estuary was dispersed by the currents, as reported by Haave et al. (2021).

3.2 Microplastics in marine fish

This study highlights the accumulation of MPs in all marine fish samples. A total of 21 species were divided into two habitat groups (10 demersal and 11 pelagic fish) (Table 1). Most marine fish were carnivores, except *Gazza minuta* and *Gerres oyena* which were omnivores. The MPs were found in the dorsal muscles, gills, and GIT of all fish samples, similar to the studies by Koongolla et al. (2020) and Maaghloud et al. (2020). In this study, the MP concentrations in the dorsal muscles, gills, and GIT were significantly different among stations ($p < 0.05$) (Figure 3(a)), commonly found in other studies Koongolla et al. (2020), Maaghloud et al. (2020), and Zhang et al. (2021).

The percentage of MPs accumulation was highest in the gill (37.49%) and GIT (37.38%), while the lowest was in the dorsal muscle (25.13%). These results indicate that MPs entered the fish mainly through the respiratory and digestive systems (Limonta et al., 2019). The gill-water interface causes the MPs to enter the fish's body readily. Our results are similar to those reported by Barboza et al. (2020) and Yona et al. (2022). Microplastic accumulation in the organs indicates MP pollution in the beach waters. Accumulation of MPs in gills can cause a decrease in respiratory efficiency and hypoxia (Movahedinia et al., 2012). In addition, MPs in the dorsal muscle can result from skin lesions and the bloodstream (Barboza et al., 2020).

Microplastics were accumulated in demersal and pelagic fish species 14.47-55.50 particles/fish (Table 1). The MP concentrations varied in marine fish with no standard threshold. The abundance of MPs and marine fish in the region might be influenced by swimming, cruising, and feeding habit (Koongolla et al., 2020; Maaghloud et al., 2020). The distribution of all marine fish species in this study may provide information on relative frequency values that can be used as a recommendation for microplastic biomonitoring. There were five species with high relative frequency (%), *Eleutheronema tetradactylum* (ET), *Eubleekeria splendens* (ES), *Leiognathus equula* (LE), *Scomberoides lysan* (SL), and *Scomberoides tala* (ST). Our results showed that the accumulation of MPs in the fish was higher than that detected by Mistri et al. (2021) in commercial marine fish from the Adriatic Sea (2.85-4.11 particles/fish), and marine fish from the coastal waters and estuary of the West China Sea (0.3-5.3 particles/fish) by Su et al. (2019).

For the demersal fish, we found a high MP accumulation of MPs was found in *E. tetradactylum*, *E. splendens*, *L. equula*, and *E. tetradactylum*, a demersal fish, had the highest number of individuals for 11 stations and accumulated the most MPs (Table 1). The highest MPs accumulation in pelagic fish was *S. lysan*, *S. tala*, and *S. lysan* the most common pelagic fish found at the research stations. These two fish species have high economic value at the research locations, and they are widely consumed by the surrounding community.

In previous studies, the highest MPs accumulation and distribution in estuarine-coastal waters area was observed in *E. tetradactylum*, suggesting its potential as an indicator species for MPs biomonitoring (Karbalaei et al., 2019; Mirad et al., 2020). This fish is an amphidromous species, so it has a high risk of accumulating MPs from the river, estuarine, and marine areas. The dominant pelagic fish family was Carangidae, this family is known to be present widely around the Atlantic, Indian, and Pacific Oceans. The Carangidae is also the fastest predator in the ocean (Maaghloud et al., 2020). Sawalman et al. (2021) reported that three species of the family of Carangidae from Barranglompo Island, Makassar, Indonesia, also accumulated MPs, similar to the results described for the Moroccan Central Atlantic Coast (Maaghloud et al., 2020). Furthermore, skipjack tuna (*K. pelamis*) and mackerel (*S. commerson*) are marine fish very popular for consumption in Indonesia that were also found to accumulate MPs (Chen et al., 2021; Syafitri et al., 2021; Yona et al., 2022).

Similar to surface seawater, MP concentrations in fish at the stations of line 1 were also higher than those of line 2. Marine fish at line 1 was more susceptible to ingesting MPs, while current velocity from surface waves can affect the ability of MPs to settle in seawater (Pequeno et al., 2021). Stations 3, 4, and 5 showed a similar pattern of MP accumulation in fish (Figure 3(a)), which was higher than the other stations. This indicates that the estuary is a protected area with a high diversity and abundance of marine fish. In addition, the estuary is a nursery area since many marine fish reproduce and spend the early part of their lives here (Pequeno et al., 2021). Current waves affect the distribution and accumulation of MPs in the estuary (Zhang et al., 2020). Accumulation of MPs in the marine fish at line 1 may be affected by hydrodynamic force, feeding habits, swimming range, and interaction with ecosystem components (Pequeno et al., 2021; Zhang et al., 2021). Species *E. tetradactylum*, *E. splendens*, *L. equula*, *S. lysan*, and *S. tala* are amphidromous fish crossing estuarine-marine ecosystems (Mirad et al., 2020). In this study, the amphidromous species have a high concentration of MPs (Figure 3(b)), which was also confirmed by Zhang et al. (2021).

Table 1. Accumulation of MPs in marine fish at all stations

Fish species	Family	Category	Body length (cm)	Body weight (g)	Number of fish at all stations	Average of MPs accumulation at all stations (particles/fish)	Relative frequency (%)
Demersal fish							
Eleutheronema tetradactylum (ET)	Polynemidae	Threadfins	14.10-30.33	70.12-257.95	144	20.31	15.49
Eubleekeria splendens (ES)	Leiognathidae	Ponyfish	12.20-18.50	40.21-60.83	100	20.54	9.86
Leiognathus equula (LE)	Leiognathidae	Ponyfish	13.36-18.80	47.12-64.31	113	18.54	9.86
Karalla daura (KD)	Leiognathidae	Ponyfish	14.18-16.35	50.36-68.51	32	14.47	2.82
Gazza minuta (GM)	Leiognathidae	Toothpony	15.13-18.02	43.70-61.11	47	14.47	5.63
Gerres oyena (GO)	Gerreidae	Silverbellies	14.12-15.28	40.15-51.02	22	17.77	2.82
Johnius belangerii (JB)	Sciaenidae	Croackers	17.90-21.30	54.02-115.00	47	17.36	5.63
Johnius dussumieri (JD)	Sciaenidae	Croackers	30.55-36.20	250.15-290.12	10	19.60	1.41
Drepane longimana (DL)	Drepaneidae	Concertina fish	17.50-18.00	50.35-55.05	2	16.00	1.41
Mystus gulio (GL)	Bagridae	Long whiskers catfish	28.20-33.70	140.93-253.78	9	22.44	9.86
Pelagic fish							
Scomberoides lysan (SL)	Carangidae	Carangids/Jack and pompanus	28.20-33.70	140.93-253.78	54	22.44	9.86
Scomberoides tala (ST)	Carangidae	Carangids/Jack and pompanus	23.70-34.70	115.12-255.15	42	19.02	7.04
Atule mate (AM)	Carangidae	Carangids/Jack and pompanus	16.35-23.41	70.35-205.35	36	17.72	4.23
Carangoides oblongus (CO)	Carangidae	Carangids/Jack and pompanus	16.80-24-50	120.25-140.12	21	20.71	4.23
Caranx ferdau (CF)	Carangidae	Carangids/Jack and pompanus	15.80-21.50	115.60-143.54	20	17.45	2.82
Caranx sexfasciatus (CS)	Carangidae	Carangids/Jack and pompanus	17.80-19.70	120.20-126-12	5	19.20	1.41
Caranx ignobilis (CI)	Carangidae	Carangids/Jack and pompanus	17.18-21.50	163.36-258.26	21	17.43	2.82
Katsuwonus pelamis (KP)	Scombridae	Mackerels	26.00-28.90	170.00-205.02	22	20.18	4.23
Scomberomorus commerson (SC)	Scombridae	Carangids/Jack and pompanus	35.52-36.10	180.50-208.60	5	28.20	1.41
Sphyraena barracuda (SB)	Sphyraenidae	Barracudas	45.00-47.20	320.20-360.20	2	55.50	2.82
Trichiurus lepturus (TL)	Trichiuridae	Largehead hair tall	51.25-52.26	142.50-145.50	2	21.50	1.41

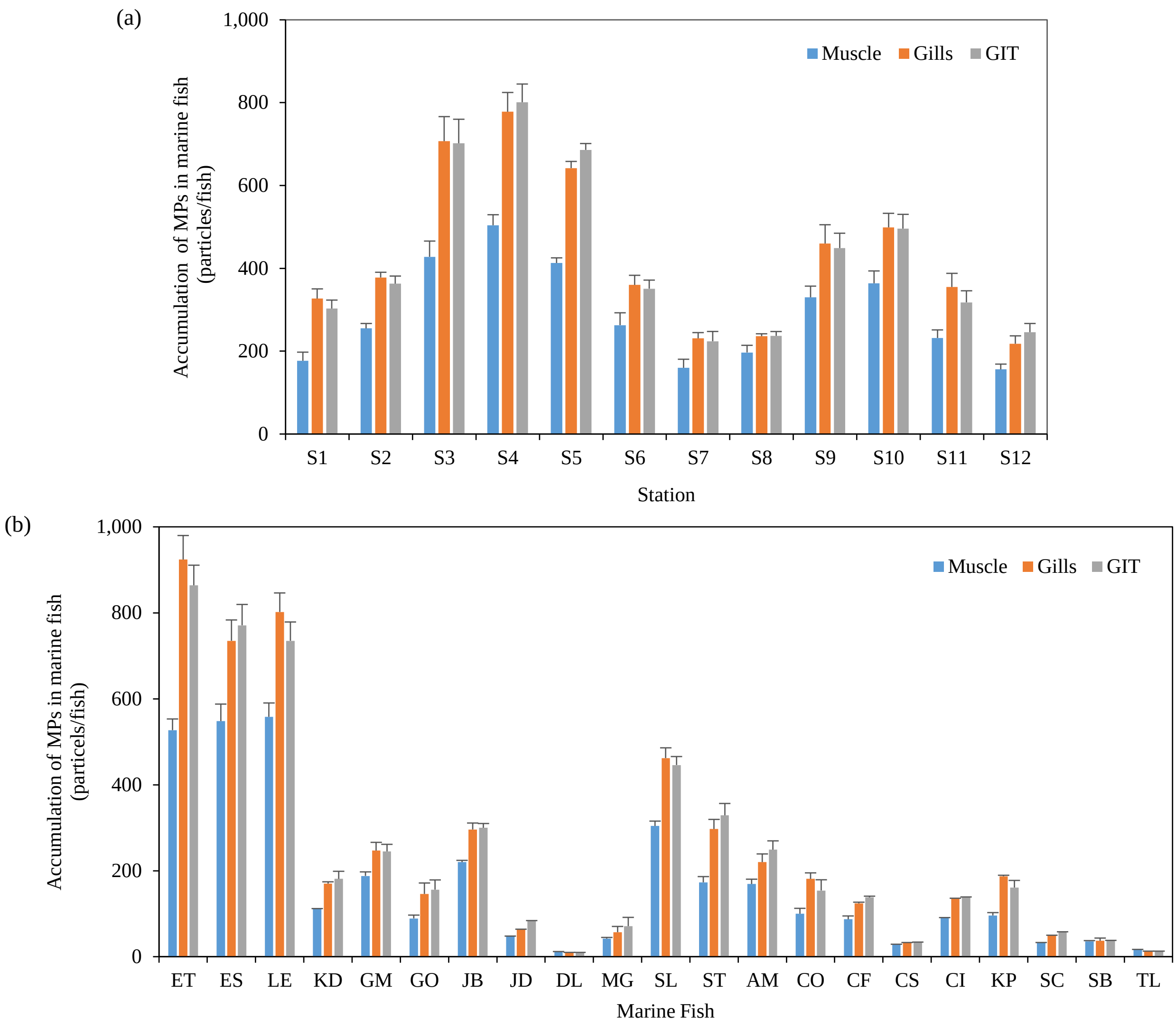

Figure 3. Accumulation of MPs in fish found in each (a) station (a) and (b) fish species

3.3 Microplastics characteristics

In this study, MPs found in the surface seawater were dominated by small particle sizes (<1.5 mm) (Figure 4(a)), similar to the results demonstrated by Guven et al. (2017) and Koongolla et al. (2020). This finding suggested that MPs in marine fish tend to be associated with MPs concentrations in surface seawater. The accumulation of MPs in marine fish may also be affected by their position in the food chains.

The shape of MPs found in surface seawater was dominated by films (73.30%), followed by fibers (13.09%), fragments (12.39%), foams (1.05%), and pellets (0.17%) (Figure 4(b)). Similar results were reported by Pattiaratchi et al. (2022), where film and fiber were the most dominant MPs in the Indian Ocean from various regions. However, in the dorsal muscle of marine fish, the most dominant MP shapes were fragments (70.62%) and fiber (14.29%). Fiber and fragments can be internalized by skin lesions or the blood (Barboza et al., 2020). For the gills and GIT, films were the most dominant MP shape (gills 74.22% and GIT 74.57%) (Figure 4(b)), although differences were found between gills and GIT. Film and fiber accumulate and trigger the perception that MPs are fish food (Galloway et al., 2017).

For MP colors in surface seawater, the most dominant colors were black, brown, and transparent, but they varied in marine fish (Figure 4(c)). Importantly, the color of MPs acts as a visual appearance similar to natural prey in marine ecosystems (Savoca et al., 2017).The most dominant MP polymers in surface seawater included PE (38%), PP (24%), and PET (24%) (Figure 4(d)). It is known that PE and PP have a lower specific gravity, thus they are more commonly found in surface seawater (Amelia et al., 2021). Similar results were reported by Rodrigues et al. (2020).

The shape of MPs found in surface seawater was dominated by films (73.30%), followed by fibers (13.09%), fragments (12.39%), foams (1.05%), and pellets (0.17%) (Figure 4(b)). Similar results were reported by Pattiaratchi et al. (2022), where film and fiber were the most dominant MPs in the Indian Ocean from various regions. However, in the dorsal muscle of marine fish, the most dominant MP shapes were fragments (70.62%) and fiber (14.29%). Fiber and fragments can be internalized by skin lesions or the blood (Barboza et al., 2020). For the gills and GIT, films were the most dominant MP shape (gills 74.22% and GIT 74.57%) (Figure 4(b)), although differences were found between gills and GIT. Film and fiber accumulate and trigger the perception that MPs are fish food (Galloway et al., 2017).

For MP colors in surface seawater, the most dominant colors were black, brown, and transparent, but they varied in marine fish (Figure 4(c)). Importantly, the color of MPs acts as a visual appearance similar to natural prey in marine ecosystems (Savoca et al., 2017). The most dominant MP polymers in surface seawater included PE (38%), PP (24%), and PET (24%) (Figure 4(d)). It is known that PE and PP have a lower specific gravity, thus they are more commonly found in surface seawater (Amelia et al., 2021). Similar results were reported by Rodrigues et al. (2020).

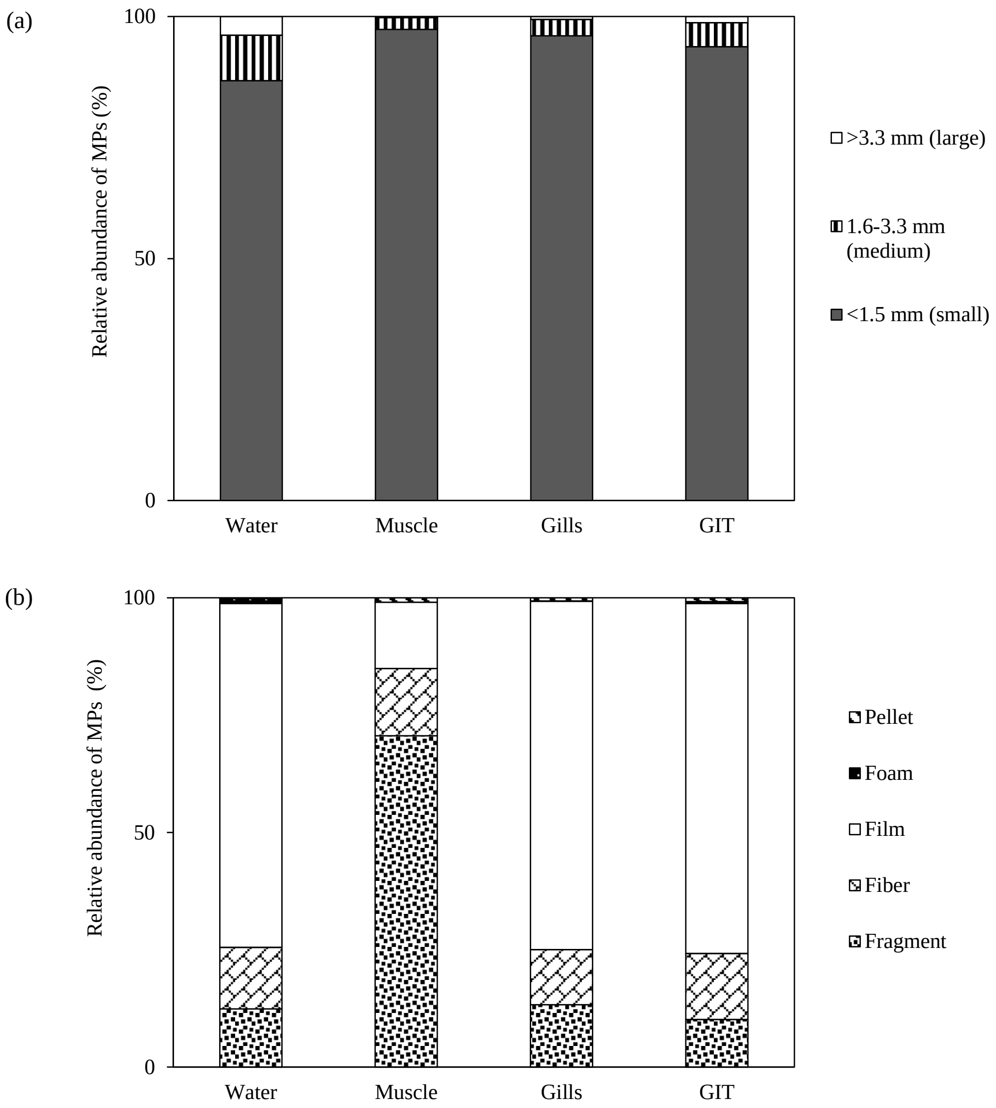

Figure 4. Relative abundance of MPs classified according to their (a) sizes, (b) shapes, (c) colors, and (d) type of polymers in water and fish organs

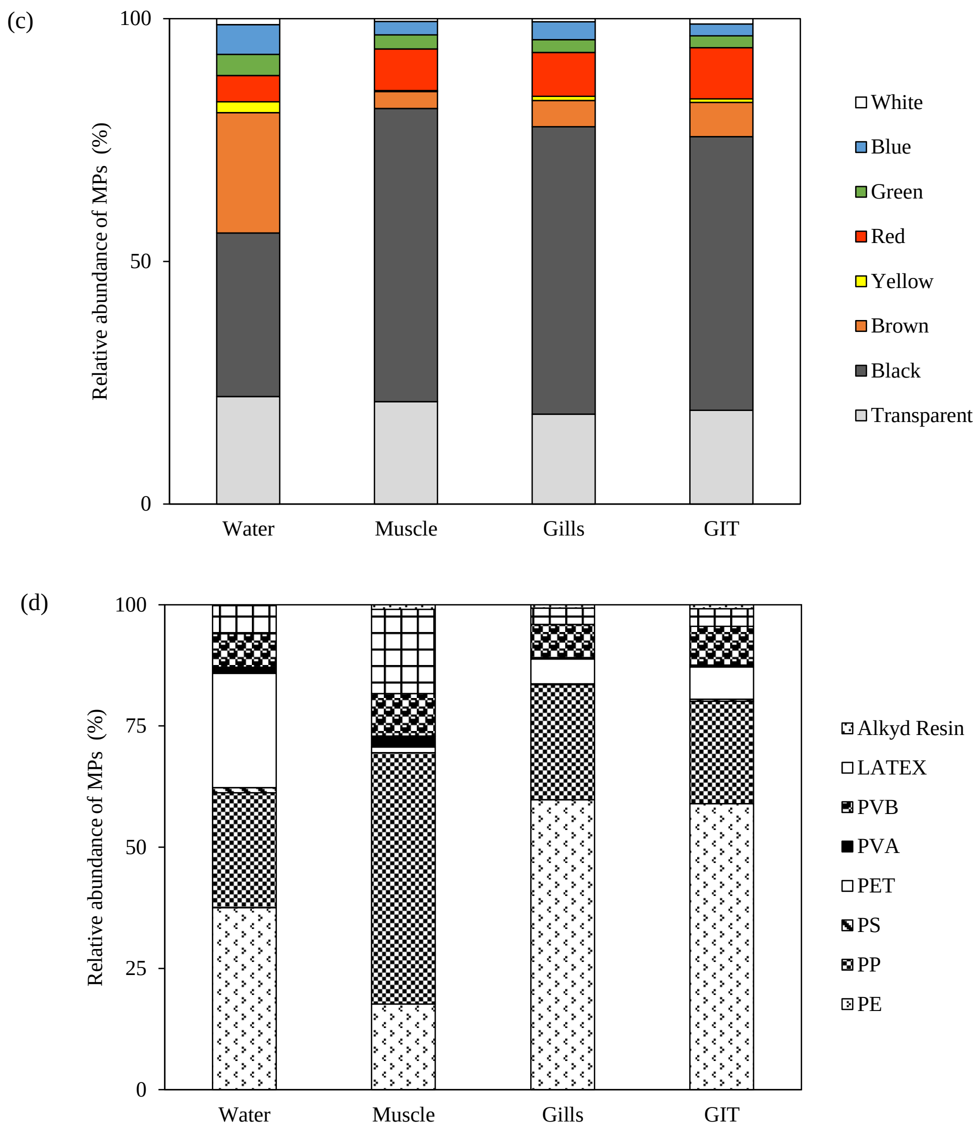

Figure 4. Relative abundance of MPs classified according to their (a) sizes, (b) shapes, (c) colors, and (d) type of polymers in water and fish organs (cont.)

Microplastic polymers that accumulated in marine fish organs were primarily PE and PP (Figure 4(d)). This result was consistent with polymers in surface seawater and other studies by Koongolla et al. (2020), Zhang et al. (2020), and Barboza et al. (2020). These two polymers are the most widely used type of thermoplastics in various human materials, such as packaging and fishery equipment, and are generally found in marine waters and biota (Andrady, 2011). Some of the risks of MPs accumulation in marine fish depend on their physical and chemical characteristics, as previously demonstrated in animal models (Barboza et al., 2020; Limonta et al., 2019). The consumption of marine fish worldwide containing MPs is inevitable, thereby exposing humans to MPs (Smyth and Elliott, 2016).

3.4 Environmental factors and PCA analysis

The results for the environmental variables are shown in Table 2. Sampling was performed from October to November 2021, which is the rainy season. In this study, air and water temperature, salinity, pH, and DO did not show significant differences between stations ($p>0.05$), as confirmed by Duncan's test analysis (Table 2). These findings highlight which estuarine-marine area had transitional conditions. However, statistically significant differences were detected between (i) low (S3 and S4) and high (S2, S5, S6, S7, and S11) air temperatures, (ii) low (S3) and high (S1, S11, and S12) water temperatures, (iii) low (S7) and high (S10) salinity, (iv) low (S3) and high (S10) pH, and (v) low (S3) and high (S5) water DO. These findings emphasize that environmental factors at the BTB stations varied between the coastal and estuary waters. Pearson correlation analysis found that the MP concentration in surface seawater did not correlate to the average air temperature, water temperature, pH, and DO. However, our findings suggest that the MP concentration in surface waters was correlated to the average salinity.

Our results are similar to those of Defontaine et al. (2020), which demonstrated the turbulent mixing effect of salt-wedge estuaries that can drastically affect the water masses and particles like MPs. Similar features were studied in the Ebro Estuary by Simon-Sánchez et al. (2019), where the estuary acted as a salinity barrier for transporting plastic waste. In this study, stations 3, 4, 9, and 10 had higher salinity levels than the other stations. As expected, the salinity of estuarine-marine waters was influenced by the hydrodynamics in these areas (Smyth and Elliott, 2016). Human activities downstream of the PRE include massive sand mining using heavy equipment, marine tourism activities, Vannamei shrimp aquaculture, and settlements. These conditions most likely contributed to MPs accumulation in the estuary and marine ecosystems (Syafiya and Hadisusanto, 2019; Utami et al., 2022).

Table 2. Environmental factors and concentration of MPs in surface seawater at each station

Stations	Air temperature (°C)	Water temperature (°C)	Salinity (‰)	pH	DO (mg/L)	MPs
S1	29.23^{c}	30.06^{h}	32.31^{e}	7.27^{fg}	6.24^{c}	24.67^{c}
S2	30.19^{e}	29.23^{f}	32.64^{f}	7.23^{de}	6.27^{cd}	14.33^{abc}
S3	28.25^{a}	27.24^{a}	33.43^{i}	6.68^{a}	5.31^{a}	25.00^{c}
S4	28.21^{a}	28.22^{c}	33.36^{i}	6.74^{b}	6.40^{d}	13.67^{abc}
S5	30.24^{e}	29.18^{ef}	32.34^{e}	6.92^{c}	6.70^{e}	21.67^{bc}
S6	30.13^{e}	28.20^{c}	32.13^{d}	7.20^{d}	6.36^{cd}	12.33^{ab}
S7	30.20^{e}	28.08^{b}	30.32^{a}	7.24^{de}	6.35^{cd}	7.00^{a}
S8	29.09^{c}	28.32^{d}	33.14^{g}	7.26^{efg}	6.32^{cd}	10.67^{ab}
S9	28.50^{b}	29.12^{e}	33.22^{h}	7.29^{g}	5.71^{b}	17.67^{abc}
S10	28.35^{ab}	29.61^{g}	33.63^{k}	7.32^{h}	6.36^{cd}	21.00^{bc}
S11	30.10^{e}	30.10^{h}	31.13^{b}	7.23^{de}	6.33^{cd}	12.67^{ab}
S12	29.60^{d}	30.02^{h}	31.29^{c}	7.25^{ef}	6.42^{d}	10.33^{ab}

Numbers followed by the same letter in the same column indicate insignificant differences with Duncan's test with at a significance level of 0.05.

It should be noted that the intensity and frequency of rain events were relatively high during the study period, causing the Progo River to increasingly discharge into the estuary area and bring various wastes to the sea. During the rainy season, starting in August, sea surface runoff transfers MPs to the coastal area, which is also influenced by environmental parameters, including salinity, wind, and other hydrodynamic conditions (Kanhai et al., 2018). In this study, the rainy season was a period of high rainfall, causing high river water discharge that increased the water output to the sea (river flush) via the estuary area. This condition contributed to the fragmentation of plastics into micro or nanoplastics (Lima et al., 2014). The contamination of MPs has been closely related to climate change as plastic production results from the extraction of fossil fuels, although it cannot be determined how much greenhouse gas emissions are produced from plastics, and the distribution of MPs in the sea also influences climate (Ford et al., 2022). This study is consistent with previous results that showed temperature and UV light to greatly contribute to the fragmentation of MPs (Gola et al., 2021).

A PCA analysis was conducted to identify which environmental variables explain the variation in MP concentration at each station. PCA analysis on environmental factors, surface seawater, and marine fish (27 active variables) showed a spatial distribution of the sampling stations in the four quadrants (Figure 5). The biplot revealed an apparent clustering of MP concentrations on the first (F1) and second (F2) axes, explaining >42.95% of the total variance. The first axis (F1) explained 23.76% of the variance, which divided the biplot according to the stations. The highest MP-contaminated seawater was found for S3, ET, MG, ES, ST, KP, SL, and LE samples. Notably, the MP concentration at S3 correlated with the salinity of the seawater. Stations S7, S12, S8, S11, and S6 had lower MP concentrations.

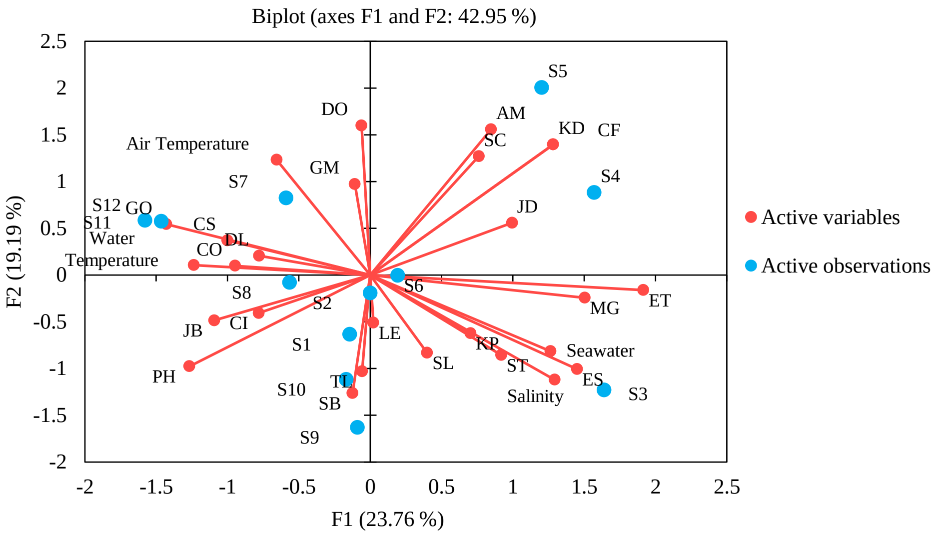

Figure 5. PCA biplot of environmental factors and MP concentration of surface seawater and marine fish

3.5 Histological analysis and MP internalization in the intestine from two demersal marine fish

The histological analysis was conducted to observe potential correlations between structural characteristics with MPs accumulation (Ahrendt et al., 2020). Several findings have revealed that the presence of MPs can affect the histology of the GIT (Limonta et al., 2019; Furukawa et al., 2004; Qiao et al., 2019). In this research, histological analyses were carried out on two demersal fish, *Eleutheronema tetradactylum* (ET) and *Leioghnathus equula* (LE), from three stations using HE and PAS-AB staining (Figure 6) following the methods of Limonta et al. (2019) and Haave et al. (2021) who analyzed the intestinal histology of zebrafish and the gut histology of several wildlife marine biotas, respectively. The two selected fish species are demersal and amphidromous, have a high relative frequency (%), and accumulate MPs. Microplastic internalization of intestinal tissue was analyzed with microscopy and FTIR analysis using MP particles from intestinal coupes. Appropriate steps were taken during the histological process to avoid the presence of artifacts (Batel et al., 2020).

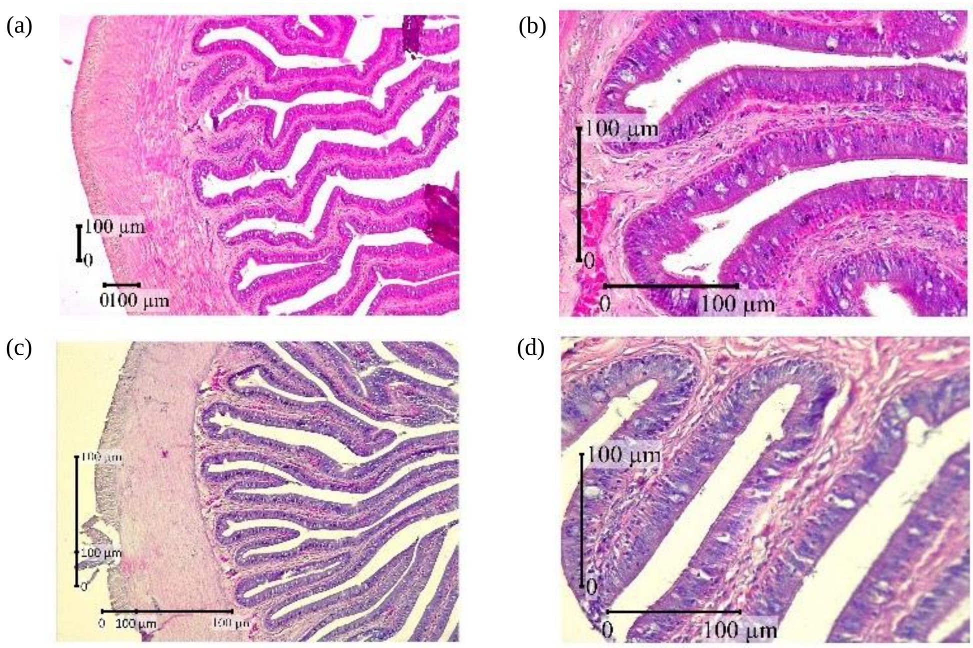

Figure 6. Histology of intestine with HE staining of ET with 100× magnification (a) and 400× magnification (b), LE with 100× magnification (c) and 400× magnification (d), histology of intestine with PAS-AB staining of ET with 100x magnification (e) and 400× magnification (f), LE with 100× magnification (g) and 400× magnification (h)

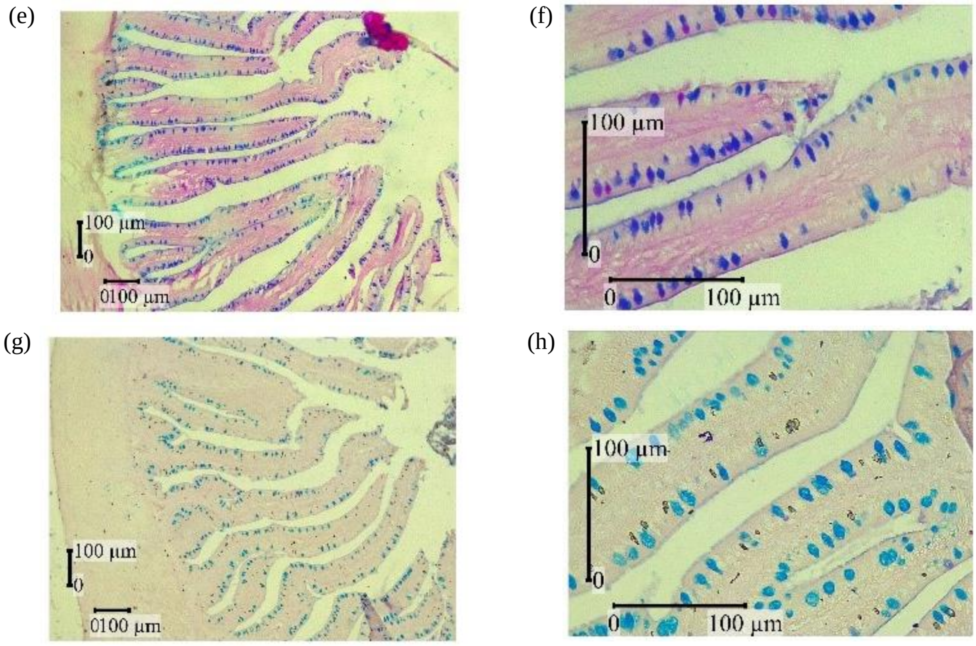

Figure 6. Histology of intestine with HE staining of ET with 100× magnification (a) and 400× magnification (b), LE with 100× magnification (c) and 400× magnification (d), histology of intestine with PAS-AB staining of ET with 100x magnification (e) and 400× magnification (f), LE with 100× magnification (g) and 400× magnification (h) (cont.)

These findings highlight, the MP particles found in the intestine and/or tissue of *E. tetradactylum* and *L. equula* (Figure 7(a-d)). Although our results differ slightly from Haave et al. (2021), who did not find MP particles in the intestinal samples, they are consistent with those of Batel et al. (2020) and Cauwenberghe et al. (2015), who detected MPs in the digestive system of blue mussels (*Mystus edulis* L.) and the zebrafish intestine, respectively. Tissues were positive for MP internalization based on physical characteristics (size, shape, and color) identified by microscopy and FTIR. The Kruskal-Wallis test on MP particles of the *E. tetradactylum* showed a significant ($p<0.05$) difference among the stations. In contrast, the Kruskal-Wallis test on MP particles of the *L. equula* did not differ significantly ($p>0.05$) among stations. This study investigated the internalization of MP particles in intestinal tissue with a focus on polymers (PP, PE, PVA, and LATEX), shapes (fragment and fiber), and colors (transparent, brown, black, red, blue, and green). Microplastics were frequently found in intestinal tissues samples. The presence of MPs in the intestinal tissues was observed by structural histology damage (Figure 7).

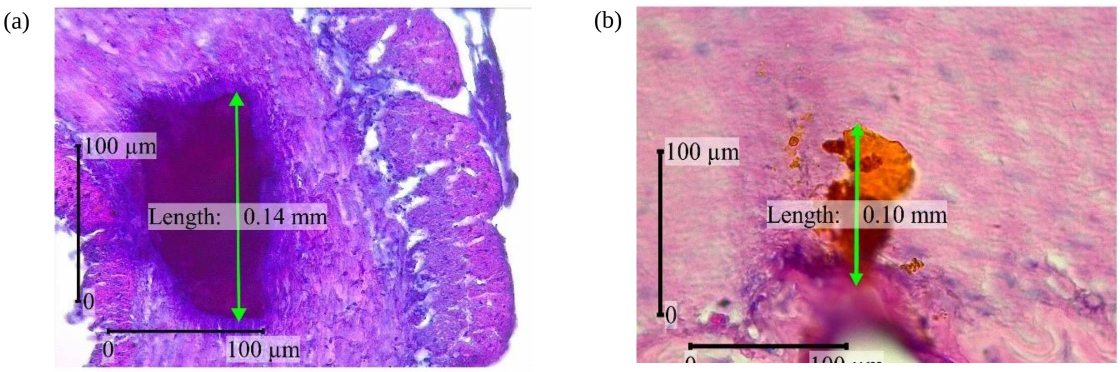

Figure 7. Internalization of MP particles for intestinal histology analysis with HE staining. Microplastics in ET intestinal samples (a-b), MPs in LE intestinal samples (c-d).

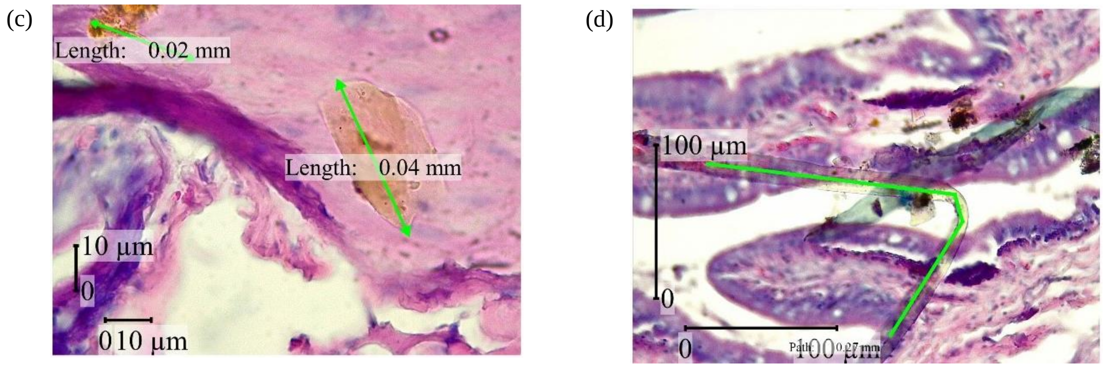

Figure 7. Internalization of MP particles for intestinal histology analysis with HE staining. Microplastics in ET intestinal samples (a-b), MPs in LE intestinal samples (c-d) (cont.).

For research related to the analysis of the impact of MPs accumulation, under natural conditions, on the integrity of the intestinal tissue using histological parameters of the villi cell, crypt cell, goblet cell, and denudation on the epithelial cell under natural exposure, please refer to Ahrendt et al. (2020) and Limonta et al. (2019). Duncan's test analysis (Table 3) confirmed most of the results were not significantly different between stations for *E. tetradactylum* and *L. equula* fish samples. These findings suggest that demersal fish have swimming ranges in both coastal and estuary waters. However, the mean crypt depth of *E. tetradactylum* and the mean villi length of *L. equula* significantly differed among stations. The Pearson correlation found that MP accumulation of MPs in GIT strongly correlated with the average intestinal villi length of *E. tetradactylum* (r=0.728), but it was weakly correlated with the average goblet cells (r=0.389). This result is similar to the study of Ahrendt et al. (2020), which showed that the concentration of MPs in the intestine causes goblet cell loss and a low mean length of the villi. In contrast, *L. equula*, showed that MPs in the GIT were weakly correlated with the average villi length (r=0.314) and were not correlated with the mean crypt depth and the number of goblet cells. This difference might have been influenced by differences in natural prey, and behavior.

Table 3. Average of histology parameters in *E. tetradactylum* (ET) and *L. equula* (LE)

Fish	Stations	Average of villi length (µm)	Average of crypt depth (µm)	Average of goblet's cell	Average of microplastics in GIT
ET	S1	485.37^{a}	75.59^{b}	46.00^{a}	13.33
	S3	498.34^{a}	65.40^{ab}	45.20^{a}	8.33
	S6	485.47^{a}	52.87^{a}	44.40^{a}	11.67
LE	S1	185.05^{a}	19.64^{a}	23.07^{a}	15.67
	S3	157.94^{ab}	15.59^{a}	20.47^{a}	7.67
	S6	269.73^{b}	28.27^{a}	24.80^{a}	6.67

Numbers followed by the same letter in the same column indicate insignificant differences with Duncan's test at a significance level of 0.05.

Accumulation of MPs in the GIT of ET and LE ranged between 8.33-13.33 particles/fish and 6.67-15.67 particles/fish, respectively. In the GIT, the most dominant MPs shape was film, fragment, and fiber. The most dominant MP polymers were PE and PP, similar to the histological sample' physical and chemical results. Therefore, MPs accumulation in the intestine is expected to affect tissue structure and functioning. The effects of MP internalization in the intestine in this study were strongly correlated with the mean villi length. Previous studies have demonstrated that the accumulation of MPs can damage the villus structure and denudation of the epithelium (Ahrendt et al., 2020). The evidence obtained by Zhao et al. (2021) in zebrafish as the animal model also confirms that fish exposed to MPs stimulate intestinal structural damage.

Additionally, this research evaluated the percentage of epithelial denudation in the intestine. Epithelial tissue acts as an important environment-organism interface with several functions, including nutrient transport and osmoregulation, and serves as a barrier against toxicants like MPs (Minghetti et al., 2017). Microplastic accumulation in the intestine causes damage to the epithelial barrier, inflammation, oxidative stress, and microbiota disorder (Jeong et al., 2017). Our study showed that *E. tetradactylum* had higher epithelial denudation than *L. equula*. The percentage of epithelial denudation in *E. tetradactylum* ranged between 70.20% to 89.52%, while *L. equula* ranged between 67.69% to 81.24% (Figure 8). A high percentage of epithelial denudation was found at station 3. This station had a high MP concentration in surface seawater. Nevertheless, the two fish species showed epithelial denudation above 50%, indicating a high level of foreign particles, including internalization of MPs in the intestine (Ahrendt et al., 2020).

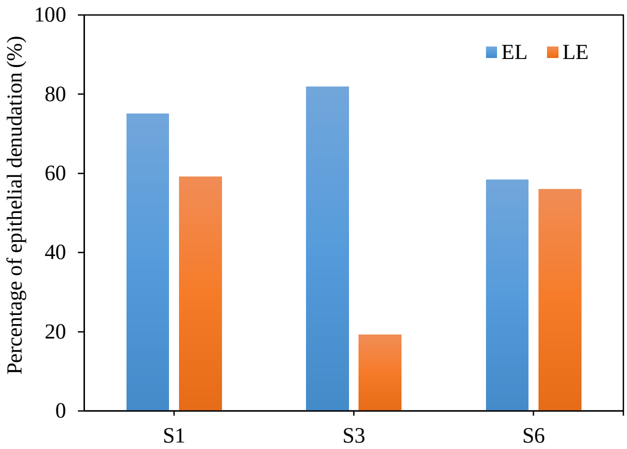

Figure 8. Percentage of epithelial denudation (%) in *E. tetradactylum* (ET) and *L. equula* (LE).

Previous studies by Furukawa et al. (2004) and Qiao et al. (2019) showed that histological analysis of the MP internalized intestine causes significant changes such as damage to epithelial, cracks in the villi, thickening of the walls, and an increase in mucus volume. In this study, the histological structure showed damage to the mean villi's length, goblet cells, and denudation of the villus epithelial cells (Figure 9). These conditions might have been caused by MPs' physical characteristics and polymers that can lead to inflammation.

Previous studies have shown that MPs can destroy the functional barrier of epithelial cells because they increase ion leakage to the lamina propria (Sendra et al., 2021). During MP internalization, the intestine will undergo lysosomal degradation, causing alkalinization and an increase in the reactive oxygen system (Sendra et al., 2021; Jeong et al., 2017). The latter will activate signal transduction mediated by p-ERK, p-38, and Nrf2 (Jeong et al., 2017). Microplastic accumulation has been correlated with the level of mRNA inflammation, such as IL-10, IL-8, IL-IB, SOD, and CAT. Previous studies have confirmed that MPs can cause damage to mucus channels and increase mucus activity, inflammation, and metabolic disorders such as microbiota addiction (Qiao et al., 2019). Microbiota disorders have been changed in gene expression studies, which correlated with changes in the regulation of epithelial integrity in the intestinal cytochrome P450 gene (CYP1A), while dysfunction of the barrier correlated with cortisol stress hormone and inflammatory cytokine release (Furukawa et al., 2004).

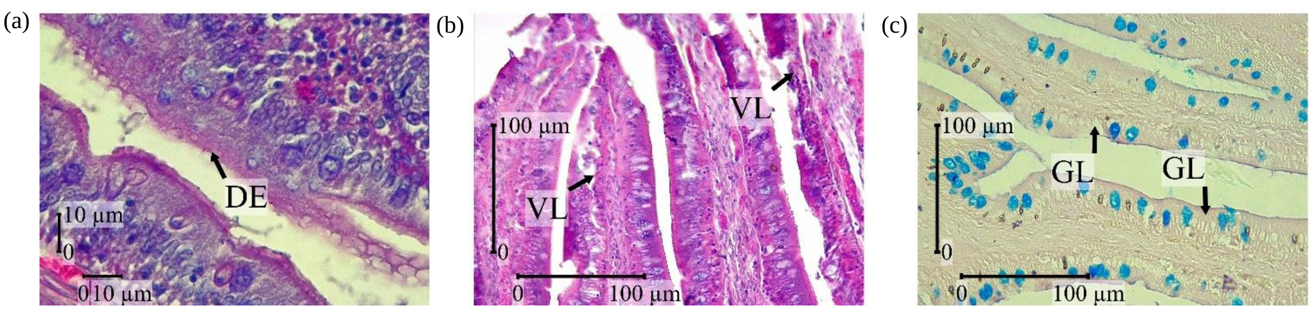

Figure 9. Structural damage to intestinal histology samples with HE and PAS-AB staining. Epithelial denudation with 1,000× magnification (a), villi cell loss (VL) with 400× magnification (b), and goblet cell loss with 400× magnification (c).

The potential of detecting MP accumulation in organs with histological analysis must be expanded. Many researchers have claimed that MPs cause structural damage based on MP particles and polymers (Ahrendt et al., 2020; Limonta et al., 2019), while other studies revealed that MPs do not induce any histological reaction (Batel et al., 2020; De Sales-Ribeiro et al., 2020). Nevertheless, additional research about MPs on the histological structure is important to clarify and understand the transfer of MPs' from the environment to the organs. The discovery of MPs in intestinal histology samples, above the background contamination, suggests the translocation of MPs to tissues of marine fish exposed in their natural habitats. The uptake and release of MPs in animal models have previously been observed (Ahrendt et al., 2020; Limonta et al., 2019; Mbugani et al., 2022), although this is one of the very few studies that have investigated MP accumulation in marine fish under natural exposure.

The structural damage to intestinal samples in this study confirms MP internalization in intestinal tissue with structural damage under naturally exposed conditions, which strongly indicates that MPs accumulation in the GIT of marine fish has a negative effect on epithelial homeostasis, villi structure, crypt structure, and goblet cell condition. Further histology and biomarker studies are needed regarding the internalization of MPs in other tissues in marine fish from different water columns under natural conditions.

4. CONCLUSION

Microplastic pollution was found in surface seawater and marine fish from the coastal waters of BTB, Special Region of Yogyakarta, Indonesia. The MP characteristics, including, size, shape, and color, varied between the different types of MPs. The dominant MP polymers were PP, PE, and PET. Station 3 contained the highest MP concentration in surface seawater Demersal and pelagic were present at the highest relative frequency, and *E. tetradactylum*, *E. splendens*, and *L. equula* (demersal), and *S. lysan* and *S.tala* (pelagic) are recommended for MP biomonitoring. Intestinal histological analysis of *E. tetradactylum* and *L. equula* and FTIR analysis showed MP internalization in tissue with structural damage. This novel study demonstrated the presence of MPs in marine fish tissues from wildlife by histological analysis. This is to our knowledge, the first study to demonstrate MPs in demersal marine fish using histological analysis in relation to the environmental MP concentration in a natural habitat. Further management and method development is needed for MPs mapping and potential accumulation in tissues under natural exposure.

ACKNOWLEDGEMENTS

This study was funded by Lembaga Pengelola Dana Pendidikan (LPDP), Final Research Grants (grant number FR1982021259420/2021). The authors thank the local fishermen of Baru and Trisik Beaches, Aditya Pertama, S.Kom, Ascarti Adaninggar, S.Si., Fitri Syamsiyah, S.Si., Anshori, S.Si., Nisrina Salsabila, S.Si, and Akbar Reza, M.Sc. for their assistance during data collection at Baru and Trisik Beaches.

REFERENCES

Abbasi S, Soltani N, Keshavarzi B, Moore F, Turner A, Hassanaghaei M. Microplastics in different tissues of fish and prawn from the Musa Estuary, Persian Gulf. Chemosphere 2018;205:80-7.

Ahrendt C, Perez-Venagas DJ, Urbina M, Gonzalez C, Echeveste P, Aldana M, et al. Microplastics ingestion cause intertidal lesions in the intertidal fish *Girella laevifrons*. Marine Pollution Bulletin 2020;151:1-6.

Ali D, Almarzoug MHA, Ali HA, Samdani MS, Hussain SA, Alarifi S, et al. Fish as bioindicators to determine the effects of pollution in river by using the micronucleus and alkaline single cell gel electrophoresis assay. Journal of King Saud University-Science 2020;32:2880-5.

Amelia TSM, Khalik WM, Ong MC, Shao YT, Pan H, Bhubalan K. Marine microplastics as vectors of major ocean pollutants and its hazard to the marine ecosystem and humans. Progress in Earth and Planetary Science 2021;8(1):1-26.

Andrady AL. Microplastics in the marine environment. Marine Pollution Bulletin 2011;62:1596-605.

Auta HS, Emenike CU, Fauziah SH. Distribution and importance of microplastics in the marine environment: A review of the sources, fate, effects, and potential solutions. Environment International 2017;102:165-76.

Barboza LGA, Lopes C, Oliveira P, Besaa F, Otero V, Henriques B, et al. Microplastics in wild fish from North East Atlantic Ocean and its potential for causing neurotoxic, lipid oxidative damage, and human health risks associated with ingestion exposure. Science of the Total Environment 2020;717:1-14.

Bastesen E, Haave M, Andersen GL, Velle G, Bodtker G, Krafft CG. Rapid landscape changes in plastic bays along the Norwegian Coastline. Frontiers in Marine Science 2021;8:1-17.

Batel A, Baumann L, Carterny CC, Cormier B, Keiter SH, Braunbeck T. Histological, enzymatic and chemical analyses of the potential effects of differently sized microplastics particles upon long-term ingestion in zebrafish (*Danio rerio*). Marine Pollution Bulletin 2020;153:1-8.

Brodeur RD, Buckley TW, Lang GM, Draper DL, Buchanan JC, Hibpshman RE. Demersal fish predators of gelatinous zooplankton in the Northeast Pacific Ocean. Marine Ecology Progress Series 2021;658:89-104.

Carbery M, O'Connor W, Thavamani P. Trophic transfer of microplastics and mixed contaminants in the marine food web and implications for human health. Environment International 2018;115:400-9.

Cauwenberghe LV, Claessens M, Vandegehuchte MB, Janssen CR. Microplastics are taken up by mussels (*Mystus edulis*) and lugworms (*Arenicola marina*) living in natural habitats. Environmental Pollution 2015;199:10-7.

Cedervall T, Hansson L, Lard M, Frohm B, Linse S. Food chain transport of nanoparticles affects behaviour and fat metabolism in fish. PLoS ONE 2012;7(2):1-7.

Chen K, Chen M, Chen T. Plastic ingestion by fish in the coastal waters of the Hengchun Peninsula Taiwan: Associated with human activity but no evidence. Ecotoxicology and Environmental Safety 2021;213:1-8.

De Sales-Ribeiro C, Brito-Casillas Y, Fernandez A, Caballero MJ. An end to the controversy over the microplastic detection and effects of pristine microplastics in fish organs. Scientific Reports 2020;10:1-19.

Defontaine S, Sous D, Tesan J, Monperrus M, Lenoble V, Lanceleur L. Microplastics in a salt-wedge estuary: Vertical structure and tidal dynamics. Marine Pollution Bulletine 2020; 160:1-29.

Ford HV, Jones NH, Davies AJ, Godley BJ, Jambeck JR, Napper IE, et al. The fundamental links between climate change and marine plastics pollution. Science of the Total Environment 2022;806:1-11.

Furukawa S, Fujita T, Shimabukuro M, Iwaki M, Yamada Y, Nakajima Y, et al. Increased oxidative stress in obesity and its impact on metabolic syndrome. Journal of Clinical Investigation 2004;114(12):1752-61.

Galloway TS, Cole M, Ceri L. Interactions of microplastics debris throughout the marine ecosystem. Nature Ecology and Evolution 2017;1:1-8.

Gola D, Tyagi PK, Arya A, Chauhan N, Agarwal M, Singh SK, et al. The impact of microplastics on marine environment: A review. Environmental Nanotechnology, Monitoring and Management 2021;16:1-6.

Group of Experts on the Scientific Aspects of Marine Environment Protection (GESAMP). Sources, Fate, and Effects of Microplastics in the Marine Environment: A Global Assessment: Volume 90. Albert Embankment, London: International Maritime Organization; 2015.

Guven O, Gokdag K, Jovanovic B, Kideys AE. Microplastics litter composition of the Turkish territorial waters of the Mediterranean Sea, and its occurrence in the gastrointestinal tract of fish. Environmental Pollution 2017;223:286-94.

Haave M, Gomeiro A, Schinheit J, Nilsen H, Olsen AB. Documentation of microplastics in tissues of wild coastal animals. Frontiers in Environmental Science 2021;9:2-12.

Hidalgo-Ruz V, Gutow L, Thompson RC, Thiel M. Microplastics in the marine environment: A review of the methods used for identification and quantification. Environmental Science and Technology 2012;46(6):3060-75.

Jeong C, Kang H, Lee M, Kim D, Han J, Hwang D, et al. Adverse effects of microplastics and oxidative stress-induced MAPK/Nrf2 pathway-mediated defense mechanisms in the marine copepod *Paracyclopina nana*. Scientific Reports 2017;7:1-11.

Jovanović B, Gokdag K, Guven O, Emre Y, Whitley EM. Virgin microplastics are not causing imminent to fish after dietary exposure. Marine Pollution Bulletin 2018;130:123-31.

Jovanović B. Ingestion of microplastics by fish and its potential consequences from a physical perspective. Integrated Environmental Assessment and Management 2017;13(3): 510-5.

Kanhai LDK, Gardfeldt K, Lyashevska O, Hassellov M, Thompson EC, O'Connor I. Microplastics in sub-surface waters of the Artic Central Basin. Marine Pollution Bulletin 2018;130:8-18.

Karami A, Golieeskardi A, Choo CK, Romano N, Ho YB, Salamatinia B. A high-performance protocol for extraction of microplastics in fish. Science of the Total Environment 2017;578:485-94.

Karbalaei S, Golieskardi A, Hamzah HB, Abdulwahid S, Hanachi P, Walker TR, et al. Abundance and characteristics of microplastics in commercial marine fish Malaysia. Marine Pollution Bulletin 2019;148:5-15.

Koongolla JB, Lin L, Pan Y, Yang C, Sun D, Liu S, et al. Occurrence of microplastics in gastrointestinal tract and gills of fish from Beibu Gulf, South China Sea. Environmental Pollution 2020;258:1-6.

Lebreton LCM, Greer SD, Borrero. Numerical modeling of floating debris in the world's oceans. Marine Pollution Bulletin 2012;64:653-61.

Lima ARA, Costa MF, Barletta M. Distribution patterns of microplastics within the plankton of a tropical study. Environmental Research 2014;132:146-55.

Limonta G, Manica A, Benkhalqu A, Bertolucci C, Abelli L, Fossi MC, et al. Microplastics induce transcriptional changes, immune response and behavioral alterations in adult zebrafish. Scientific Reports 2019;9:1-11.

Lundebye AK, Lusher AL, Bank MS. Marine microplastics and seafood implications for food security. In: Bank MS, editor. Microplastics in the Environment: Pattern and Process: Environmental Contamination Remidiation and Management. Norway: Institute of Marine Research; 2022. p. 131-52.

Maaghloud H, Houssa R, Ouansafi S, Bellali F, El Bouqdaoi K, Charouki N, et al. Ingestion of microplastics by pelagic fish from the Moroccan Central Atlantic coast. Environmental Pollution 2020;261:1-10.

Mbugani JJ, Machiwa JE, Shilla DA, Kimaro W, Joseph D, Khan FR. Histomorphological damage in the small intestine of Wami Tilapia (*Oreochormis urolepis*) (Norman, 1922) exposed to microplastics remain long after depuration. Microplastics 2022;1:240-53.

McNeish RE, Kim LE, Barret HA, Mason SA, Kelly JJ, Hoellein TJ. Microplastic in riverine fish is connected to species traits. Scientific Reports 2018;8(1):1-12.

Minghetti M, Drieschner C, Bramaz N, Schug H, Schirmer K. A fish intestinal epithelial barrier model established from the rainbow trout (*Oncorhychus mykiss*) cell line, RtgutGC. Cell Biology and Toxicology 2017;33:539-55.

Mirad A, Yoswaty D, Thamrin. Identification of microplastic waste in seawater and the digestive organs of senangin fish (*E. tetradactylum*) at Dumai City Sea Waters. Asian Journal of Aquatic Sciences 2020;3(3):248-59.

Mistri M, Scoponi M, Sfriso AA, Munari C, Curiotto M, Sfiso A, et al. Microplastics contamination in protected areas of the Gulf of Venice. Water Air Soil Pollution 2021;232:1-9.

Movahedinia A, Abtahi B, Bahmani M. Gill histopathological lesions of the Sturgeons. Asian Journal of Animal and Veterinary Advances 2012;7:710-7.

Pattiaratchi C, van der Mheen M, Schlundt C, Narayanaswamy BE, Sura A, Hajbane S, et al. Plastics in the Indian Ocean-sources transport, distribution, and impacts. Ocean Science 2022;18:1-28.

Pequeno J, Antunes J, Dhimmer V, Bessa F, Sobral P. Microplastics in marine and estuarine species from the coast of Portugal. Frontiers in Environmental Science 2021;9:1-12.

Prakoso AA. Identification and Staging of DIY's south coast tourism activity zone. Jurnal Arsitektur dan Perencanaan 2018;1:240-9.

Qiao R, Sheng C, Lu Y, Zhang Y, Ren H, Lemos B. Microplastics induce intestinal inflammation, oxidative stress, and disorders of metabolome and microbiome in zebrafish. Science of the Total Environment 2019;662:246-53.

Ratucoreh CY, Retnoaji B. The growth and histology structure of Indonesian eel (*Angilla bicolor bicolor* McClelland, 1844) fed with microalgae. Proceedings of the AIP Conference Proceedings; 2018 Aug 15-16; Faculty of Biology Universitas Gadjah Mada, Yogyakarta: Indonesia; 2018.

Rodrigues D, Antunes J, Otero V, Sobral P, Costa MH. Distribution patterns of microplastics in seawater surface at a Portuguese Estuary and Marine Park. Frontiers in Environmental Science 2020;8:1-15.

Sahubawa L. The Study of economic potential distribution of marine resources on the south coast of the Special Region of Yogyakarta as an effort to accelerate investment. Jurnal Teknosains 2015;4:101-98.

Savoca MS, Tyson CW, McGill M, Slager CJ. Odours from marine plastic debris induce food search behaviours in a forage fish. Proceedings of The Royal Society B: Biological Sciences 2017;284:1-8.

Sawalman R, Zamani NP, Werorilangi S, Ismet MS. Spatial and temporal distribution of microplastics in the surface waters of Barranglompo Island, Makassar. IOP Conference Series: Earth and Environmental Science 2020;860:1-10.

Sendra M, Pereiro P, Yeste MP, Mercado L, Figueras A, Vovoa B. Size matters: Zebrafish (*Danio rerio*) as a model to study toxicity of nanoplastics from cells to whole organism. Environmental Pollution 2021;268:1-13.

Simon-Sánchez L, Gralaud M, Garcia-Orellana J, Ziveri P. River deltas as hotspots of microplastics accumulation: The case study of the Ebro River (NW Mediterranean). Science of the Total Environment 2019;687:1186-96.

Smyth K, Elliot M. Effects of changing salinity on the ecology of the marine environments. In: Solan M, Whiteley N, editors. Stressors in the Marine Environment: Physiological and Ecological Responses; Societal Implications. New York: Oxford University Press; 2016. p. 161-74.

Su L, Deng H, Li B, Chen Q, Pettigrove V, Wu C, et al. The occurrence of microplastic in specific in commercially caught fishes from coast and estuary area of east China. Journal of Hazardous Materials 2019;365:716-24.

Sun X, Liang J, Zhu M, Zhao Y, Zhang B. Microplastics in seawater and zooplankton from the Yellow Sea. Environmental Pollution 2018;242:585-95.

Syafitri J, Hamdani H, Pratama RI, Ismail MR. Microplastics accumulation in gastrointestinal tract of sea fish landed at TPI Gaung Pandang, West Sumatera. Global Scientific Journals 2021;9(9):509-19.

Syafiya A, Hadisusanto S. Macrozoobenthos community in the sand mining area of the Progo River. Jurnal Manusia dan Lingkungan 2019;26(2):52-61.

Tasseron P, Zinsmeister H, Rambonnet L, Hiemstra A, Siepman D, van Emmerik T. Plastics hotspot mapping in urban water systems. Geosciences 2020;10:1-11.

Utami I, Resdianningsih K, Rahmawati S. The findings of microplastics in sediment of the Progo and Opak Rivers, Bantul Regency. Jurnal Riset Daerah 2022;22:Article No. 1412.

van Sebille E, Aliani S, Law KL, Maximenko N, Alsina JM, Bagaev A, et al. The physical oceanography of the transport of floating marine debris. Environmental Research Letters 2020;15:2-23.

Wieczorek AM, Morrison L, Croot PL, Allcock L, MacLoughlin E, Savard O, et al. Frequency of microplastics in mesopelagic fishes from the Northwest Atlantic. Frontiers in Marine Sciences 2018;5:1-9.

Woodall LC, Sanchez-Vidal A, Canals M, Paterson GLJ, Coppock R, Sleight V, et al. The deep sea is a major sink for microplastic debris. Royal Society Open Science 2014;1:1-8.

Yan M, Nie H, Xu K, He Y, Hu Y, Huang, et al. Microplastics abundance, distribution and composition in the Pearl River along Guangzhou City and Pearl River estuary, China. Chemosphere 2019;217:879-86.

Yona D, Eviatri MR, Wardana DS, Pitaloka DA, Ningrum D, Fuad MAF, et al. Microplastics in organs of commercial marine fishes from five fishing points in Java Island, Indonesia. Indonesian Journal of Marine Science 2022;27(3):199-214.

Yu F, Yang C, Zhu Z, Bai X, Ma J. Adsorption behavior of organic pollutants and metals on micro/nanoplastics in the aquatic environment. Science of the Total Environmental 2019;694:1-11.

Zhang C, Wang S, Sun D, Pan Z, Zhou A, Xie S, et al. Microplastics pollution in surface water from east coastal areas of Guangdong, South China and preliminary study on microplastics biomonitoring using two marine fish. Chemosphere 2020;256:1-8.

Zhang K, Hamidian AH, Tubic A, Zhang Y, Fang JKH, Wu C, et al. Understanding plastic degradation and microplastic formation in the environment: A review. Environmental Pollution 2021;274:1-14.

Zhao Y, Qiao R, Zhang S, Wang G. Metabolomic profiling reveals the intestinal toxicity of different length of microplastic fibers on zebrafish (*Danio rerio*). Journal of Hazardous Materials 2021;403:1-10.

Hydrogeochemistry of Two Major Mid-hill Lentic Water Bodies for Irrigation of the Central Himalaya, Nepal

Babi Kumar Kafle[1,2], Chhatra Mani Sharma[3], Smriti Gurung[2], Nani Raut[2], Kumud Raj Kafle[2], Rita Bhatta[1,2], Lekhendra Tripathee[4], Rukumesh Paudyal[4], Junming Guo[4], Shichang Kang[4,5], and Bed Mani Dahal[2*]

[1]*Department of Chemical Science and Engineering, School of Engineering, Kathmandu University, Nepal*
[2]*Department of Environmental Science and Engineering, School of Science, Kathmandu University, Nepal*
[3]*Central Department of Environmental Science, Institute of Science and Technology, Tribhuvan University, Kirtipur, Kathmandu, Nepal*
[4]*State Key Laboratory of Cryospheric Science, Northwest Institute of Eco-Environment and Resources, Chinese Academy of Sciences, Lanzhou, China*
[5]*University of Chinese Academy of Sciences, Beijing, China*

ARTICLE INFO

Received: 9 Sep 2022
Received in revised: 19 Dec 2022
Accepted: 27 Dec 2022
Published online: 22 Feb 2023
DOI: 10.32526/ennrj/21/202200195

Keywords:
Lake Phewa/ Kulekhani Reservoir/ Water chemistry/ Irrigation/ Water quality

*** Corresponding author:**
E-mail: bedmani@ku.edu.np

ABSTRACT

The concentration and composition of different salts in natural water bodies determine the water quality for various purposes. This study assesses the water quality of two mid-mountain lentic water bodies, Lake Phewa and Kulekhani Reservoir. For this purpose, selected physico-chemical parameters along with major ions such as HCO_3^-, SO_4^{2-}, PO_4^{3-}, NO_3^-, Cl^-, Ca^{2+}, Mg^{2+}, Na^+, K^+, and NH_4^+ were analyzed. Major ions were analyzed using ion chromatography, anions by DX-600 and cations by Dionex ISC-2500 ion chromatographs. The sources of major ions were determined by using the Gibbs diagram, Piper plot, and Scatter plots. Dissolved oxygen, ammonia and phosphate showed seasonal variations in both lakes. The concentrations of cations are in the order of $Ca^{2+} > Na^+ > Mg^{2+} > K^+$ in both water bodies. However the trend of anions had small variations for Cl^- and SO_4^{2-} in Lake Phewa ($HCO_3^- > Cl^- > SO_4^{2-} > NO_3^-$) and Kulekhani Reservoir ($HCO_3^- > SO_4^{2-} > Cl^- > NO_3^-$). The Piper plot and equiline plots indicated that the water chemistry is dominantly controlled by the dissolution of carbonate minerals and to a limited extent by weathering of silicate minerals. This is further supported by the Gibbs plot showing bedrock geology as the main source of major ions. The overall study indicates that the hydrogeochemistry of these water bodies is controlled by local geology and is suitable for irrigation purposes.

1. INTRODUCTION

Freshwater ecosystems serve multiple purposes and are widely used for domestic purposes, fisheries, recreation, irrigation, and hydroelectricity (Biswas, 2008). However, these ecosystems are undergoing deterioration (Wu and Sun, 2016) making water quality one of the growing environmental concerns (Juma et al., 2014). The quality of water in any ecosystem provides significant information about the available resources for supporting life in that ecosystem and its suitability for human use (Destouni et al., 2017). The importance of water quality to public health and aquatic life is a well-established fact and there is a great need to assess water quality (Gao et al., 2017) for various uses. Freshwater catchment areas and drainage basins are affected by natural processes including rainfall, erosion, and hydrological features (Bhat and Pandit, 2014). Furthermore, the quality of surface water is mainly governed by a range of anthropogenic activities including agricultural and industrial activities (Bhatnagar and Sillanpää, 2010; Gautam et al., 2019; Mayanglambam and Neelam, 2020). Accordingly, many freshwater bodies have become polluted in different parts of the world thereby making them unsuitable for various uses.

Nepal is endowed with rich freshwater resources in the form of rivers, lakes, glaciers, ice, and snow. Nevertheless, with a growing dependency on

Citation: Kafle BK, Sharma CM, Gurung S, Raut N, Kafle KR, Bhatta R, Tripathee L, Paudyal R, Guo J, Kang S, Dahal BM. Hydrogeochemistry of two major mid-hill lentic water bodies for irrigation of the Central Himalaya, Nepal. Environ. Nat. Resour. J. 2023;21(2):171-185. (https://doi.org/10.32526/ennrj/21/202200195)

water for various uses, water availability and quality have become major concerns, particularly in urban and peri-urban areas. For instance, the Bagmati and other rivers in the heart of the capital Kathmandu are heavily polluted with organic and inorganic components (Sada, 2012; Paudyal et al., 2016; Tripathee et al., 2016; Prajapati et al., 2020). Likewise, lakes and wetlands are also facing similar problems (Gautam et al., 2019; Lamsal et al., 2019; Khatiwada et al., 2021). Therefore, water quality assessment is crucial in planning and developing sustainable management strategies for freshwater bodies.

The concentration of dissolved ions depends on water flow paths, and the interactions between rock and water (Nordstrom, 2011). The geochemical study of surface water allows us to obtain important information on the chemical weathering of rock/soil (Han and Liu, 2004). Chemical weathering processes would supply major ions to solution from all lithology to water sources. The ions in lake water are affected by rock characteristics such as porosity, lithology, hydro geomorphology, precipitation, and permeability of the topsoil (Ansari et al., 2015; Haque et al., 2020). Sediments of Tertiary age (mixed sandstone and shale) outcrop the length of southern Nepal in the Siwalik Range. Many mineral veins are present in those areas of the crystalline rocks. Veins of sulphide ores (including pyrite, chalcopyrite, arsenopyrite, and galena) occur in the Markhu-Kulekhani-Arkhaule area. Pyrite (iron sulphide) has also been recorded in black shale deposits in the Andhi Mohan Ghat area of the Gandaki region (Khan and Tater, 1969). For a trace element to be mobile in fresh water it must at least be present in the source rocks, it must be in sufficient quantities, it must be soluble, and it must be in the path of water flow (Nordstrom, 2011).

Comprehensive water quality assessments involve analyses of physical, chemical, and biological components (Bi et al., 2021). These components and parameters may vary depending upon the water use. Physico-chemical characterization, particularly an assessment of major ions, has long been accepted as an established practice to assess water quality. Major ions from aquatic ecosystems reflect the ionic contribution of bedrock geology, land use, and disturbances in the catchments (Feller, 2005). Furthermore, these ions form important cellular components of the biota (Kamunde and Wood, 2003). The concentrations of major ions present in water bodies thus have implications on productivity, the relative abundance of biota, and, accordingly, water use. This study assesses the water quality of lake Phewa and Kulekhani Reservoir two important freshwater lentic systems in Nepal especially focusing on their physico-chemical characterization and suitability of water for irrigation.

2. METHODOLOGY

2.1 Study area

Lake Phewa (Figure 1), located in the city of Pokhara in Gandaki Province, Nepal, has multiple uses. It is a stream-fed and dam-regulated semi-natural freshwater lake in the subtropical mountain area. It has a surface area of 5.23 km^2 with a mean depth of 8.6 m. The watershed area of the lake is 110 km^2 (Suwal, 2013). The main inlet in Phewa Lake is Harpan Khola (Khola means stream in Nepali) while the outlet is present at the dam and the water ultimately flows into the Seti River. Lake-dependent tourism, fishery, and irrigation form the basis of livelihoods for local communities (Pokharel, 2008; Shrestha and Aryal, 2011). In the year 2019 alone, nearly 1.2 million tourists visited the city (Joshi and Dahal, 2019). The common fishes found in the Phewa Lake are silver carp (*Hypophthalmichthys molitrix*), bighead carp (*Aristichthys nobilis*), grass carp (*Ctenopharyngodon idella*), Nile tilapia (*Oreochromis niloticus*) and common carp (*Cyprinus carpio*) (Gurung et al., 2005).

The Kulekhani Reservoir (Figure 1), located in Bagmati Province in Central Nepal, generates hydroelectricity and is also used for cage fishery (Gurung et al., 2010). The main source of water for the reservoir is the Chitlang Khola and other smaller streams. The reservoir, with a water storage capacity of 85.3 million m^3, produces 31 MW and 32 MW of electricity from Kulekhani I and Kulekhani II power stations, respectively (Kafle et al., 2019). The major fish species reared in cage culture are bighead carp (*Aristichthys nobilis*) and silver carp (*Hypophthalmichthys molitrix*) (Saund and Shrestha, 2007). However, the increasing number and volume of fish cages and the use of agrochemicals in the catchment area are the major causes of water pollution (Njiru et al., 2017) in the reservoir. Furthermore, in recent years, the number of domestic tourists visiting the reservoir and nearby areas has increased.

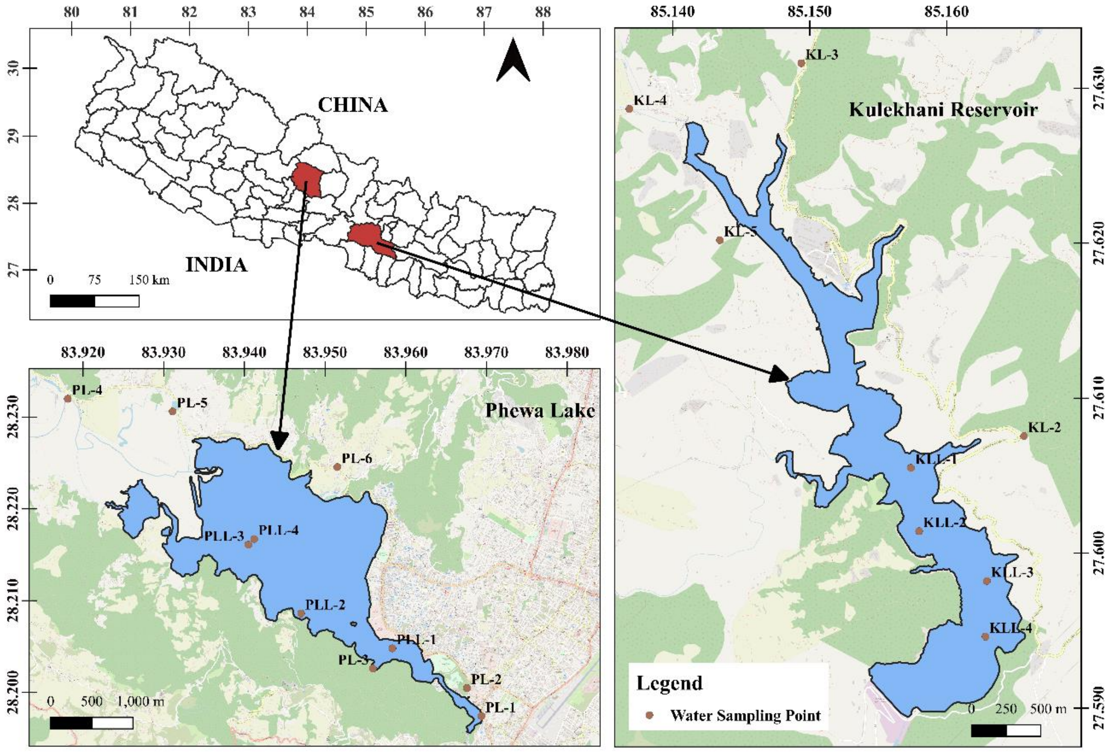

Figure 1. Location map of the study area showing sampling sites in Phewa Lake and Kulekhani Reservoir

2.2 Sampling and analysis

Sampling was conducted during October 2017 (autumn); February 2018 (winter); April 2018 (spring); and July 2018 (summer) encompassing four different seasons. Water samples were collected from nine sites (five from inlets and four from the reservoir) from the Kulekhani Reservoir and 10 sites (six from inlets and four from the main lake) from Phewa Lake (Figure 1). The sampling sites were selected based on accessibility but were representatives of inlets, outlets, and interiors of lakes.

The physico-chemical parameters such as dissolved oxygen (DO), pH, electrical conductivity (EC), temperature, turbidity, and total dissolved solids (TDS) were measured on-site with portable probes (Wagtech and LUTRON). From each site, 1,000 mL water samples were collected in high-density polyethylene (HDPE) bottles for the analysis of the major ions, viz. HCO_3^-, SO_4^{2-}, PO_4^{3-}, NO_3^-, Cl^-, Ca^{2+}, Mg^{2+}, Na^+, K^+, and NH_4^+. The sampling bottles were rinsed with the lake water in the respective sampling sites before sample collection. The samples were immediately stored in an icebox until they were transported to the laboratory for further analysis.

The samples for major ions were analyzed using ion chromatography. The cations (Na^+, K^+, Ca^{2+}, Mg^{2+}, and NH_4^+) were analyzed using an ion chromatograph (DX-600) with an IonPac CS12A analytical column, IonPac CG12A guard column, 20 mmol//L methane sulfonic acid (MSA) eluent, and CSRS 300 continuous self-regeneration cation suppressor. Similarly, anions (Cl^-, SO_4^{2-}, NO_3^-, and NO_2^-) were analyzed by Dionex ISC-2500 ion chromatograph using an IonPac AS11-HC analytical column, IonPac AG11-HC guard column, 20 mmol/L potassium hydroxide (KOH) eluent, and ASRS 300 continuous self-regeneration anion suppressor. Bicarbonate concentration was calculated using the ion balance of total cations and anions (Tripathee et al., 2014).

The sources of major ions were determined by using the Gibbs diagram, Piper plot, and Scatter plots. Important irrigation water quality parameters such as sodium absorption ratio (SAR), sodium percentage (%Na), and Kelley's ratio (KR) were estimated by following Ayers and Westcot (1985), Richards (1954), and Nagaraju et al. (2014) respectively (Table 1). Furthermore, the United States Salinity Laboratory (USSL) diagram (USSL, 1954) and the Wilcox diagrams were used for the further interpretation of irrigation water quality.

Kruskal-Wallis and One Way Analysis of Variance methods were used for comparing nonparametric and parametric data, respectively.

Table 1. Irrigation water quality parameters

Parameters	Equations	References
Sodium absorption ratio (SAR)	$\mathrm{SAR} = \frac{\mathrm{Na^+}}{\left(\sqrt{\frac{1}{2}(\mathrm{Ca^{2+}} + \mathrm{Mg^{2+}})}\right)}$	Ayers and Westcot (1985)
Sodium percentage (%Na)	$(\mathrm{Na^+})\% = \frac{(\mathrm{Na^+} + \mathrm{K^+})}{(\mathrm{Ca^{2+}} + \mathrm{Mg^{2+}} + \mathrm{Na^+} + \mathrm{K^+})} \times 100$	Richards (1954)
Kelley's ratio (KR)	$\mathrm{KR} = \frac{\mathrm{Na^+}}{\mathrm{Ca^{2+}} + \mathrm{Mg^{2+}}} \times 100$	Kelley (1963)

3. RESULTS AND DISCUSSION

3.1 Physico-chemistry of water

The mean concentrations of different physico-chemical parameters of water samples from Phewa Lake and Kulekhani Reservoir are summarized in Tables 2 and 3, respectively. The average concentration of DO in Phewa Lake (7.36±2.32 mg/L) and Kulekhani Reservoir (10.98±3.50 mg/L) are consistent with previous studies in other subtropical lakes in Nepal such as Ghodaghodi Lake, Begnas Lake, and Phewa Lake (Table 4). Slight variations in DO concentrations in the water bodies may be due to differences in temperature and timing of samplings (Gurung et al., 2018). DO is a parameter that is often ignored in water quality studies and yet it can have a significant impact on plant health, root development, fertilizer, and water uptake as well as yield.

Phewa Lake water is slightly alkaline (7.51±0.87 pH value) in spring whereas Kulekhani Reservoir is alkaline (8.30±0.73 pH value) in spring and monsoon seasons. The pH value is proportional to the concentration of carbon dioxide, carbonate, and bicarbonate equilibrium and it is more affected due to the change in the physico-chemical condition of a water body (Sarkar et al., 2020). pH correlates with electric conductivity and total alkalinity (Kothari et al., 2021). Most of the water bodies in Nepal have been reported to be alkaline, possibly, at least in part, due to anthropogenic sources such as the use of detergents (Kannel et al., 2007). The pH values in the present study are within the range of Nepal quality guidelines for irrigation (CBS, 2012). High pH (>7.0) may reduce the availability of various metals and micronutrients to plants causing deficiency symptoms. High pH is often accompanied by high alkalinity whereas low pH (<5.0) may result in toxic high levels of metals like iron and manganese (He et al., 2005). Based on the pH values, the water from Phewa Lake is more suitable for irrigation in the spring season than in other seasons, whereas in Kulekhani Reservoir the water is relatively more suitable for irrigation in spring and summer seasons.

Table 2. Physico-chemical composition (average±SD) of the surface water in Phewa Lake

Parameters (average±SD)	Autumn	Spring	Summer	Winter
Temp (°C)	23.28±2.03[ca]	22.59±2.95[ab]	22.51±5.73[a]	19.92±6.77[b]
DO (mg/L)	6.76±0.88[a]	9.01±1.58[bd]	6.91±2.70[c]	7.53±2.89[d]
pH	6.86±0.31[ac]	8.77±0.76[b]	7.76±1.91[cd]	7.40±1.90[ad]
TDS (mg/L)	48.00±41.41[a]	40.57±27.09[a]	36.56±23.73[a]	39.05±25.62[a]
Conductivity (µS/cm)	96.33±82.96[a]	85.57±50.94[a]	76.67±45.36[a]	85.56±59.80[a]
Turbidity (NTU)	2.73±1.45[a]	2.96±0.74[a]	2.38±1.05[a]	2.38±1.08[a]
Hardness (mg/L)	20.25±21.29[a]	20.40±8.16[a]	13.65±9.64[a]	19.05±20.89[a]
Sulphate (mg/L)	0.01±0.00[a]	0.46±0.39[b]	0.33±0.35[ba]	0.32±0.33[bc]
Bicarbonate (mg/L)	31.01±33.95[bc]	32.32±36.45[ab]	25.94±32.23[ac]	37.11±49.25[b]
Ammonia (mg/L)	0.35±0.28[ac]	0.73±0.17[b]	0.42±0.35[c]	0.46±0.34[ab]
Chloride (mg/L)	1.12±1.93[ac]	0.32±0.16[bc]	0.26±0.16[ab]	0.98±3.61[c]
Nitrate (mg/L)	0.34±10.24[a]	0.03±0.02[ab]	0.02±0.02[b]	0.06±0.12[ac]
Phosphorus (mg/L)	1.44±0.89[a]	0.16±0.02[bc]	0.17±0.05[ac]	0.16±0.12[c]
Sodium (mg/L)	2.56±3.17[a]	0.86±0.39[a]	0.79±0.37[a]	2.30 ±7.76[a]
Potassium (mg/L)	0.90±1.12[a]	0.37±0.19[a]	0.32±0.19[a]	0.65±1.59[a]
Calcium (mg/L)	5.84±5.26[c]	7.20±2.69[bc]	4.68±3.38[d]	6.28±6.07[c]
Magnesium (mg/L)	1.38±2.01[ab]	0.59±0.41[bc]	0.48±0.36[b]	0.81±1.49[c]

*Different alphabets in superscript indicate a significant difference in the mean values (p<0.05).

Table 3. Physico-chemical composition (average±SD)of the surface water in Kulekhani Reservoir

Parameters (average±SD)	Autumn	Spring	Summer	winter
Temp (°C)	16.98±3.33^{c}	20.06±1.94^{dc}	16.48±1.94^{ac}	9.10±1.75^{b}
DO (mg/L)	7.15±2.82^{da}	9.88±1.68^{bc}	11.89±1.73^{b}	14.99±1.73^{cd}
pH	7.74±0.66^{ac}	8.77±0.53^{bd}	8.85±0.50^{b}	7.84±0.50^{cd}
TDS (mg/L)	95.07±28.99^{a}	114.75±63.87^{a}	114.57±63.13^{a}	117.12±63.94^{a}
Conductivity (μS/cm)	190.21±59.06^{a}	187.27±62.50^{bc}	185.19±62.85^{c}	192.15±58.71^{ac}
Turbidity (NTU)	2.48±1.58^{a}	3.37±1.07^{a}	9.07±20.64^{a}	2.57±1.05^{a}
Hardness (mg/L)	38.34±12.29^{abc}	29.94±19.79^{ac}	39.80±11.42^{ad}	54.08±18.45^{bd}
Sulphate (mg/L)	1.13±0.45^{a}	0.63±0.48^{a}	1.07±0.96^{a}	1.16±0.45^{a}
Bicarbonate (mg/L)	56.81±17.96^{cb}	40.67±25.60^{ac}	56.81±17.96^{ba}	94.01±47.90^{b}
Ammonia (mg/L)	0.14±0.23^{c}	0.10±0.13^{ac}	1.47±1.64^{b}	1.42±1.64^{ba}
Chloride (mg/L)	0.87±0.49^{a}	0.48±0.35^{a}	0.85±0.81^{a}	0.88±0.66^{a}
Nitrate (mg/L)	0.42±0.24^{a}	0.01±0.02^{a}	0.38±0.86^{a}	0.46±0.43^{a}
Phosphorus (mg/L)	1.59±0.91^{a}	0.22±0.01^{ac}	0.16±0.04^{cb}	0.07±0.04^{b}
Sodium (mg/L)	4.34±1.57^{a}	1.59±0.91^{b}	2.99±2.43^{ab}	8.88±14.58^{ca}
Potassium (mg/L)	1.52±0.50^{a}	0.64±0.43^{bc}	1.07±1.00^{ab}	1.43±0.53^{ca}
Calcium (mg/L)	11.60±3.20^{bc}	10.11±5.99^{ac}	13.92±4.18^{ab}	17.08±4.67^{b}
Magnesium (mg/L)	2.20±1.19^{a}	1.14±1.20^{a}	1.22±0.79^{a}	2.78±1.95^{a}

*Different alphabets in superscript indicate a significant difference in the mean values ($p<0.05$).

Table 4. Comparisons of the present study with the results from previous studies on different lakes from Nepal

Lakes	Begnas Lake	Phewa Lake	Rara Lake	Ghodaghodi Lake	Phewa Lake	Kulekhani Reservoir
References	Khadka and Ramanathan (2013)	Khadka and Ramanathan (2021)	Gurung et al. (2018)	Pant et al. (2020)	Present study	Present Study
DO (mg/L)	8.82	10.41	NA	5.54	7.58	10.98
pH	7.27	7.94	7.34	7.96	7.48	8.30
Conductivity (μS/cm)	90.51	86.45	193.85	142.00	86.73	188.70
Sulphate (mg/L)	7.26	9.16	2.15	4.80	0.18	1.00
Bicarbonate (mg/L)	25.31	28.25	122.15	49.00	33.09	62.00
Chloride (mg/L)	2.57	1.57	0.46	6.60	1.20	0.70
Nitrate (mg/L)	5.34	5.29	0.55	2.10	0.14	0.31
Phosphorus (mg/L)	0.09	0.08	NA	NA	0.50	0.56
Sodium (mg/L)	3.89	3.33	0.74	5.50	2.81	4.44
Potassium (mg/L)	1.42	1.40	1.48	2.10	0.80	1.16
Calcium (mg/L)	7.03	8.69	20.64	16.00	6.39	13.17
Magnesium (mg/L)	1.97	1.84	11.78	2.40	1.02	1.83

There was no significant seasonal variation in TDS values for both water bodies. The average TDS value for the Kulekhani Reservoir was 108.13± 53.19 mg/L and that of Phewa Lake was 41.20±28.77 mg/L. The TDS values in natural waters are generally in the range of 50 to 250 mg/L, despite areas of especially hard water or high salinity, its value may be as high as 500 mg/L (Omer, 2019). TDS levels should be below 640 mg/L to avoid problems in plugs and below 960 mg/L to avoid problems with other plant growing conditions. TDS levels above 2,000 mg/L are very likely to cause plant growth problems (Samuel et al., 2021).

There is no significant seasonal variation in EC for either water body except in autumn in the Kulekhani Reservoir. The average level of EC in Phewa Lake (90.28±65.62 μS/cm) and Kulekhani Reservoir (188.70±58.21 μS/cm) are similar to other lakes of Nepal such as Begnas Lake, Phewa Lake (previous study), Rara Lake, and Ghodaghodi Lake

(Table 4). EC of lake water has a strong interrelationship with pollution levels (Das et al., 2006). These EC values are within the range of CBS (2012) guidelines, i.e., 400 µS/cm. Elevated EC levels in water can damage growth media and rooting function resulting in nutrient imbalances and water uptake issues. Similarly, turbidity also did not show seasonal variations in either water body. The average level of turbidity in Phewa Lake and Kulekhani Reservoir were 2.43±1.02 NTU and 4.37±10.30 NTU, respectively. Turbidity is caused by particles, suspended or dissolved, in water that scatter light making the water appear cloudy. Nutrients are the leading source of impairment to lakes, ponds, and reservoirs (USEPA, 2000).

The average concentration of sulphate (SO_4^{2-}) in Phewa Lake (0.20±0.25 mg/L) and Kulekhani Reservoir (1.00±0.63 mg/L) were relatively low in comparison with previous studies in Begnas Lake, Phewa Lake, Rara Lake, and Ghodaghodi Lake (Table 4). Sulfur is an essential plant nutrient and sulfur addition is often needed in fertilizer (Gilbert, 1951). The average concentration of bicarbonates (HCO_3^-) in Phewa Lake (32.88±46.50 mg/L) and Kulekhani Reservoir (62.087±34.870 mg/L) are within the range of previous studies in Begnas Lake, Phewa Lake, Rara Lake, and Ghodaghodi Lake (Table 4). The cumulative effect of carbonates (CO_3^{2-}), bicarbonates (HCO_3^-), and hydroxide ions is represented by the alkalinity. A high concentration of bicarbonates is problematic because it increases the pH of the growth media which can cause various nutrient problems, e.g., iron and manganese deficiency, calcium, and magnesium imbalance (Horneck et al., 2011).

There is a significant seasonal variation of ammonia (NH_4^+) ($p<0.05$) for both water bodies. It was significantly higher during summer and winter in Kulekhani (H=18.17, $p<0.001$) and during summer in Lake Phewa (F=12.61, $p<0.001$). The average concentration of NH_4^+ in Phewa Lake and Kulekhani Reservoir were 0.40±0.34 mg/L and 0.78±1.70 mg/L, respectively. Nitrogen is a critical plant nutrient, and it can be beneficial for irrigation when present in water but should be accounted for in the overall fertilization program considering the other form of Nitrogen (Fageria and Baligar, 2005).

Chloride did not differ seasonally in the Kulekhani Reservoir, but it showed a significantly higher concentration in winter compared to summer in Phewa Lake (H=12.11, $p<0.007$). Nevertheless, the average concentration of chloride in Phewa Lake (1.17±3.59 mg/L) and Kulekhani Reservoir (0.77 ±0.60 mg/L) were within the range of previous studies in Nepalese lentic water bodies (Table 4). Chloride can damage plants from excessive foliar absorption (with sprinkler systems) or excessive root uptake (with drip irrigation). Most plants can tolerate chloride up to 100 mg/L although as little as 30 mg/L can be problematic in a few sensitive plants (Fipps, 2003).

Nitrate did not show significant seasonal variation in the Kulekhani Reservoir, but it was significantly lower in summer compared to the winter and autumn seasons in Phewa Lake (H=19.45, $p<0.001$). The average concentration of nitrate in Phewa lake (0.14±0.20 mg/L) and Kulekhani Reservoir (0.32±0.51 mg/L) were relatively low compared to previous studies in other nearby lakes (Table 4). The level of nitrogen should be less than 300 mg/L according to Nepal quality guidelines for aquaculture and 5 mg/L for irrigation as per CBS (2012).

The average concentration of phosphate in Phewa Lake (0.48±0.71 mg/L) and Kulekhani Reservoir (0.51±0.77 mg/L) was relatively high compared to previous studies in other nearby lakes (Table 4), and it showed a significant seasonal variation in both water bodies, particularly it was higher in winter in Kulekhani (H=31.36, $p<0.05$) and autumn in Lake Phewa (H=22.01, $p<0.001$). Phosphorous levels above 5 mg/L may cause antagonism and deficiencies in other nutrients and its levels in water need to be considered in the overall fertilization program (Bindraban et al., 2020).

There is no seasonal variation of sodium in Phewa Lake, but it significantly varied seasonally in the Kulekhani Reservoir having the lowest concentration in spring (H=12.96, $p<0.005$). The average concentration of sodium in Phewa Lake (2.73±7.61 mg/L) and the Kulekhani Reservoir (4.45±7.64 mg/L) was consistent with previous studies in similar lakes in Nepal (Table 4). High sodium in the irrigation water can impact both the soil and the plant and can also be toxic to many plants (Safdar et al., 2019).

The average concentration of calcium in Phewa Lake (6.45±6.30 mg/L) and Kulekhani Reservoir (13.18± 50.16 mg/L) was relatively high compared to previous studies in other Nepalese lakes (Table 4). Calcium compounds occur naturally in surface water, and their concentrations are mainly determined by the carbonate balance (Potasznik and Szymczyk, 2015). Calcium enters the freshwater systems through weathering of rocks, especially limestone, and from the leaching and runoff of forest soils. Like calcium, magnesium is washed from rocks like dolomite $[CaMg(CO_3)_2]$ and magnesite $(MgCO_3)$ and subsequently enters the water bodies as runoff.

The average concentration of magnesium in Phewa Lake (1.02±1.73 mg/L) and Kulekhani Reservoir (1.83±1.47 mg/L) were relatively high compared with other lakes (Table 4). Anthropogenic sources of magnesium include fertilizer, cattle feed, and chemical industries (Potasznik and Szymczyk, 2015). Chemical industries add magnesium to plastics and other materials as a fire protection measure. Magnesium sulphate is applied in beer breweries, and magnesium hydroxide is applied as a flocculant in wastewater treatment plants. Magnesium is also a mild laxative.

There is no significant seasonal variation in hardness in Phewa Lake, but a significant seasonal variation was observed in the Kulekhani Reservoir ($p<0.05$). The average level of hardness in Phewa Lake and Kulekhani Reservoir were 20.28±22.36 mg/L and 40.54±17.58 mg/L, respectively. Since calcium and magnesium are essential plant nutrients, moderate levels of hardness of 100 to 150 mg/L are considered ideal for plant growth (Boman et al., 2002).

3.2 Ionic composition and hydro-geochemistry of the lake water

The concentrations of cations are in the order $Ca^{2+} > Na^{+} > Mg^{2+} > K^{+}$ for both water bodies whereas those of the anions are in the order $HCO_3^- > Cl^- > SO_4^{2-} > NO_3^-$ in Phewa Lake; and $HCO_3^- > SO_4^{2-} > Cl^- > NO_3^-$ in Kulekhani Reservoir. The dominance of Ca^{2+} and HCO_3^- in freshwater bodies has been frequently reported on global as well as regional scales (Wetzel, 2001). Previous studies on Nepalese lakes and rivers have also reported similar findings (Gurung et al., 2018; Sharma et al., 2021; Khadka and Ramanathan, 2021; Bhatta et al., 2022).

From the Piper plot, it is seen that, in both water bodies, cations are found to be distributed in the calcium type and that of anions in the HCO_3^- zone (Figure 2). The plot also indicates that the majority of samples are located on the Ca^{2+}-Mg^{2+}-HCO_3^- hydro-geochemical facies. It indicates that the water chemistry is dominantly controlled by the congruent dissolution of carbonate minerals and to a limited extent by incongruent weathering of silicate minerals in the surface sediments. The dissolved salts in freshwater lakes are low as these are derived from atmospheric precipitation and chemical weathering (Kilham, 1990). The pattern of Ca^{2+}-Mg^{2+}-HCO_3^- is considered the source of water from carbonate dissolution and atmospheric precipitation (Asare-Donkor et al., 2018). Since the lake watersheds are held by both types of rock at the sources, they contribute to making both alkalinity and acidity in the water (Kafle et al., 2019).

The major mechanisms that control lake water chemistry can be interpreted with the help of the Gibbs diagram (Gibbs, 1970; Marandi and Shand, 2018) which shows bedrock geology as the source of major ions in both water bodies.

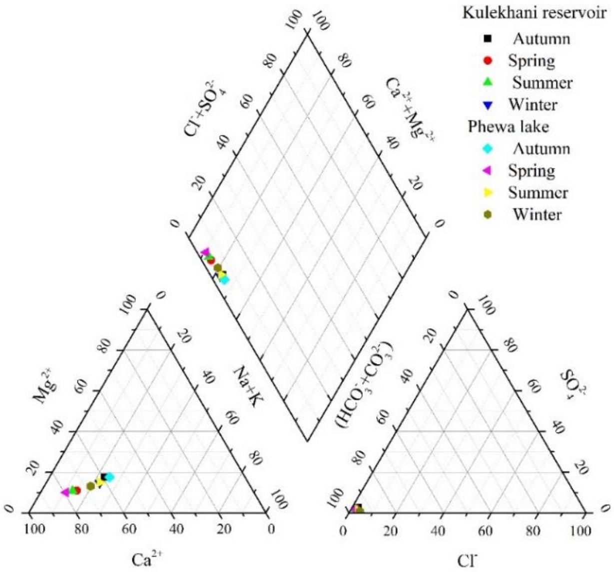

Figure 2. Piper plot of Kulekhani Reservoir and Phewa Lake

The (Ca^{2+} + Mg^{2+}) vs. (HCO_3^- + SO_4^{2-}) graph illustrates the processes of mineralization of ground water (Kumar et al., 2020). Several studies on Himalayan lakes revealed the dominance of Ca^{2+} and Mg^{2+} among the cations and HCO_3^- among the anions in lake waters (Mayanglambam and Neelam, 2020). The relatively higher concentration of HCO_3^- indicates an intense weathering catchment area rocks and organic matter decomposition in the area (Figure 3). Other factors responsible for the abundance and variation in major cations (Ca^{2+}, Na^+, Mg^{2+}, and K^+) and anions (HCO_3^-, SO_4^{2-}, PO_4^{3-}, NO_3^-, and Cl^-) in surface water are controlled by weathering, atmospheric precipitation, and possible atmospheric activities (Pollock, 2011).

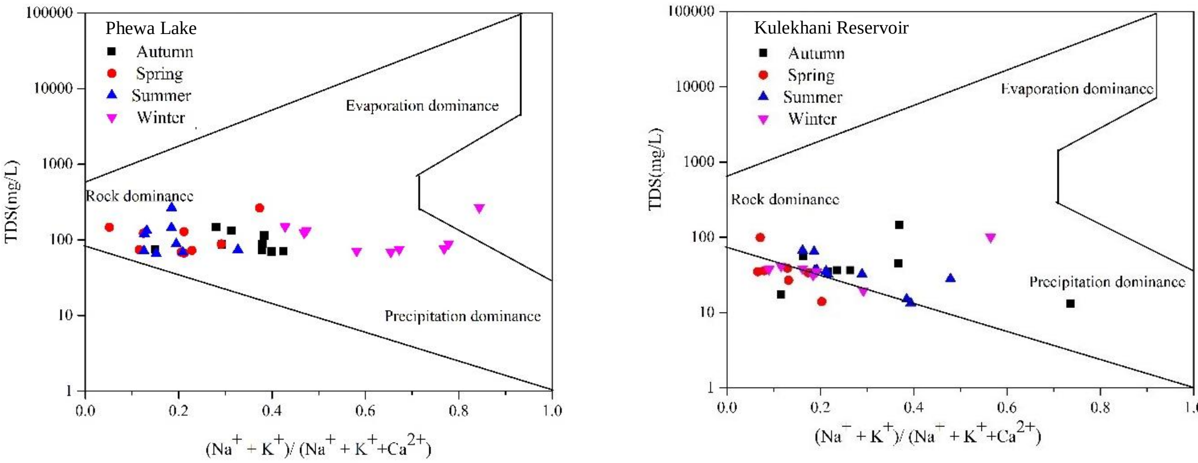

Figure 3. Gibbs diagram of Kulekhani Reservoir and Phewa Lake

Data points along or near the 1:1 line are attributed to carbonate and sulphate mineral weathering (Figure 4). Those that fall above the 1:1 line resulted from the effects of the reverse ion exchange processes in the system. Data points that fall below the equiline are deemed to have also resulted from the dissolution of carbonates. The points of the Scatter plot of alkali metals (Ca^{2+} + Mg^{2+}) vs TZ^+ (total cations) are slightly below 1:1 equiline (Figures 4(a) and 4(a')) indicating the dominance of alkaline earth metals over alkali metals suggesting carbonate weathering as the dominant control mechanism over silicate weathering. This fact is also verified by the similar information obtained in the Gibbs diagram (Figure 3). Furthermore, Ca^{2+} + Mg^{2+} vs. HCO_3^- + SO_4^{2-} (Figures 4(b) and 4(b')) points lying below the equiline further confirms carbonate weathering with only a minor contribution from silicate weathering along with the ion exchange process. Ca^{2+} + Mg^{2+} vs. HCO_3^- points also lie below the equiline indicating very low concentrations of SO_4^{2-} (Figures 4(d) and 4(d')). In general, the weathering of carbonate rocks is more effective (12 times) than that of silicate rocks (Gaillardet et al., 1999), and similar observations have been reported in many freshwater bodies across the lesser Himalayan region (Jeelani and Shah, 2006; Saini et al., 2008).

The Scatter plot of Na^+ + K^+ vs. TZ^+ in a 1:6 ratio indicates that water is relatively deficient in Na^+ + K^+ (Figures 4(c) and 4(c')). The samples mostly fall on or near the 1:1 equiline suggesting HCO_3^- is balanced by Ca^{2+} and Mg^{2+} while the monsoon samples fall below the equiline indicating HCO_3^- needs to be balanced also by Na^+ + K^+, in addition to Ca^{2+} + Mg^{2+}. The Scatter plot of Ca^{2+} + Mg^{2+} vs. HCO_3^- + SO_4^{2-} shows that the sampling points fall mostly below 1:1 equiline requiring a portion of HCO_3^- and SO_4^{2-} to be balanced by Na^+ + K^+ from weathering of silicate.

Sodium ion is ubiquitous in water, owing to the high solubility of its salts and the abundance of sodium-containing mineral deposits (Arega, 2020). Potassium is an important element for aquatic animal and plant species, although the least abundant of four major elements (Ca^{2+} > Mg^{2+} > Na^+ > K^+) in natural waters based on esthetic considerations. World Health Organization has established a drinking water guideline of 200 mg/L of sodium. Sodium levels in drinking water are typically less than 20 mg/L but can vary in different countries.

In a freshwater system, chloride is generally a minor component of the total ionic composition. The mean concentration of chloride in river waters is about 8 mg/L (Wetzel, 1983). However, chloride from anthropogenic sources is increasingly identified as a significant pollutant of freshwater lakes and streams (Gillis, 2011). The concentration of chloride is within the range of the Nepal standard for drinking water i.e., 250 mg/L (CBS, 2012) because the average concentration of chloride was 1.20 mg/L in Phewa Lake and 0.70 mg/L in the Kulekhani Reservoir. In Phewa Lake, it is consistent with the previous study (1.57 mg/L) by Khadka and Ramanathan (2021). In the Kulekhani Reservoir, the concentration of chloride is relatively lower than in other lakes but slightly higher than in Rara Lake (Table 4).

From these results, it is evident that the main source of major ions in both the water bodies can be attributed to their geology. The Phewa Lake watershed predominantly lies on the Kuncha formation rocks that comprise phyllite and phyllitic quartize (Stöcklin and Bhattarai, 1977). The rock types indicate the contribution in the lake water with mild acidic anions in most of the seasons. The southwestern parts of the watershed are composed of quartzite rock named the Fagfog Quartzite Formation that has massive white and pinkish white quantize and the northwestern part has phyllite with quartz veins with little carbonate content. However, in the rainy season (monsoon), the nearby Ghachok and Tallakot Formation (Yamanaka et al., 1982) plays the main role in contributing to alkalinity in the water of its carbonate contents. This comparative result shows that Phewa Lake water is a little more acidic compared with the Kulekhani Reservoir water as also indicated by Kafle et al. (2019).

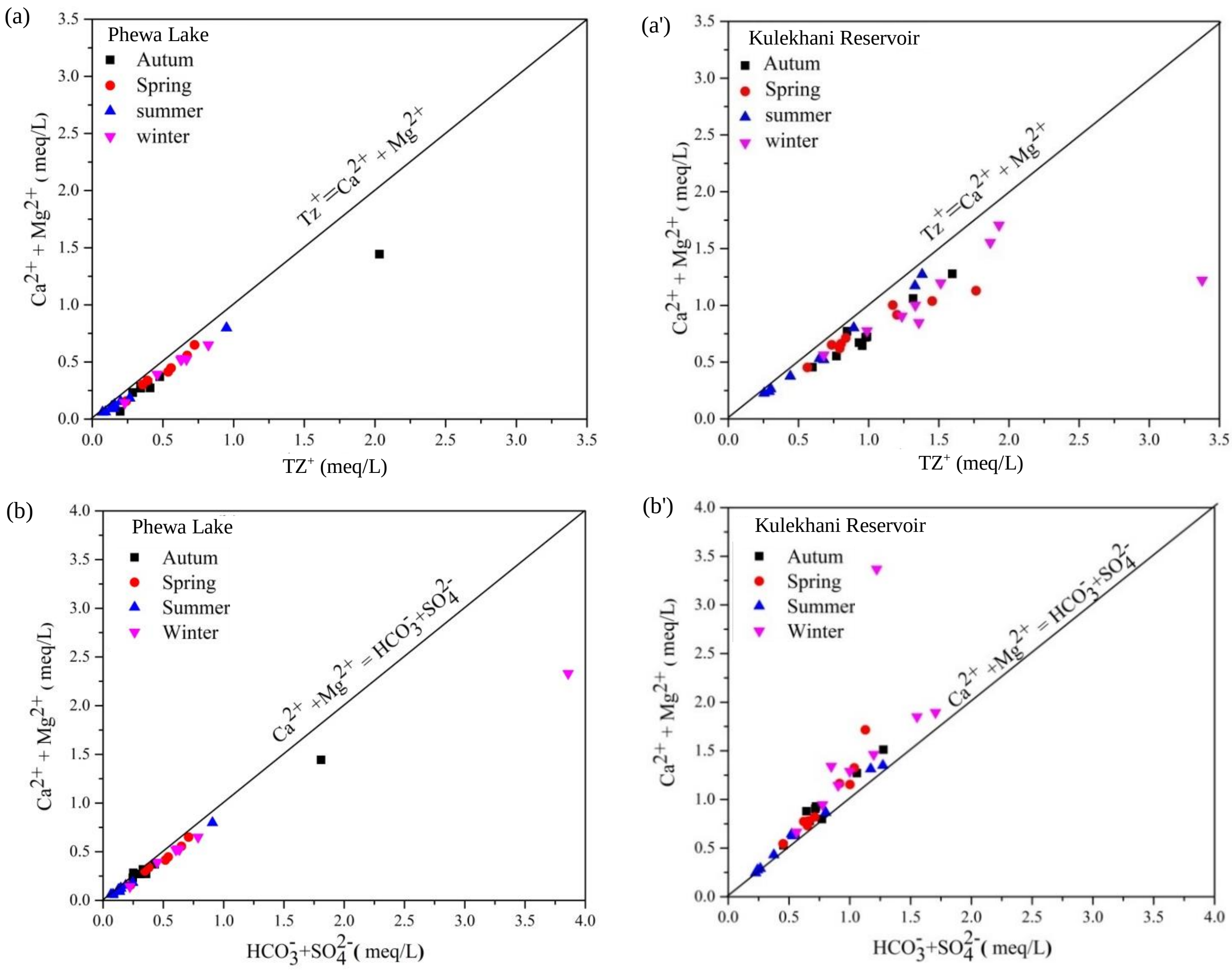

Figure 4. Scatter diagrams showing: (a),(a') $Ca^{2+} + Mg^{2+}$ vs. TZ^{+}; (b),(b') $Ca^{2+} + Mg^{2+}$ vs. $HCO_3^- + SO_4^{2-}$; (c),(c') $Na^+ + K^+$ vs. TZ^+ ; (d),(d') $Ca^{2+} + Mg^{2+}$ vs. HCO_3^- for Phewa Lake and Kulekhani Reservoir

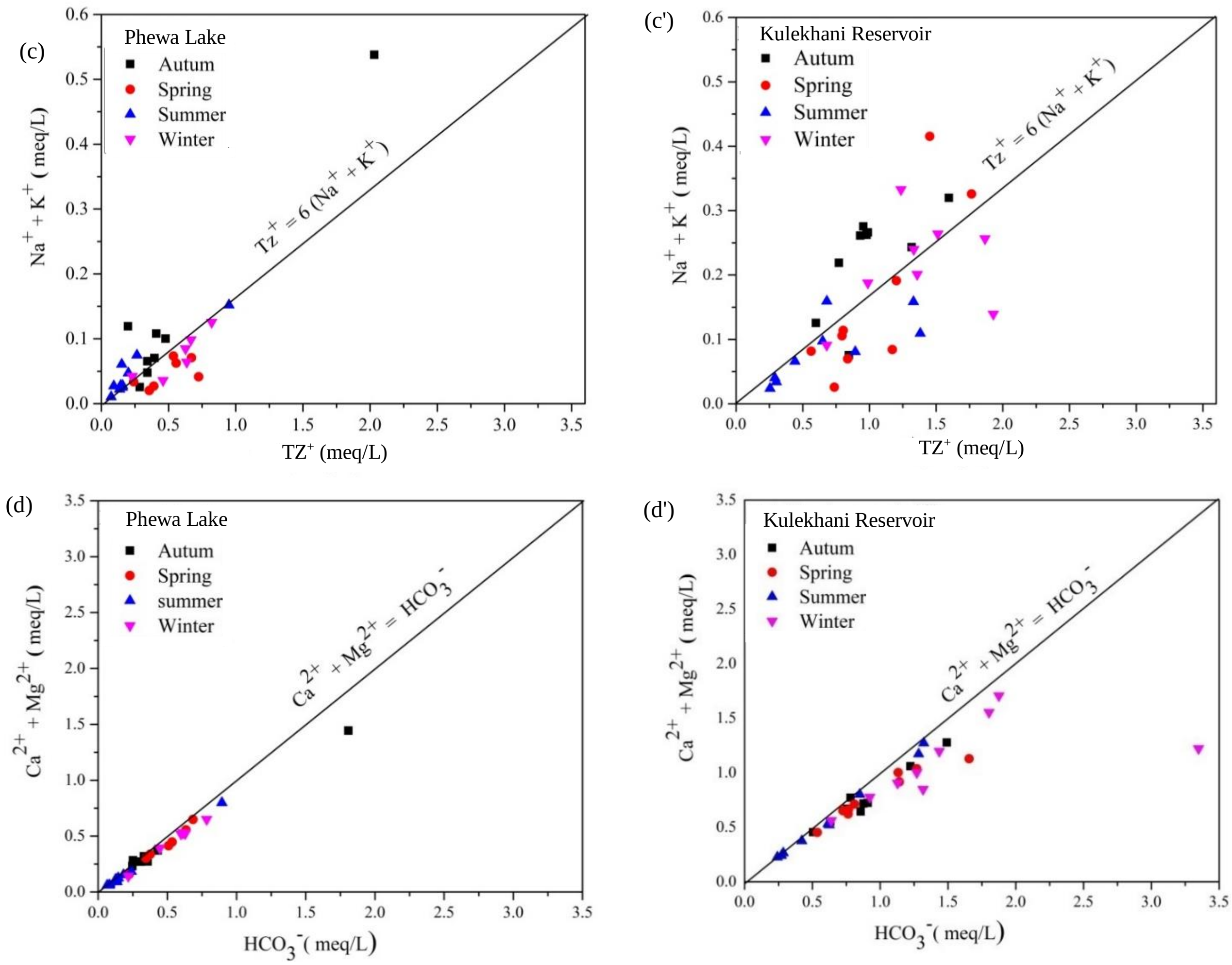

Figure 4. Scatter diagrams showing: (a),(a') $Ca^{2+} + Mg^{2+}$ vs. TZ^+; (b),(b') $Ca^{2+} + Mg^{2+}$ vs. $HCO_3^- + SO_4^{2-}$; (c),(c') $Na^+ + K^+$ vs. TZ^+ ; (d),(d') $Ca^{2+} + Mg^{2+}$ vs. HCO_3^- for Phewa Lake and Kulekhani Reservoir (cont.)

In the Kulekhani watershed, the carbonate and silicate rocks are prominent. The reservoir water with cations ($Ca^{2+} + Mg^{2+}$) is contributed from the north side inlet streams, which flow from calcareous Markhu Formations (coarse crystalline marble) and Chandragiri limestone and Chitlang slate made of argillaceous limestone (Stöcklin and Bhattarai, 1977; Stöcklin, 1980). The reservoir itself is situated along a part of the Markhu formation which contributes to the alkalinity in the water. Similarly, the acidic rocks are situated in the western and southern part of the lake watershed that has silicate rocks with granite that contribute to a mild acidic anion (Neupane et al., 2017).

3.3 Water quality for irrigation

The water samples are classified for irrigation purposes as US Salinity Laboratory (USSL, 1954) classification shown in the USSL diagram (Figure 5). It is classified into four types - C1, C2, C3, and C4 based on salinity hazard and S1, S2, S3, and S4 based on sodium hazard. Based on the USSL diagram most of the samples fall under the C1S1 (low salinity and low sodium) category, which can be used for irrigation in most soil types. A few samples are in the C2S1 category indicating the suitability of the lake waters for irrigation (Figure 5).

Likewise, the Wilcox diagram (Wilcox, 1955) revealed good water quality (Figure 6) for irrigation. According to the categorization of the Wilcox diagram, the irrigation water quality falls mostly in the excellent to good category and only a few samples are in the good to permissible category.

Sodium is an important ion used for the classification of irrigation water because its reaction with soil reduces its permeability. Excessive amounts of EC and Na^+ content in agricultural water may also decrease the osmotic gradient and reduce the ingestion of nutrients from the soil by plants (Saleh et al., 1999).

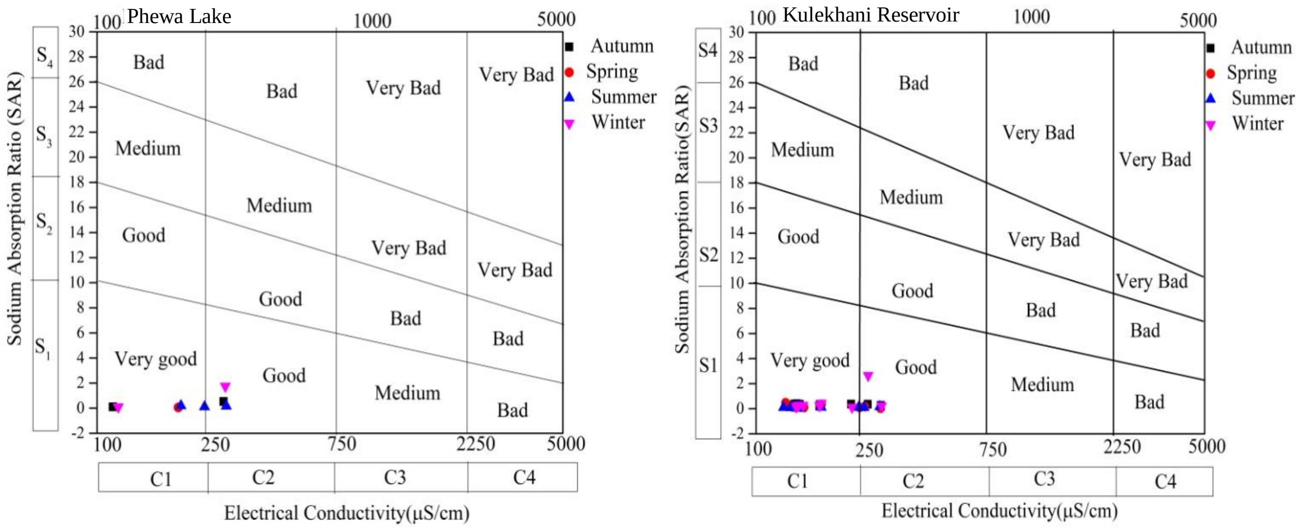

Figure 5. USSL diagram showing the relation between SAR and electrical conductivity

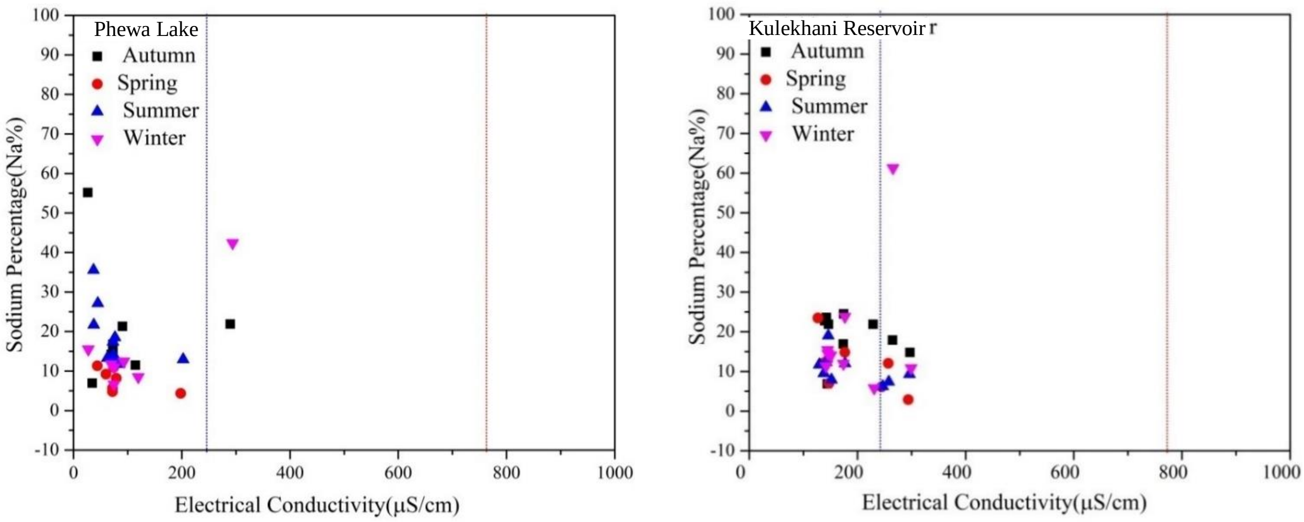

Figure 6. Wilcox diagram for Kulekhani Reservoir and Phewa Lake

The mean values of different irrigation water quality attributes are presented in Tables 5 and 6. All the values comply with Nepal's standard of irrigation water quality (CBS, 2012). Sodium values reflected that the water was under the category of good to excellent (20-40 Na%). As per Nepal water quality guidelines for irrigation, a sodium percentage of less than 70 mg/L is recommended for irrigation water (CBS, 2012), and up to 460 mg/L depending upon the sensitivity of crops. Furthermore, the Wilcox diagram showed that most of the samples were good for irrigation (Figure 6). SAR is used to measure the alkali/sodium level to determine the harmful level of crops. Na^+ replaces the exchangeable Ca^{2+} and Mg^{2+} ions; the high Na^+ content of irrigation water changes the soil characteristics and reduces crop yield.

The computed SAR values in the present study ranged between 0.04 to 2.64 (Table 5). The SAR values of the Phewa Lake ranged between 0.04 and 1.75 meq/L with an overall average value of 0.20 meq/L, whereas it ranged between 0.04 and 2.64 meq/L with an overall average value of 0.29 meq/L in the Kulekhani Reservoir (Table 5).

The value of Kelley's ratio less than one is suitable for irrigation and greater than one is unsuitable for irrigation purposes. In the Kulekhani Reservoir, the KR ranged from 0.03 to 1.69 in four different seasons, with an average of 0.22 (Table 6).

Table 5. Average sodium percentage and sodium absorption ratio (SAR) in lake waters during four seasons in Kulekhani Reservoir and Phewa Lake

Seasons	Sodium percentage (%Na)			Sodium absorption ratio (SAR)		
	Min	Max	Average±SD	Min	Max	Average±SD
Kulekhani Reservoir						
Autumn	6.67	24.50	19.00±5.60	0.09	0.39	0.31±0.01
Spring	2.99	23.48	11.46±5.90	0.04	0.47	0.20±0.13
Summer	6.27	19.02	10.61±3.81	0.06	0.25	0.13±0.06
Winter	5.78	61.26	18.76±16.64	0.12	2.64	0.51±0.80
Phewa Lake						
Autumn	11.48	55.16	20.38±14.88	0.05	0.61	0.25±0.20
Spring	4.36	11.33	7.78±2.88	0.04	0.13	0.08±0.03
Summer	11.75	35.54	18.54±7.66	0.05	0.25	0.13±0.06
Winter	6.63	42.39	15.44±12.22	0.07	1.75	0.36±0.61

Table 6. Kelley's ratio of water samples from Kulekhani Reservoir and Phewa Lake during four seasons

Rank	Kelley's ratio	Quality	Number of samples				Percentage of water samples
			Autumn	Spring	Summer	Winter	
Kulekhani Reservoir							
1	<1.0	Suitable	9	9	9	8	97.20
2	>1.0	Unsuitable	0	0	0	1	2.80
Phewa Lake							
1	<1.0	Suitable	7	7	10	7	96.90
2	>1.0	Unsuitable	1	0	0	0	3.10

According to Richards (1954) classification, a value of SAR less than 10 is excellent, 10 to 18 is good, 18 to 26 is doubtful, and greater than 26 is unsuitable for irrigation uses. Based on the classification, both water bodies are excellent for irrigation purposes. Based on Kelley's ratio, 97.20% of the water samples from the Kulekhani Reservoir are suitable for irrigation purposes having a KR ratio of less than 1. Similarly, the KR values from Phewa Lake varied from 0.05 to 1.63 and the average value was 0.25. The present study shows that 96.90% of water samples are found to be suitable for irrigation purposes.

4. CONCLUSION

The study focused on water quality assessments of two mid-hill lakes in Nepal; Phewa Lake and Kulekhani Reservoir. The suitability for irrigation of the water from the lakes was evaluated based on water physico-chemical parameters, SAR index, Wilcox plot, Kelley's ratio, and Sodium percentage. Samples from all four seasons were analyzed for dissolved oxygen, pH, conductivity, temperature, turbidity, total dissolved solids, major ions, and important salts. Dissolved oxygen, ammonia, and phosphate showed seasonal variations in both lakes. However, chloride and nitrate had seasonal variations in Lake Phewa only, and sodium had seasonal variations in Kulekhani only. The concentrations of cations are in the same order of abundance, namely Ca^{2+} > Na^{+} > Mg^{2+} > K^{+} in both water bodies. However, the trend of anions had small variations for Cl^{-} and SO_4^{2-} in Lake Phewa (HCO_3^{-} > Cl^{-} > SO_4^{2-} > NO_3^{-}) and Kulekhani Reservoir (HCO_3^{-} > SO_4^{2-} > Cl^{-} > NO_3^{-}). The water chemistry of both mid-hill lakes is dominantly controlled by the dissolution of carbonate minerals from watershed bedrock as the main source of major ions, which was clearly reflected by a Piper plot and Gibbs diagram. Based on the KR values and SAR index more than 96 percent of water samples were suitable for irrigation purposes. Although the water chemistry of the middle mountains of Nepal is substantially affected by local geology, the water is suitable for irrigation in all seasons.

ACKNOWLEDGEMENTS

We express our thanks to Shrija Tuladhar and Sushma Manandhar for their assistance in the field data collection and laboratory works. George Vernon Byrd deserves our sincere thanks for correcting English language. Bed Mani DAHAL, the Principal Investigator, and his team were supported for research by University Grants Commission- Nepal (Grant # CRG-72/73-S&T-07). The Second Tibetan Plateau

Scientific Expedition and Research Program (STEP) (Grant No. 2019QZKK0605), the Strategic Priority Research Program of the Chinese Academy of Sciences, Pan Third Pole Environment Study for a Green Silk Road (Pan-TPE) (XDA20040501, and the Asia-Pacific Network for Global Change Research (APN) (CRRP2021-12MY-Paudyal) partially supported this study.

REFERENCES

Ansari MA, Deodhar A, Kumar US, Khatti VS. Water quality of few springs in outer Himalayas-A study on the groundwater-bedrock interactions and hydrochemical evolution. Groundwater for Sustainable Development 2015;1(1-2): 59-67.

Arega T. Sodium and potassium analysis of drinking water quality assessment and its health effects in Ethiopia: A retrospective study. Journal of Oral Health Dentistry 2020;4(1):261-6.

Asare-Donkor NK, Ofosu JO, Adimado AA. Hydrochemical characteristics of surface water and ecological risk assessment of sediments from settlements within the Birim River basin in Ghana. Environmental Systems Research 2018;7(1):1-7.

Ayers RS, Westcot DW. Water Quality for Agriculture. Rome, Italy: Food and Agriculture Organization of the United Nations; 1985.

Bhat SA, Pandit AK. Surface water quality assessment of Wular Lake, a Ramsar site in Kashmir Himalaya, using discriminant analysis and WQI. Journal of Ecosystems 2014;1-18:Article No. 724728 .

Bhatnagar A, Sillanpää M. Utilization of agro-industrial and municipal waste materials as potential adsorbents for water treatment-a review. Chemical Engineering Journal 2010; 157(2-3):277-96.

Bhatta R, Gurung S, Joshi R, Tuladhar S, Regmi D, Kafle BK, et al. Spatio-temporal hydrochemistry of two selected Ramsar sites (Rara and Ghodaghodi) of west Nepal. Heliyon 2022;8(11):1-11.

Bi S, Wang L, Li Y, Zhang Z, Wang Z, Ding X, et al. A comprehensive method for water environment assessment considering trends of water quality. Advances in Civil Engineering 2021;1-8:Article No. 5548113.

Bindraban PS, Dimkpa CO, Pandey R. Exploring phosphorus fertilizers and fertilization strategies for improved human and environmental health. Biology and Fertility of Soils 2020; 56(3):299-317.

Biswas AK, Integrated water resources management: Is it working? International Journal of Water Resources Development 2008;24(1):5-22.

Boman BJ, Wilson PC, Ontermaa EA. Understanding water quality parameters for citrus irrigation and drainage systems [Internet]. 2002 [cited 2022 October 19]. Available from: https://itc.tamu.edu/files/2018/05/CIR1406.pdf.

Central Bureau of Statistic Nepal (CBS). Environmental Statistics of Nepal. Kathmandu, Nepal: Central Bureau of Statistic, National Planning Commission Secretariat, Government of Nepal; 2012.

Das R, Samal NR, Roy PK, Mitra D. Role of electrical conductivity as an indicator of pollution in shallow lakes. Asian Journal of Water, Environment and Pollution 2006;3(1):143-6.

Destouni G, Fischer I, Prieto C. Water quality and ecosystem management: Data-driven reality check of effects in streams and lakes. Water Resources Research 2017;53(8):6395-406.

Fageria NK, Baligar VC. Enhancing nitrogen use efficiency in crop plants. Advances in Agronomy 2005;88:97-185.

Feller MC. Forest harvesting and streamwater inorganic chemistry in western north America: A review. Journal of the American Water Resources Association 2005;41(4):785-811.

Fipps G. Irrigation water quality standards and salinity management strategies [Internet]. 2003 [cited 2022 Oct 21]. Available from: https://twon.tamu.edu/wp-content/uploads/sites/3/2021/06/irrigation-water-quality-standards-and-salinity-management-strategies-1.pdf.

Gaillardet J, Dupré B, Louvat P, Allegre CJ. Global silicate weathering and CO_2 consumption rates deduced from the chemistry of large rivers. Chemical Geology 1999;159(1-4): 3-30.

Gao JM, Wu L, Chen YP, Zhou B, Guo JS, Zhang K, et al. Spatiotemporal distribution and risk assessment of organotins in the surface water of the Three Gorges Reservoir Region, China. Chemosphere 2017;171:405-14.

Gautam D, Bhattarai S, Sigdel R, Jandug CM, Mujahid A, Bijaya GCD. Climatic variability and wetland resources in Rupa Lake Catchment, Nepal. North American Academic Research 2019;2(12):82-91.

Gibbs RJ. Mechanisms controlling world water chemistry. Science 1970;170(3962):1088-90.

Gilbert FA. The place of sulfur in plant nutrition. The Botanical Review 1951;17(9):671-91.

Gillis PL. Assessing the toxicity of sodium chloride to the glochidia of freshwater mussels: Implications for salinization of surface waters. Environmental Pollution 2011;159(6): 1702-8.

Gurung TB, Wagle SK, Bista JD, Joshi PL, Batajoo R, Adhikari P, et al. Participatory fisheries management for livelihood improvement of fishers in Phewa Lake, Pokhara, Nepal. Himalayan Journal of Sciences 2005;3(5):47-52.

Gurung TB, Mulmi RM, Kalyan KC, Wagle G, Pradhan GB, Upadhayaya K, et al. Cage fish culture: An alternative livelihood option for communities displaced by reservoir impoundment in Kulekhani, Nepal. In: Silva SS, Davy FB, editors. Success Stories in Asian Aquaculture. Dordrecht: Springer; 2010. p. 85-102.

Gurung S, Gurung A, Sharma CM, Jüttner I, Tripathee L, Bajracharya RM, et al. Hydrochemistry of lake Rara: A high mountain lake in western Nepal. Lakes and Reservoirs: Research and Management 2018;23(2):87-97.

Han G, Liu CQ. Water geochemistry controlled by carbonate dissolution: A study of the river waters draining karst-dominated terrain, Guizhou Province, China. Chemical Geology 2004;204(1-2):1-21.

Haque S, Kannaujiya S, Taloor AK, Keshri D, Bhunia RK, Ray PK, et al. Identification of groundwater resource zone in the active tectonic region of Himalaya through earth observatory techniques. Groundwater for Sustainable Development 2020;10:Article No. 100337.

He ZL, Yang XE, Stoffella PJ. Trace elements in agroecosystems and impacts on the environment. Journal of Trace Elements in Medicine and Biology 2005;19(2-3):125-40.

Horneck DA, Sullivan DM, Owen JS, Hart JM. Soil Test Interpretation Guide. Oregon, USA: Oregon State University; 2011.

Jeelani GH, Shah AQ. Geochemical characteristics of water and sediment from the Dal Lake, Kashmir Himalaya: Constraints on weathering and anthropogenic activity. Environmental Geology 2006;50(1):12-23.

Joshi S, Dahal R. Relationship between social carrying capacity and tourism carrying capacity: A case of Annapurna Conservation Area, Nepal. Journal of Tourism and Hospitality Education 2019;9:9-29.

Juma DW, Wang H, Li F. Impacts of population growth and economic development on water quality of a lake: Case study of Lake Victoria Kenya water. Environmental Science and Pollution Research 2014;21(8):5737-46.

Kafle BK, Dahal BM, Sharma CM, Kafle KR, Gurung S, Raut N, et al. Physicochemical characterization of water samples from Lake Phewa and Kulekhani Reservoir, Nepal. Proceedings of the Agriculture and Society in Changing Climate International Conference; 2019 Aug 17-19; Hotel View Bhrikuti, Lalitpur: Nepal; 2019.

Kamunde C, Wood CM. The influence of ration size on copper homeostasis during sublethal dietary copper exposure in juvenile rainbow trout, Oncorhynchus mykiss. Aquatic Toxicology 2003;62(3):235-54.

Kannel PR, Lee S, Kanel SR, Khan SP, Lee YS. Spatial-temporal variation and comparative assessment of water qualities of urban river system: A case study of the river Bagmati (Nepal). Environmental Monitoring and Assessment 2007;129(1): 433-59.

Kelley WP. Use of saline irrigation water. Soil Science 1963; 95(6):385-91.

Khadka UR, Ramanathan AL. Major ion composition and seasonal variation in the Lesser Himalayan Lake: Case of Begnas Lake of the Pokhara Valley, Nepal. Arabian Journal of Geosciences 2013;6(11):4191-206.

Khadka UR, Ramanathan AL. Hydrogeochemical analysis of Phewa Lake: A lesser Himalayan Lake in the Pokhara Valley, Nepal. Environment and Natural Resources Journal 2021; 19(1):68-83.

Khan RH, Tater JM. Radiometric Dates of Some Nepalese Rocks. Kathmandu, Nepal: His Majesty's Government of Nepal, Ministry of Industry and Commerce; 1970.

Khatiwada JR, Adhikari JN, Rijal D, Sharma LN. Freshwater biodiversity in Western Nepal: A review. Nepalese Journal of Zoology 2021;5(1):34-46.

Kilham P. Mechanisms controlling the chemical composition of lakes and rivers: Data from Africa. Limnology and Oceanography 1990;35(1):80-3.

Kothari V, Vij S, Sharma S, Gupta N. Correlation of various water quality parameters and water quality index of districts of Uttarakhand. Environmental and Sustainability Indicators 2021;9:Article No. 100093.

Kumar P, Mahajan AK, Kumar A. Groundwater geochemical facie: implications of rock-water interaction at the Chamba City (HP), Northwest Himalaya, India. Environmental Science and Pollution Research 2020;27(9):9012-26.

Lamsal P, Atreya K, Ghosh MK, Pant KP. Effects of population, land cover change, and climatic variability on wetland resource degradation in a Ramsar listed Ghodaghodi Lake Complex, Nepal. Environmental Monitoring and Assessment 2019;191(7):1-6.

Marandi A, Shand P. Groundwater chemistry and the Gibbs Diagram. Applied Geochemistry 2018;97:209-12.

Mayanglambam B, Neelam SS. Geochemistry and pollution status of surface sediments of Loktak Lake, Manipur, India. SN Applied Sciences 2020;2(12):1-6.

Nagaraju A, Kumar KS, Thejaswi A. Assessment of groundwater quality for irrigation: A case study from Bandalamottu lead mining area, Guntur District, Andhra Pradesh, South India. Applied Water Science 2014;4(4):385-96.

Neupane P, Kafle KR, Dahal BM, Sharma CM, Raut N, Gurung S, et al. Sediment load and its source identification: A comparative study of Lake Phewa and Kulekhani reservoir, Nepal. Proceedings of the 11th Asian Regional Conference of IAEG; 2017 Nov 28-30; Hotel Yak and Yeti, Kathmandu: Nepal; 2017.

Njiru J, Waithaka E, Aloo PA. An overview of the current status of Lake Naivasha Fishery: Challenges and management strategies. The Open Fish Science Journal 2017;10:1-11.

Nordstrom DK. Hydrogeochemical processes governing the origin, transport and fate of major and trace elements from mine wastes and mineralized rock to surface waters. Applied Geochemistry 2011;26(11):1777-91.

Omer NH. Water quality parameters. In: Summers JK editor. Water Quality-Science, Assessments and Policy. 2019. p. 1-34.

Pant RR, Pal KB, Bishwakarma K, Thapa LB, Dangol A, Dawadi B,et al. Application of multivariate approaches to the hydro-chemical assessment of the Ghodaghodi Lake, Sudurpaschim Province, Nepal. Nepal Journal of Science and Technology 2020;19(2):46-54.

Paudyal R, Kang S, Sharma CM, Tripathee L, Sillanpää M. Variations of the physicochemical parameters and metal levels and their risk assessment in urbanized Bagmati River, Kathmandu, Nepal. Journal of Chemistry 2016;1-14:Article No. 6025905.

Pokharel S. Conservation of Phewa Lake of Pokhara, Nepal. Nepal: Ministry of Culture, Tourism and Civil Aviation, Government of Nepal; 2008.

Pollock SJ. Assessing Groundwater/surface Water Connectivity and the Effect on Groundwater Quality in Alexandra, Central Otago [dissertation]. Central Otago, University of Otago; 2011.

Potasznik A, Szymczyk S. Magnesium and calcium concentrations in the surface water and bottom deposits of a river-lake system. Journal of Elementology 2015;20(3):677-92.

Prajapati RN, Lama S, Khadka S, Gauli S, Gaire T. A study of basic water quality in dry season in Manohara River in Nepal. Journal of Water Resource Research and Development 2020;3(3):1-5.

Richards LA. Diagnosis and Improvement of Saline and Alkali Soils. Washington D.C., USA: United States Department of Agriculture; 1954.

Sada R. Hanumante River: Emerging uses, competition and implications. Journal of Science and Engineering 2012;1:17-24.

Safdar H, Amin A, Shafiq Y, Ali A, Yasin R, Shoukat A, et al. A review: Impact of salinity on plant growth. Nature and Science 2019;17(1):34-40.

Saini RK, Swain S, Patra A, Khanday GJ, Gupta H, Purushothaman P, et al. Water chemistry of three Himalayan Lakes: Dal (Jammu and Kashmir), Khajjiar (Himachal Pradesh) and Nainital (Uttarakhand). Himalayan Geology 2008;655(2648):Article No. 2300.

Saleh AA, El-Meleigy SA, Ebad FA, Helmy MA, Jentschke G, Godbold DL. Base cations ameliorate Zn toxicity but not Cu toxicity in sugar beet (*Beta vulgaris*). Journal of Plant Nutrition and Soil Science 1999;162(3):275-9.

Samuel S, Michael A, Iliya M. Analysis of water quality of small scale irrigation scheme in Kwadon, yamaltu-debalga of gombe state. EQA-International Journal of Environmental Quality 2021;41:33-9.

Sarkar R, Ghosh AR, Mondal NK. Comparative study on physicochemical status and diversity of macrophytes and zooplanktons of two urban ponds of Chandannagar, WB, India. Applied Water Science 2020;10(2):1-8.

Saund TB, Shrestha J. Fish and benthic fauna in Kulekhani Reservoir, Makwanpur. Nepal Journal of Science and Technology 2007;8:63-8.

Sharma CM, Kang S, Tripathee L, Paudyal R, Sillanpää M. Major ions and irrigation water quality assessment of the Nepalese Himalayan rivers. Environment, Development and Sustainability 2021;23(2):2668-80.

Shrestha AB, Aryal R. Climate change in Nepal and its impact on Himalayan glaciers. Regional Environmental Change 2011; 11(1):65-77.

Stöcklin J, Bhattarai KD. Geology of the Kathmandu Area and Central Mahabharat range. Himalaya, Nepal: Department of Mines and Geology/UNDP; 1977.

Stöcklin J. Geology of Nepal and its regional frame: Thirty-third William Smith lecture. Journal of the Geological Society 1980;137(1):1-34.

Suwal RC. Eco-tourism in Nepal: A Case Study of Phewa Lake Area, Pokhara [dissertation]. Kathmandu, Tribhuvan University; 2013.

Tripathee L, Kang S, Huang J, Sharma CM, Sillanpää M, Guo J, et al. Concentrations of trace elements in wet deposition over the Central Himalayas, Nepal. Atmospheric Environment 2014;95:231-8.

Tripathee L, Kang S, Sharma CM, Rupakheti D, Paudyal R, Huang J, et al. Preliminary health risk assessment of potentially toxic metals in surface water of the Himalayan Rivers, Nepal. Bulletin of Environmental Contamination and Toxicology 2016;97(6):855-62.

United States Salinity Laboratory (USSL). Diagnosis and Improvement of Saline and Alkali Soils. Washington D.C., USA: USDA; 1954. p. 69-81.

United States Environmental Protection Agency (USEPA). National Water Quality Inventory 1998 Report to Congress. USEPA 841-R-OO-OOl. Washington D.C., USA: Office of Water; 2000. p. 413.

Wetzel RG. Periphyton of freshwater ecosystems. Proceedings of the First International Workshop on Periphyton of Freshwater Ecosystems; 1982 Sept 14-17; Växjö: Sweden; 1983.

Wetzel RG. Limnology: Lake and River Ecosystems. Gulf Professional Publishing; 2001.

Wilcox L. Classification and Use of Irrigation Waters (No. 969). Washington D.C., USA: United States Department of Agriculture; 1955.

Wu J, Sun Z. Evaluation of shallow groundwater contamination and associated human health risk in an alluvial plain impacted by agricultural and industrial activities, mid-west China. Exposure and Health 2016;8(3):311-29.

Yamanaka H, Yoshida M, Arrita K. Terrace landforms and quaternary deposit around Pokhara Valley, central Nepal. Journal of Nepal Geological Society 1982;2:113-42.

Environment and Natural Resources Journal 2023; 21(2): 186-197

Evaluation of Land Use Land Cover Changes in Nan Province, Thailand, Using Multi-Sensor Satellite Data and Google Earth Engine

Jiratiwan Kruasilp[1,2], Sura Pattanakiat[1*], Thamarat Phutthai[1], Poonperm Vardhanabindu[1], and Pisut Nakmuenwai[1]

[1]*Faculty of Environment and Resource Studies, Mahidol University, Nakhon Pathom 73170, Thailand*
[2]*Geo-informatics and Space Technology Development Agency, Bangkok 10210, Thailand*

ARTICLE INFO

Received: 13 Sep 2022
Received in revised: 16 Jan 2023
Accepted: 18 Jan 2023
Published online: 15 Feb 2023
DOI: 10.32526/ennrj/21/202200200

Keywords:
Random forest/ Synthetic Aperture Radar/ Change detection/ Google Earth Engine/ Land management policy

*** Corresponding author:**
E-mail: sura44@gmail.com

ABSTRACT

Land use and land cover (LULC) conversion has become a chronic problem in Nan province. The primary factors of changes are lacking arable land, agricultural practices, and agriculture expansion. This study evaluated the usefulness of multi-sensor Landsat-5 (LS5), Landsat-8 (LS8), Sentinel-1 (S1), and Sentinel-2 (S2) satellite data for monitoring changes in LULC in Nan province, Thailand during a 30-year period (1990-2019), using a random forest (RF) model and the cloud-based Google Earth Engine (GEE) platform. Information of established land management policies was also used to describe the LULC changes. The median composite of the input variables selection from multi-sensor data were used to generate datasets. A total of 36 datasets showed the overall accuracy (OA) ranged from 51.70% to 96.95%. Sentinel-2 satellite images combined with the Modified Soil-Adjusted Vegetation Index (MSAVI) and topographic variables provided the highest OA (96.95%). Combination of optical (i.e., S2 and LS8) and S1 Synthetic Aperture Radar (SAR) data expressed better classification accuracy than individual S1 data. Forest cover decreased continuously during five consecutive periods. Coverage of maize and Pará rubber trees rapidly expanded in 2010-2014. These changes indicate an adverse consequence of the established economic development promoted by industrial and export agriculture. The findings strongly support the use of the RF technique, GEE platform and multi-sensor satellite data to enhance LULC classification accuracy in mountainous area. This study recommended that certain informative and science-based evidence will encourage local policymakers to identify priority areas for land management and natural resource conservation.

1. INTRODUCTION

Land use and land cover (LULC) are changing globally as a result of human activity and land development. In Thailand, LULC changes affect local communities. Accurate, timely, and reliable spatial and temporal information on LULC in mountain areas is crucial, but the information are still lacking. Thailand is often under heavy cloud cover and experiences frequent precipitation. Such weather conditions can affect utilization of optical satellite data in LULC monitoring by reducing image quality. In addition, the optical satellite data sets such as LANDSAT, Satellite Pour l'Observation de la Terre (SPOT), or Moderate Resolution Imaging Spectroradiometer (MODIS) contain limitations. As data acquisitions over the country could be accomplished only a few days per year. Taken together, timely LULC analysis is limited when the single optical sensor data is used.

There has been increasing interest in synthetic aperture radar (SAR) remote sensing, which is sensitive to vegetation structure and can be applied under all weather and environmental conditions (Dobson et al., 1992). However, SAR data has not been widely used for LULC monitoring in Thailand due to the difficulty of image processing operation when compared with optical sensor data. Increasing understanding of the utility of SAR images helps

Citation: Kruasilp J, Pattanakiat S, Phutthai T, Vardhanabindu P, Nakmuenwai P. Evaluation of land use land cover changes in Nan Province, Thailand, using multi-sensor satellite data and Google Earth Engine. Environ. Nat. Resour. J. 2023;21(2):186-197. (https://doi.org/10.32526/ennrj/21/202200200)

driving operational LULC monitoring. Recently, earth observations produce a variety of data across spatial and temporal extents and resolutions. It is desirable to use multi-source data in order to extract LULC information. Therefore, multi-source data can provide superior classification results and fulfill the gaps in data acquisition from single sensor data (Richards, 2012). On the other hand, no study in Thailand has reported the effects of different input variables selecting from multi-sensor satellite data on the accuracy of LULC classification.

Currently, numerous image classification techniques based on remote sensing data were established to improve the accuracy of LULC classification. One of the most robust and generally used techniques of supervised classification techniques for LULC monitoring is Random forest (RF) (Gislason et al., 2006). RF is an ensemble classifier based on bagging to construct many individual decision trees, which is a powerful nonparametric statistical model used to handle non-linear relations. RF is a versatile and smart machine learning technique that can perform both regression and classification tasks using a multitude of decision trees and a statistical technique to produce more accurate and stable predictions (Biau and Scornet, 2016). Compared to other classifiers such as Maximum Likelihood Classification (MLC), Artificial Neural Network (ANN) and Support Vector Machine (SVM), the advantages of RF are processing efficiency on large and multi-source data sets, handling a large number of input variables without variable deletion, and requiring less time for model training (Belgiu and Drăguţ, 2016). Thus, RF is the most frequently used algorithms for satellite image processing over the last 10 years, particularly LULC classification (Rodriguez-Galiano et al., 2012; Balzter et al., 2015; Chakraborty et al., 2016).

To manage multi-sensor datasets at the regional scale, Google Earth Engine (GEE) has been increasingly used in LULC studies in recent years (Amani et al., 2020; Tamiminia et al., 2020). GEE is a free cloud computing platform using JavaScript code for planetary-scale geospatial analyses; it is useful for storing and processing large datasets (Gorelick et al., 2017). GEE provides massive volumes of global time-series satellite images, such as daily MODIS data, Landsat archives dating back to the early 1980s, and Sentinel-1 (S1) and Sentinel-2 (S2) images (Kumar and Mutanga, 2018). Multi-temporal Landsat data were applied to generate LULC maps using machine learning classifier through GEE platform, which showed a consistent and effective overall classification. The result achieved mapping accuracy of greater than 70% (Tsai et al., 2018). In Thailand, GEE is not widely used for operation LULC classification. Therefore, using multi-sensor satellite data and GEE platform is being challenged for robust operational long-term LULC monitoring over the country.

The objective of this study was to evaluate LULC changes in Nan province from 1990 to 2019 using multi-sensor satellite data. A Random forest (RF) classifier was used in conjunction with the GEE platform. Furthermore, the changes in LULC in relation to established land management policies in the province over the last 30 years were revealed.

2. METHODOLOGY

2.1 Study area

The study area is located in Nan province, Thailand (Figure 1), in the easternmost part of Northern Thailand (central coordinates: 100°46' 44.36" E, 18°47'1.61" N), and is bordered by Lao PDR. Nan consists of 15 districts and 99 sub-districts, covering a total area of 12,142.12 km^2. According to the Köppen-Geiger climate map, the region has a tropical savanna climate (Aw) (Peel et al., 2007) with an annual average temperature of around 27°C and average precipitation of around 1,000-1,200 mm per year. The most notable characteristic of the province is its mountain area (87.2%; 600-1,200 meters above mean sea level), which has an average slope of >30%. Nan is flat only in its central valley region, which covers 12.8% of the study area. The dominant forest ecosystems include mixed deciduous forest, evergreen forest, and dry dipterocarp forest. The population of the province was 476,727 in 2020; the main employment sector is agriculture (92.84%) (The Bureau of Registration Administration, 2020).

2.2 Data acquisition

2.2.1 Satellite datasets and topographic variables

This study used multi-sensor satellite data, including S1, S2 MSI S2, Landsat-5 TM (LS5), and Landsat-8 OLI (LS8) images taken over Nan province during 1990 to 2019. These images were selected according to availability on the GEE platform, which covered the study period. The input selected bands of the satellites are given in Table 1. All satellite images were acquired throughout the growing season to eliminate the influence of seasonal variations in vegetation. In addition, topographic variables consisting of elevation and slope maps were derived from 30-m spatial resolution Shuttle Radar Topography Mission (SRTM) digital elevation models (DEM) based on the WGS84 Geoid model. All datasets were acquired from the US Geological Survey (USGS) website (http://earthexplorer.usgs.gov/) and integrated into the cloud-based GEE platform.

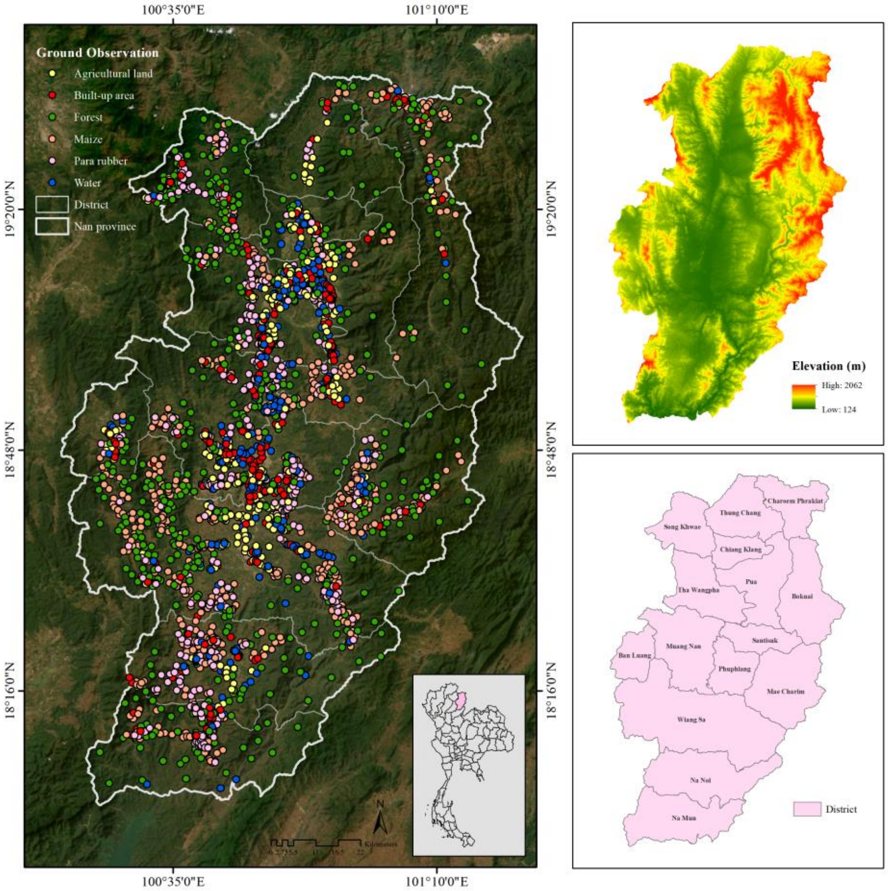

Figure 1. Map of the study area in Nan Province, Thailand. Ground observation map in 2019 (left), elevation map (top right), and administrative boundary map (bottom right).

Table 1. Summary of satellite datasets used in the analysis

Satellite	Data characteristics			
	Sensor	Resolution (m)	Band/Mode	Acquisition
Landsat-5 TM	Optical	30	Visible (band 1 - 3) NIR (band 4) SWIR (band 5)	1990, 1998, 2007, 2010
Landsat-8 OLI	Optical	30	Visible (band 2 - 4) NIR (band 5) SWIR (band 6)	2014, 2019
Sentinel-2 MSI	Optical	10, 20	Visible (band 2 - 4) NIR (band 8) SWIR (band 11)	2019
Sentinel-1 GRD	SAR	10	Dual polarization (VV and VH)	2014, 2019

2.2.1 Ground observations and training data

Ground observation data were collected during the growing season in 2019. In-situ data consisting of digital photographs, longitudes, latitudes, and detailed descriptions of the LULC classes were obtained through ground observations. Six major LULC classes including agricultural land, built-up area, forest, Pará rubber trees, maize, and water were utilized in this study. Additionally, regions of interest (ROIs) for each LULC class were delineated by visual interpretation of high-resolution Google Earth images, based on advanced knowledge of LULC data acquired through past and ongoing fieldwork (Liu et al., 2018; Sarzynski et al., 2020). Training using an RF classifier and accuracy assessments of LULC maps were conducted using ground observation and ROI data.

2.3 Random forest classification based on Google Earth Engine

2.3.1 Satellite image pre-processing

For optical images pre-processing, LS5, LS8, and S2 surface reflectance images were retrieved from GEE repository. All selected satellite data were calculated for the median image of each study year, which was clipped to the study area boundary. The study area located in the mountain area, where it is subject to cloud cover conditions. Cloud and cloud shadow masking operation using pixel quality assurance band from Landsat surface reflectance images generated from the C programming language implementation of Function of Mask (CFMask) algorithm, was performed to overcome this obstacle (Foga et al., 2017). Meanwhile, the QA60 band was used to mask out clouds from the S2 images. Then, five spectral indices, including the Normalized Difference Vegetation Index (NDVI), Normalized Difference Moisture Index (NDMI), Modified Normalized Difference Water Index (MNDWI), Normalized Difference Built-up Index (NDBI), and Modified Soil-Adjusted Vegetation Index (MSAVI) were calculated from selected images in order to increase the accuracy of LULC classification (Phan et al., 2020). The calculated spectral indices were used as input for LULC classification (Zha et al., 2003; Gitelson, 2004; Xu, 2006; Campbell and Wynne, 2011; DeVries et al., 2015). The specifications of the selected spectral indices are presented in Table 2.

Table 2. Specifications of the spectral indices

Spectral index	Formula
Normalized Difference Vegetation Index	$\frac{\text{NIR} - \text{RED}}{\text{NIR} + \text{RED}}$
Normalized Difference Moisture Index	$\frac{\text{NIR} - \text{SWIR}}{\text{NIR} + \text{SWIR}}$
Modified Normalized Difference Water Index	$\frac{\text{GREEN} - \text{SWIR}}{\text{GREEN} + \text{SWIR}}$
Normalized Difference Built-up Index	$\frac{\text{SWIR} - \text{NIR}}{\text{SWIR} + \text{NIR}}$
Modified Soil-Adjusted Vegetation Index	$\frac{2\text{NIR} + 1 - \sqrt{(2\text{NIR} + 1)^2 - 8(\text{NIR} - \text{RED})}}{2}$

For SAR images pre-processing, S1 Level-1 Ground Range Detected (GRD) images were retrieved from the GEE image library. Orbit restitution, thermal noise removal, terrain correction and radiometric calibration were performed using the Sentinel-1 toolbox on the GEE platform. In addition, S1 images were filtered using refined Lee filter on the GEE platform to reduce speckle noise and preserve content of texture information (Lee et al., 2009). Grey-Level Co-occurrence Matrix (GLCM) is the most popular and approved approach for texture feature extraction. It can improve classification by reducing heterogeneity and preserving boundaries of the same LULC types. The different GLCM texture variables reported in previous studies have increased LULC classification accuracy (Hall-Beyer, 2017; Numbisi et al., 2019; Tavares et al., 2019). In this study, four GLCM texture variables, including variance, contrast, entropy, and correlation, were extracted from backscattering of S1 images. Variance is the dispersion around the average pixel values within a defined window. The depth and smoothness of the image texture structure is reflected by Contrast. Entropy is used to measure the randomness of a gray-level distribution. Correlation is the predictability and linear relationship of the neighboring pixels, which reflects similarity of image texture in a horizontal or vertical direction (Haralick, 1979).

2.3.2 Image classification and LULC change detection using a pixel-based RF classifier

Topographic, optical and SAR products were integrated as features of the classifier input. Each satellite images in 1990, 1998, 2007, 2010, 2014, and

2019 were classified into six major LULC classes including agricultural land, built-up area, forest, para rubber, maize, and water classes. We created six clusters on the GEE platform consisting of (1) LS5/LS8/S1 + spectral indices/GLCM + Topographic variables; (2) LS5/LS8/S1 + spectral indices/GLCM; (3) LS5/LS8/S1; (4) LS5/LS8/S2 + Individual spectral indices + Topographic variables; (5) Combination of LS8/S2 with S1 polarizations + spectral indices + GLCM + Topographic variables; and (6) Combination of LS8/LS2 with S1 polarization. A total of 36 datasets were grouped within six clusters as presented in Table 3. These datasets were selected for evaluation of different input variables selection impact on the accuracy of LULC classification (Phan et al., 2020).

RF supervised machine learning algorithm and GEE platform were utilized to produce LULC maps in 1990, 1998, 2007, 2010, 2014, and 2019. The RF classification was performed using different datasets, including optical spectral bands, five spectral indices, SAR polarizations, four GLCM texture variables for each polarization, and combination of optical and SAR data. Annual cloud free composites of each chosen year were created by using the median reflectance pixel values of the collection (Huang et al., 2010). With a minimum of two tuning parameters requirement, the number of classification trees desired was set at 100 to provide a reliable error estimation and to maintain the computation times. The number of predictor variables used to split a node was set at the square root of the number of input variables (Cutler et al., 2007). All input data were resampled to a resolution of 10 m using a bicubic interpolation to harmonize the different datasets (Vizzari, 2022; De Luca et al., 2022). LULC changes were identified by applying a post-classification comparison method to five consecutive periods: 1990-1998, 1998-2007, 2007-2010, 2010-2014, and 2014-2019 (Tewkesbury et al., 2015).

2.3.3 Accuracy assessment

Accuracy assessment of LULC classification was performed using the confusion matrix, which is accepted as the standard descriptive reporting tool for accuracy assessment (Congalton and Green, 2019). The combination of ground observations and stratified random sampling based on multiple high-resolution Google Earth images were randomly selected to train the RF classifier (70% of pixels from each LULC class) and validate samples (the remaining 30% of pixels) (Belgiu and Drăguţ, 2016). The matrix was used to compute the kappa coefficient (K), overall accuracy (OA), user's accuracy (UA) and producer's accuracy (PA). K is the measurement of RF performance. The possible K values range from -1 (very poor agreement) to 1 (excellent agreement). OA values representing for average percentage of correctly classified pixel range from 0 (no pixel correctly classified) to 1 (100% of pixels are well classified). PA is the measurement of omission error (underestimation) while UA is the measurement of commission error (overestimation).

2.4 Land management policies in Nan Province

Land management policies in Nan Province were collected from governance and online news reports. Thanks to these data, we could confirm results of the LULC changes across the study area for the period 1990-2019. It was found that the forest concession – a policy instrument to implement forest harvesting, promotion of agricultural extension, and infrastructural modernization – resulted in declining of forest from 85% in 1964 to 60% in 2018. To establish an increasing number of protected areas, national parks, and wildlife sanctuaries, the Royal Thai Government officially banned all commercial logging in natural forests in 1989 (Lakanavichian, 2001). This action aimed to encourage projects for maize and Pará rubber plantations in 1981 and 2005, respectively (Thailand Environment Institute, 2012). In the early 21st century, opium was replaced by maize plantation, which was one of the factors of deforestation severity. Rapid booming of maize production resulting in the decline of prices, particularly in 2007. Meanwhile, promoting of Pará rubber plantation occurred as an alternative crop since 2005.

Given all the factors mentioned above, a strategic plan for the province has been promoted to initiate for less adverse environmental impact and increased sustainable consumption of natural resources. It is essential to better understand the sequelae of underlying LULC conversion before effective land use planning. Therefore, the LULC changes would provide the potential information required for design and implementation of natural resources policies, strategies, and legislation. Workflow of the data processing is illustrated in Figure 2.

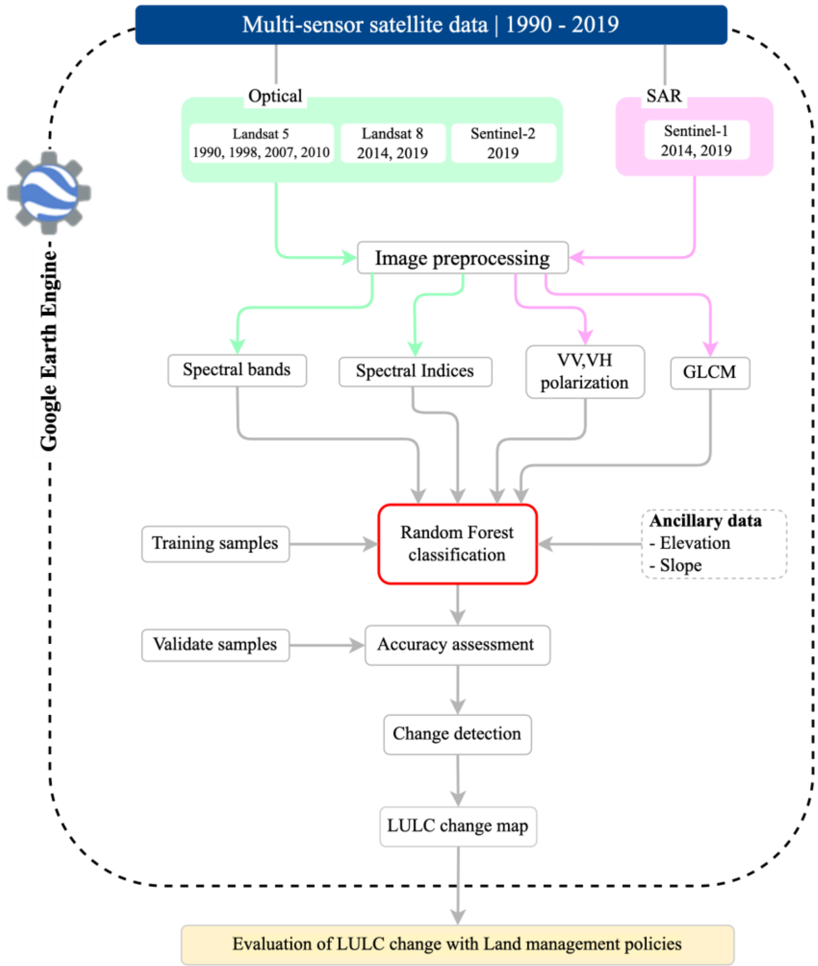

Figure 2. Workflow of data processing

3. RESULTS AND DISCUSSION

3.1 LULC classification based on multi-sensor satellite data using RF via the GEE platform

This study demonstrated the potential of multi-sensor satellite data for monitoring LULC changes in Nan province. In this study, the overall accuracy (OA) of LULC classification for datasets (L01-L36), which were categorized into six clusters, ranged from 51.70% to 96.95% (Table 3). Producer's accuracies (PA) and user's accuracy (UA) values of each dataset ranged from 0.61 to 0.99 and 0.73 to 1, respectively. Dataset L31 in cluster 4 (i.e., S-2 B2, B3, B4, B8, B11, MSAVI, slope, and elevation) provided the highest OA (96.95%; kappa coefficient=0.96), while dataset L15 in cluster 3 (i.e., S1 VV) produced the lowest OA (51.70%; kappa coefficient =0.42). For all clusters, spectral feature bands from LS5, LS8, S2, and a combination of multi-sensor satellite data yielded OA values >85%. This presented high OA compared with previous study using only single sensor (OA<80%) (Phan et al., 2020). Single sensor of optical data was also performed in this study (cluster 3). However, the OA was 85%, which was higher than their study but still lower than OA from multi-sensor. In terms of the SAR data, S1 data alone in clusters 1-3 yielded much lower OA values than LS8, S2, and a combination of multi-sensor satellite data, with an OA <80%. S1 data alone did not provide acceptable classification accuracy in the study area. Possible reasons for this include the low ability of the backscatter intensity feature to identify vegetation, and deep penetration of the C-band into crowns on medium-sized branches (Abdikan et al., 2016). Additionally, similarity between forest backscatter and Pará rubber trees in mountain areas may have decreased the classification accuracy. The results for clusters 5-6 revealed that a combination of multi-sensor satellite images and ancillary variables increased the OA by >12%. Combining optical and SAR satellite images using the RF model resulted in high LULC classification accuracy. This indicated that, compared with utilizing only S2, LS, or S1 data, improvements in classification accuracy could be achieved by combining optical and SAR satellite images. This result aligned with those of De Alban et al. (2018) and Torbick et al. (2016). Due to their different wavelengths, optical and SAR data respond to different surface characteristics (Zhu et al., 2012). Nevertheless, they provided comparable OA for all LS-8 and S2 spectral bands with the topographic data. However, only the spectral feature bands from S2 images had (slightly) higher OA values than LS8 images. Likewise, combinations of S2 and S1 images provided higher OA than combinations of LS8 and S1 images (cluster 5-6). These findings indicate that the LULC classification results were affected by the spatial resolution of the satellite data obtained by different sensors.

Classification using an RF model and the GEE platform was more accurate than that using maximum likelihood classification (MLC) model in the same study area (Paiboonvorachat and Oyana, 2011). Paiboonvorachat and Oyana (2011) reported OA <86% by using MLC model in Nan province. MLC is a traditional technique, which relies on second order statistics of Gaussian probability density model for each class. The pixel samples are required to have a normal distribution of the data in each class, but some classes are non-normally distributed data. Therefore, this is a significant disadvantage of MLC because input data are regularly non-normal distribution. The GEE platform allows for rapid processing of multi-sensor satellite data, because image downloading and local data storage are not necessary. In contrast, several Thai organizations publishing official national reports of natural resources use conventional techniques for operational image processing, which require expensive hardware and on-premises software.

Table 3. Overall accuracy (%) from the classification results for each datasets

Cluster	Datasets	Variable	OA (%)
1	L1	Landsat-5 B1, B2, B3, B4, B5, NDVI, NDMI, MNDWI, MSAVI, NDBI, slope, elevation	93.65
	L2	Landsat-8 B2, B3, B4, B5, B6, NDVI, NDMI, MNDWI, MSAVI, NDBI, slope, elevation	94.79
	L3	Sentinel-2 B2, B3, B4, B8, B11, NDVI, NDMI, MNDWI, MSAVI, NDBI, slope, elevation	96.42
	L4	Sentinel-1 VV, VV_contrast, VV_var, VV_ent, VV_corr, slope, elevation	70.75
	L5	Sentinel-1 VH, VH_contrast, VH_var, VH_ent, VH_corr, slope, elevation	75.51
	L6	Sentinel-1 VV, VV_contrast, VV_var, VV_ent, VV_corr, VH, VH_contrast, VH_var, VH_ent, VH_corr, slope, elevation	75.21
2	L7	Landsat-5 B1, B2, B3, B4, B5, NDVI, NDMI, MNDWI, MSAVI, NDBI	87.03
	L8	Landsat-8 B2, B3, B4, B5, B6, NDVI, NDMI, MNDWI, MSAVI, NDBI	89.19
	L9	Sentinel-2 B2, B3, B4, B8, B11, NDVI, NDMI, MNDWI, MSAVI, NDBI	91.33
	L10	Sentinel-1 VV, VV_contrast, VV_var, VV_ent, VV_corr	55.10
	L11	Sentinel-1 VH, VH_contrast, VH_var, VH_ent, VH_corr	57.37
3	L12	Landsat-5 B1, B2, B3, B4, B5	85.07
	L13	Landsat-8 B2, B3, B4, B5, B6	89.32
	L14	Sentinel-2 B2, B3, B4, B8, B11	91.23
	L15	Sentinel-1 VV	51.70
	L16	Sentinel-1 VH	58.28
	L17	Sentinel-1 VV, VH	59.64
4	L18	Landsat-5 B1, B2, B3, B4, B5, NDVI, SLOPE, ELEVATION	93.40
	L19	Landsat-5 B1, B2, B3, B4, B5, MSAVI, SLOPE, ELEVATION	93.91
	L20	Landsat-5 B1, B2, B3, B4, B5, MNDWI, SLOPE, ELEVATION	92.39
	L21	Landsat-5 B1, B2, B3, B4, B5, NDBI, SLOPE, ELEVATION	93.65
	L22	Landsat-5 B1, B2, B3, B4, B5, NDMI, SLOPE, ELEVATION	93.40
	L23	Landsat-8 B2, B3, B4, B5, B6, NDVI, slope, elevation	95.33
	L24	Landsat-8 B2, B3, B4, B5, B6, NDMI, slope, elevation	95.06
	L25	Landsat-8 B2, B3, B4, B5, B6, MNDWI, slope, elevation	94.79
	L26	Landsat-8 B2, B3, B4, B5, B6, MSAVI, slope, elevation	95.33
	L27	Landsat-8 B2, B3, B4, B5, B6, NDBI, slope, elevation	94.66
	L28	Sentinel-2 B2, B3, B4, B8, B11, NDVI, slope, elevation	95.54

Table 3. Overall accuracy (%) from the classification results for each datasets (cont.)

Cluster	Datasets	Variable	OA (%)
	L29	Sentinel-2 B2, B3, B4, B8, B11, NDMI, slope, elevation	95.59
	L30	Sentinel-2 B2, B3, B4, B8, B11, MNDWI, slope, elevation	95.74
	L31	Sentinel-2 B2, B3, B4, B8, B11, MSAVI, slope, elevation	96.95
	L32	Sentinel-2 B2, B3, B4, B8, B11, NDBI, slope, elevation	95.33
5	L33	Landsat-8 B2, B3, B4, B5, B6, NDVI, NDMI, MNDWI, MSAVI, NDBI, Sentinel-1 VV, VV_contrast, VV_var, VV_ent, VV_corr, VH, VH_contrast, VH_var, VH_ent, VH_corr, slope, elevation	95.67
	L34	Sentinel-2 B2, B3, B4, B8, B11, NDVI, NDMI, MNDWI, MSAVI, NDBI, Sentinel-1 VV, VV_contrast, VV_var, VV_ent, VV_corr, VH, VH_contrast, VH_var, VH_ent, VH_corr, slope, elevation	96.14
6	L35	Landsat-8 B2, B3, B4, B5, B6, Sentinel-1 VV, VH	91.70
	L36	Sentinel-2 B2, B3, B4, B8, B11, Sentinel-1 VV, VH	92.31

Remarkably, and similar to Mishra et al. (2019), higher OA was obtained in this study by integrating textural features, backscatter intensity, and topographic variables. This was likely due to the texture characteristic, which is an intrinsic spatial feature that effectively represents spatial relationships, particularly in SAR images (Du et al., 2015). The present findings showed that the integration of spectral indices (NDVI, NDMI, MNDWI, MSAVI, and NDBI) from optical sensors and topographic variables (i.e., slope and elevation) can increase LULC classification accuracy. The NDVI is commonly used for efficient classification in tropical forests. Interestingly, the MSAVI enhanced classification accuracy significantly more than the other spectral indices in this study. The loss of forest cover in Nan province has decreased vegetation coverage, but the influence of background soil signals, which are problematic for the NDVI, could be reduced for the MSAVI (Guo et al., 2019; Wen et al., 2020). This result supported the advantage of MSAVI over NDVI which was similar to the finding of Vargas et al. (2021).

Important topographic variables for improving LULC classification accuracy in this study were slope and elevation, because these variables can overcome the similarity of shadow on mountain terrain with the spectral characteristics of waters. This result was supported by previous studies showing that the combination of topographic variables with satellite data provided higher classification accuracy than individual datasets (Wagle et al., 2020; Waśniewski et al., 2020). Likewise, Dobrinić et al. (2021) strongly recommended that topographic variables produced major classification enhancements as an input feature, which was also observed in this study.

3.2 Evaluation of LULC changes by land management policies in Nan province over the last 30 years

The datasets yielding the highest OA values were used to produce LULC maps for 6 study years: 1990, 1998, 2007, 2010, 2014, and 2019 (Figure 3). All LULC classes had producer's accuracies (PA) and user's accuracy (UA) values >0.95. Water was the most differentiable object (PA and UA=0.99 and 1.00, respectively). From 1990 to 2019, the major type of LULC was forest area (70.28%), followed by agricultural area (26.56%). Forest area decreased from 8,533.67 km^2 in 1990 to 7,621.22 km^2 in 2019. Agriculture dominated flat and low-slope areas. A >7-fold increase in maize plantation area was seen between 1990 (159.90 km^2) and 2019 (1,240.87 km^2), whereas the Pará rubber tree area showed a 6.5-fold increase from 2007 to 2019. Slight increases in built-up and water areas were observed, from 1.26% in 1990 to 1.83% in 2019, and 0.58% in 1990 to 0.81% in 2019, respectively.

Over the last three decades (1990-2019), the maize plantation area showed the largest expansion (676.03%), followed by Pará rubber tree (100%) and built-up (45.16%) areas. The smallest expansion, of 39.45%, was that of water area. Agricultural area exhibited the largest decrease, of 22.76%, followed by forest (10.69%) (Figure 4). Across the five consecutive periods, forest was the only area that experienced a continuous decrease, due to its conversion into maize and Pará rubber tree plantation areas. Figure 5 illustrates the forest conversion between 1990 and 2019. Overall forest changed area totally distributed over 1,298.34 km^2. The Pará rubber tree and water areas expanded most between 2007 and 2010 (165.05% and 12.24%, respectively). Maize area expansion was greatest between 1990 and 1998

(256.33%). During the past 30 years, maize and Pará rubber trees have become the dominant monoculture crops in the mountain study area. During that period, both crops were expensive and in high demand on global markets (Pongkijvorasin and Teerasuwannajak, 2019). Their increased cultivation arose from the promotion of industrial and export agriculture by the Thai government and the implementation of a capitalist economic model (Rossi, 2014; Darlington, 2019). The water area was also increased to supply crop plantations. However, the maize plantation area decreased during 2014-2019, by 17.62%, which was related to an increase in the agricultural area. This may be due to the implementation of a strategic plan to grow alternative cash crops to maize, with the aim of reducing adverse effects on the environment.

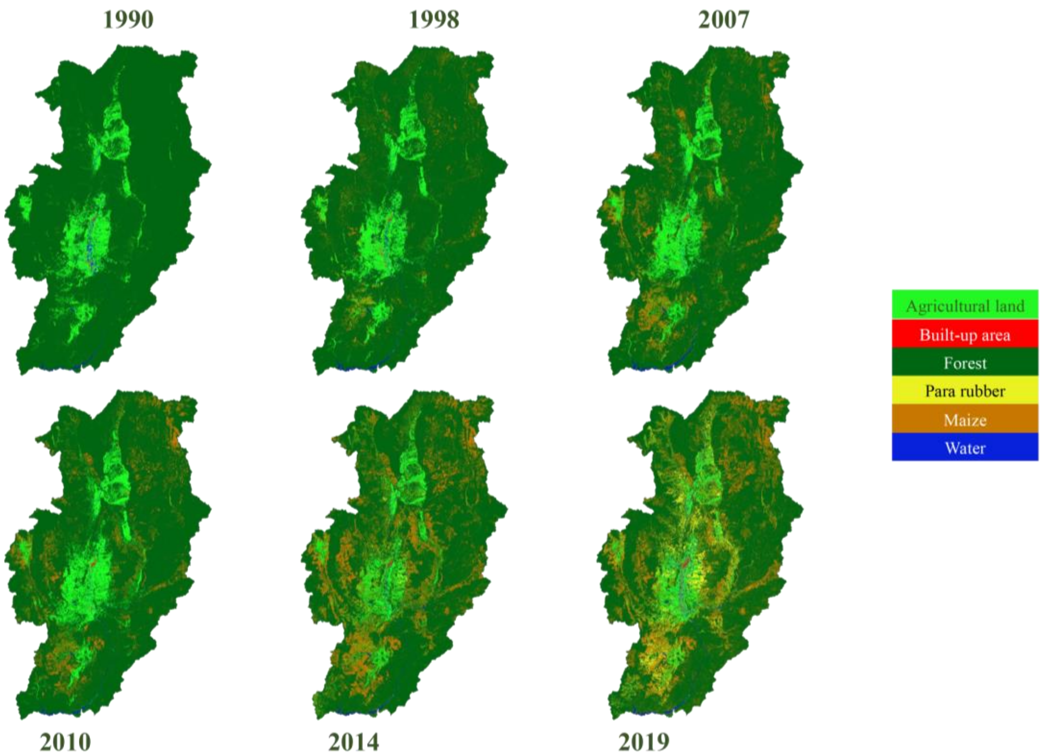

Figure 3. LULC changes between 1990 and 2019 according to the RF classifier

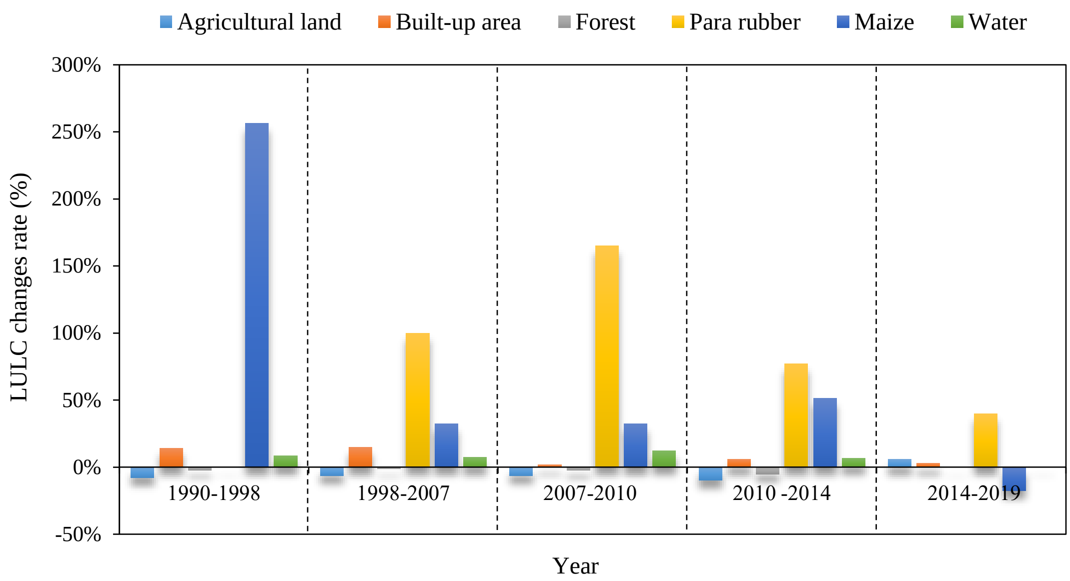

Figure 4. Percentage changes in LULC categories over five consecutive periods

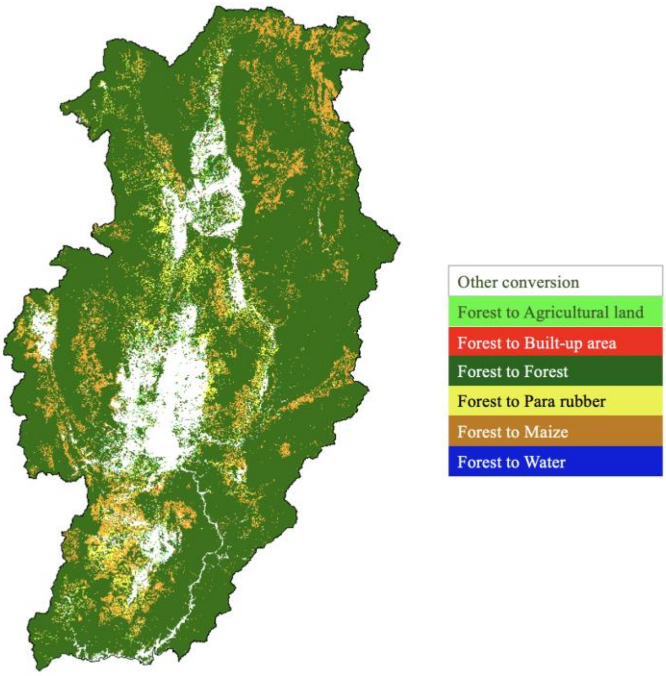

Figure 5. Forest conversion between 1990 and 2019

In the study area, economic measures implemented by the private sector, such as credit provision and market offerings, were among the major drivers of unsustainable land use (Humidtropics, 2015). Forest can be considered as unoccupied land, and there is a lack of awareness of sustainable natural resource use practices. Many farmers transitioned from subsistence farming and small-scale production to cash crops, intensive mono-crop agriculture, and contract farming, as promoted by the government and agro-industrial companies, to generate more income and enhance their quality of life (Darlington, 2019). Even though forest changes are high in Nan province, Agarwal et al. (2022) reported that community managed forests were well conserved due to a strong protection against deforestation by the community. This is a principal key for natural resource management, particularly in forest areas, for sustainable land use and management.

4. CONCLUSION

This study represents the first long-term (30 years) assessment of LULC change in Nan province. Evaluation of the potential of multi-sensor satellite data (i.e., optical and SAR images) to produce LULC change maps in five consecutive periods using an RF model and cloud-computing platform (GEE) was performed. Land management policies were used to clarify the changes of LULC in each period. This study highlighted the advantages of RF classifier in conjunction with GEE platform which can display great performance in rapid processing of multi-sensor satellite data and ability to deal with high-dimensional data. Using GEE platform for LULC change assessment is clearly beneficial for classification purposes and could be used to leverage the operational classification process. The highest overall accuracy was achieved using Sentinel-2 spectral bands, MSAVI, and topographic variables. MSAVI showed an advantage over NDVI in the area of decreased vegetation coverage. Major LULC classification could be enhanced by using topographic variables. In terms of SAR data, the combination of optical (i.e., S2 and LS8) and SAR images expressed better classification accuracy than individual S1 data. Regarding established land management policies, forest areas revealed extensive encroachment in Nan province during the study period. These are consequences of extensive conversion of forest to maize and Pará rubber tree areas. Taken together, geoinformatics and remote sensing technology as well as land management policies will provide certain informed and science-based decisions to guide policymakers in improvement of sustainable natural resource management plan and monitoring.

ACKNOWLEDGEMENTS

The authors would like to thank Geo-Informatics and Space Technology Development Agency (GISTDA), Bangkok, Thailand for supporting research materials and providing research facilities. We thank the anonymous reviewers and editors for their insightful comments and suggestions.

REFERENCES

Abdikan S, Sanli FB, Ustuner M, Calò F. Land cover mapping using SENTINEL-1 SAR data. Proceedings of the International Archives of the Photogrammetry, Remote Sensing and Spatial Information Sciences, XLI-B7, 2016 XXIII ISPRS Congress; 2016 Jul 12-19; Prague: Czech Republic; 2016.

Agarwal S, Sairorkham B, Sakitram P, Lambin EF. Effectiveness of community forests for forest conservation in Nan Province, Thailand. Journal of Land Use Science 2022;17(1):307-23.

Amani M, Ghorbanian A, Ahmadi SA, Kakooei M, Moghimi A, Mirmazloumi SM, et al. Google earth engine cloud computing platform for remote sensing big data applications: A comprehensive review. IEEE Journal of Selected Topics in Applied Earth Observations and Remote Sensing 2020;13: 5326-50.

Balzter H, Cole B, Thiel C, Schmullius C. Mapping CORINE land cover from Sentinel-1A SAR and SRTM digital elevation kodel data using random forests. Remote Sensing 2015;7(11):14876-98.

Belgiu M, Drăguţ L. Random forest in remote sensing: A review of applications and future directions. ISPRS Journal of Photogrammetry and Remote Sensing 2016;114:24-31.

Biau G, Scornet E. A random forest guided tour. TEST 2016; 25(2):197-227.

Campbell JB, Wynne RH. Introduction to Remote Sensing. New York, USA: Guilford Press; 2011.

Chakraborty A, Sachdeva K, Joshi PK. Mapping long-term land use and land cover change in the central Himalayan region using a tree-based ensemble classification approach. Applied Geography 2016;74:136-50.

Congalton RG, Green K. Assessing the Accuracy of Remotely Sensed Data: Principles and Practices, 3rd ed. Boca Raton, USA: CRC Press; 2019.

Cutler DR, Edwards TC, Beard KH, Cutler A, Hess KT, Gibson J, et al. Random forests for classification in ecology. Ecology 2007;88(11):2783-92.

Darlington SM. Buddhist integration of forest and farm in Northern Thailand. Religions 2019;10(9):Article No. 521.

De Alban JDT, Connette GM, Oswald P, Webb EL. Combined Landsat and L-Band SAR data improves land cover classification and change detection in dynamic tropical landscapes. Remote Sensing 2018;10(2):Article No. 306.

De Luca G, M.N. Silva J, Di Fazio S, Modica G. Integrated use of Sentinel-1 and Sentinel-2 data and open-source machine learning algorithms for land cover mapping in a Mediterranean region. European Journal of Remote Sensing 2022;55(1):52-70.

DeVries B, Decuyper M, Verbesselt J, Zeileis A, Herold M, Joseph S. Tracking disturbance-regrowth dynamics in tropical forests using structural change detection and Landsat time series. Remote Sensing of Environment 2015;169:320-34.

Dobrinić D, Gašparović M, Medak D. Sentinel-1 and 2 Time-Series for vegetation mapping using random forest classification: A case study of Northern Croatia. Remote Sensing 2021;13(12):Article No. 2321.

Dobson MC, Ulaby FT, LeToan T, Beaudoin A, Kasischke ES, Christensen N. Dependence of radar backscatter on coniferous forest biomass. IEEE Transactions on Geoscience and Remote Sensing 1992;30(2):412-5.

Du P, Samat A, Waske B, Liu S, Li Z. Random forest and rotation forest for fully polarized SAR image classification using polarimetric and spatial features. ISPRS Journal of Photogrammetry and Remote Sensing 2015;105:38-53.

Foga S, Scaramuzza PL, Guo S, Zhu Z, Dilley RD, Beckmann T, et al. Cloud detection algorithm comparison and validation for operational Landsat data products. Remote Sensing of Environment 2017;194:379-90.

Gislason PO, Benediktsson JA, Sveinsson JR. Random Forests for land cover classification. Pattern Recognition Letters 2006; 27(4):294-300.

Gitelson AA. Wide dynamic range vegetation index for remote quantification of biophysical characteristics of vegetation. Journal of Plant Physiology 2004;161(2):165-73.

Gorelick N, Hancher M, Dixon M, Ilyushchenko S, Thau D, Moore R. Google Earth Engine: Planetary-scale geospatial analysis for everyone. Remote Sensing of Environment 2017;202:18-27.

Guo B, Yang F, Han B, Fan Y, Chen S, Yang W, et al. A model for the rapid monitoring of soil salinization in the Yellow River Delta using Landsat 8 OLI imagery based on VI-SI feature space. Remote Sensing Letters 2019;10(8):796-805.

Hall-Beyer M. Practical guidelines for choosing GLCM textures to use in landscape classification tasks over a range of moderate spatial scales. International Journal of Remote Sensing 2017;38(5):1312-38.

Haralick RM. Statistical and structural approaches to texture. Proceedings of the IEEE 1979;67(5):786-804.

Huang C, Thomas N, Goward SN, Masek JG, Zhu Z, Townshend JRG, et al. Automated masking of cloud and cloud shadow for forest change analysis using Landsat images. International Journal of Remote Sensing 2010;31(20):5449-64.

Humidtropics. Situational Analysis in Support of the Development of Integrated Agricultural Systems in the Upland Areas of Nan Province, Thailand. Chiang Mai, Thailand: International Institute of Tropical Agriculture; 2015.

Kumar L, Mutanga O. Google Earth Engine applications since inception: Usage, trends, and potential. Remote Sensing 2018;10(10):Article No. 1509.

Lakanavichian S. Forests out of bounds: Impacts and effectiveness of logging bans in natural forests in Asia-Pacific. Bangkok, Thailand: FAO; 2001.

Lee JS, Wen JH, Ainsworth TL, Chen KS, Chen AJ. Improved sigma filter for speckle filtering of SAR imagery. IEEE Transactions on Geoscience and Remote Sensing 2009;47(1): 202-13.

Liu X, Hu G, Chen Y, Li X, Xu X, Li S, et al. High-resolution multi-temporal mapping of global urban land using Landsat images based on the Google Earth Engine Platform. Remote Sensing of Environment 2018;209:227-39.

Mishra VN, Prasad R, Rai PK, Vishwakarma AK, Arora A. Performance evaluation of textural features in improving land use/land cover classification accuracy of heterogeneous landscape using multi-sensor remote sensing data. Earth Science Informatics 2019;12(1):71-86.

Numbisi FN, Van Coillie FMB, De Wulf R. Delineation of cocoa agroforests using multiseason Sentinel-1 SAR images: A low grey level range reduces uncertainties in GLCM texture-based mapping. ISPRS International Journal of Geo-Information 2019;8(4):Article No. 179.

Paiboonvorachat C, Oyana TJ. Land-cover changes and potential impacts on soil erosion in the Nan watershed, Thailand. International Journal of Remote Sensing 2011;32(21): 6587-609.

Peel MC, Finlayson BL, McMahon TA. Updated world map of the Köppen-Geiger climate classification. Hydrology and Earth System Sciences 2007;11(5):1633-44.

Phan TN, Kuch V, Lehnert LW. Land cover classification using Google Earth Engine and random forest classifier: The role of image composition. Remote Sensing 2020;12(15):Article No. 2411.

Pongkijvorasin S, Teerasuwannajak KT. A study of farmer's decision and incentive scheme to reduce highland maize farming in Thailand. International Journal of Agricultural Sustainability 2019;17(3):257-70.

Richards JA. Remote Sensing Digital Image Analysis. Heidelberg, Germany: Springer; 2012.

Rodriguez-Galiano VF, Ghimire B, Rogan J, Chica-Olmo M, Rigol-Sanchez JP. An assessment of the effectiveness of a random forest classifier for land-cover classification. ISPRS Journal of Photogrammetry and Remote Sensing 2012;67:93-104.

Rossi A. Environmental subjects and displays of political order: The case of ecology monks in Northern Thailand. Antropologia 2014;1(1):127-42.

Sarzynski T, Giam X, Carrasco L, Lee JSH. Combining radar and optical imagery to map oil palm plantations in Sumatra, Indonesia, using the Google Earth Engine. Remote Sensing 2020;12(7):Article No. 1220.

Tamiminia H, Salehi B, Mahdianpari M, Quackenbush L, Adeli S, Brisco B. Google Earth Engine for geo-big data applications: A meta-analysis and systematic review. ISPRS Journal of Photogrammetry and Remote Sensing 2020;164:152-70.

Tavares PA, Beltrão NES, Guimarães US, Teodoro AC. Integration of Sentinel-1 and Sentinel-2 for classification and LULC mapping in the urban area of Belém, Eastern Brazilian Amazon. Sensors 2019;19(5):Article No. 1140.

Tewkesbury AP, Comber AJ, Tate NJ, Lamb A, Fisher PF. A critical synthesis of remotely sensed optical image change detection techniques. Remote Sensing of Environment 2015; 160:1-14.

Thailand Environment Institute. Report on the Sub-Global Assessment (SGA) for NAN, Thailand 2012. Thailand: Thailand Environment Institute; 2012. (in Thai).

The Bureau of Registration Administration. Thailand population [Internet]. 2020 [cited 2022 Feb 25]. Available from: https://stat.bora.dopa.go.th/new_stat/webPage/statByYear.php/. (in Thai).

Torbick N, Ledoux L, Salas W, Zhao M. Regional mapping of plantation extent using multisensor imagery. Remote Sensing 2016;8(3):Article No. 236.

Tsai YH, Stow D, Chen HL, Lewison R, An L, Shi L. Mapping vegetation and land use types in Fanjingshan national nature reserve using Google Earth Engine. Remote Sensing 2018;10(6):Article No. 927.

Vargas TF, Vázquez IT, Gómez RA. Remote sensing based forest canopy opening and their spatial representation. Forest Science and Technology 2021;17(4):214-24.

Vizzari M. PlanetScope, Sentinel-2, and Sentinel-1 data integration for object-based land cover classification in Google Earth Engine. Remote Sensing 2022;14(11):Article No. 2628.

Wagle N, Acharya TD, Kolluru V, Huang H, Lee DH. Multi-temporal land cover change mapping using Google Earth Engine and ensemble learning methods. Applied Sciences 2020;10(22):Article No. 8083.

Waśniewski A, Hościło A, Zagajewski B, Moukétou-Tarazewicz D. Assessment of Sentinel-2 Satellite images and random forest classifier for rainforest mapping in Gabon. Forests 2020;11(9):Article No. 941.

Wen Y, Guo B, Zang W, Ge D, Luo W, Zhao H. Desertification detection model in Naiman Banner based on the albedo-modified soil adjusted vegetation index feature space using the Landsat8 OLI images. Geomatics, Natural Hazards and Risk 2020;11(1):544-58.

Xu H. Modification of normalised difference water index (NDWI) to enhance open water features in remotely sensed imagery. International Journal of Remote Sensing 2006;27(14):3025-33.

Zha Y, Gao J, Ni S. Use of normalized difference built-up index in automatically mapping urban areas from TM imagery. International Journal of Remote Sensing 2003;24(3):583-94.

Zhu Z, Woodcock CE, Rogan J, Kellndorfer J. Assessment of spectral, polarimetric, temporal, and spatial dimensions for urban and peri-urban land cover classification using Landsat and SAR data. Remote Sensing of Environment 2012;117:72-82.

INSTRUCTION FOR AUTHORS

Publication and Peer-reviewing processes of Environment and Natural Resources Journal

Environment and Natural Resources Journal is a peer reviewed and open access journal that is published in six issues per year. Manuscripts should be submitted online at https://ph02.tci-thaijo.org/index.php/ennrj/about/submissions by registering and logging into this website. Submitted manuscripts should not have been published previously, nor be under consideration for publication elsewhere (except conference proceedings papers). A guide for authors and relevant information for the submission of manuscripts are provided in this section and also online at: https://ph02.tci-thaijo.org/index.php/ennrj/author. All manuscripts are refereed through a **single-blind peer-review** process.

Submitted manuscripts are reviewed by outside experts or editorial board members of **Environment and Natural Resources Journal**. This journal uses double-blind review, which means that both the reviewer and author identities are concealed from the reviewers, and vice versa, throughout the review process. Steps in the process are as follows:

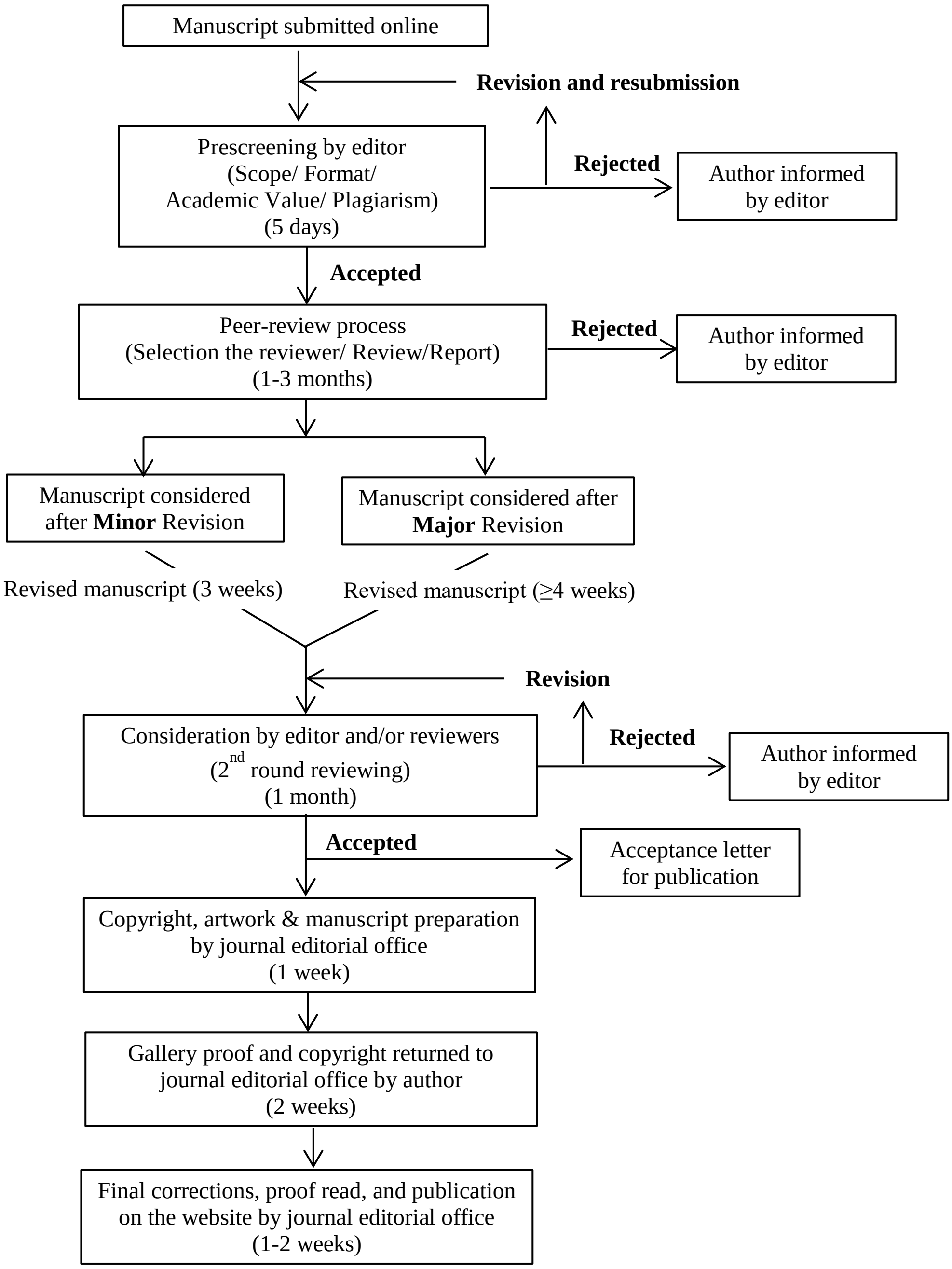

The Environment and Natural Resources Journal (EnNRJ) accepts 2 types of articles for consideration of publication as follows:

- *Original Research Article:* Manuscripts should not exceed 3,500 words (excluding references).
- *Review Article (by invitation):* This type of article focuses on the in-depth critical review of a special aspect in the environment and also provides a synthesis and critical evaluation of the state of the knowledge of the subject. Manuscripts should not exceed 6,000 words (excluding references).

Submission of Manuscript

Cover letter: Key points to include:

- Statement that your paper has not been previously published and is not currently under consideration by another journal
- Brief description of the research you are reporting in your paper, why it is important, and why you think the readers of the journal would be interested in it
- Contact information for you and any co-authors
- Confirmation that you have no competing interests to disclose

Manuscript-full: Manuscript (A4) must be submitted in Microsoft Word Files (.doc or .docx). Please make any identifying information of name(s) of the author(s), affiliation(s) of the author(s). Each affiliation should be indicated with superscripted Arabic numerals immediately after an author's name and before the appropriate address. Specify the Department/School/Faculty, University, Province/State, and Country of each affiliation.

Manuscript-anonymized: Manuscript (A4) must be submitted in Microsoft Word Files (.doc or .docx). Please remove any identifying information, such as authors' names or affiliations, from your manuscript before submission and give all information about authors at title page section.

Reviewers suggestion *(mandatory)*: Please provide the names of 3 potential reviewers with the information about their affiliations and email addresses. *The recommended reviewers should not have any conflict of interest with the authors. Each of the reviewers must come from a different affiliation and must not have the same nationality as the authors.* Please note that the editorial board retains the sole right to decide whether or not the recommended potential reviewers will be selected.

Preparation of Manuscript

Manuscript should be prepared strictly as per guidelines given below. The manuscript (A4 size page) must be submitted in Microsoft Word (.doc or .docx) with Times New Roman 12 point font and a line spacing of 1.5. *The manuscript that is not in the correct format will be returned and the corresponding author may have to resubmit*. The submitted manuscript must have the following parts:

Title should be concise and no longer than necessary. Capitalize first letters of all important words, in Times New Roman 12 point bold.

Author(s) name and affiliation must be given, especially the first and last names of all authors, in Times New Roman 11 point bold.

Affiliation of all author(s) must be given in Times New Roman 11 point italic.

Abstract should indicate the significant findings with data. A good abstract should have only one paragraph and be limited to 250 words. Do not include a table, figure or reference.

Keywords should adequately index the subject matter and up to six keywords are allowed.

Text body normally includes the following sections: 1. Introduction 2. Methodology 3. Results and Discussion 4. Conclusions 5. Acknowledgements 6. References

Reference style must be given in Vancouver style. Please follow the format of the sample references and citations as shown in this Guide below.

Unit: The use of abbreviation must be in accordance with the SI Unit.

Format and Style

Paper Margins must be 2.54 cm on the left and the right. The bottom and the top margin of each page must be 1.9 cm.

Introduction is critically important. It should include precisely the aims of the study. It should be as concise as possible with no sub headings. The significance of problem and the essential background should be given.

Methodology should be sufficiently detailed to enable the experiments to be reproduced. The techniques and methodology adopted should be supported with standard references.

Headings in Methodology section and Results and Discussion section, no more than three levels of headings should be used. Main headings should be typed (in bold letters) and secondary headings (in bold and italic letters). Third level headings should be typed in normal and no bold, for example;

2. Methodology
2.1 Sub-heading
2.1.1 Sub-sub-heading

Results and Discussion can be either combined or separated. This section is simply to present the key points of your findings in figures and tables, and explain additional findings in the text; no interpretation of findings is required. The results section is purely descriptive.
Tables Tables look best if all the cells are not bordered; place horizontal borders only under the legend, the column headings and the bottom.
Figures should be submitted in color; make sure that they are clear and understandable. Please adjust the font size to 9-10, no bold letters needed, and the border width of the graphs must be 0.75 pt. *(Do not directly cut and paste them from MS Excel.)* Regardless of the application used, when your electronic artwork is finalized, please 'save as' or convert the images to TIFF (or JPG) and separately send them to EnNRJ. The images require a resolution of at least 300 dpi (dots per inch). If a label needed in a figure, its font must be "Times New Roman" and its size needs to be adjusted to fit the figure without borderlines.

All Figure(s) and Table(s) should be embedded in the text file.

Conclusions should include the summary of the key findings, and key take-home message. This should not be too long or repetitive, but is worth having so that your argument is not left unfinished. Importantly, don't start any new thoughts in your conclusion.

Acknowledgements should include the names of those who contributed substantially to the work described in the manuscript but do not fulfill the requirements for authorship. It should also include any sponsor or funding agency that supported the work.

References should be cited in the text by the surname of the author(s), and the year. This journal uses the author-date method of citation: the last name of the author and date of publication are inserted in the text in the appropriate place. If there are more than two authors, "et al." after the first author' name must be added. Examples: (Frits, 1976; Pandey and Shukla, 2003; Kungsuwas et al., 1996). If the author's name is part of the sentence, only the date is placed in parentheses: "Frits (1976) argued that . . ."

Please be ensured that every reference cited in the text is also present in the reference list (and vice versa).

In the list of references at the end of the manuscript, full and complete references must be given in the following style and punctuation, arranged alphabetically by first author's surname. Examples of references as listed in the References section are given below.

Book
Tyree MT, Zimmermann MH. Xylem Structure and the Ascent of Sap. Heidelberg, Germany: Springer; 2002.

Chapter in a book
Kungsuwan A, Ittipong B, Chandrkrachang S. Preservative effect of chitosan on fish products. In: Steven WF, Rao MS, Chandrkachang S, editors. Chitin and Chitosan: Environmental and Friendly and Versatile Biomaterials. Bangkok: Asian Institute of Technology; 1996. p. 193-9.

Journal article
Muenmee S, Chiemchaisri W, Chiemchaisri C. Microbial consortium involving biological methane oxidation in relation to the biodegradation of waste plastics in a solid waste disposal open dump site. International Biodeterioration and Biodegradation 2015;102:172-81.

Published in conference proceedings
Wiwattanakantang P, To-im J. Tourist satisfaction on sustainable tourism development, amphawa floating marketSamut songkhram, Thailand. Proceedings of the 1st Environment and Natural Resources International Conference; 2014 Nov 6-7; The Sukosol hotel, Bangkok: Thailand; 2014.

Ph.D./Master thesis

Shrestha MK. Relative Ungulate Abundance in a Fragmented Landscape: Implications for Tiger Conservation [dissertation]. Saint Paul, University of Minnesota; 2004.

Website

Orzel C. Wind and temperature: why doesn't windy equal hot? [Internet]. 2010 [cited 2016 Jun 20]. Available from: http://scienceblogs.com/principles/2010/08/17/wind-and-temperature-why-doesn/.

Report organization:

Intergovernmental Panel on Climate Change (IPCC). IPCC Guidelines for National Greenhouse Gas Inventories: Volume 1-5. Hayama, Japan: Institute for Global Environmental Strategies; 2006.

Remark

** Please be note that manuscripts should usually contain at least 15 references and some of them must be up-to-date research articles.*

** Please strictly check all references cited in text, they should be added in the list of references. Our Journal does not publish papers with incomplete citations.*

Changes to Authorship

This policy of journal concerns the addition, removal, or rearrangement of author names in the authorship of accepted manuscripts:

Before the accepted manuscript

For all submissions, that request of authorship change during review process should be made to the form below and sent to the Editorial Office of EnNRJ. Approval of the change during revision is at the discretion of the Editor-in-Chief. The form that the corresponding author must fill out includes: (a) the reason for the change in author list and (b) written confirmation from all authors who have been added, removed, or reordered need to confirm that they agree to the change by signing the form. Requests form submitted must be consented by corresponding author only.

After the accepted manuscript

The journal does not accept the change request in all of the addition, removal, or rearrangement of author names in the authorship. Only in exceptional circumstances will the Editor consider the addition, deletion or rearrangement of authors after the manuscript has been accepted.

Copyright transfer

The copyright to the published article is transferred to Environment and Natural Resources Journal (EnNRJ) which is organized by Faculty of Environment and Resource Studies, Mahidol University. The accepted article cannot be published until the Journal Editorial Officer has received the appropriate signed copyright transfer.

Online First Articles

The article will be published online after receipt of the corrected proofs. This is the official first publication citable with the Digital Object Identifier (DOI). After release of the printed version, the paper can also be cited by issue and page numbers. DOI may be used to cite and link to electronic documents. The DOI consists of a unique alpha-numeric character string which is assigned to a document by the publisher upon the initial electronic publication. The assigned DOI never changes.

Mahidol University

Wisdom of the Land

Research and Academic Service Section, Faculty of Environment and Resource Studies, Mahidol University
999 Phutthamonthon 4 Rd, Salaya, Nakhon Pathom 73170, Phone +662 441-5000 ext. 2108 Fax. +662 441 9509-10
E-mail: ennrjournal@gmail.com Website: https://www.tci-thaijo.org/index.php/ennrj